Deoxygenation and hydrogenation of biomass-derived molecules over multifunctional catalysts

Thesis submitted in accordance with the requirements of the University of Liverpool for the degree of Doctor in Philosophy

by

Mshari Ayad N. Alotaibi

November 2012

Abstract

Deoxygenation and hydrogenation of biomass-derived molecules over multifunctional catalysts

PhD thesis by Mshari A. Alotaibi

The aim of this work was to investigate heterogeneous catalysis of the deoxygenation of renewable feedstocks for value-added chemicals and fuels using heteropoly acids. The main focus was on $H_3PW_{12}O_{40}$ (HPW) and its Cs acidic salt $Cs_{2.5}H_{0.5}PW_{12}O_{40}$ (CsPW), which have sufficiently high thermal stability, with decomposition temperatures of 450 and > 500 °C, respectively. These compounds have very strong Brønsted acidity and are well documented as acid catalysts. They were used for the deoxygenation and hydrogenation of propionic acid, methyl isobutyl ketone (MIBK) and diisobutyl ketone (DIBK) in the gas phase. For comparison, zeolite catalysts doped with Pt were examined for the deoxygenation of MIBK. CsPW was doped with Pd, Pt, Cu and Ru metals using the impregnation method, while Pt was doped on zeolites by ion exchange. The catalysts under study were characterised using various physical and chemical techniques.

CsPW and CsPW-supported Pd, Pt and Cu catalysts were found to be stable in the deoxygenation of propionic acid. They retained the Keggin structure of their polyanion (primary structure), as well as the CsPW crystal structure (secondary structure), after reaction at 400 °C in H_2, whereas HPW decomposed above 350 °C in N_2. The reaction was found to involve several pathways including ketonisation, decarbonylation, decarboxylation and hydrogenation, leading to the partial or total deoxygenation of propionic acid. HPW/SiO_2 and CsPW, both in H_2 and in N_2, exhibited ketonisation activity between 250 and 300 °C to yield 3-pentanone, CsPW being more selective than HPW. At 400 °C, HPW and CsPW were active for the decarbonylation and decarboxylation of propionic acid to yield ethene and ethane respectively. Loading Pd or Pt onto CsPW greatly enhanced decarbonylation in flowing H_2, but had little effect in N_2. Similar performance was exhibited by Pd and Pt on SiO_2, giving almost 100% selectivity to ethene in H_2. These results are consistent with the hydrodeoxygenation of propionic acid on Pd and Pt, suggesting that hydrogenolysis of the C-C bond plays an essential role. Cu catalysts were active in the hydrogenation of the C=O bond to yield propanal and 1-propanol. Turnover rates of propionic acid conversion on metal catalysts followed the order Pd > Pt > Cu.

Pt/CsPW was found to be a very efficient catalyst for the selective one-step hydrodeoxygenation of biomass-derived aliphatic ketones MIBK and DIBK to yield 2-methylpentane (MP) and 2,6-dimethylheptane (DMH) under mild conditions at 100 °C and 1 bar pressure without isomerisation of the carbon backbone via a metal-acid bifunctional mechanism. For MIBK hydrogenation, the mechanism involves MIBK hydrogenation to MP-ol on metal sites followed by MP-ol dehydration on acid sites to form olefin and finally olefin hydrogenation to 2MP on metal sites. Pt/ZSM-5 matched the catalytic performance of Pt/CsPW at 200 °C, but considerable isomerisation of MP took place at this temperature. This shows that the strong acidity of CsPW is essential for the high efficiency of the Pt/CsPW catalyst.

Publications

Published papers

1- Mshari A. Alotaibi, Elena F. Kozhevnikova, Ivan V. Kozhevnikov, Efficient hydrodeoxygenation of biomass-derived ketones over bifunctional Pt-polyoxometalate catalyst, Chem. Comm. 48 (2012) 7194.

2- Mshari A. Alotaibi, Elena F. Kozhevnikova, Ivan V. Kozhevnikov, Hydrogenation of methyl isobutyl ketone over bifunctional Pt-zeolite catalyst, J. Catal. 293 (2012) 141.

3- Mshari A. Alotaibi, Elena F. Kozhevnikova, Ivan V. Kozhevnikov, Deoxygenation of propionic acid on heteropoly acid and bifunctional metal-loaded heteropoly acid catalysts: Reaction pathways and turnover rates, Appl. Catal. A 247-248 (2012) 32.

Oral Presentations

1- Mshari A. Alotaibi, Elena F. Kozhevnikova, Ivan V. Kozhevnikov, Gas phase deoxygenation and hydrogenation of propionic acid on heteropoly acid catalysts, 15th International Congress on Catalysis, Munich, Germany, July 2012.

2- Mshari A. Alotaibi, Elena F. Kozhevnikova, Ivan V. Kozhevnikov, Deoxygenation of biomass-derived Molecules over Multifunctional Polyoxometalate catalysts in the Gas Phase , IX International Conference, St. Petersburg, Russia, October 2012.

Poster presentations

1- Mshari A. Alotaibi, Elena F. Kozhevnikova, Ivan V. Kozhevnikov, Poster Day, University of Liverpool, March 2011.

2- Mshari A. Alotaibi, Elena F. Kozhevnikova, Ivan V. Kozhevnikov, 5th SIC2011 Conference, Coventry, UK, June 2011.

3- Mshari A. Alotaibi, Elena F. Kozhevnikova, Ivan V. Kozhevnikov, EuropaCat X Congress, Glasgow, UK, August 2011.

4- Mshari A. Alotaibi, Elena F. Kozhevnikova, Ivan V. Kozhevnikov, IchemE meeting, Oxford, UK, September 2011.

5- Mshari A. Alotaibi, Elena F. Kozhevnikova, Ivan V. Kozhevnikov, Open Day, University of Liverpool, November 2011.

6- Mshari A. Alotaibi, Elena F. Kozhevnikova, Ivan V. Kozhevnikov, 15th International Congress on Catalysis, Munich, Germany, July 2012.

7- Mshari A. Alotaibi, Elena F. Kozhevnikova, Ivan V. Kozhevnikov, 3rd NORSC meeting, York, UK, October 2012.

Acknowledgements

I would like to express my sincere thanks to my supervisor, Prof. Ivan V. Kozhevnikov, for his kind support and guidance during my study. He always gave me sound advice that helped me to achieve my aims. By benefiting from his experience, I learned many fundamental skills and acquired much invaluable knowledge of catalysis.

Many thanks are due to Dr. Elena F. Kozhevnikova for her kind assistance in conducting experiments throughout my laboratory work. I appreciate the value of her work in our group to solve the technical issues.

I would also like to thank all members of the technical support team in the Chemistry Department, especially James Mulvihill, Charles Clavering, Gordon Bostock, Paul Fargin and Richard Dewson.

Thanks are due to Dr. Jennifer Nicholls for the XRD analysis of catalysts and to Prof. Gordon Tatlock and Dr. Robert Hetterley for TEM and STEM-EDX measurements.

Let me also extend my thanks to past and present members of my group: Ali Alsalme, Abdullah Alhanash, Sarah Frodsham, Mike Craven, Hossein Bayahia and Rana Yahya.

Endless thanks and love go out my parents for their support and encouragement. I also wish to gratefully thank my brothers and sisters for all of the things that they have done for me to help me achieve my goals.

Special thanks to my wife and my children for standing by me during my life and my study. Without their help I could not have completed my work successfully.

Finally, the scholarship from Salman Bin Abdulaziz University is gratefully acknowledged. I also appreciate the financial management of the Saudi Arabia Cultural Bureau in the UK.

List of abbreviations

BET	Brunauer-Emett-Teller
CsPW	Caesium salt ($Cs_{2.5}$) of phosphotungstic acid ($H_3PW_{12}O_{40}$)
DIBK	Diisobutyl ketone
DMH	Dimethyl heptane
DMH-ol	Dimethyl heptanol
DSC	Differential Scanning Calorimetry
DTG	Derivative Thermogravimetry
DRIFT	Diffuse Reflectance Infrared Fourier Transform spectroscopy
FTIR	Fourier Transform Infrared spectroscopy
GC	Gas Chromatography
HPA	Heteropoly Acid
HPW	$H_3PW_{12}O_{40}$
ICP	Inductively Coupled Plasma atomic emission spectroscopy
MIBK	Methyl isobutyl ketone
MP	Methyl pentane
MP-ol	Methyl pentanol
MS	Mass Spectroscopy
POM	Polyoxometalate
TCD	Thermal Conductivity Detector
TGA	Thermogravimetric Analysis
TOF	Turnover Frequency
TPR	Temperature Programmed Reduction
XRD	X-ray Diffraction

Content

1. Introduction

1.1 Heterogeneous catalysis

A catalyst is a material that facilitates a chemical reaction and makes the reaction go faster without itself undergoing chemical change during the process. It can in most cases release a different reaction pathway [1]. Catalysis is the change in the reaction rate caused by the catalyst. Commercially, more than 90% of industrial chemical processes, producing building materials, medicines and food, for example, are catalysed; therefore, catalysis is very important economically [2, 3]. Heterogeneous catalysis, where the catalyst and reactant are in different phases, has been extensively utilised in oil refining and bulk chemical production. This largely involves the application of solid heterogeneous catalysts in the vapour phase system [4]. Industrially, heterogeneous catalysis has the advantages of ease of treatment, recycling and product separation. Conversely, the main drawbacks of homogeneous catalysis are the difficulty and cost of product separation [4, 5]. Historically, the use of heterogeneous catalysis can be traced back to the early 19^{th} century, when an oxidation reaction over platinum was one of the first heterogeneous catalysis reactions discovered by Faraday [6, 7]. Table 1.1 shows selective examples of major industrial processes using heterogeneous catalysis [1].

Table 1.1 Examples of major industrial processes using heterogeneous catalysis [1]

Process	**Catalyst**	**Reactants**	**Product**	**End usage**
Haber-Bosch NH_3 synthesis	Magnetite (Fe)	H_2, N_2	NH_3	Fertilizer, gunpowder, explosives
Methanol synthesis	$Cu/ZnO/Al_2O_3$	CO, CO_2, H_2	CH_3OH	Bulk chemicals, fuel
Fischer-Tropsch	Co, Fe	Coal, natural gas	C_5-C_{11} hydrocarbons	Automotive fuel
Cracking	Zeolites	Long alkanes, C_{12+}	C_7-C_9 alkanes	Fuel, detergents
Alkylation	Zeolites, clays, silicates	C_3-C_5 alkanes	C_7-C_9 isoalkanes	High-octane fuel
Dehydrogenation/ reforming	Pt/ Al_2O_3	Alkanes	Alkenes	Polymers, bulk chemicals
Hydrodesulphurisation	Co/Mo sulphides	Diesel fuel	Sulphur-free diesel	Automotive fuel
Hydrocracking	Pt on zeolites or aluminosilicates	Aromatic mixtures	Saturated hydrocarbons	Automotive/ aviation fuel
Isomerisation	H-ZSM-5 zeolites	Xylenes, toluene	p-Xylene	Polymers, bulk chemicals
Polymerisation	Ti, Ziegler-Natta	Ethane	Polyethylene	Polymers, bulk chemicals
Oxidation	Vanadium oxide	Xylenes	Phthalic acid	Polymers

The principle of heterogeneous catalytic reactions can be represented by the simple example in Figure 1.1, according to the following steps [3]:

1- Substrate molecules diffuse through the gas phase to the surface of the catalyst.

2- The molecular form of the substrate is adsorbed upon the surface.

3- The molecules (depending on the strength of their bonds) may dissociate into atoms.

4- The dissociated molecules react together on the surface to form adsorbed product. This is often recognised as the rate-determining step in a catalytic reaction.

5- Finally, the adsorbed product desorbs from the surface into the gas phase.

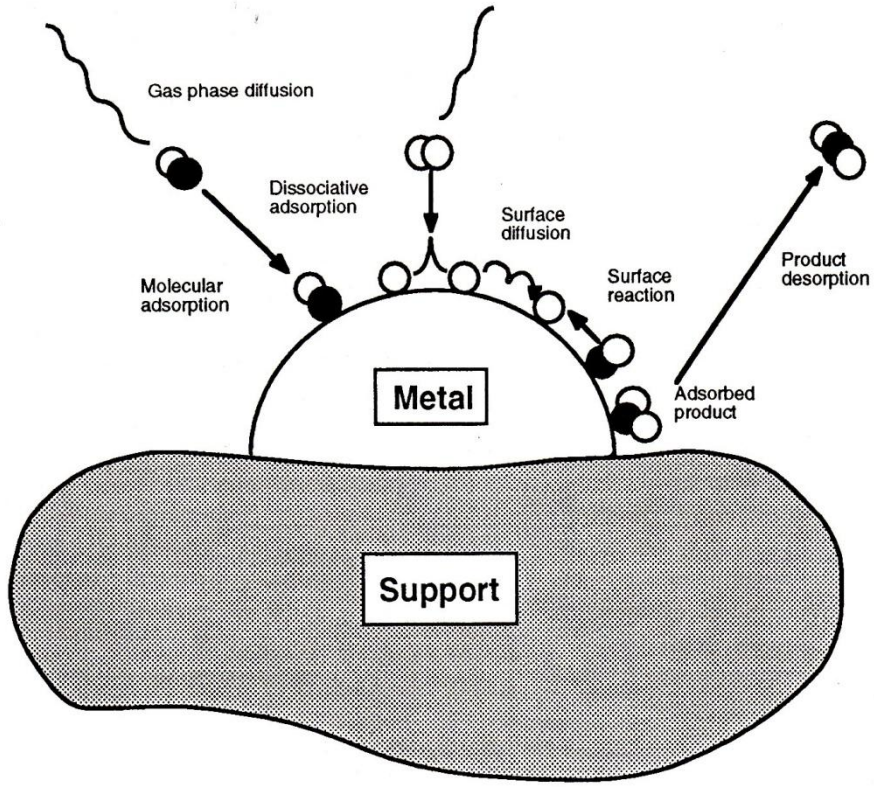

Figure 1.1 Molecular and atomic processes during heterogeneous catalysis [3]

To design, develop or choose the appropriate catalyst for any particular catalytic reaction, a number of factors must be taken into account [3, 8]. First of all, the active phase of the catalyst is fundamental to its preparation and to determining that the catalyst has the right kinetic reaction parameters, represented as high yield per unit time. The second factor is its surface area. In most cases, to produce an optimised yield, the catalyst should have a high surface area. However, some reactions need a moderate surface area to prevent an undesirable reaction with an intermediate material. Thirdly,

the longevity and strength of the catalyst are both very important. Resistance to any critical changes in the reaction bed may depend on the catalyst's strength, while there are industrial benefits from its longevity. The fourth factor is the stability of the catalyst during the reaction, as it has been found that almost all catalysts undergo deactivation with time of reaction. This can most commonly be attributed to three factors: 1) coke formation on some catalysts through the reaction of hydrocarbon compounds; 2) poisoning, which can reduce active sites on the catalyst and which may arise from reactions with impurities in industrial feedstocks; 3) sintering of a deposited metal, which reduces the surface area and the influence of the metal. The fifth factor to be considered in choosing a catalyst is that its shape will significantly affect its strength and stability. The external morphological characteristics of a catalyst must be appropriate for the catalytic process. Next, the catalyst must be environmentally friendly, minimising toxic by-products of the reaction, while the catalyst itself must not release toxic material into the environment. Regenerable and recyclable catalysts are highly desirable environmentally. In addition to these factors, the combined cost of the catalyst and the process must be lower than the selling price of the product.

1.2 Multifunctional catalysis

The need for sustainable catalysis in terms of economic and environmental feasibility has driven the development of catalyst synthesis and catalytic processes. In order to reduce waste, energy consumption, intermediate isolation steps and cost, tandem (cascade, domino) catalysis processes have been developed, introducing environmentally friendly technologies with high selectivity for desirable products and

high reactant conversion [9, 10]. As can be seen in Figure 1.2, for step-by-step processes, intermediates must be separated and sometimes purified after each step with a large amount of waste (solid arrows), making these operations costly and time consuming. On the other hand, tandem processes (broken arrows), such as those occurring in the cells of living organisms, can overcome most of these disadvantages of traditional step-by-step catalysis [11].

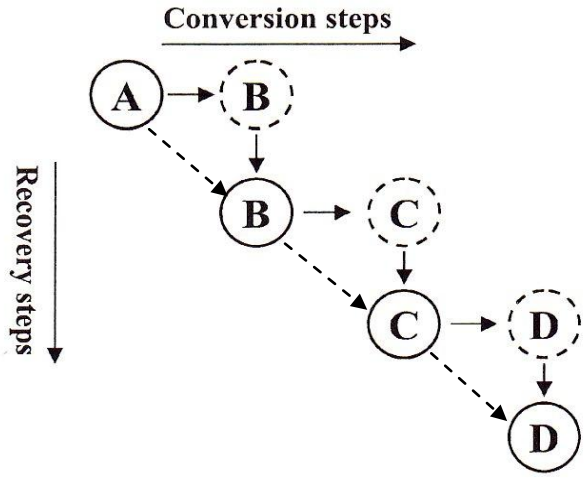

Figure 1.2 Recovery step after each conversion step in a traditional multistep organic reaction [11]. Broken arrows represent a tandem process to produce the final product without intermediate separation.

Utilisation of one-pot reactions to produce the final product without intermediate isolation is an attractive alternative process to traditional organic reactions. This type of process, as seen in Figure 1.3, can overcome thermodynamic limitations for highly energetic intermediate compounds by balancing equilibrium-limited endothermic steps with exothermic steps to produce the target product [11, 12].

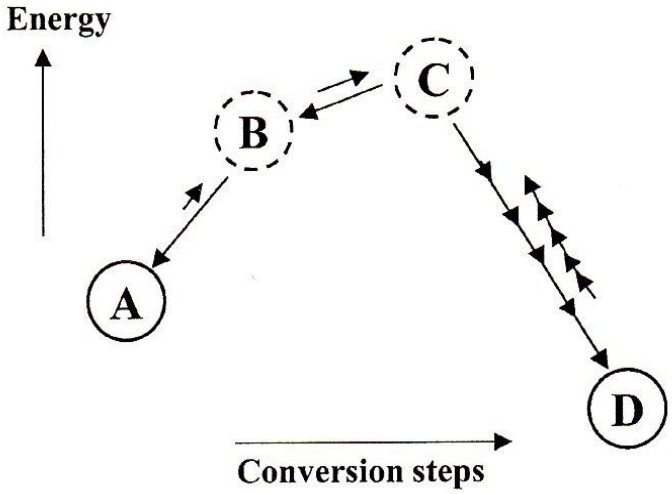

Figure 1.3 Potential energy of tandem process to overcome thermodynamic barriers in multistep synthesis [11]

One of the important steps in creating a tandem process is designing a multifunctional catalyst, which can be defined as having two or more active sites. These work simultaneously to catalyse a multistep sequential reaction in a one-pot system. Thus, multifunctional catalysis is considered important for the future development of sustainable catalytic processes in organic petrochemical manufactures [11, 13].

Multifunctional catalysts have been widely utilised in the production of organic compounds by tandem catalysis. In the most common cases, these catalysts contain one or two transition metals on acidic and/or basic sites as support. The major issue in their preparation is that these active sites must be precisely tuned to suit the reaction system and work synergistically [11-13].

Extensive heterogeneous catalysis research using multifunctional catalysts has concentrated on improving catalysts comprising transition metals on an active support having acidic and/or basic sites for multistage reactions. For instance, in early studies,

Pt supported multifunctional catalysts were found to be efficient in the isomerisation of paraffins, hydroisomerisation of naphthenes and hydrocracking of paraffins [14-17]. Furthermore, the one-pot synthesis of methyl isobutyl ketone (MIBK) from acetone has been widely investigated over multifunctional catalysts. The process involves acid-catalysed formation of diacetone alcohol (DA), which is then dehydrated to mesityl oxide (MO), followed by hydrogenation of MO to MIBK on metal function, as shown in Scheme 1.1.

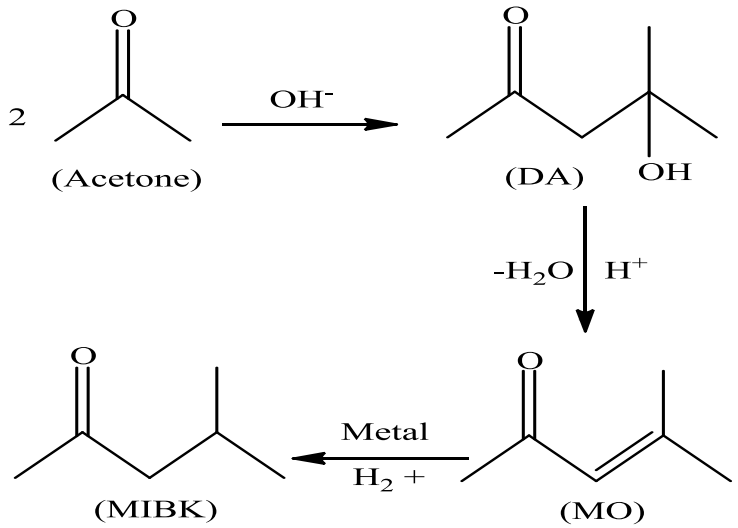

Scheme 1.1 One-pot synthesis of MIBK from acetone over multifunctional catalysts

1.3 Heteropoly acids

1.3.1 Introduction to heteropoly acids

Heteropoly acids (HPAs) comprise polyoxometalate anions which have metal-oxygen clusters in their structure [18]. Heteropolyanions have the general chemical formula $[X_xM_mO_y]^{q-}$ ($x \leq m$), where X is the heteroatom, which is also known as the central

atom if it is located in the centre of the polyanion, and M is the addenda atom, while x, m and y are the number of atoms X, M and O respectively. Typical heteroatoms are P^{5+}, As^{5+}, Si^{4+}, Ge^{4+} and B^{3+}. In most cases, Mo (VI) and W (VI) are used as addenda atoms because of a favourable combination of ionic radius and charge, as well as accessibility of empty *d* orbitals for metal-oxygen π bonding. On the other hand, less frequently utilised addenda atoms are V (V) or Nb (V), or mixed elements of these atoms [18, 19].

Heteropolyanions synthesise by a self-assembly process in an aqueous solution, as represented in equation 1.1 [20]:

$$12WO_4^{2-} + HPO_4^{2-} + 23H^+ \longrightarrow PW_{12}O_{40}^{3-} + 12H_2O \qquad (1.1)$$

Berzelius was the first scientist to discover a heteropoly compound, in 1826. Since then, many studies have been reported regarding the synthesis of heteropoly compounds and many attempts have been made to explain their structure [19]. Among the various types of HPA compounds, the Keggin structure is an important milestone because of its thermal stability and availability [19, 20]. Other HPA derivatives are the Wells-Dawson, Anderson-Evans and Dexter-Silverton structures [19].

Heteropoly compounds have found numerous applications as catalysts, offering significant economic and environmental benefits [19-21] related to their unique structural mobility and multifunctionality. Research into these compounds is a rapidly growing field: in 1996 alone, more than 600 publications and 120 patents were identified as being concerned with HPA chemistry and technology, mainly related to catalysis [19, 22].

In general, heteropoly acids and their salts in the solid state are ionic crystals [19, 23]. Structurally, the heteropoly anion itself is denoted a primary structure, which

can be found in solution, while as a solid material, it consists of large polyanions, cations, water molecules and other molecules, which are called secondary structures. In addition, the tertiary structure of HPAs in the solid state has been found to have a more influential function in catalytic reactions. The assembly of its primary and secondary particles, its pore structure and the distribution of protons and cations are vital features of these structures, as shown in Figure 1.4 [20].

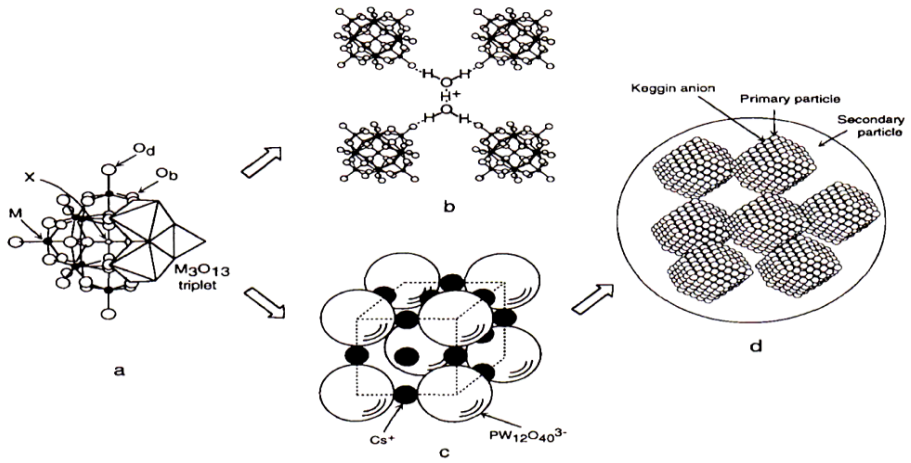

Figure 1.4 Primary, secondary, and tertiary structures of heteropoly compounds: (a) primary structure (Keggin structure, $XM_{12}O_{40}$); (b) secondary structure ($H_3PW_{12}O_{40}{\cdot}6H_2O$); (c) secondary structure ($Cs_3PW_{12}O_{40}$ unit cell); (d) tertiary structure of bulk $Cs_{2.5}H_{0.5}PW_{12}O_{40}$

1.3.2 The Keggin structure

The Keggin structure, which was discovered in 1933, was the first recognised type of HPA. It is representative of the majority of these compounds and is the most popular in catalysis. The preference for this type comes from its availability and thermal stability. For these reasons, the most widely utilised Keggin HPA compounds, such as

$H_3PW_{12}O_{40}$, $H_3PMo_{12}O_{40}$, $H_4SiW_{12}O_{40}$ and $H_4SiMo_{12}O_{40}$, are typically available commercially. The chemical formula of Keggin heteropolyanions can be shown as $[XM_{12}O_{40}]^{x-8}$, where X is the heteroatom, x is its oxidation state and M is the addenda atom (usually W^{6+} or Mo^{6+}) [19, 20].

In terms of its composition, the Keggin anion has a diameter of 12 Å and consists of a central XO_4 tetrahedron surrounded by twelve edge and corner sharing MO_6 octahedra, arranged in four groups of three edge sharing M_3O_{13} which are linked with the central XO_4 tetrahedron, as can be seen in Figure 1.5 [19].

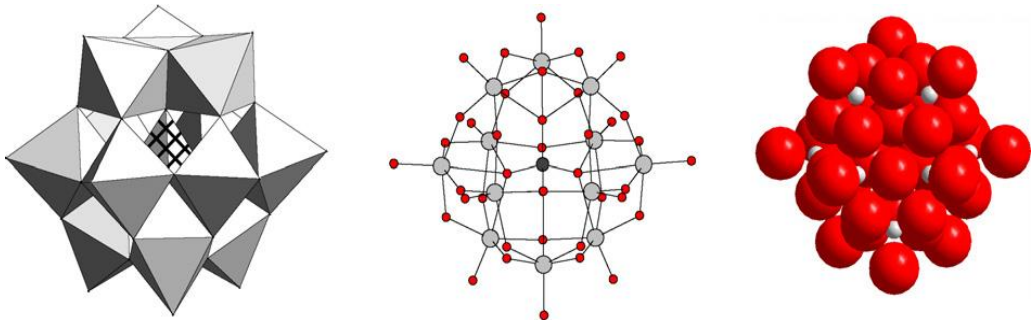

Fig. 1.5 The structure of the Keggin heteropolyanion $[\alpha\text{-}XM_{12}O_{40}]^{n-}$ in polyhedral (left), ball-and-stick (centre) and space-filling (right) representations

Four types of oxygen atom can be discriminated in the Keggin structure: terminal M=O, M-O-M edge-bridge shared within M_3O_{13} group, M-O-M corner-bridge connecting two different M_3O_{13} and internal X-O-M. These oxygen types can be clearly distinguished by ^{17}O NMR as well as fingerprint spectra by Fourier transform infrared spectroscopy (FTIR) in the range of 600-1100 cm^{-1} [19, 20, 24].

1.3.3 Thermal stability of HPAs

Since the composition stability of HPAs in aqueous media is strongly dependent on the pH of the solution, the thermal stability of solid HPAs is very important to their use in heterogeneous catalysis [19, 20]. Some HPA compounds are satisfactorily stable and applicable at relatively high temperatures, up to 300-350 °C. However, regarding the regeneration temperature of HPAs, e.g. in the decoking process, there is a crucial issue of their low thermal stability. Practically, thermal stability is measured by thermogravimetric analysis (TGA), DTA, differential scanning calorimetry (DSC), X-ray diffraction (XRD), infrared spectroscopy (IR) and solid state NMR. Generally, the Keggin structure is the most thermally stable of HPA structures. This stability can be measured in terms of thermal decomposition temperature, defined as the temperature at which all acidic protons are lost, as presented in Scheme 1.2 [18, 19, 25].

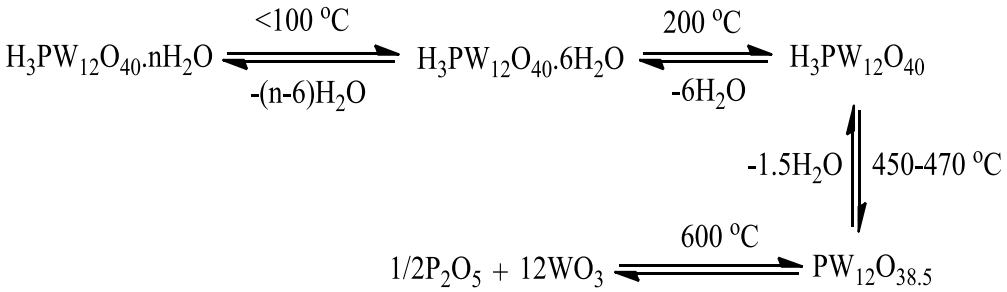

$H_3PW_{12}O_{40}.nH_2O \rightleftharpoons H_3PW_{12}O_{40}.6H_2O \rightleftharpoons H_3PW_{12}O_{40}$

$H_3PW_{12}O_{40} \rightleftharpoons 1/2P_2O_5 + 12WO_3 \rightleftharpoons PW_{12}O_{38.5}$

Scheme 1.2 Thermal decomposition of $H_3PW_{12}O_{40}$ hydrate [25]

The decomposition temperature of the most commonly utilised Keggin HPA compounds, as estimated by the TGA technique, decreases in the following order [19, 25, 26]:

$H_3PW_{12}O_{40}$ > $H_4SiW_{12}O_{40}$ > $H_3PMo_{12}O_{40}$ > $H_4SiMo_{12}O_{40}$.
(465 °C) (445 °C) (375 °C) (350 °C)

It is obvious that $H_3PW_{12}O_{40}$ has the highest thermal stability among the Keggin type of HPAs. However, the onset of thermal decomposition of solid HPAs actually occurs at temperatures lower than those measured by TGA [19].

Heteropoly salts are more stable than their parent acids, although their stability depends on the countercation. Cs and K salts are stable around their melting points, while ammonium salt has a lower thermal stability than those mentioned above, but higher than the hydrogen form of its parent acid [26]. For example, $Cs_{2.5}H_{0.5}PW_{12}O_{40}$, the highest acidic salt, starts to decompose noticeably at 500 °C, which means that it has better thermal stability than $H_3PW_{12}O_{40}$ [27].

1.3.4 Redox properties of HPAs

The redox chemistry of HPAs has been central to much research and has found various catalytic applications. Characteristically, it can be estimated by various methods such as rates of reduction of HPAs and from the ESR and XPS spectra of reduced HPAs [19, 26]. The results obtained by these methods are significantly affected by the purity of the samples and the method of reduction, while the redox properties can be controlled by changing factors such as the heat of oxide formation, ionic potential and electronegativity [20, 26].

In MO_6 octahedra in Keggin-type HPAs, which as explained above have one terminal oxygen atom M=O per addenda atom, the lowest unoccupied molecular orbital (LUMO) is a nonbonding metal-centred orbital. As a result, Keggin-type HPAs are easily reduced, most often to form mixed-valence species which then retain the structure of the parent oxidised anions [19]. This may explain the importance of Keggin HPAs in oxidation reactions.

The oxidation potential of HPAs depends strongly on their addenda atoms and less on their heteroatoms. Their oxidation potentials are thus in the following order of addenda atoms [18, 19, 24]:

$$V\ (V) > Mo\ (VI) >> W\ (VI)$$

From the first aspect of redox properties, the reduction by hydrogen molecules of Keggin HPAs ($H_3PM_{12}O_{40}$) where M = W or Mo undergoes three steps:

$$\underset{\text{I}}{x H_2 + PM_{12}O_{40}^{3-}\ (\text{surface})} \rightleftharpoons \underset{\text{II}}{2xH^+\ (\text{bulk}) + PM_{12}O_{40}^{(3+2x)-}\ (\text{bulk})} \qquad (1)$$

$$\underset{\text{II}}{2xH^+\ (\text{bulk}) + PM_{12}O_{40}^{(3+2x)-}\ (\text{bulk})} \longrightarrow \underset{\text{III}}{PM_{12}O_{40-x}^{3-}\ (\text{bulk}) + xH_2O\ (\text{bulk})} \qquad (2)$$

$$xH_2O\ (\text{bulk}) \longrightarrow xH_2O\ (\text{gas}) \qquad (3)$$

In the first step, $2xH^+$ are present between polyanions and $2xe^-$ are present in the polyanion without producing water. In this case, the number of electrons formed per anion is variable and depends on the addenda atom. In the second step, the protons formed react with the oxygen of the polyanion to produce water, which then evolves into the gas phase in the last step [26].

Keggin HPAs in the solid state have very fast diffusion of protons and electrons (redox carriers), as proven by the rates of reduction, since the isotopic equilibration of H_2-D_2 in the gas phase and in the entire solid phase is very rapid at 300 °C. This has been emphasised by electronic conductivity at 200-250 °C, since the measurement depended strongly on the composition of HPAs and on thermal treatment. On the other hand, a kinetic study has shown that step (1) is very rapid, while step (2) is slow. Depending on the addenda atoms, in step (1), the equilibrium favours the backward

reaction with $H_3PW_{12}O_{40}$. By contrast, $H_3PMo_{12}O_{40}$ favours the forward reaction [26, 28].

From the second aspect of redox properties, the reoxidation of HPAs is fast and reversible when the extent of reduction is low. For example, in the case of $H_3PMo_{12}O_{40}$, regarding the equations of the three steps mentioned above, the redox route from I to II is very fast and reversible, while from II to III it is very fast near the surface and slow in the bulk and both are reversible. On the other hand, the redox cycle from I to III' (excessively reduced species) is slow and often irreversible [20, 26].

There is strong interest in the modification of the redox properties of HPAs, especially for industrial use as oxidation catalysts, by varying the addenda atoms. Nevertheless, the redox mechanism has not yet been clarified. For instance, substitution of Mo in $H_3PMo_{12}O_{40}$ by V results in a decreased rate of reduction by hydrogen and makes it less reversible than $H_3PMo_{12}O_{40}$ [26]. It has been reported that the activity of Keggin HPAs in their reduction by hydrogen molecules using temperature-programmed reduction (TPR) increases in the order: $H_3PW_{12}O_{40} \approx H_3SiW_{12}O_{40} < H_3PMo_2W_{10}O_{40} < H_3PMo_6W_6O_{40} \approx H_3PMo_{12}O_{40} \leq H_4SiMo_{12}O_{40} \approx H_5PMo_{10}V_2O_{40}$ [19, 29].

1.3.5 Acidity of HPAs

Heteropoly acids are known as strong Brønsted acids [19, 20, 24], being stronger than conventional solid acids such as SiO_2-Al_2O_3, H_3PO_4/SiO_2 and HX and HY zeolites [26]. The acidity of Keggin-type HPAs in solution and in the solid state has been extensively reported [18-20, 30]. The proton sites of HPAs are a very important characteristic which dominates their activity. Regarding the acidity of HPAs, six types of acidic sites are present in these catalysts [19, 20, 26]:

1. Proton sites in the HPA itself, such as $H_3PW_{12}O_{40}$.
2. Proton sites in its acidic salts, such as $Cs_{2.5}H_{0.5}PW_{12}O_{40}$.
3. Lewis acid sites in salts (metal countercations, e.g. in $La^{III}[PMo_{12}O_{40}]$).
4. Proton sites formed by the reduction of salts:

$$Pd_2[SiW_{12}O_{40}] + 4\,[H] \longrightarrow 2\,Pd^0 + H_4[SiW_{12}O_{40}]$$

5. Proton sites generated by partial hydrolysis of polyanions:

$$[PW_{12}O_{40}]^{3-} + 2\,H_2O \longrightarrow [PW_{11}O_{39}]^{7-} + [WO_3] + 4\,H^+$$

6. Proton sites generated by dissociation of coordinated water:

$$Ln(H_2O)_n^{3+} \longrightarrow Ln(H_2O)_n(OH)^{2+} + H^+$$

1.3.5.1 Proton structure

The proton structure is essential to understanding the activity of HPAs and how their crystal structure is produced by connecting the neighbouring heteropoly anions [18]. Two kinds of protons have been found in solid state HPAs, as represented in Figure 1.6: hydrated protons (a) and non-hydrated protons (b) [18, 19]. The former are highly mobile and thus responsible for the extremely high proton conductivity of crystalline HPA hydrates, whereas non-hydrated protons are much less mobile and are assumed to remain on the oxygen atoms surrounding the polyanion [18, 19].

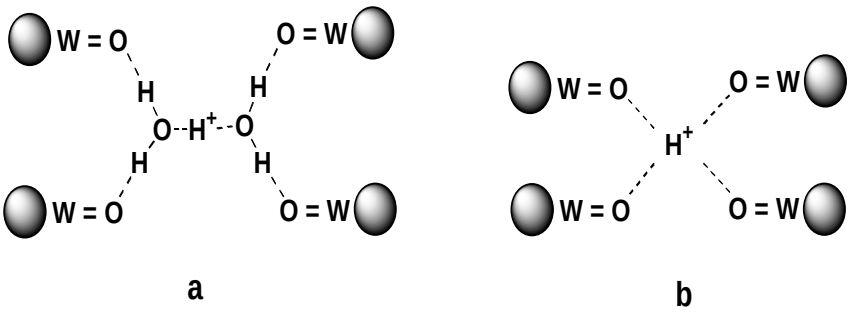

Figure 1.6 Schematic structures of (a) bulk proton sites in $H_3PW_{12}O_{40}.6H_2O$ and (b) anhydrous $H_3PW_{12}O_{40}$ [19].

The surface proton sites in solid HPAs are stronger than the bulk sites and are therefore very important for heterogeneous acid catalysis. Generally, crystalline HPAs have low surface area (1-5 $m^2\ g^{-1}$) and low porosity (<0.1 $cm^3\ g^{-1}$) [18-20, 26, 31]. The protons are localised on the bridging oxygen atoms in the surface of heteropoly anions when HPAs are supported on inert porous materials such as silica to improve their porosity and exposed surface area [18].

1.3.5.2 Acidity of solid HPAs

Solid HPAs form ionic crystals consisting of heteropoly anions, variable hydrated protons (H^+, H_3O^+, $H_5O_2^+$) and crystallisation water. This crystal structure depends on the amount of crystallisation water. Heat treatment reduces the amount of water, thereby reducing the number of acid sites and increasing their strength [19]. Thus, the strength and number of acid sites on solid HPAs can be controlled by adjusting their composition [20].

Thermal desorption of basic molecules such as pyridine and ammonia determines the acid properties of solid acids. The acid strengths of HPAs and SiO_2/Al_2O_3 have been compared by adsorption of pyridine [20]. The pyridine

molecules on SiO_2/Al_2O_3 are desorbed completely at 300 °C, while they remain adsorbed in $H_3PW_{12}O_{40}$ at the same temperature, indicating that $H_3PW_{12}O_{40}$ is a very strong acid.

Using temperature-programmed desorption (TPD) of ammonia, Izumi *et al.* [32] found that the order of acid strength of HPAs in terms of the temperature of ammonia desorption was as follows:

$$H_3PW_{12}O_{40} > H_4SiW_{12}O_{40} \geq H_3PMo_{12}O_{40} > H_4SiMo_{12}O_{40}$$
$$592\ °C \qquad 532\ °C \qquad 463\ °C \qquad 423\ °C$$

The identical order of acid strength was obtained by ammonia sorption using a calorimetric technique [18, 32, 33]. In addition, the activities of HPAs are in the same order in heterogeneous and in homogeneous systems [18, 20], while values for heat of ammonia absorption further prove that HPAs are stronger than zeolites or simple oxides. For example, the initial heat of NH_3 adsorption was 195 kJ mol^{-1} for $H_3PW_{12}O_{40}$, 150 kJ mol^{-1} for HZSM-5 and 140 kJ mol^{-1} for γ-Al_2O_3 [20].

1.3.5.3 Acidity of solid HPA salts

The nature of the countercations in heteropoly salts is an important determinant of their acidity, porosity, solubility and thermal stability. For instance, salts with small cationic radius, such as Li^+ (0.68Å) and La^{3+} (1.02Å), seem to be like their parent HPAs: they are non-porous, dissolve easily in water and have low surface areas (< 10 $m^2\ g^{-1}$), whereas salts with large cationic radius, such as Cs^+ (1.67 Å) and NH_4^+ (1.43 Å), are water-tolerant, having bimodal porosity and surface areas > 100 $m^2\ g^{-1}$ [18, 19]. As these salts are usually prepared by stoichiometric precipitation from aqueous solutions, residual quantities of protons remain and are responsible for their activity [34]. The

effect of substitution of protons in Keggin HPAs by 1A, 2A and 3B group monovalent cations has been investigated in the isomerisation of 1-butene and the dehydration of alcohol [35-37].

Okuhara *et al.* [20, 33, 38] demonstrated that $Cs_{2.5}H_{0.5}PW_{12}O_{40}$ has strong acid sites and a relatively high surface area (100-200 $m^2\ g^{-1}$) , as shown in Figure 1.7, and is a very efficient solid acid catalyst as well as being water tolerant, which means that it is suitable for reactions where water is either the reaction medium or a by-product. In addition, the pore size of $Cs_xH_{3-x}PW_{12}O_{40}$ can be controlled via its caesium content [39, 40].

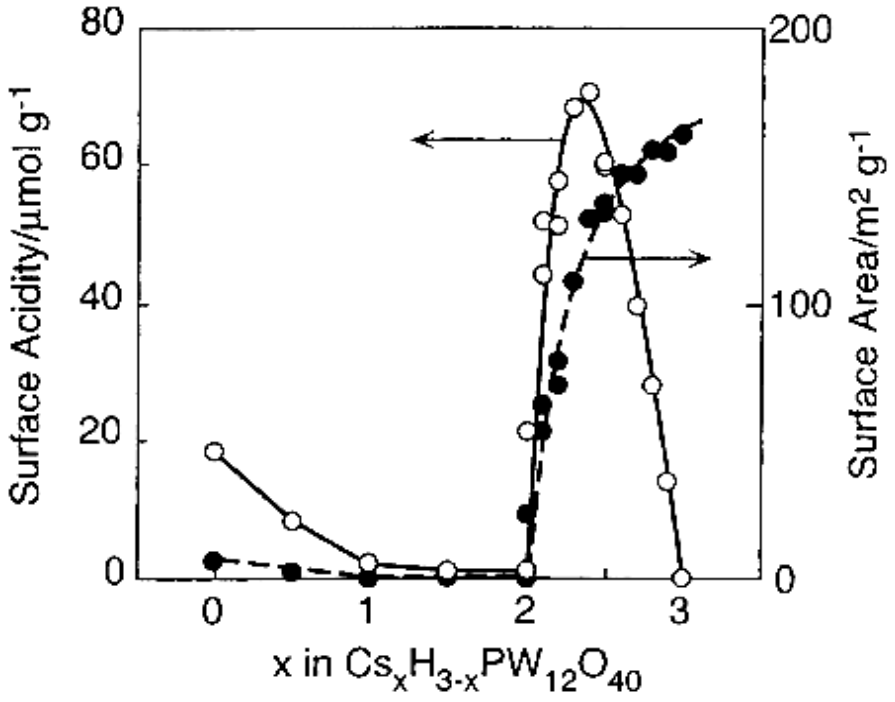

Figure 1.7 Surface acidity and surface area of $Cs_xH_{3-x}PW_{12}O_{40}$ as a function of Cs content, x [40]

1.3.5.4 Acidity of supported HPAs

Because of the low surface area of bulk HPAs, there is much interest in the loading of these solid acids on supported acidic or neutral materials such as silica, alumina, active carbon or ion-exchange resin; thus they are very important for catalytic applications [18-20, 26, 28, 31, 32, 41, 42]. The catalytic activity and acidity of supported HPAs greatly depends on the type of support, the HPA loading and the conditions of pretreatment [18, 19]. On the other hand, basic solids such as MgO are not favoured for use as supports, because they tend to decompose HPAs [19].

Silica (SiO_2) is the material most often used as a carrier of HPAs. It is relatively inert towards HPAs at certain loading percentages, although some chemical interaction takes place between them. As shown in Figure 1.8, the acidity of $H_3PW_{12}O_{40}$ decreases when it is loaded on SiO_2, as revealed by microcalorimetry of NH_3 adsorption [19]. The thermal stability of HPAs supported on silica is comparable to that of unsupported HPAs or slightly lower [18, 20, 43]. It has been found that at low $H_3PW_{12}O_{40}$ loading, 20% and less, the supported $H_3PW_{12}O_{40}$ loses more than 80% of its proton sites because of the strong interaction between $H_3PW_{12}O_{40}$ and SiO_2 [18, 32]. In contrast, molybdenum HPAs decompose at low loading due to their very strong interaction with SiO_2 but retain the Keggin structure at high loading [44, 45]. According to microcalorimetry of NH_3 adsorption, the acid strength of $H_3PW_{12}O_{40}$ supported on various carriers increases in the following order: activated carbon < α-Al_2O_3 < SiO_2 [19].

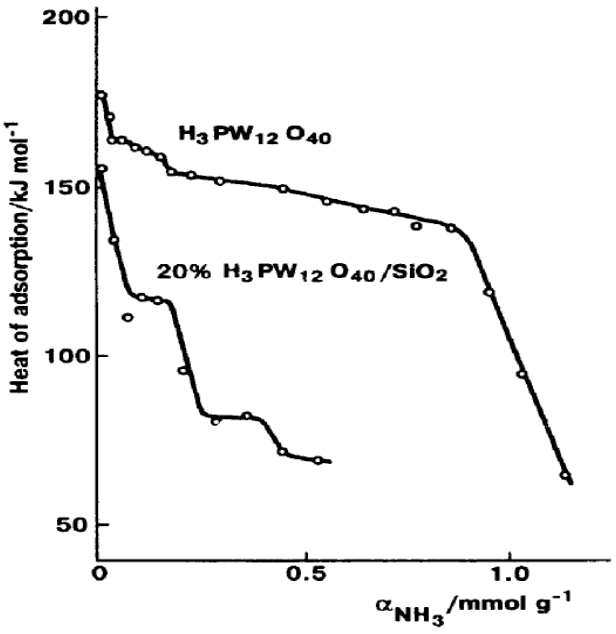

Figure 1.8 Differential heat of ammonia adsorption onto $H_3PW_{12}O_{40}$ and 20% $H_3PW_{12}O_{40}/SiO_2$ measured at 150 °C after pretreatment at 300 °C/10^{-3} mmHg [19].

1.3.6 Heterogeneous catalysis by HPAs

Heteropoly acids comprising polyoxometalates (POMs), i.e. metal-oxygen cluster anions, have found numerous applications as catalysts, offering significant economic and environmental benefits [19, 20, 31]. Nevertheless, the crucial issue of their low thermal stability limits their application in terms of reaction temperature, especially during the regeneration process of removing carbonaceous deposits (coke) from the catalyst surface [18, 19, 25].

Misono *et al.* [20, 46] demonstrated that there are three different kinds of heterogeneous catalysis by solid HPAs: surface catalysis, bulk type I (pseudoliquid catalysis) and bulk type II catalysis, as seen in Figure 1.9.

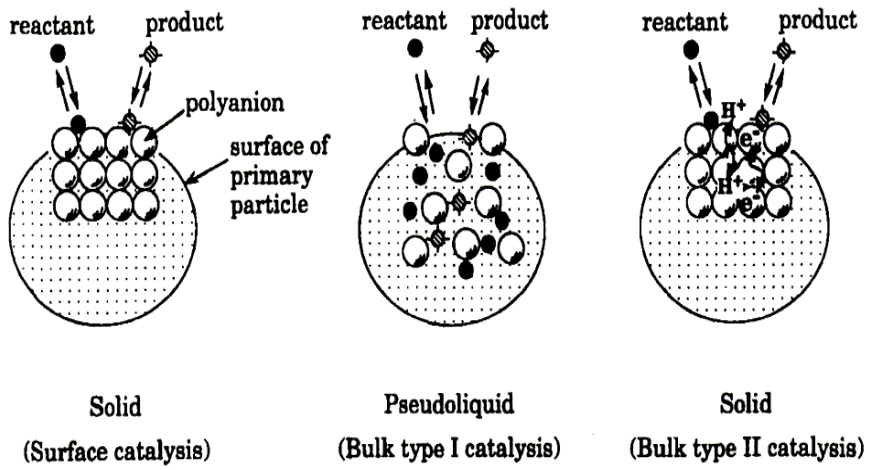

Figure 1.9 Types of heterogeneous catalysis by solid HPAs [20]

In the first case, the catalytic reaction takes place on the surface of a solid catalyst, i.e. the external surface of the catalyst and its pore walls, while bulk type I, where the reaction happens between polyanions, is found in acidic catalysis at low temperature, such as in acid forms and some salts. A typical example of catalysis type II is redox catalysis, which occurs at high temperature accompanied by the rapid migration of redox carriers (protons and electrons) onto the bulk of the solid catalyst. In addition, reaction on the surface of a solid catalyst may occur in this type [20]. Extensive examples of heterogeneous catalytic reactions by HPAs have been reviewed [19, 20, 26, 40, 47].

There are main factors dominating the acid catalysis of solid HPAs: the behaviour of the pseudo-liquid, acidity and basicity. In principle, the acidic properties are practically controlled by three factors [20]:

1. The structure and composition of heteropoly anion itself.
2. The countercation.
3. Dispersion on the support.

1.3.7 Metal doped HPAs in multifunctional catalysis

The potential of solid HPAs as multifunctional catalysts has been documented as depending on the flexibility of substitution of their texture (secondary structure). Their composition can be modified to introduce other chemical functions such as metal functionality [18-20]. However, little research has been done using HPAs as multifunctional catalysts in multistep reactions [48].

As stated above, amongst HPA compounds, $Cs_{2.5}H_{0.5}PW_{12}O_{40}$ has been found to have strong solid acidity as well as a relatively high surface area. Therefore, it has been widely utilised as an acidic carrier of chosen metals in multifunctional catalysts to process multistage reactions [40, 46]. For example, the one-pot synthesis of MIBK from acetone has been successfully investigated using palladium metal (Pd) on $Cs_{2.5}H_{0.5}PW_{12}O_{40}$ [48]. This reaction comprises three steps, as explained in section 1.2. Alhanash *et al.* [49] report that ruthenium (Ru) doped $Cs_{2.5}H_{0.5}PW_{12}O_{40}$ is a very productive multifunctional catalyst for glycerol hydrogenolysis to form propanediol.

Pd and Pt-doped solid HPAs have been employed in *n*-alkane isomerisation [27]. In addition, (-)-menthol has been formed in one step by conversion of (+)-citronellal over Pd-PW/SiO_2 [50]. This reaction occurs in two steps, the first over an acid function and the second over a metal function, as shown in Scheme 1.3.

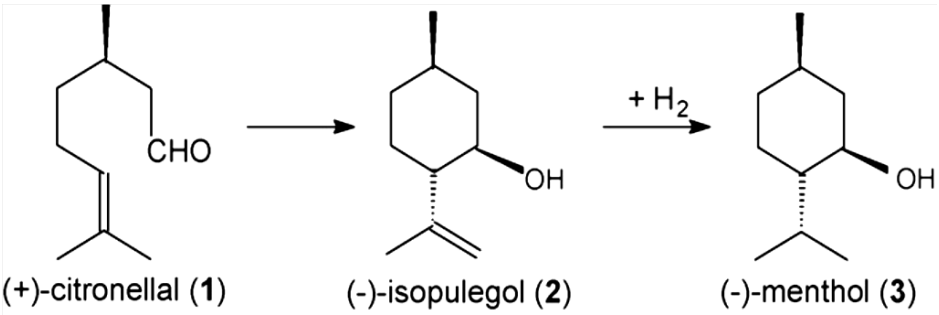

Scheme 1.3 One-pot formation of (-)-menthol from (+)-citronellal over Pd-PW/SiO_2 [50].

Regarding the deactivation and regeneration of HPAs in organic reactions, Kozhevnikov and co-workers studied the effect of doping HPAs with platinum group metals on the nature of coke formation, because it is the main reason for catalyst deactivation [51, 52]. After metal deposition only soft coke was produced and this could be burned under air at 350 °C to regenerate the HPA catalysts before their thermal decomposition (≈500 °C).

1.4 Zeolites

1.4.1 Structure and properties

Zeolites are crystalline microporous materials (pore diameter ≤ 2 nm) whose framework consists of silica and aluminium oxide tetrahedra connected by shared oxygen atoms. A negative charge arises on the aluminium oxide because of a difference of valence between Al^{3+} and Si^{4+} which is neutralised by an extra-framework cation. Generally, based on the crystallographic unit cell, the structural formula of zeolites can be represented by [53]:

$$M_{x/n}\,[(AlO_2)_x(SiO_2)_y]\,.\,wH_2O,$$

where n is the valence of cation M, w is the number of water molecules per unit cell, and x and y are the total number of tetrahedra per unit cell. The primary structural units, SiO_4 and AlO_4, link together to form a wide variety of ranges and cages called secondary building units (SBUs) [53]. A number of repeating SBUs can be connected together by oxygen atoms to build extensive networks of channels, channel junctures and cavities with molecular dimensions that characterise the structure of zeolites and result in a high surface area, which is a desirable property for catalysis [53, 54]. These well-defined pore dimensions allow zeolites to be utilised for specific applications. In addition to their pore dimensions, zeolites are classified according to their Si/Al ratio [55]. Figure 1.10 shows the most frequently encountered zeolite structures.

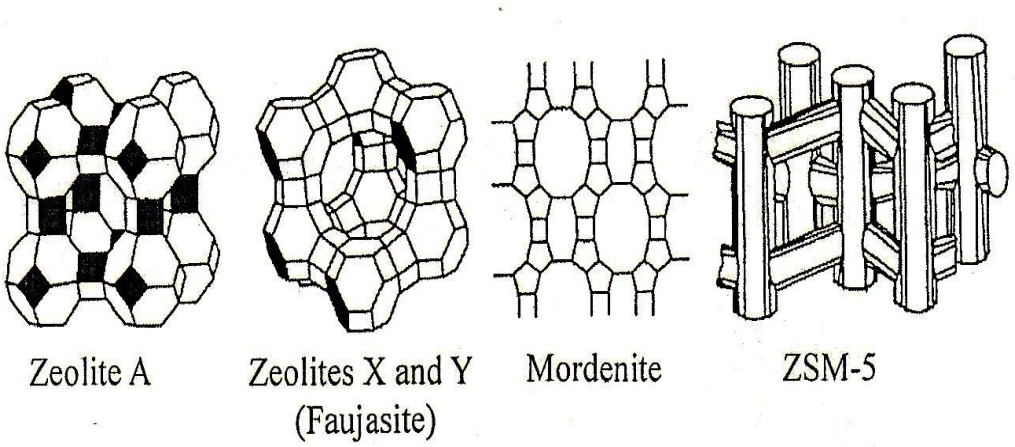

Figure 1.10 Structures of the most frequently encountered zeolites [55]

Zeolites may be classified as natural and synthetic. Natural forms are present in very large quantities, but their structures and properties are restricted, whereas zeolites can be synthesised with a wide choice of pore structures and properties [53].

Statistically, about 2.5 million metric tons of natural zeolites are consumed per year, while the consumption of synthetic zeolites is approximately 1.7-2 million metric tons per year [56].

1.4.1.1 Acidity

The acidity of zeolites is one of the most important properties in their application. The possibility of changing and controlling the acidity type and strength of zeolites has led to their widespread use in oil refining, petrochemicals and fine chemicals [55].

As can be seen in Figure 1.11 [57], synthesised zeolites are normally prepared by using Na^+ ions to neutralise framework charges. However, Na^+ ions can be readily exchanged to create Brønsted acid sites by introducing hydroxyl groups into the pore structure. These are created by the treatment of Na^+ with by either ammonium or polyvalent cations, followed by heating. Further heating removes water molecules from the proton structure and leads to the formation of Lewis sites [53, 55, 58].

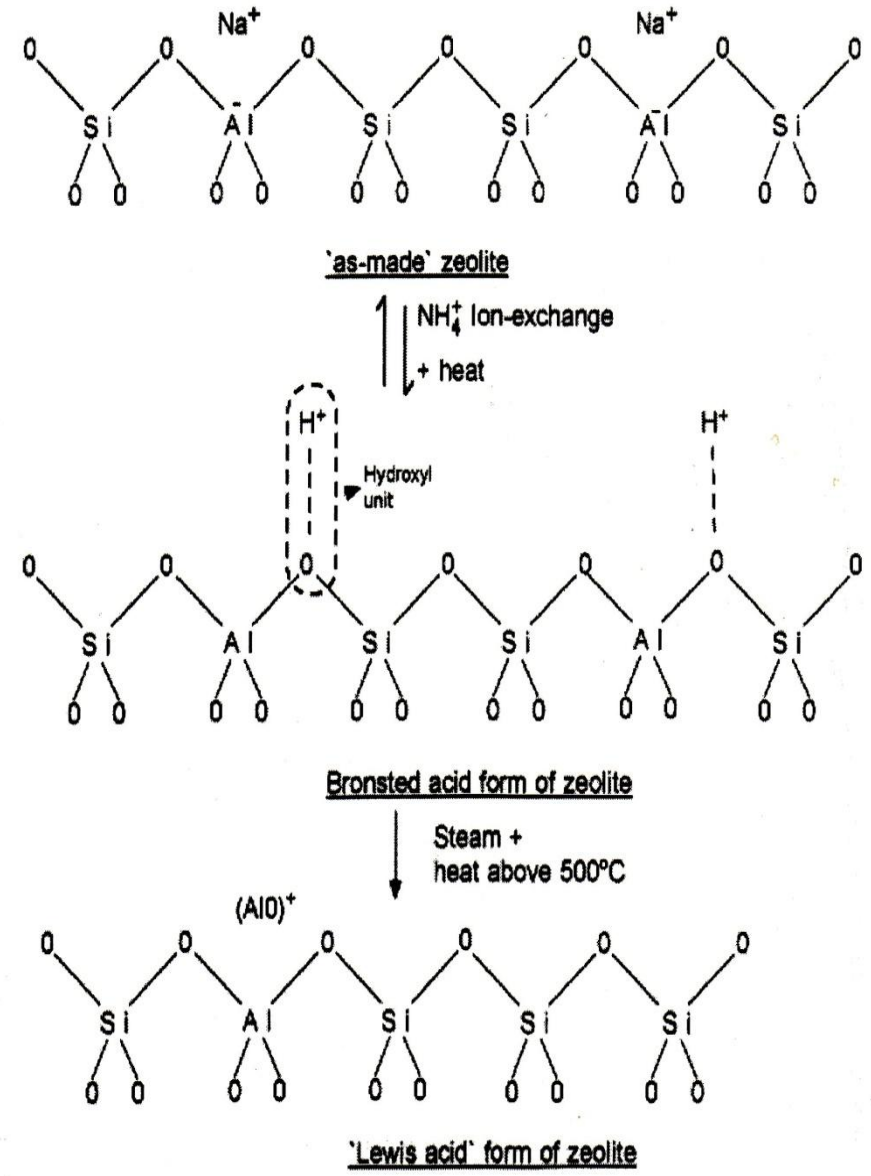

Figure 1.11 Development of internal acidity of zeolites by exchanging NH_4^+ cation [57].

In a particular catalytic reaction over zeolite, the acidity is evaluated in terms of the total numbers of Brønsted and Lewis sites, their strength distribution and their location [59]. Adsorption of basic molecules such as ammonia and pyridine is commonly used to determine the acidic properties of zeolites using experimental techniques such as TPD and FTIR. Theoretically, each acidic site is created by

exchanging one ammonium molecule into the zeolite framework. Therefore, the acidity is determined by calculating the ratio of SiO_2 to Al_2O_3 in the framework [59]. It has been found that the acid strength of zeolites with the same Si/Al ratio decreases in the following order: H-ZSM-5 > H-MOR > H-Beta > H-Y, which illustrates the effect of framework type [60-62]. It is of interest that the catalytic activities of Brønsted acid sites was found to depend on the structure and chemical composition of zeolites, specifically on the Si/Al ratio [63]. In general, increasing the Si/Al ratio increases the number of strong Brønsted sites, despite a reduction in the total number of acid sites [59, 64-67]. As aluminium atoms induce a higher degree of electron contribution than silicon, the strength of acid sites reduces when the number of neighbouring aluminium atoms increases. This results in a strong interaction between oxygen charge and proton-oxygen [68, 69]. The catalytic activity of zeolites increases when the Si/Al ratio increases [70]; that is, it depends strongly on the zeolite framework [62]. In addition, it has been proven that Brønsted sites, rather than Lewis sites, are the main source of the catalytic activity of zeolites. It is doubted whether Lewis sites play any practically important role in acid-catalysed reactions. Nevertheless, under certain conditions, they do have an indirect effect on catalytic activity by enhancing the strength of nearby Brønsted sites [71].

1.4.1.2 Shape selectivity

The particular pore sizes of zeolites make them selective for molecules which have dimensions of the same order of magnitude. The well-defined pores can discriminate reactants and/or products by their shape and/or size as the molecules differ in their diffusion through the pore structure [71, 72]. Unlike traditional acidic catalysts, zeolites

seem to be designed to admit specific reactant substrates which produce selective molecules.

The main cause of deactivation of acidic catalysts, including zeolites, is coke formation, but this can be overcome by controlling the pore structure, exploiting the property of shape selectivity in zeolites. ZSM-5, which has unique dimensions with 10 oxygen ring size pores and lacks large supercages of smaller windows size, was found to restrict the formation of coke, which is responsible for blocking zeolite pores [59, 73].

Three types of shape selectivity are distinguished, as shown schematically in Figure 1.12 [55, 59, 71]:

1. Reactant shape selectivity: Reactants with molecular dimensions corresponding to the pore size can pass through to the active sites inside the pore structure, while those of different dimensions will be hindered.
2. Product shape selectivity: Products which have certain dimensions can diffuse into the pores and leave through the channels.
3. Restricted transition state shape selectivity: In the case of a specific parallel or consecutive reaction, when its intermediate or transition states cannot be accommodated inside the zeolite pores because they need more space than is available, this reaction will be prohibited.

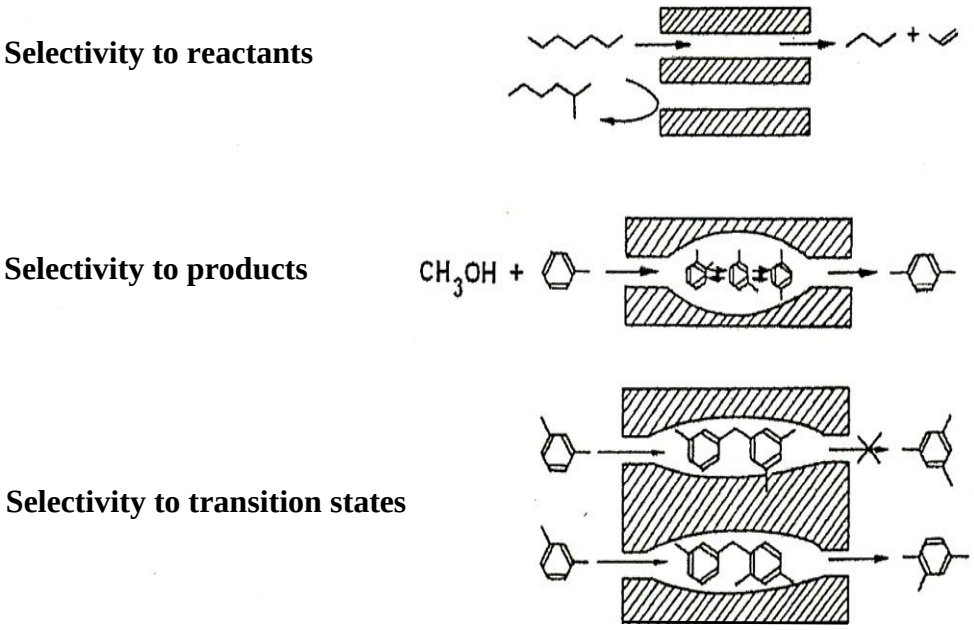

Figure 1.12 Three types of shape selectivity in zeolites [55]

1.4.2 Heterogeneous catalysis by zeolites

Zeolites show hydrophobic properties as the Si/Al ratio increases; consequently, their affinity towards reactants increases. Well defined pore structures, a wide range of acid site distributions and high thermal stability, as well as their high surface area, make them suitable for separation processes, adsorption applications and heterogeneous catalysis. Indeed, heterogeneous catalysis by zeolites is a particularly interesting field, offering economic and environmental advantages [55, 71].

More than 40% of industrial processes use zeolites as catalysts [74]. According to this survey, ZSM-5 is the most widely used zeolite type, accounting for 42% of zeolite applications. The ease of modification of their properties has drawn much attention to the application of zeolites as catalysts, but it is difficult to modify independently any one of these properties, such as acid strength, porosity or acid site density [55, 75]. Perot *et al.* [75] demonstrated that dealumination of zeolite reduced

the density of acid sites while increasing their strength, thus changing the porosity of the mesopores.

One of the best known reactions over a zeolite with strong acidic sites such as ZSM-5 is the cracking of paraffins, where the catalyst forms carbonium ions by protonation of paraffins such as n-hexane and n-butane to produce hydrogen gas, olefins and paraffins at high temperatures [55]. Isomerisation of xylene is an example of shape selectivity for *para*-isomers using modified ZSM-5 [76]. *Para*-xylene has high diffusivity through the channels of ZSM-5 compared to other isomers. Peters and co-workers [77] studied the esterification of acetic acid with butanol over a variety of zeolite catalysts, emphasising the influence of the zeolite structure and reporting that the catalytic activity in respect to this reaction increased in the order of ZSM-5 (12.5) < H-MOR (45) < H-Beta (12.5) < H-USY (20), where the Si/Al ratio is in brackets. The low activity of H-ZSM-5 resulted from internal diffusion limitations in this catalyst of medium pore size, despite similarities to H-Beta in terms of acid sites. It was found that a one-dimensional channel in H-MOR was blocked and that this caused its low activity, although the channel size of H-MOR is similar to that of H-USY, as the latter has high activity related to its framework structure.

As the mass transport limitations of reactants and/or products are critical for reaction by zeolites, the pores can be changed to mesopores by decreasing the size of zeolite crystals or by increasing the pore size to overcome diffusional limitations [78, 79]. Hartmann reports that mesoporous zeolites offer resistance to deactivation and increased activity [78]. Examples of heterogeneous catalysis reactions over an extensive range of zeolites are reported in detail [53, 56, 72, 74, 80].

1.4.3 Metal doped zeolites in multifunctional catalysis

Because of their high surface area, thermal stability and shape selectivity, zeolites are extensively utilised as acidic supports for multifunctional catalysis. However, the properties of metal-doped zeolites as catalysts depend mainly on details of the preparation method, including the type of metal precursor, the degree of calcination and reduction, and the loading of the metal. All of these factors strongly affect the dispersion of the metal over the zeolite structure, the particle size of the metal and the position of the metal. In addition, it is very important to balance the acid strength of the zeolite and the metal function to demonstrate the effect on the catalytic activity of metal-doped zeolite catalysts by controlling these factors [81].

Heterogeneous bifunctional metal-acid catalysis using zeolite doped with metal atoms (usually Pd or Pt) has received much attention for use in multistep reactions such as the one-pot synthesis of MIBK from acetone over Pt and Pd metals supported on zeolites [82-84]. As described in section 1.2, this reaction involves three steps which can be performed simultaneously over metal-doped zeolite. Another example of a multistep reaction over metal-doped zeolite is the formation of (-)-menthol from (+)-citronellal in one pot over Pt-loaded H-Beta [85]. Further examples of catalytic applications of zeolites in multistep reactions are reported [86].

1.5 Deoxygenation of biomass-derived molecules

1.5.1 Introduction

Efficient utilisation of biomass resources is a major goal for academia and industry [87, 88]. Increasing concerns over climate change and diminishing petroleum resources drive the search for sustainable, economic and eco-friendly alternative routes for chemical production from renewable sources. It has been estimated that by 2030, the proportion of transportation fuel and chemicals produced from biomass resources will be 20% and 25% respectively [89]. The use of biomass-derived phenolics, alcohols, carboxylic acids, ketones, carbon dioxide and other oxygenates can significantly reduce greenhouse gas emission, diversify energy sources and improve energy security [87-91].

Biomass can be converted to derive transportation fuels and chemicals in various ways, mainly by thermochemical and catalytic processes [88, 92, 93]. The former are non-catalytic processes that involve high temperature treatment of substrates, such as gasification, liquefaction and pyrolysis, while the latter entail the removal of most or all of the oxygen atoms from reactants using catalysts to enhance their energy intensity and stability or to reduce their viscosity. In most cases C-C bonds are coupled between intermediates to augment the molecular weight of the final product [91, 94].

1.5.2 Deoxygenation of carboxylic acids

Carboxylic acids are readily available from natural resources and are attractive as renewable raw materials for the production of value-added chemicals and biofuel

components [87, 88]. For fuel applications, carboxylic acids require the reduction of their oxygen content, i.e. deoxygenation [95]. Therefore, much recent research has focused on the deoxygenation of carboxylic acids using heterogeneous catalysis [96-102].

The thermal and catalysed decomposition of lower C_1-C_3 acids in the gas phase has been addressed in considerable detail ([103-106] and references therein). The decomposition of formic acid is straightforward due to the simplicity of this molecule. In the case of acetic and propionic acids, which are more relevant to biomass-derived higher carboxylic acids, the products are more varied, reflecting the wider variety of possible reaction pathways. Both dehydration via C-O bond cleavage and decarboxylation via C-C bond cleavage occur in the pyrolysis of C_1-C_3 carboxylic acids. Thus, propionic acid dehydrates between 496 and 580 °C to form methylketene (Equation 1.2), simultaneously decarboxylating to produce CO_2 and ethane (Equation 1.3) [99]. Further decomposition of methylketene gives CO and ethene together with other hydrocarbon products, resulting in the decarbonylation of propionic acid (Equation 1.4) [103, 106].

$$CH_3CH_2COOH \rightarrow CH_3CH{=}C{=}O + H_2O \qquad (1.2)$$

$$CH_3CH_2COOH \rightarrow C_2H_6 + CO_2 \qquad (1.3)$$

$$CH_3CH_2COOH \rightarrow C_2H_4 + CO + H_2O \qquad (1.4)$$

In the catalysed decomposition of carboxylic acids, the process depends on the catalyst. On metal surfaces, the decomposition may occur via surface carboxylate intermediates [104, 105]. Surface acetate species give ketene by dehydrogenation accompanied by C-O bond cleavage, as well as CO_2 and CH_4 by C-C bond cleavage.

On metal oxide surfaces, carboxylic acids are adsorbed both in molecular form and as carboxylates. These surface species may decompose via dehydration and/or decarboxylation, giving ketene, CO_2, CO and hydrocarbons. Principal decomposition products on metal oxide catalysts often include ketones with $2n–1$ carbon atoms, such as acetone and 3-pentanone for acetic and propionic acid respectively (Equation 1.5) [104, 107].

$$2\ CH_3CH_2COOH \rightarrow (CH_3CH_2)_2CO + CO_2 + H_2O \qquad (1.5)$$

Current studies of the catalysed deoxygenation of higher carboxylic acids have focused on liquid-phase and gas-phase processes, either in the presence of H_2 (hydrodeoxygenation) or in hydrogen-free systems [96-102, 108]. The principal concern has been to discover active catalysts that are selective towards deoxygenation and stable in the presence of CO, CO_2 and water, the inevitable by-products of carboxylic acid deoxygenation.

Gas-phase deoxygenation appears more promising, given its technological and environmental benefits. Acid deoxygenation can occur via decarboxylation and decarbonylation pathways, as illustrated above for propionic acid (Equations 1.3 and 1.4). Decarboxylation yields CO_2 and C_{n-1} alkane, whereas decarbonylation yields CO, water and C_{n-1} alkene. Both reactions are thermodynamically favourable at elevated temperatures (e.g. 300 °C) [102]. Since CO/CO_2 selectivity may be affected by the reversible water-gas shift reaction, $CO + H_2O \rightarrow CO_2 + H_2$, it cannot be used to discriminate reliably between these pathways [97, 101].

Supported Pd and Ni, among other metals, are frequently chosen as the catalysts for acid deoxygenation. Early on, $7\%Pd/SiO_2$ was found to be an efficient catalyst for

acid deoxygenation in the gas phase; for example, it decarboxylated octanoic acid to yield 97% of heptane at 330 °C in an H_2 flow [100]. Although by stoichiometry H_2 is not required for decarboxylation (Equation 1.3), the reaction does not occur under N_2 in a hydrogen-free system.

Gas-phase deoxygenation of oleic acid over 2%Pd/C at 380 °C in an H_2–N_2 flow yields a mixture of heptadecane and heptadecenes, with the alkane/alkene ratio increasing with an increase in the H_2/N_2 ratio [101].

On the other hand, the deoxygenation of carboxylic acids in liquid-phase batch systems has been demonstrated to occur under H_2 or N_2 pressure with a wide variety of supported metal catalysts [96-99, 102, 108]. Murzin and co-workers carried out extensive studies of the deoxygenation of fatty acids in liquid phase over various metals such as Pd, Pt, Ni, Ru, Rh, Os and mixtures of them, supported on oxides and active carbon [96, 102, 109-111]. Pd/C was reported to be the most efficient catalyst for the liquid-phase deoxygenation of stearic acid [102]. However, solvents and pressure must be applied to achieve these reactions.

Immer and co-workers have demonstrated that an addition of 10% H_2 to an He flow improves the stability of a Pd/C catalyst in the liquid-phase deoxygenation of C_{18} fatty acids [97]. However, Fu *et al.* [108] found that Pt/C was a more active catalyst than Pd/C for the deoxygenation of palmitic acid with the existence of supercritical water in reaction media at 370 °C, with more than 90% selectivity of pentadecane and without H_2 addition.

Chen *et al.* [112] have demonstrated the effect of Ru on different supports (C, ZrO_2, and Al_2O_3) in the deoxygenation of C_2-C_4 carboxylic acids in aqueous phase.

They report that carboxylic acids at high temperature deoxygenated to hydrocarbons with a tendency to form methane as the main product, as well as at high Ru loading, while at low temperature the reaction tends to be hydrogenation to produce alcohols. In their study, the deoxygenation reaction decreased, depending on the type of support, in the order of Ru/C > Ru/Zr_2O > Ru/Al_2O_3, indicating the influence of the surface acidity of the support, the interaction between Ru and the support and the state of the Ru species, as studied by the NH_3-TPD, H_2-TPR and CO-FTIR techniques.

The catalytic conversion of carboxylic acids to ketones, ketonisation, is of particular interest and has been the target of much applied and fundamental research [113]. It is always competitive with aldehyde formation. Ketonisation (Equation 1.5) allows for the partial deoxygenation of carboxylic acids to be achieved, accompanied by their carbon backbone upgrade. It is catalysed by many metal oxide and oxide-like catalysts ([114-116] and references therein). A ceria-zirconia catalyst has been reported for the ketonisation of C_4-C_6 carboxylic acids derived from renewable carbohydrate feedstocks (glucose and sorbitol) to convert these acids into transportation fuels [117].

Pestman *et al.* [118] tested a variety of oxides as catalysts of the ketonisation of acetic acid. Oxides of Bi, Pb, Mg and Zn, which exhibited activity for acetone formation, are all basic oxides and have low lattice energy, except magnesium oxide. In this case, acetone is formed by the decomposition of bulk acetate at the start of the reaction. On the other hand, oxides with high lattice energy, such as γ-alumina, TiO_2 and ZrO_2 exhibited activity for acetone formation on the surface of the catalysts without decomposition of bulk acetates. Furthermore, iron and vanadium oxides have been found to form acetone [107]. In this study, acetic acid was not the only subject of the ketonisation reaction: other carboxylic acids with high numbers of α-hydrogen atoms

were also tested. The results indicate that the ketonisation pathway is suspended as the number of α-hydrogen atoms in the carboxylic acid decreases, because this favours aldehyde formation.

Red mud, a waste material which consists of a mixture of iron oxides, titanium oxide and complexes of sodium alumina-silicate, has been tested as a catalyst for the ketonisation of carboxylic acids [113]. Ketones were formed by selectivity in the range of 40-60% when red mud was either pre-reduced by a mix of formic and acetic acid or reduced in situ by H_2 at a reaction temperature of 360 °C.

Propionic acid has been used as a feed substrate for a ketonisation reaction to yield 3-pentanone in the liquid phase. The product is a raw material for organic syntheses that can also be used as a solvent in paints and fragrances. Various supported and unsupported oxides have been reviewed for the ketonisation of propionic acid, as well as other carboxylic acids [119].

Several mechanisms have been proposed for the ketonisation of carboxylic acids, including: (i) decomposition of metal carboxylate; (ii) via acid anhydride intermediate; (iii) via β-keto acid intermediate and (iv) via ketene intermediate route [104, 107, 114].

The hydrogenation of carboxylic acids can also be used for their partial or total deoxygenation. Hydrogenation over metal oxides has attracted interest as an environmentally friendly route to aldehydes (Equation 1.6) [114].

$$RCOOH + H_2 \rightarrow RCHO + H_2O \qquad (1.6)$$

Aldehydes are extensively used for manufacturing fragrances and flavours. In addition, they are utilised as intermediates in the production of agrochemicals, dyes and pharmaceuticals. A range of aldehydes can be produced on a small or medium scale by different methods, including the partial oxidation and dehydrogenation of alcohols and the Rosenmund reduction of acid chlorides. However, these methods have many drawbacks, such as large amounts of waste, low yield and unattractive by-products [120, 121]. Some methods of producing aldehydes are not applicable industrially because they involve individual multistep and stoichiometric reactions rather than catalysis, such as the reduction of esters or carboxamides by lithium aluminium hydride or one of its derivatives [122, 123].

Compelling evidence has been obtained for the reaction occurring via the Mars-van Krevelen mechanism [114, 124], which can be explained in two steps depending on the oxygen lattice (Figure 1.13). In the first step, oxygen in the lattice reacts with a reducing adsorbate, i.e. hydrogen molecules. This reaction produces water, which is then desorbed, creating an oxygen vacancy (a). In the second step, an oxidant, i.e. acetic acid, refills this vacancy, thus forming acetaldehyde (b).

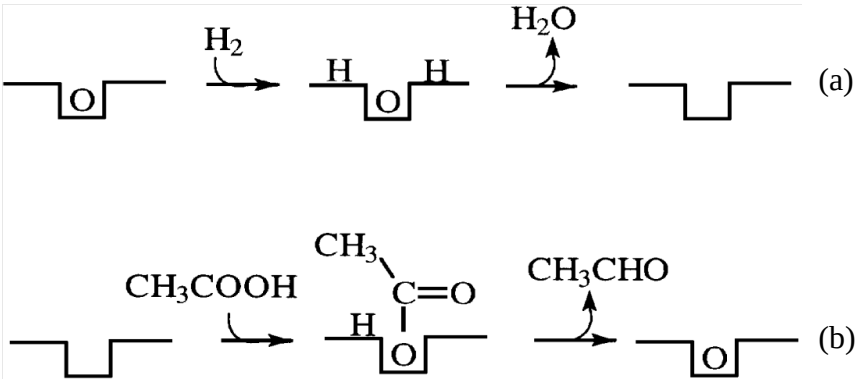

Figure 1. 13 Formation of acetaldehyde via the Mars-van Krevelen mechanism [124]

In this mechanism, when the strength of the metal-oxygen bond is too high, the first step will be very slow, because the oxygen will be strongly bound to the lattice, making it difficult to create vacancies. On the other hand, if the bond strength is too low, the second step will restrict the reaction, resulting in weak extraction of oxygen from the oxidant molecules. Thus, an oxide with an intermediate metal-oxygen bond strength is ideally used as a catalyst in this mechanism.

Pestman *et al.* [124] extensively studied the relationship between aldehyde selectivity and metal-oxygen bond strength in various metal oxides. They found that those of intermediate M-O bond strength, such as oxides of Fe, Sn, Ge or V, whose oxidation states can be easily changed, exhibited high selectivity for aldehyde. The best catalyst was Fe_2O_3, with selectivity greater than 80%. Conversely, TiO_2 and ZrO_2 have strong M-O bonds and showed low selectivity, although these oxides were found to be selective for the hydrogenation of aromatic carboxylic acids.

The addition of Pt to these oxides was found to enhance the catalytic activity and selectivity for hydrogenation. This can be explained by the dissociation of hydrogen molecules on metals and their transformation to hydrogenation sites in the oxide phase [124, 125].

Mitsubishi developed a commercial process for the hydrogenation of aromatic acids using a Cr_2O_3/ZrO_2 oxide catalyst and of aliphatic acids using a Cr_2O_3 catalyst to produce the corresponding aldehydes with ≥ 90% yield [114]. It has been reported that the redox properties of catalysts, as well as their acid-base properties, play an essential role in the carboxylic acid hydrogenation reaction [114, 121]. Metal oxides possessing weak redox properties with moderate acid or basic sites may be efficient in producing aldehyde.

The hydrogenation of benzoic acid was carried out by Holderich *et al.* [126], who report that the weakly acidic ZnO catalyst as well as possessing relatively strong basic sites exhibited excellent selectivity of 96% for benzaldehyde, with 100% conversion of acid. They also demonstrated that strong acid sites led to toluene formation by consecutive hydrogenation of benzaldehyde, together with coke formation.

P-Mo-V heteropoly compounds of Keggin structure have been studied as catalysts for the gas-phase hydrogenation and ketonisation of aliphatic carboxylic acids. However, due to their relatively low thermal stability (< 400 °C), these POMs decompose in situ to form Mo and V oxides, which are the true catalysts, rather than the POMs themselves [127, 128]. Related to these studies, increasing the Cs content in P-Mo-V catalysts by a certain amount increased their selectivity for aldehyde.

1.5.3 Hydrodeoxygenation of biomass-derived ketones

Today's best known biofuels, biodiesel and bioethanol, are derived from food crops (oils, grains or sugars) [88, 89], which results in unsustainable pressures on the global food and arable land supply. Second-generation biofuels will be produced largely from a combination of non-food sources such as cellulosic biomass, inedible oils and algal oils [129]. Biomass-based butanol (also called biobutanol) is expected to play a major role in the next generation of biofuels and has a number of advantages over ethanol: 85% butanol/gasoline blends can be used in unmodified petrol engines [130]. It can be transported in existing gasoline pipelines and produces more power than ethanol. Biobutanol can be produced fermentatively from cereal crops, sugar cane, sugar beet, etc., but can be also produced from cellulosic raw materials. Biobutanol production is

largely based on the traditional acetone-butanol fermentation of carbohydrates by *Clostridium* strains, which yields butanol together with acetone and ethanol in a mass ratio of 6:3:1 [131, 132]. Therefore, if the biobutanol project goes ahead as planned, it will produce a large surplus of acetone, so finding new outlets for acetone, preferably in the transportation fuel sector, would greatly improve the economy of biobutanol production.

It is well known that acetone can be transformed into C_6, C_9 and larger organic molecules by aldol condensation, which is employed in the industrial production of MIBK and diisobutyl ketone (DIBK) (Scheme 1.4) for use as solvents in paints, coatings and resins. The synthesis can be carried out as a one-pot process using a bifunctional catalyst, as described in section 1.2.

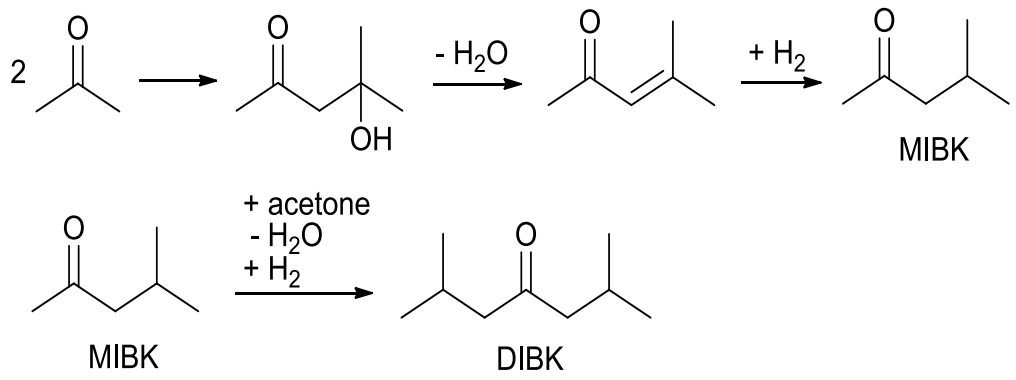

Scheme 1.4 MIBK and DIBK production from acetone

Global annual demand for MIBK is over 300,000 tons. Among the many multifunctional catalysts which have been successfully used to synthesise it from acetone in liquid and gas phases in industrial one-pot systems are Pd supported on cation exchange resins and on zirconium phosphate [133], Pd and Pt on zeolites [82-84,

134], Pd on $Cs_{2.5}H_{0.5}PW_{12}O_{40}$ [48], Pd on Cr^{3+}-Zn^{2+} mixed oxide [135, 136], Pd on MgO/SiO_2 [137], Pt, Pd, Ni and copper on activated carbon [138, 139], Pd on Nb_2O_5 [140] and Pd on $ALPO_4$-11 and SAPO-11 [141]. Further examples of multifunctional catalysts in the heterogeneous catalysis of various reactions are given in various reviews [6, 9, 12, 142].

MIBK and DIBK can be hydrogenated to alkanes, 2-methylpentane (MP) and 2,6-dimethylheptane (DMH). These alkanes match those in gasoline and could therefore be blended with straight-run gasoline, then subjected to standard catalytic reforming [143] to enhance the octane rating and used through the existing fuel infrastructure. However, to the best of our knowledge, there is little data available on the catalytic hydrogenation of MIBK and DIBK.

1.6 Objectives and thesis outline

The efficient utilisation of biomass resources is a major goal for academia and industry. Increasing concerns over climate change and diminishing petroleum resources drives the search for sustainable, economic and eco-friendly alternative routes by which chemicals can be produced from renewable sources. In this context, the deoxygenation of biomass-derived products such as carboxylic acids and ketones has received much attention as a renewable source of raw materials for the production of value-added chemicals and biofuel components. The reactions involved include decarboxylation, decarbonylation, ketonisation and dehydrogenation of oxygenate compounds. Recently, heteropoly compounds have found numerous applications as catalysts, offering significant economic and environmental benefits.

The aim of this work is to investigate key reaction pathways of the gas-phase deoxygenation of propionic acid catalysed by HPAs and metal-doped HPAs with proven on-stream stability. Propionic acid is chosen as a representative of carboxylic acids with the number of carbon atoms $n \leq 6$ derived from carbohydrate feedstocks. The chosen catalysts are tungstophosphoric Keggin heteropoly acid $H_3PW_{12}O_{40}$ (HPW) and its Cs acidic salt $Cs_{2.5}H_{0.5}PW_{12}O_{40}$ (CsPW), which possess sufficiently high thermal stability, with decomposition temperatures of 450 °C and > 500 °C respectively. These compounds have a very strong Brønsted acidity and are well documented as acid catalysts. In addition, Pd-, Pt- and Cu-doped CsPW have been chosen for study as bifunctional metal-acid catalysts. In particular, it should be interesting to compare Pd and Pt catalysts with Cu catalysts, because they preferably catalyse C=C and C=O bond hydrogenation respectively. These catalysts are compared with the corresponding SiO_2-supported metal catalysts regarding their selectivity and turnover rate. The reactions were carried out under hydrogen and nitrogen gases.

The gas phase hydrodeoxygenation of MIBK and DIBK were also investigated using bifunctional catalysts possessing both acid and metal sites. First, a number of conventional supported metal catalysts comprising Pd, Pt, Ru and Cu supported on silica and active carbon were tested for MIBK hydrogenation. Next, bifunctional metal-HPA catalysts comprising Pt, Pd, Ru, or Cu supported on Keggin heteropoly salt $Cs_{2.5}H_{0.5}PW_{12}O_{40}$ (CsPW) were utilised. After working under optimum conditions and promising metal efficiency, DIBK was tested as a reactant in multifunctional catalysis reactions. In addition, platinum-doped zeolites were investigated as bifunctional catalysts of the MIBK hydrodeoxygenation reaction. The effects of various reaction parameters, acid and metal functions will be discussed, as will the reaction mechanisms.

The physical and chemical properties of the catalysts were characterised using such techniques as TGA, DSC, XRD, IR, inductively coupled plasma atomic emission spectroscopy (ICP), TPR, elemental analysis (C, H analysis), hydrogen and nitrous oxide chemisorption.

Chapter 1 presents definitions and an outline account of the application of heterogeneous and multifunctional catalysis, in addition to a brief introduction to heteropoly acids and zeolites. The literature on the deoxygenation of biomass-derived molecules to produce value-added chemicals is reviewed, with particular attention to carboxylic acids and ketones.

Chapter 2 provides a description of the methods which were used in catalyst preparation. The techniques of catalyst characterisation and the gas-phase catalytic reaction testing procedures are described.

In chapter 3, the results of catalyst characterisation techniques are elucidated and there follows a description of the structure and physiochemical properties of the fresh and used catalysts.

Chapter 4 reports an investigation of the catalytic performance of HPW, CsPW and Pd-, Pt- and Cu-doped CsPW in gas-phase propionic acid deoxygenation reactions, in comparison with the corresponding SiO_2-supported metal catalysts. The reaction pathways are suggested.

Chapter 5 reports an examination of the catalytic activity of bifunctional catalysts, consisting of Pd, Pt, Ru and Cu based on C, SiO_2 and CsPW, in a gas-phase MIBK hydrodeoxygenation reaction. DIBK was submitted as a reactant under optimum conditions. In addition, the mechanism of this reaction is discussed.

Chapter 6 reports the use of Pt-doped zeolites (H-ZSM-5, H-Beta, and H-Y) as bifunctional metal-acid catalysts of the gas-phase hydrodeoxygenation of MIBK.

Finally, **Chapter 7** draws conclusions from the results of the catalytic study and the characterisation of the catalysts.

References

[1] G. Rothenberg, Catalysis: Concepts and Green Applications, Wiley-VCH, Weinheim, 2008.

[2] J.M. Thomas, W.J. Thomas, Principles and Practice of Heterogeneous Catalysis, VCH, Weinheim, 1997.

[3] M. Bowker, The Basis and Applications of Heterogeneous Catalysis, Oxford University Press Inc., New York, 1998.

[4] R.A. Sheldon, H.v. Bekkum, Fine Chemicals through Heterogeneous Catalysis, Wiley, Chichester, 2001.

[5] W. Keim, Green Chem. 5 (2003) 105.

[6] S.M. George, Chem. Rev. 95 (1995) 475.

[7] G.C. Bond, Heterogeneous Catalysis: Principles and Applications, Second ed., Oxford, 1987.

[8] G. Ertl, H. Knozinger, J. Weitkamp, Preparation of Solid Catalysts, Wiley-VCH, Germany, 1999.

[9] J.C. Wasilke, S.J. Obrey, R.T. Baker, G.C. Bazan, Chem. Rev. 105 (2005) 1001.

[10] F.X. Felpin, E. Fouquet, ChemSusChem. 1 (2008) 718.

[11] A. Bruggink, R. Schoevaart, T. Kieboom, Org. Process Res. Dev. 7 (2003) 622.

[12] M.J. Climent, A. Corma, S. Iborra, Chem. Rev. 111 (2011) 1072.

[13] B. Cornils, W.A. Herrmann, R. Schlogl, H.-C. Wong, Catalysis from A to Z: A concise Encyclopedia, Wiley-VCH, New York, 2000.

[14] F.G. Ciapetta, J.B. Hunter, Ind. Eng. Chem. 45 (1953) 147.

[15] F.G. Ciapetta, J.B. Hunter, Ind. Eng. Chem. 45 (1953) 155.

[16] V. Haensel, G.R. Donaldson, Ind. Eng. Chem. 43 (1951) 2102.

[17] H. Heinemann, G.A. Mills, J.B. Hattman, F.W. Kirsch, Ind. Eng. Chem. 45 (1953) 130.

[18] I.V. Kozhevnikov, Chem. Rev. 98 (1998) 171.

[19] I.V. Kozhevnikov, Catalysts For Fine Chemical Synthesis, Catalysis by Polyoxometalates, Wiley Chichester, 2002.

[20] T. Okuhara, N. Mizuno, M. Misono, Adv. Catal. 41 (1996) 113.

[21] M.N. Timofeeva, Appl. Catal. A 256 (2003) 19.

[22] D.E. Katsoulis, Chem. Rev. 98 (1998) 359.

[23] L.C.W. Baker, D.C. Glick, Chem. Rev. 98 (1998) 3.

[24] M.T. Pope, Heteropoly and Isopoly Oxometalates, Springer, Berlin, 1983.

[25] I.V. Kozhevnikov, J. Mol. Catal. A 262 (2007) 86.

[26] N. Mizuno, M. Misono, Chem. Rev. 98 (1998) 199.

[27] K. Na, T. Okuhara, M. Misono, J. Chem. Soc. Faraday T. 91 (1995) 367.

[28] N. Mizuno, M. Misono, J. Phys. Chem. 93 (1989) 3334.

[29] K. Katamura, T. Nakamura, K. Sakata, M. Misono, Y. Yoneda, Chem. Lett. (1981) 89.

[30] J.B. Moffat, Polyhedron 5 (1986) 261.

[31] J.B. Moffat, Metal-Oxygen Clusters: The Surface and Catalytic Properties of Heteropoly Oxometalates, Kluwer, New York, 2001.

[32] Y. Izumi, R. Hasebe, K. Urabe, J. Catal. 84 (1983) 402.

[33] T. Okuhara, T. Nishimura, H. Watanabe, M. Misono, J. Mol. Catal. 74 (1992) 247.

[34] J.B. Moffat, J. Mol. Catal. 52 (1989) 169.

[35] M.A. Parent, J.B. Moffat, Catal. Lett. 60 (1999) 191.

[36] M.A. Parent, J.B. Moffat, J. Catal. 177 (1998) 335.

[37] M.A. Parent, J.B. Moffat, Catal. Lett. 48 (1997) 135.

[38] T. Okuhara, T. Nishimura, H. Watanabe, K. Na, M. Misono, Stud. Surf. Sci. Catal. 90 (1994) 419.

[39] T. Okuhara, T. Nishimura, M. Misono, Chem. Lett. (1995) 155.

[40] T. Okuhara, Chem. Rev. 102 (2002) 3641.

[41] I.V. Kozhevnikov, K.I. Matveev, Appl. Catal. 5 (1983) 135.

[42] I.V. Kozhevnikov, Catal. Rev. 37 (1995) 311.

[43] C. Rocchicciolideltcheff, M. Amirouche, G. Herve, M. Fournier, M. Che, J.M. Tatibouet, J. Catal. 126 (1990) 591.

[44] C. RocchiccioliDeltcheff, A. Aouissi, S. Launay, M. Fournier, J. Mol. Catal. A 114 (1996) 331.

[45] K. Bruckman, M. Che, J. Haber, J.M. Tatibouet, Catal. Lett. 25 (1994) 225.

[46] M. Misono, Chem. Comm. (2001) 1141.

[47] T. Okuhara, N. Mizuno, M. Misono, Appl. Catal. A 222 (2001) 63.

[48] R.D. Hetterley, E.F. Kozhevnikova, I.V. Kozhevnikov, Chem. Comm. (2006) 782.

[49] A. Alhanash, E.F. Kozhevnikova, I.V. Kozhevnikov, Catal. Lett. 120 (2008) 307.

[50] K.A.D. Rocha, P.A. Robles-Dutenhefner, E.M.B. Sousa, E.F. Kozhevnikova, I.V. Kozhevnikov, E.V. Gusevskaya, Appl. Catal. A 317 (2007) 171.

[51] M.R.H. Siddiqui, S. Holmes, H. He, W. Smith, E.N. Coker, M.P. Atkins, I.V. Kozhevnikov, Catal. Lett. 66 (2000) 53.

[52] M. Musawir, E.F. Kozhevnikova, I.V. Kozhevnikov, J. Mol. Catal. A 262 (2007) 93.

[53] H. Van Bekkum, E. M. Flanigen, P. A. Jacobs, J.C. Jansen, Introduction to Zeolite Science and Practice, 2nd ed., Elsevier, Amsterdam, 2001.

[54] J.W. Ward, J. Catal. 9 (1967) 225.

[55] B.C. Gates, Catalytic Chemistry, Wiley, 1992.

[56] B. Yilmaz, U. Muller, Top. Catal. 52 (2009) 888.

[57] D.M. Al-Dhiayan, Ph.D Thesis, *The synthesis and Characterisation of Metal Substituted Pentasil Zeolites*, Department of Chemistry, UMIST, UK, 1995.

[58] W.M. Meier, D.H. Olson, Atlas of Zeolite Structure Types, Butterworths, 1987.

[59] F.R. Ribeiro, F. Alvarez, C. Henriques, F. Lemos, J.M. Lopes, M.F. Ribeiro, J. Mol. Catal. A 96 (1995) 245.

[60] S.G. Hegde, R. Kumar, R.N. Bhat, P. Ratnasamy, Zeolites 9 (1989) 231.

[61] M. Brandle, J. Sauer, J. Am. Chem. Soc. 120 (1998) 1556.

[62] D. Barthomeuf, Mater. Chem. Phys. 17 (1987) 49.

[63] V.R. Choudhary, D.B. Akolekar, J. Catal. 125 (1990) 143.

[64] W.J. Mortier, J. Catal. 55 (1978) 138.

[65] G.J. Kramer, R.A. Vansanten, J. Am. Chem. Soc. 115 (1993) 2887.

[66] I.N. Senchenya, V.B. Kazansky, S. Beran, J. Phys. Chem. 90 (1986) 4857.

[67] S. Kato, K. Nakagawa, N. Ikenaga, T. Suzuki, Catal. Lett. 73 (2001) 175.

[68] R.A. van Santen, D.P. de Bruyn, C.J.J. den Ouden, B. Smit, in: E.M.F. H. van Bekkum, J.C. Jansen (Eds.), Studies in Surface Science and Catalysis, Elsevier, 1991, pp. 317-358.

[69] A. Corma, F.V. Melo, D.J. Rawlence, Zeolites 10 (1990) 690.

[70] B. Coq, J. Pardillos, F. Figueras, Appl. Catal. 62 (1990) 281.

[71] J. Weitkamp, Solid State Ionics 131 (2000) 175.

[72] A. Corma, J. Catal. 216 (2003) 298.

[73] L.Y. Fang, S.B. Liu, I. Wang, J. Catal. 185 (1999) 33.

[74] K. Tanabe, W.F. Holderich, Appl. Catal. A 181 (1999) 399.

[75] G. Perot, M. Guisnet, J. Mol. Catal. 61 (1990) 173.

[76] Y.G. Li, H. Jun, Appl. Catal. A 142 (1996) 123.

[77] T.A. Peters, N.E. Benes, A. Holmen, J.T.F. Keurentjes, Appl. Catal. A 297 (2006) 182.

[78] M. Hartmann, Angew. Chem. Int. Edit. 43 (2004) 5880.

[79] C.H. Christensen, K. Johannsen, I. Schmidt, C.H. Christensen, J. Am. Chem. Soc. 125 (2003) 13370.

[80] M. Stocker, Micropor. Mesopor. Mat. 82 (2005) 257.

[81] M.D. Romero, A. deLucas, J.A. Calles, A. Rodriguez, Appl. Catal. A 146 (1996) 425.

[82] P.P. Yang, Y.C. Shang, J.F. Yu, J. Wang, M.L. Zhang, T.G. Wu, J. Mol. Catal. A 272 (2007) 75.

[83] L. Melo, G. Giannetto, L. Cardozo, A. Llanos, L. Garcia, P. Magnoux, M. Guisnet, F. Alvarez, Catal. Lett. 60 (1999) 217.

[84] P.Y. Chen, S.J. Chu, W.C. Lin, K.C. Wu, C.L. Yang, Zeolites and Microporous Crystals 83 (1994) 481.

[85] P. Mertens, F. Verpoort, A.N. Parvulescu, D. De Vos, J. Catal. 243 (2006) 7.

[86] E.G. Derouane, Microporous and Mesoporous Solid Catalysts, Wiley, 2007.

[87] A. Corma, S. Iborra, A. Velty, Chem. Rev. 107 (2007) 2411.

[88] E.L. Kunkes, D.A. Simonetti, R.M. West, J.C. Serrano-Ruiz, C.A. Gartner, J.A. Dumesic, Science 322 (2008) 417.

[89] G.W. Huber, J.A. Dumesic, Catal. Today 111 (2006) 119.

[90] P. Gallezot, ChemSusChem. 1 (2008) 734.

[91] D.M. Alonso, J.Q. Bond, J.A. Dumesic, Green Chem. 12 (2010) 1493.

[92] D. Mohan, C.U. Pittman, P.H. Steele, Energ. Fuel 20 (2006) 848.

[93] T.P. Vispute, H.Y. Zhang, A. Sanna, R. Xiao, G.W. Huber, Science 330 (2010) 1222.

[94] K.C. Kwon, H. Mayfield, T. Marolla, B. Nichols, M. Mashburn, Renew. Energ. 36 (2011) 907.

[95] T.V. Choudhary, C.B. Phillips, Appl. Catal. A 397 (2011) 1.

[96] H. Bernas, K. Eranen, I. Simakova, A.R. Leino, K. Kordas, J. Myllyoja, P. Maki-Arvela, T. Salmi, D.Y. Murzin, Fuel 89 (2010) 2033.

[97] J.G. Immer, M.J. Kelly, H.H. Lamb, Appl. Catal. A 375 (2010) 134.

[98] P.T. Do, M. Chiappero, L.L. Lobban, D.E. Resasco, Catal. Lett. 130 (2009) 9.

[99] Y. Takemura, A. Nakamura, H. Taguchi, K. Ouchi, Ind. Eng. Chem. Prod. Rd. 24 (1985) 213.

[100] W.F. Maier, W. Roth, I. Thies, P.V. Schleyer, Chem. Ber-Recl. 115 (1982) 808.

[101] M. Arend, T. Nonnen, W.F. Hoelderich, J. Fischer, J. Groos, Appl. Catal. A 399 (2011) 198.

[102] M. Snare, I. Kubickova, P. Maki-Arvela, K. Eranen, D.Y. Murzin, Ind. Eng. Chem. Res. 45 (2006) 5708.

[103] P.G. Blake, K.J. Hole, J. Phys. Chem. 70 (1966) 1464.

[104] K.S. Kim, M.A. Barteau, Langmuir 4 (1988) 945.

[105] J.L. Davis, M.A. Barteau, Langmuir 5 (1989) 1299.

[106] P.G. Blake, K.J. Hole, J. Chem. Soc. B (1966) 577.

[107] R. Pestman, A. Vanduijne, J.A.Z. Pieterse, V. Ponec, J. Mol. Catal. A 103 (1995) 175.

[108] J. Fu, X.Y. Lu, P.E. Savage, Energ. Environ. Sci. 3 (2010) 311.

[109] I. Simakova, O. Simakova, P. Maki-Arvela, D.Y. Murzin, Catal. Today 150 (2010) 28.

[110] S. Lestari, P. Maki-Arvela, K. Eranen, J. Beltramini, G.Q.M. Lu, D.Y. Murzin, Catal. Lett. 134 (2010) 250.

[111] S. Lestari, P. Maki-Arvela, H. Bernas, O. Simakova, R. Sjoholm, J. Beltramini, G.Q.M. Lu, J. Myllyoja, I. Simakova, D.Y. Murzin, Energ. Fuel 23 (2009) 3842.

[112] L.A. Chen, Y.L. Zhu, H.Y. Zheng, C.H. Zhang, B. Zhang, Y.W. Li, J. Mol. Catal. A 351 (2011) 217.

[113] E. Karimi, I.F. Teixeira, L.P. Ribeiro, A. Gomez, R.M. Lago, G. Penner, S.W. Kycia, M. Schlaf, Catal. Today 190 (2012) 73.

[114] T. Yokoyama, N. Yamagata, Appl. Catal. A 221 (2001) 227.

[115] O. Nagashima, S. Sato, R. Takahashi, T. Sodesawa, J. Mol. Catal. A 227 (2005) 231.

[116] A.D. Murkute, J.E. Jackson, D.J. Miller, J. Catal. 278 (2011) 189.

[117] C.A. Gaertner, J.C. Serrano-Ruiz, D.J. Braden, J.A. Dumesic, J. Catal. 266 (2009) 71.

[118] R. Pestman, R.M. Koster, A. van Duijne, J.A.Z. Pieterse, V. Ponec, J. Catal. 168 (1997) 265.

[119] M. Renz, Eur. J. Org. Chem. (2005) 979.

[120] W. Rachmady, M.A. Vannice, J. Catal. 209 (2002) 87.

[121] T. Yokoyama, N. Fujita, Appl. Catal. A 276 (2004) 179.

[122] A.M. Baro, W. Erley, Surf. Sci. 112 (1981) L759.

[123] J.C. Cavalier, E. Chornet, Surf. Sci. 60 (1976) 125.

[124] R. Pestman, R.M. Koster, J.A.Z. Pieterse, V. Ponec, J. Catal. 168 (1997) 255.

[125] R. Pestman, R.M. Koster, E. Boellaard, A.M. van der Kraan, V. Ponec, J. Catal. 174 (1998) 142.

[126] W.F. Holderich, J. Tjoe, Appl. Catal. A 184 (1999) 257.

[127] H. Benaissa, P.N. Davey, E.F. Kozhevnikova, I.V. Kozhevnikov, Appl. Catal. A 351 (2008) 88.

[128] H. Benaissa, P.N. Davey, Y.Z. Khimyak, I.V. Kozhevnikov, J. Catal. 253 (2008) 244.

[129] P.d. Sustainable Boifuels: Prospects and Challenges, The Royal Society, UK, 2008.

[130] P. Durre, Ann. N. Y. Acad. Sci. 1125 (2008) 353.

[131] V.V. Zverlov, O. Berezina, G.A. Velikodvorskaya, W.H. Schwarz, Appl. Microbiol. Biot. 71 (2006) 587.

[132] D.T. Jones, D.R. Woods, Microbiol. Rev. 50 (1986) 484.

[133] H.-J.A. K. Weissermel, Industrial Organic Chemistry, 3rd ed., VCH, Weinheim, 1997.

[134] T.J. Huang, W.O. Haag, US Patent 4339606, 1982.

[135] E.F. Kozhevnikova, I.V. Kozhevnikov, J. Catal. 238 (2006) 286.

[136] F. Al-Wadaani, E.F. Kozhevnikova, I.V. Kozhevnikov, J. Catal. 257 (2008) 199.

[137] J.J. Gamman, S.D. Jackson, F.A. Wigzell, Ind. Eng. Chem. Res. 49 (2010) 8439.

[138] G. Waters, O. Richter, B. Kraushaar-Czarnetzki, Ind. Eng. Chem. Res. 45 (2006) 6111.

[139] G. Waters, O. Richter, B. Kraushaar-Czarnetzki, Ind. Eng. Chem. Res. 45 (2006) 5701.

[140] Y. Higashio, T. Nakayama, Catal. Today 28 (1996) 127.

[141] S.M. Yang, Y.M. Wu, Appl. Catal. A 192 (2000) 211.

[142] D.E. Fogg, E.N. dos Santos, Coordin. Chem. Rev. 248 (2004) 2365.

[143] B.G.R. H. A. Wittcoff, Industrial Organic Chemicals, Wiley, N. Y., 1996.

2. Experimental

2.1 Introduction

This chapter describes the methods of catalyst preparation used in this work. Characteristic techniques that have been utilised to identify the properties of catalysts such as stability, porosity, surface area, structure, elemental content and metal dispersion are explained in detail. Finally, there is an account of the experimental setup and reaction procedure, as well as calculations of conversion and product selectivity.

2.2 Materials

All solvents and chemical precursors used were bought from Aldrich unless stated otherwise. Propionic acid (99.0 %), MIBK (99.0 %) and DIBK (98.0 %) were used as reactants; decane (>99.0 %) as GC standard; $HPW.xH_2O$ (>99.9 %), Cs_2CO_3 (99.9 %), silica Aerosil 300 (S_{BET}=300 $m^2\ g^{-1}$), $Pd(OAc)_2$ (98.0 %), $Pt(acac)_2$ from Alfa Aesar, $Cu(NO_3)_2.xH_2O$, $RuCl_3.xH_2O$ (99.9 %) and $H_2PtCl_6.xH_2O$ (99.0 %) for catalyst preparation; $2CuO.Cr_2O_3$, platinum group metal catalysts (Pt, Pd and Ru supported on active carbon) from Johnson Matthey and zeolites H-ZSM-5 (Si/Al = 12, S_{BET} = 403 $m^2\ g^{-1}$), H-Y (Si/Al = 15, S_{BET} = 780 $m^2\ g^{-1}$) and NH_4-Beta (Si/Al = 12, S_{BET} = 680 $m^2\ g^{-1}$) from Zeolyst International as commercial catalysts; ammonia solution (>30 % NH_3), HCl and HNO_3 for preparing ICP samples. All gases were supplied by BOC.

2.3 Catalyst Preparation

2.3.1 Preparation of silica-supported HPW

Silica-supported $H_3PW_{12}O_{40}$ catalyst, HPW/SiO_2, containing 30 % HPW, was prepared by wet impregnation [1]. A suspension of 7 g Aerosil 300 silica in 50-70 ml aqueous solution, containing a certain amount of HPW, was stirred in a closed glass vessel for 3-4 h and left overnight at room temperature for ageing, followed by drying at 45 °C/3 kPa using a rotary evaporator. The catalyst was then dried at 150 °C/0.1 kPa under vacuum for 1.5 h. All of the solid catalysts used in this work were sieved into a powder of 45-180 μm particle size.

2.3.2 Preparation of HPW caesium salts ($Cs_xH_{3-x}PW_{12}O_{40}$)

Caesium salts with various amounts of caesium ions were prepared by the dropwise addition of a stoichiometric quantity of aqueous Cs_2CO_3 (0.47 M) to an aqueous solution of $H_3PW_{12}O_{40}$ (0.75 M) at 40 °C with continuous stirring [2]. The precipitate obtained was aged in aqueous mixture for 48 h at room temperature and dried in a rotary evaporator at 45 °C/3 kPa, then in an oven at 150 °C/0.1 kPa for 1.5 h. Two kinds of HPW caesium salt, with varying amounts of caesium, were prepared ($Cs_{2.5}H_{0.5}PW_{12}O_{40}$ and $Cs_3PW_{12}O_{40}$). The elemental content of these catalysts was detected using ICP analysis.

2.3.3 Preparation of Pd and Pt-doped $Cs_{2.5}H_{0.5}PW_{12}O_{40}$

0.5 % Pd-doped $Cs_{2.5}H_{0.5}PW_{12}O_{40}$, designated Pd-$Cs_{2.5}H_{0.5}PW_{12}O_{40}$, was prepared by stirring $Cs_{2.5}H_{0.5}PW_{12}O_{40}$ powder with 0.02 M $Pd(OAc)_2$ solution in benzene at room temperature for 1 h, followed by slow evaporation of the benzene in a rotary evaporator

at room temperature [3]. After drying, the catalyst was calcined under vacuum at 150 °C/0.1 kPa, then reduced in an oven by a hydrogen flow at 250 °C for 2 h.

0.5 % Pt-doped $Cs_{2.5}H_{0.5}PW_{12}O_{40}$ was made by the same procedure that was used for the preparation of the Pd-doped caesium acidic salt, using $Pt(acac)_2$ (platinum bis acetylacetonate) as a metal precursor for this preparation.

2.3.4 Preparation of Cu-doped $Cs_{2.5}H_{0.5}PW_{12}O_{40}$

5 % $Cu/Cs_{2.5}H_{0.5}PW_{12}O_{40}$ was prepared by wet impregnation of $Cu(NO_3)_2.xH_2O$ on $Cs_{2.5}H_{0.5}PW_{12}O_{40}$ [4]. The water/solid ratio used to prepare this catalyst was 1.46 ml g^{-1}. After impregnation, the catalyst was dried overnight in an oven, then calcined at 400 °C in an air flow. Finally, the sample was reduced by hydrogen flow at 400 °C for 2 h. The water content of the copper nitrate was determined by thermogravimetric analysis (TGA).

2.3.5 Preparation of Ru-doped $Cs_{2.5}H_{0.5}PW_{12}O_{40}$

0.5 and 5.0 % $Ru/Cs_{2.5}H_{0.5}PW_{12}O_{40}$ were prepared by wet impregnation. A certain amount of $Cs_{2.5}H_{0.5}PW_{12}O_{40}$ was added to 0.1 M of $RuCl_3$ aqueous solution. The mixture was stirred for 24 h at room temperature, then dried at 60 °C in a rotary evaporator. The Ru catalysts were reduced under hydrogen flow at 250 °C for 2 h [5].

2.3.6 Preparation of Pd, Pt and Cu-doped SiO_2

0.5 % Pd, 0.5 % Pt and 5 % Cu-doped SiO_2 were separately prepared. Aerosil 300 silica was used with certain amount of metal precursor, adopting the procedure described for $Cs_{2.5}H_{0.5}PW_{12}O_{40}$ metal-doped catalyst preparation.

2.3.7 Preparation Pt-doped zeolites

First, NH_4-Beta was converted to H-Beta by air calcination at 550 °C for 4 h at a rate of 5 °C min^{-1}. Pt-doped zeolites (H-ZSM-5, H-Y and H-Beta) were prepared by the ion exchange method [6, 7], involving adsorption of Pt(II) on to a zeolite framework from 0.01 M aqueous solution of $Pt(NH_3)_4(NO_3)_2$. The slurry was aged at room temperature under stirring for 24 h, then filtered and washed twice with 100 ml of distilled water. Dried catalyst was calcined in air at 450 °C at a heating rate of 0.2 °C min^{-1} for 2 h, then reduced by H_2 at 400 °C for 2 h. The Pt loading on zeolite catalysts was determined by ICP analysis.

2.4 Catalyst characterisation techniques

2.4.1 Surface area and porosity analysis

Most heterogeneous catalysts are porous solid materials whose pore texture (surface area, pore volume and pore size distribution) can be determined by the preparation method [8]. These parameters are in turn essential in determining the activity, stability and selectivity of the catalyst. In particular, in gas phase catalytic reactions, the rate of product formation depends on the available surface area of catalyst. Pore size at sufficient volume is required to pass reactants through the catalyst lattice and the distribution of pore size on the catalyst surface is also important [9]. Therefore, it is necessary to determine the surface area and porosity of these materials, on which comparable results depend. It is noteworthy that the total surface area of a porous catalyst will be much higher than the external surface area because of the contribution

of the pore walls. Most heterogeneous catalysts have a total surface area of 1-1000 $m^2 g^{-1}$, whereas their external surface area is between 0.01 and 10 $m^2 g^{-1}$ [8].

IUPAC classifies the pores of solid materials into three classes in terms of their size as follows [8, 10, 11]:

- Micropores of < 2 nm and ultramicropores < 0.7 nm
- Mesopores between 2 and 50 nm
- Macropores > 50 nm.

Several techniques can be utilised to measure the surface area of a catalyst and characterise its porous texture [8, 12, 13]. One of the most common is nitrogen adsorption at its boiling temperature (-196 °C). A well defined way of calculating the total surface area of a porous solid material is the Brunauer-Emmett-Teller (BET) method, developed in 1938 [8, 14], which uses the following equation:

$$A_s = (V_m/22414)\, N_a \sigma \qquad (2.1)$$

where A_s is the surface area of catalyst, V_m is the monolayer volume of adsorbate, N_a is the Avogadro number (6.022×10^{23} mol^{-1}), σ is the area covered by one nitrogen molecule (0.162 nm^2) and the constant number 22414 is the molar volume of N_2 (ml mol^{-1}) under standard conditions [8].

The BET measurements in this work were conducted on a Micromeritics ASAP 2000 adsorption apparatus. All catalyst samples were first treated externally at 150 °C under vacuum for 1.5 h. Each pretreated sample (typically 0.2 g) was placed in a sample tube and degassed on the instrument at 250 °C until the pressure reached 8 μmHg. After removing all gases, the sample was allowed to cool at room

temperature, then the sample tube was immersed in liquid nitrogen. Finally, the gas pressure was allowed to reach equilibrium before a number (≈55) of subsequent nitrogen doses were applied in order to gain an adsorption isotherm.

2.4.2 Inductively coupled plasma atomic emission spectroscopy (ICP-AEC)

ICP-AEC is an atomic spectroscopic analytical technique which utilises as its excitation source a plasma (a gas with a high proportion of ions and electrons, created by heating gases such as argon at 6000 K) and which is able to detect a wide range of atoms at very low concentrations. When dissolved samples are submitted to ICP-AEC they emit light at characteristic wavelengths, which are converted to electrical signals that can be detected quantitatively to determine the concentration of elements in the sample [15].

ICP-AEC was used in this work to determine the Cs content in the HPW catalysts and the Pt content in the doped zeolites prepared by ion exchange. It was kindly preformed by G. Miller using the Spectro Ciros emission spectrometer which is available in the Department of Chemistry at Liverpool University.

2.4.3 Powder X-ray diffraction (XRD)

XRD is an important technique for studying the phase structure of solid materials. Since X-rays have wavelengths equivalent to the spacing of atoms in crystals, they can pass through these materials to give characteristic diffraction patterns. The angle of scattering of X-rays is affected by various factors which obey Bragg's law (equation 2.2) [16].

$$n\lambda = 2d\sin\theta \qquad (2.2)$$

where n is the order of the reflection (an integer value), λ is the incident X-ray wavelength, d is the lattice planar spacing and θ is the diffraction angle.

Useful information which can be obtained from the X-ray diffractogram includes the dimensions and symmetries of the unit cell, the crystallinity of solid materials and the average particle size, which can be calculated using the Scherrer equation (2.3):

$$t = 0.9\lambda/B \cos\theta \qquad (2.3)$$

where t is the particle size, λ is the incident X-ray wavelength, B is the full width at half the maximum of the diffraction peak, and θ is the diffraction angle. Related to this equation, the particle size of Cu-doped was measured in this work [17].

XRD of the catalysts studied was conducted using a Bruker D8 Advance diffractometer in Bragg-Brantano geometry, equipped with a Ge monochromator giving Cu Kα radiation (λ = 0.154 nm) which is available in the Department of Chemistry at Liverpool University.

2.4.4 Temperature programmed reduction (TPR)

TPR is a method mainly used to investigate hydrogenation catalysts, especially metal catalysts. It provides information about the best reduction conditions of the metal oxide precursor and explores the formation of different precursor phases and their oxidation states. It can also be used to optimise catalyst pretreatment. However, experimental parameters such as weight of catalyst sample, heating rate, particle size and gas flow rate affect the TPR profile of a catalyst [18].

H_2-TPR of catalysts in this study was carried out on a Micromeritics TPD/TPR 2900 apparatus equipped with a thermal conductivity detector (TCD) as pictured in Figure 2.1. Catalyst samples (20-30 mg) were heated to 800 °C at a rate of 10 °C min^{-1} in an H_2-N_2 (5:95) gas flow (60 ml min^{-1}).

Figure 2.1 Micromeritics TPD/TPR 2900 apparatus

2.4.5 N_2O chemisorption

Determination of metal atoms exposed on supported catalysts is vital to understanding the catalyst's activity. Metals with high dispersion are generally preferred in catalytic reactions. For practical reasons, gas adsorption methods are commonly utilised for measurement of metal dispersion [19].

Although copper catalysts have been widely utilised to catalyse hydrogenation reactions, it remains uncertain which Cu oxidation states are present in the active phase,

so not only the distribution of the oxidation states of surface Cu atoms but also the dispersion of Cu atoms on supported catalysts will be difficult to determine [20].

Weak reversible chemisorption and nonstoichiometric adsorption of commonly used gases such as CO and H_2 complicates surface Cu measurement, while using O_2 as a probe adsorbate causes bulk oxidation, making it inappropriate to use the adsorption of these gases to measure the dispersion of Cu atoms. Alternatively, dissociative N_2O adsorption is often used, followed by TPR, to measure Cu dispersion [20, 21].

In this study, the dispersion of Cu metal in 5 % Cu/CsPW and 5 % Cu/SiO_2 was determined using N_2O chemisorption followed by H_2-TPR [21]. Prior to N_2O chemisorption, a catalyst sample (150 mg) was reduced in a hydrogen flow (20 ml min^{-1}) in a Micromeritics TPD/TPR 2900 apparatus at 400 °C for 0.5 h with a temperature ramp rate of 10 °C min^{-1}, then cooled to room temperature and treated at this temperature with a gas mixture containing 1 % N_2O in nitrogen at a flow rate of 60 ml min^{-1} for 15 min to convert the surface Cu atoms to Cu_2O. Finally, the amount of Cu_2O was determined by H_2-TPR, increasing the temperature to 400 °C as described above. The copper metal dispersion, defined as the ratio of the number of metal atoms present at the surface to the total number of metal atoms in the catalyst, $D = Cu_s/Cu_{total}$, was calculated assuming a stoichiometry of $Cu_s/N_2O = 2$ and $Cu_s/H = 1$, according to the following equations ([21] and references therein):

$$2Cu_s + N_2O \rightarrow (Cu_s)_2O + N_2 \qquad (2.4)$$

$$(Cu_s)_2O + H_2 \rightarrow 2Cu_s + H_2O \qquad (2.5)$$

The average diameter of Cu particles, *d*, was calculated from the equation *d* (nm) = 1.1/*D* [20]. For 5 % Cu/SiO_2, the metal particle size was also determined by XRD using the Scherrer equation.

2.4.6 H_2 chemisorption

Dispersion of Pd, Pt and Ru on supported catalysts in this study was calculated using the pulse H_2 chemisorption method, which is well known to determine metal dispersion on supported catalysts [22, 23]. The titration of oxygen adsorbed on reduced metal sites by H_2 (H_2-O_2 titration) is a more sensitive and suitable analytic method, as it has been used widely to determine Pt [22], Rh [24], Pd [23] and Ru [25] dispersions.

Using H_2-O_2 titration, each metal (Pd, Pt and Ru)-doped catalyst in this study was reduced by H_2 in a flow of 20 ml min^{-1} at 250 °C for 2 h to ensure that the metal (M) was completely converted to M^0. The reduced sample was then exposed to air at room temperature to allow O_2 to adsorb onto the metal atoms on the catalyst surface (M_s) at an M_s-O ratio of 1:1, where O is an oxygen that adsorbs without immediate desorption back to the atmosphere [26]. A catalyst sample (50 mg) was placed in a glass sample tube connected to a Micromeritics TPD/TPR 2900 instrument and stabilised at 100 °C under nitrogen flow. 50 µl pulses of pure H_2 (heated to 75 °C) were injected in the flow at 3 min intervals until the catalyst was saturated with hydrogen. Equation 2.6 shows the stoichiometry of the H_2 titration [22, 23].

$$M_s\text{-}O + 3/2H_2 \rightarrow M_s\text{-}H + H_2O \qquad (2.6)$$

The volume of hydrogen adsorbed onto the catalyst surface was measured by integrating areas under the peaks detected by the TCD, which was displayed on the monitor. Continuous pulses were applied until no further adsorption was observed, then

the total volume of H_2 adsorbed was calculated, based on each injection being 50 µl of H_2 at 75 °C. The dispersion and average metal particle diameter were calculated as shown in equations 2.7-2.10 [27].

$$V_{348K}\ (\mu l\ ) = \sum \{50 - [(\ PA_{ads}/PA_{av}) \text{ x } 50] \qquad (2.7)$$

where V_{348K} is the total volume of H_2 adsorbed at 75 °C (348 K), PA_{ads} is the peak area of adsorbed H_2 and PA_{av} is the average peak area of at least four injections with no H_2 adsorption.

$$V_{273\ K}\ (\mu l\ ) = V_{348K} \times (273/348) \qquad (2.8)$$

Equation 2.8 gives the total volume of adsorbed H_2 at 0 °C (273 K).

$$D = \frac{V_{273K}\ (ml) \times A_r\ (g/mol)}{M_{cat}\ (g) \times 22414\ (ml/mol) \times C_M \times 1.5} \qquad (2.9)$$

where D is the metal dispersion, A_r is the atomic weight of metal, M_{cat} is the weight of catalyst used in the experiment, the constant number 22414 is the molar volume of H_2 under standard conditions, C_M is the content of metal as a fraction of catalyst weight and 1.5 is the stoichiometry of H_2 adsorbed to metal adsorbent. The average diameter of metal particles, d, was obtained from the empirical equation 2.10 [23].

$$d\ (nm) = 0.9/D \qquad (2.10)$$

2.4.7 Scanning transmission electron microscopy (STEM) with energy dispersive X-ray emission (EDX) microanalysis

The average particle sizes of some doped catalysts used in this study were determined, using STEM for the 5%Cu/SiO_2 catalyst, while STEM coupled with an energy dispersive X-ray (EDX) detector was utilised to generate a three-dimensional mapped image of the surface of 0.5%Pd/CsPW in order to verify the sizes of palladium particles on the surface of the catalyst. STEM and STEM-EDX measurements were kindly done by Prof. G. Tatlock and Dr. R. Hetterley and are gratefully acknowledged.

2.4.7.1 STEM

A directed beam of electrons was tunnelled between the tip of a probe and the surface of a catalyst, creating an electrical signal. The surface of the catalyst was scanned by the probe, then a computer program was used to generate an image of the catalyst surface. This measurement was carried out under a high vacuum to strengthen the signal [28]. The mean diameter of surface metal particles was calculated as $d_s = \Sigma n_i d_i^3 / \Sigma n_i d_i^2$, where n_i is the number of metal particles of a diameter d_i.

2.4.7.2 STEM-EDX

To develop a picture of the catalyst surface, STEM can be equipped with an energy dispersive X-ray emission detector and placed close to the sample grid. It can thus generate an elemental image of the surface of the catalyst. Practically, when the electron beam passes through the sample, electrons from lower energy shells may be excited and driven out from their energy state, leaving holes. These are filled by electrons from higher energy shells in a process which causes the emission of X-rays with energy equivalent to the difference in energy between two electron shells where

the transition occurs. The X-ray emission lines generated are characteristic of the elements contained within the catalyst [28].

The sample was suspended in ethanol and placed on a STEM grid and left for drying before the analysis. This was performed on a VGHB601UX scanning transmission electron microscope (STEM) operated at 100 kV equipped with an Oxford Pentafet energy dispersive X-ray detector (EDX).

2.4.8 Thermogravimetric analysis (TGA)

The aim of the TGA technique is to study changes in sample weight accompanying increased programmed heating of the sample. These may refer to physical or chemical changes, which can be calculated as percentage values. The instrumentation consists of a high precision balance upon the sample holder, placed inside a furnace which is then heated electrically at a linear rate under a gas flow (typically nitrogen or air). The thermal stability of solid catalysts can be ranked according to their decomposition temperatures, obtained from the TGA curve. Another application of TGA when the procedure is run under air is the determination of coke formation on a spent catalyst. It also enhances catalyst preparation by allowing the weight of precursors to be determined precisely. A derivative thermogravimetric (DTG) weight loss curve can be used to display the point at which the loss of weight becomes most apparent [29].

TGA was carried out on a Perkin-Elmer TGA 7 instrument under nitrogen flow at a heating rate of 20 ºC min^{-1} to raise the temperature from room temperature to 700 ºC. A typical TGA/DTG curve of the $H_3PW_{12}O_{40}$ catalyst is shown in Figure 2.2 as an example.

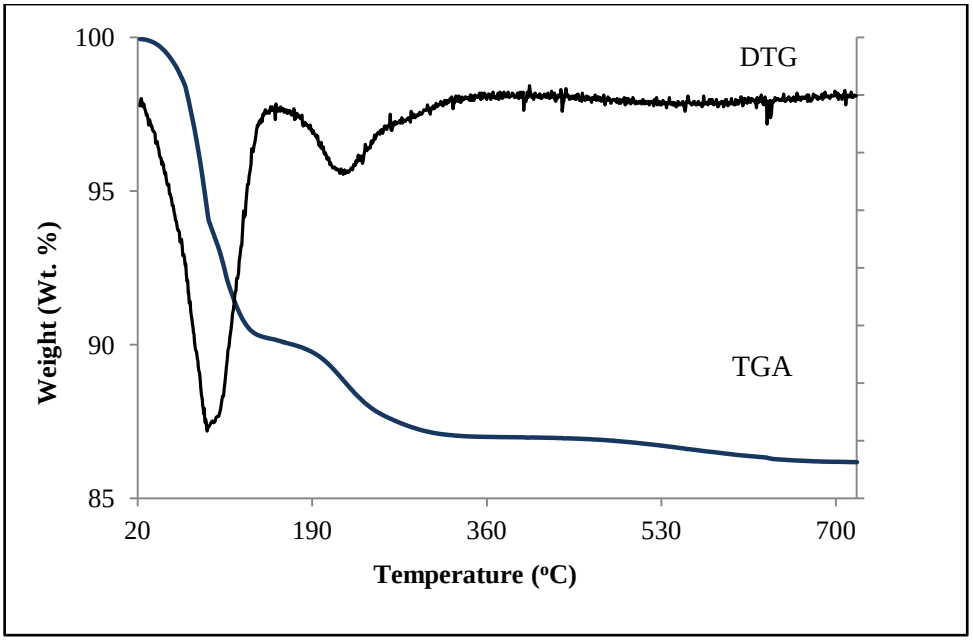

Figure 2.2 TGA/DTG of $H_3PW_{12}O_{40}$

2.4.9 Fourier transform infrared spectroscopy (FTIR)

The structure of a solid catalyst is a very important characteristic, which can be determined by infrared spectroscopy [15]. In this work, diffuse reflectance infrared Fourier transform (DRIFT) spectroscopy was utilised to examine the Keggin structure of the heteropoly acids used, to determine the nature of acidic sites by pyridine adsorption in all of the catalysts used and to detect CO, CO_2 and methylketene in propionic acid deoxygenation reactions.

The Keggin structure of the prepared HPA catalysts was investigated before and after reaction in the range of 500-1200 cm^{-1} as a fingerprint. In addition, Brønsted and Lewis acid sites were determined in the regions of 1540 and 1450 cm^{-1} respectively by pyridine adsorption. Samples were degassed under vacuum for about 2 h at 150 °C, then a small amount of the catalyst (5 mg) was mixed with KBr powder (45 mg) and

thoroughly blended. DRIFT spectra of catalysts were taken on a Nicolet NEXUS FTIR spectrometer at room temperature under N_2 atmosphere.

The same instrument, equipped with a gas cell of 10 cm path length, was used to detect CO, CO_2 and methylketene among the products of propionic acid deoxygenation in the downstream gas flow. For this purpose, methylketene (b.p. -23 °C [30]) was separated from CO using a dry ice trap, then thawed in an N_2 flow to transfer it into the gas cell.

2.4.10 Elemental analysis

Combustion analysis is a valuable method of measuring the amount of C and H in solid samples. It was used in this work to measure the C and H content of spent catalysts, in order to study the effect of carbonaceous deposits on catalyst performance. It was carried out on a Thermo Flash EA 1112 series analyzer, which is available in the Department of Chemistry at Liverpool University.

2.4.11 Differential scanning calorimetry (DSC)

The determination of the number of acid sites, their distribution and their strength is very important in studying the acidity of solid materials. A common method of doing this is DSC, using the ammonia pulse chemisorption technique [31, 32].

DSC experiments in this work were performed using a Setaram TGA-DSC 111 analyser (Figure 2.3), whose design comprised two open refractory tubes placed in a furnace. The detection unit was located centrally between the tubes to ensure that the sample cell was completely enclosed by the detector and that the results were thus accurate. A symmetrical microbalance was placed at the top of the calorimetric block,

which was in the vertical position. The suspension members of the microbalance were brought into line with the axis of each tube. A cell was hooked onto the end of each suspension member and brought into the detection area by sliding the microbalance.

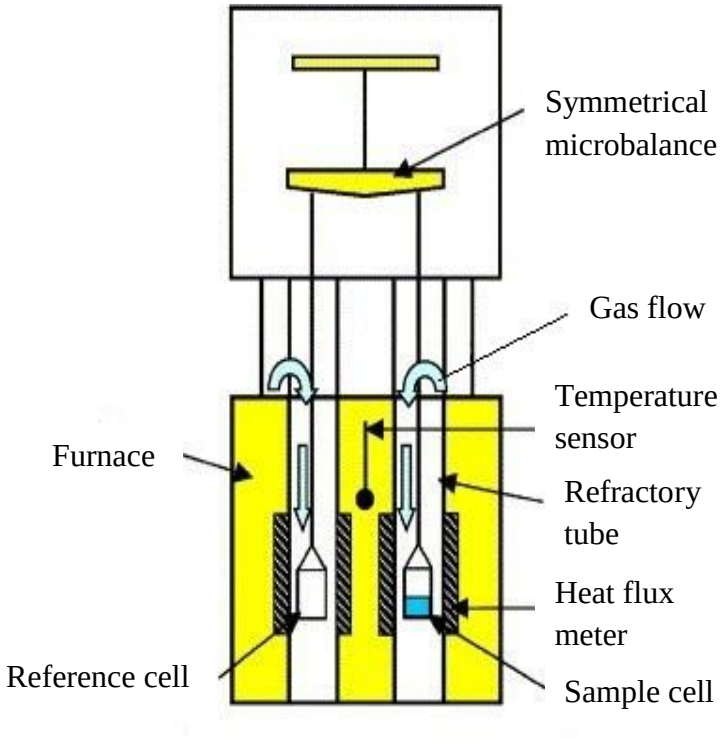

Figure 2.3 TGA-DSC diagrammatic cross section [33]

In this work, the sample was pretreated at 300 °C for 1 h with a temperature ramp rate of 5 °C min^{-1} under He gas at a flow rate of 30 ml min^{-1} to eliminate water molecules. The programmed temperature was reduced to 100 °C and held for about 2 h until the sample weight stabilised. The analysis was begun by pulsing ammonia consecutively, carried by the He gas flow. Sufficient time (20 min) was allowed after each injection for ammonia adsorption to be completed and equilibrium to be reached. The weight obtained and the corresponding heat of ammonia adsorption were recorded.

2.5 Catalytic reaction studies

2.5.1 Deoxygenation of propionic acid in the gas phase

Deoxygenation of propionic acid was carried out in the gas phase both in flowing H_2 and in a hydrogen-free system (in N_2). The catalysts were tested at 250-400 °C under atmospheric pressure in a Pyrex fixed-bed down-flow reactor of 28 cm length and 9 mm internal diameter with a catalyst bed located at the centre. The reactor was fitted with an on-line gas chromatograph using Varian Star 3400 CX instrument with a 30 m x 0.25 mm HP INNOWAX capillary column (column A) and a flame ionisation detector (FID), as shown in Figure 2.4. For a more accurate analysis of C_1-C_3 hydrocarbon products, a 60 m x 0.32 mm GSGasPro capillary column (column B) was used, which allowed for full separation of these hydrocarbons. The temperature in the reactor was controlled by a Eurotherm controller using a thermocouple placed at the top of the catalyst bed. The gas feed contained 2.0 % propionic acid in N_2 or H_2 as a carrier gas. The acid was fed by passing the carrier gas flow, controlled by a Brooks mass flow controller, through a stainless steel saturator, which held liquid propionic acid at 47 °C to maintain the chosen reactant concentration. The downstream gas lines and valves were heated to 180 °C to prevent substrate and product condensation. The gas feed entered the reactor at the top at a flow rate of 10 ml min^{-1} unless stated otherwise (space time W/F = 8.0 h g mol^{-1}, where W is the catalyst weight (g) and F the total molar flow rate (mol h^{-1}). The reactor was packed with 0.2 g catalyst powder of 45-180 μm particle size. Prior to reaction, the catalysts were pre-treated in H_2 for 1 h at the reaction temperature. Once the reaction had started, the downstream gas flow was analysed by the online GC to obtain propionic acid conversion and product selectivity.

Figure 2.4 Gas phase reaction equipment setup

Reactant substrate conversion and product yield and selectivity were calculated using the following equations.

$$\text{Conversion of reactant substrate (\%)} = \frac{Moles\ of\ substrate\ reacted}{Moles\ of\ substrate\ fed} \times 100 \qquad (2.11)$$

$$\text{Product yield (\%)} = \frac{Moles\ of\ product}{Moles\ of\ substrate\ fed} \times 100 \qquad (2.12)$$

The selectivity was defined as moles of product formed per mole of substrate converted and quoted in mole per cent. In this work, it is more convenient to calculate product selectivity from substrate conversion and product yield that mentioned in previous equations as following equation:

$$\text{Product selectivity (\%)} = \frac{Product\ yield}{Substrate\ conversion} \times 100 \qquad (2.13)$$

The rates of propionic acid conversion over different metal catalysts were measured at 250 °C under differential conditions within the conversion range < 10%. To fit these conditions, the weight of catalyst was reduced to 0.050 g and diluted with 0.15 g silica. In addition, at differential conditions the reaction activation energy, E_a, was calculated using the Arrhenius equation (2.14).

$$k = Ae^{-\frac{Ea}{RT}} \qquad (2.14)$$

where k is the reaction rate constant, A is the pre-exponential factor, R is the gas constant and T is the absolute temperature. Activation energy can be calculated from the straight line obtained by plotting ln k versus 1/T using this equation:

$$\ln k = \ln A - \frac{Ea}{RT} \qquad (2.15)$$

2.5.2 Hydrodeoxygenation of MIBK and DIBK in the gas phase

The hydrogenation of MIBK and of DIBK was carried out in the gas phase in flowing H_2. The catalysts were tested at 100-400 °C under atmospheric pressure in the same GC which was used for the deoxygenation of propionic acid. MIBK and DIBK were placed in the saturator at appropriate temperatures to maintain the chosen reactant concentration at a flow rate of 20-100 ml min^{-1}. The reactor was packed with 0.2 g of catalyst. In some cases, to reduce reaction rate, a smaller amount of catalyst was used as a homogeneous mixture with silica of a total weight of 0.2 g. Prior to reaction, the catalysts were pretreated in H_2 for 1 h at the reaction temperature. Reactant conversion, product selectivity and kinetic parameters were calculated using the equations presented above.

2.6 Product analysis

2.6.1 Gas chromatography

Gas chromatography can be used to separate compounds in a mixture by converting them to a volatile gas. The mobile phase, comprising the volatile mixture together with a carrier gas such as He, Ar, N_2 or H_2, migrates through a column consisting of a solid or liquid stationary phase. Volatile compounds pass through the column at different rates, depending on their boiling points [15].

Figure 2.5 displays the schematic of typical GC. A split/splitless injector introduces a controlled quantity of the sample into the column where the separation step occurs. The present study used a capillary column. Separated compounds, solutes, enter a detector such as flame ionisation detector (FID), where they are mixed with H_2 and air, then burned at a small metal jet. This causes the formation of ions in proportion to the concentration of ions derived from the solutes. The electrical conductivity of the flame and the current are interpreted to determine these proportions.

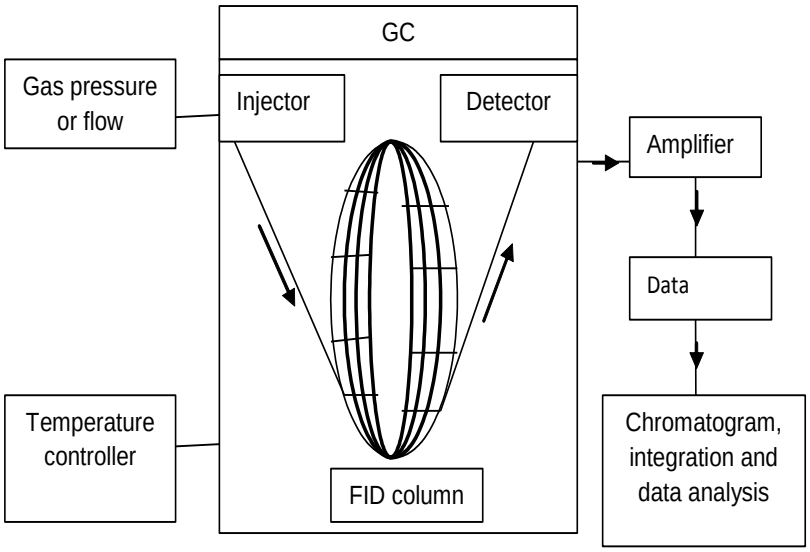

Figure 2.5 Schematic diagram of typical GC

2.6.2 Quantitative analysis of products using GC

The internal standard method was utilised to quantify all compounds that were used as reactants or expected as products. This method relies on the addition of a constant concentration of a chosen standard to a different concentration of analyte, all of which are diluted in a solvent. Therefore, the ratios of peak areas of analyte to the standard will depend on analyte concentrations, not on the actual amounts injected. Concentrations can thus be calculated using the following equation:

$$M/M_o = K \times S/S_o \qquad (2.16)$$

where M/M_o is the molar ratio of an analyte to a standard, S/S_o is the peak area ratio of an analyte to a standard and K is the molar calibration factor, derived from the linear plot of equation 2.16. In this work, decane was used as standard to calibrate organic compounds for all reactions and toluene as the solvent.

For gas phase deoxygenation of propionic acid, Table 2.1 lists the molecular weights, boiling points, retention times and calibration factors for all components.

Table 2.1 Molecular weights, boiling points, retention times and calibration factors for all components involved in the gas phase propionic acid deoxygenation

Compound	M wt ($g\ mol^{-1}$)	Boiling point (°C)	Retention time (min)	Calibration factor (K)
Propionic acid	74.08	141	8.9	4.37
Propanal	58.08	46	1.7	7.85
Propan-1-ol	60.10	97	4.1	6.92
3-Pentanone	86.13	100	3.3	2.64
Propionic anhydride	130.14	167	7.0	8.65
Light hydrocarbons	-	-	1.2	-
Methane[a]	16.04	-164	4.4	1.5
Ethane[a]	30.07	-89	4.7	3.0
Ethene[a]	28.05	-103	4.8	2.8
Propene[a]	42.08	-47	5.9	4.3

a) Retention times using column B, calibration factors were estimated using decane as standard related to the effective carbon-atom number [34].

Typical GC chromatograms for gas phase deoxygenation of propionic acid are shown in Figures 2.6 and 2.7, while the conditions of the columns and detector are represented in Figures 2.8 and 2.9. The calibration plots for the main products formed in this reaction are shown in Figure 2.10 (A-D).

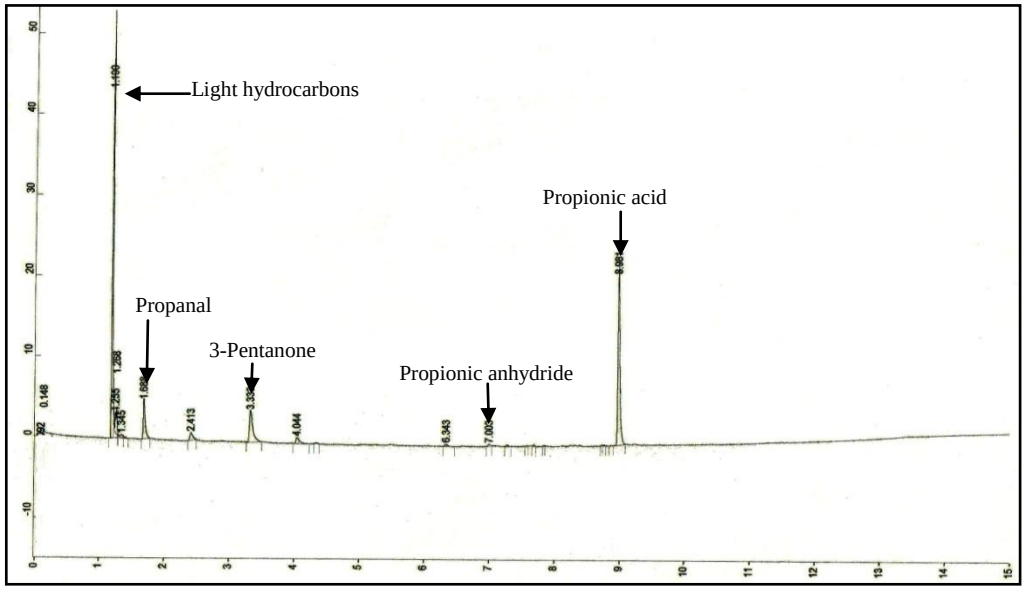

Figure 2.6 GC chromatogram of deoxygenation of propionic acid over 5.0 % Cu/CsPW using column A

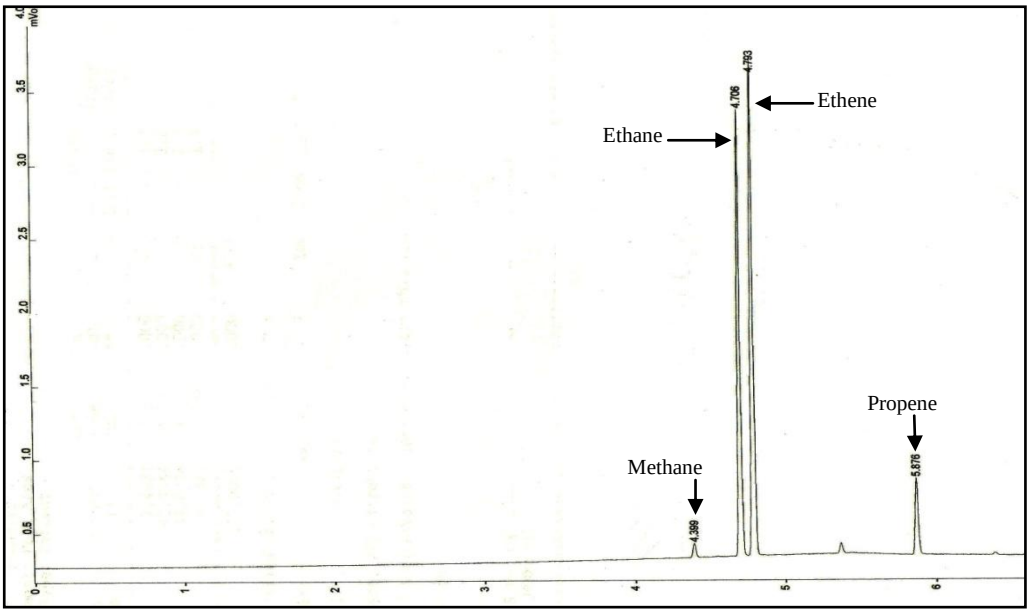

Figure 2.7 GC chromatogram for light hydrocarbon from deoxygenation of propionic acid over 5.0 % Cu/SiO_2 using column B.

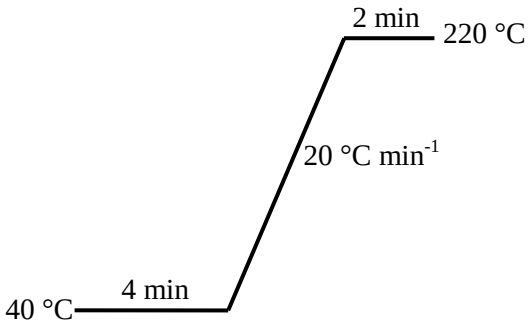

Injector temperature = 250 °C

Detector temperature = 250 °C

Figure 2.8 Conditions of column A and detector of GC analysis for deoxygenation of propionic acid.

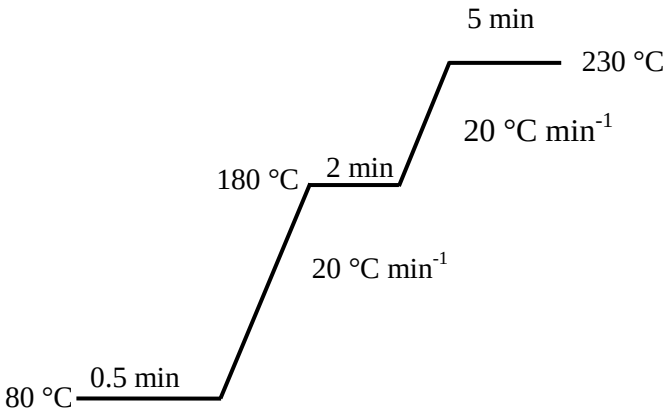

Figure 2.9 Conditions of column B of GC analysis for all reactions tested

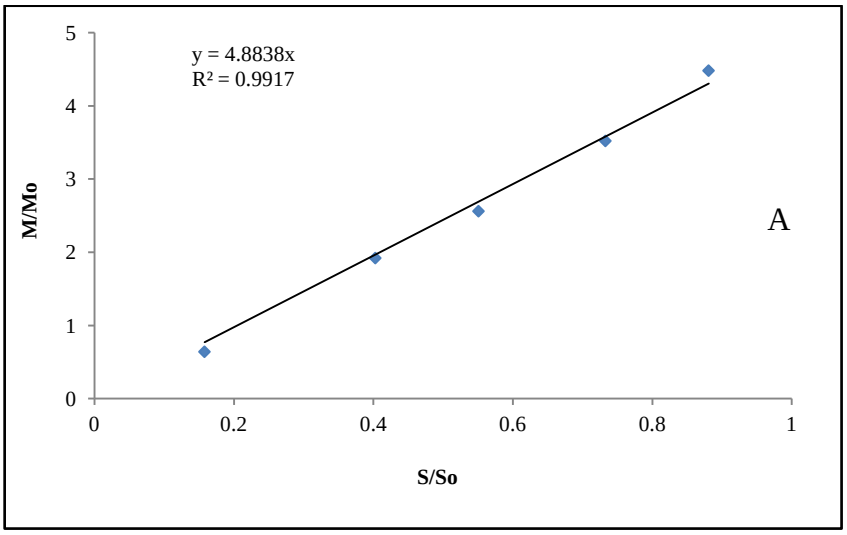

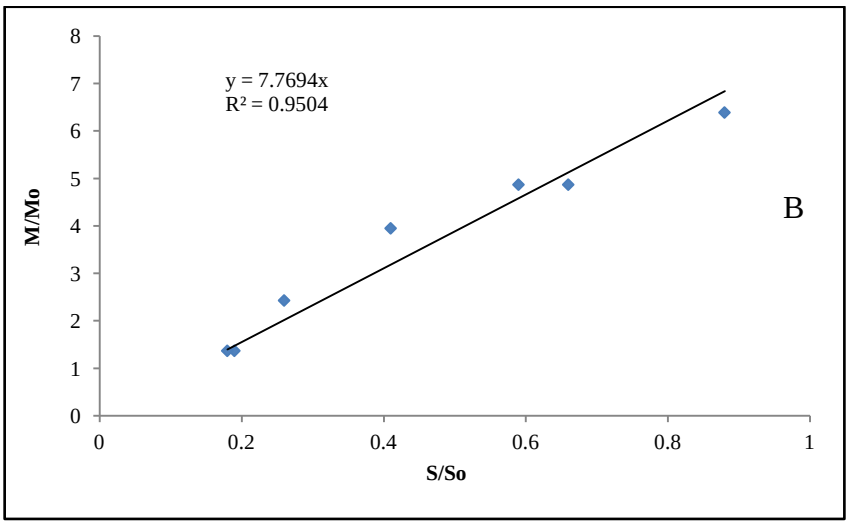

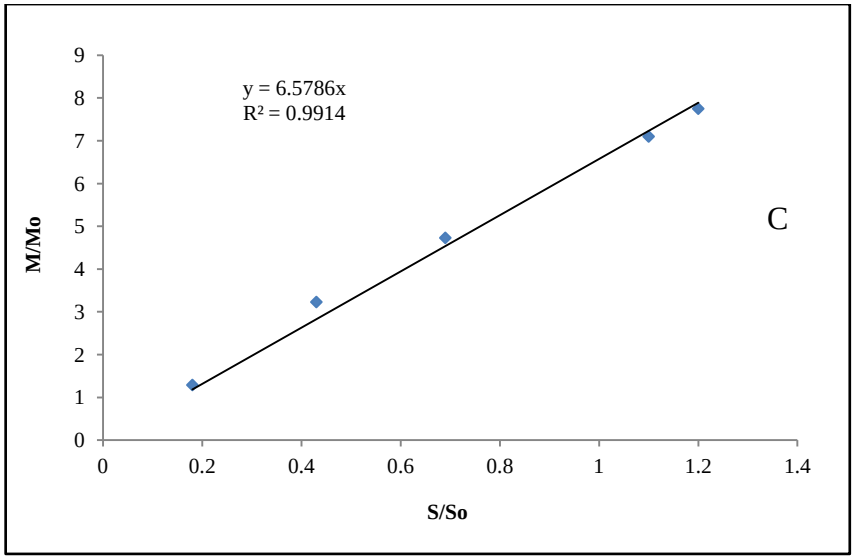

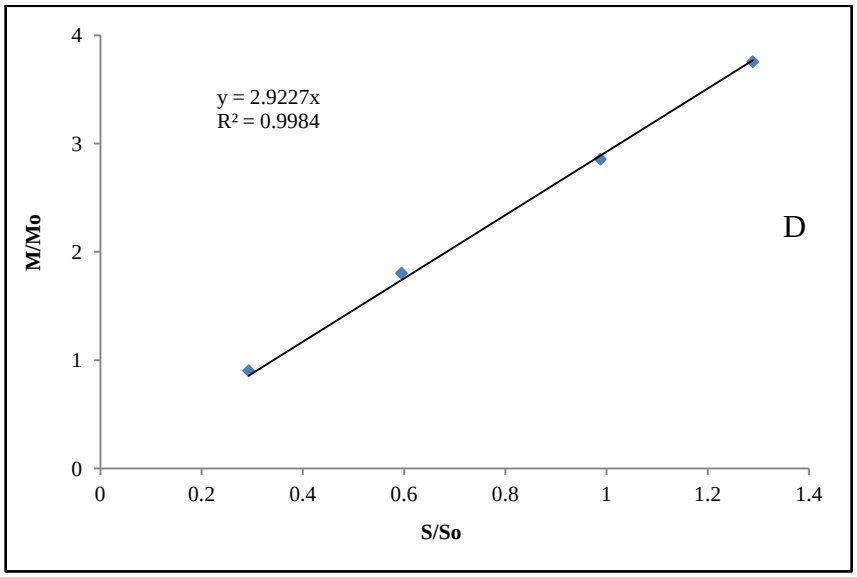

Figure 2.10 Calibration plots for the main products produced in the gas phase deoxygenation of propionic acid using decane as standard: A) propionic acid, B) propanal, C) propan-1-ol, D) 3-pentanone.

For the gas phase hydrodeoxygenation of MIBK and DIBK, molecular weights, boiling points, retention times and calibration factors for all components are given in Table 2.2.

Table 2.2 Molecular weights, boiling points, retention times, and calibration factors for all components involved in the gas phase hydrodeoxygenation of MIBK and DIBK

Compound	M wt ($g\ mol^{-1}$)	Boiling point (°C)	Retention time (min)	Calibration factor (K)
MIBK	100.16	117	3.00	1.95
DIBK	142.20	168	4.56	1.59
2-Methylpentane	86.18	60	1.24, 9.60[a]	1.85
2,6-Dimethylheptane	128.25	135	1.67	1.33
4-Methyl-2-pentanol	102.17	131	4.44	1.82
2,6-Dimethyl-4-heptanol	144	179	6.00	1.30
3-Methylpentane[a]	86.18	63	9.73	1.85
n-Hexane[a]	86.18	68	9.88	1.85
2,3-Dimethylbutane[a]	86.18	58	9.40	1.85

[a] Retention times using column B. The K factors for 2-Methylpentane isomers were assumed to be the same value.

Examples of GC traces for hydrodeoxygenation of MIBK and DIBK over selected catalysts are shown in Figures 2.11-2.13, while Figure 2.14 shows the conditions of the column and detector. Finally, the calibration plots for some products obtained in these reactions are displayed in Figure 2.15 (A-E).

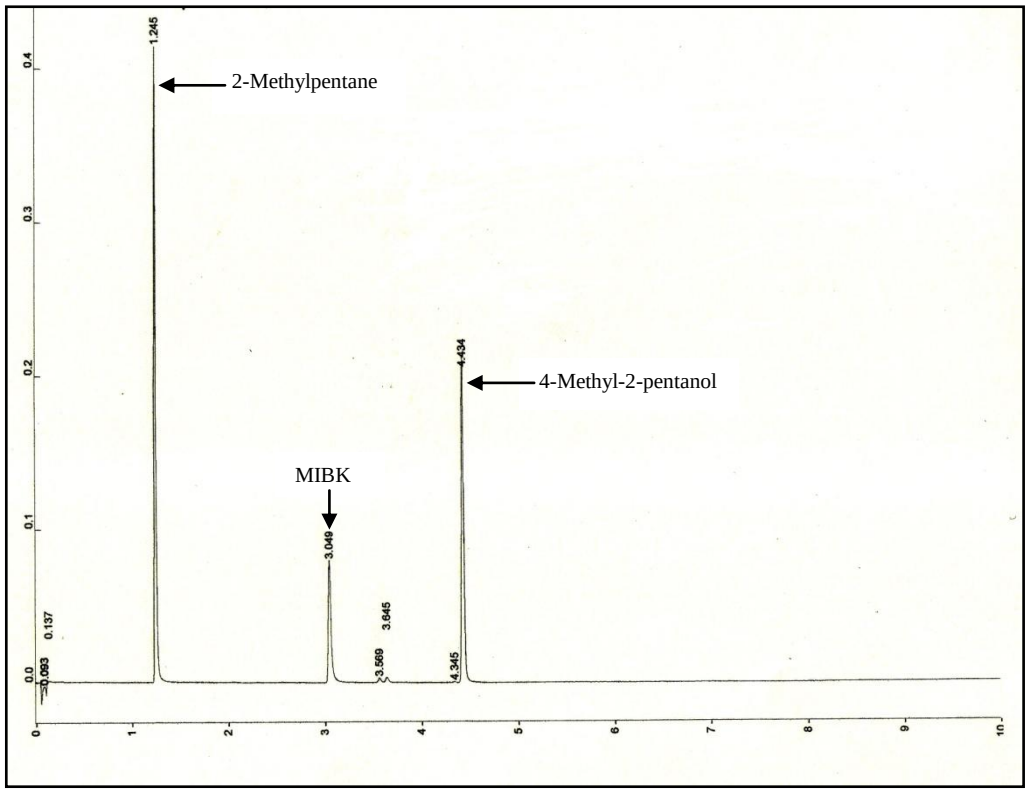

Figure 2.11 GC trace of MIBK hydrodeoxygenation over Pt/ZSM-5 using column A

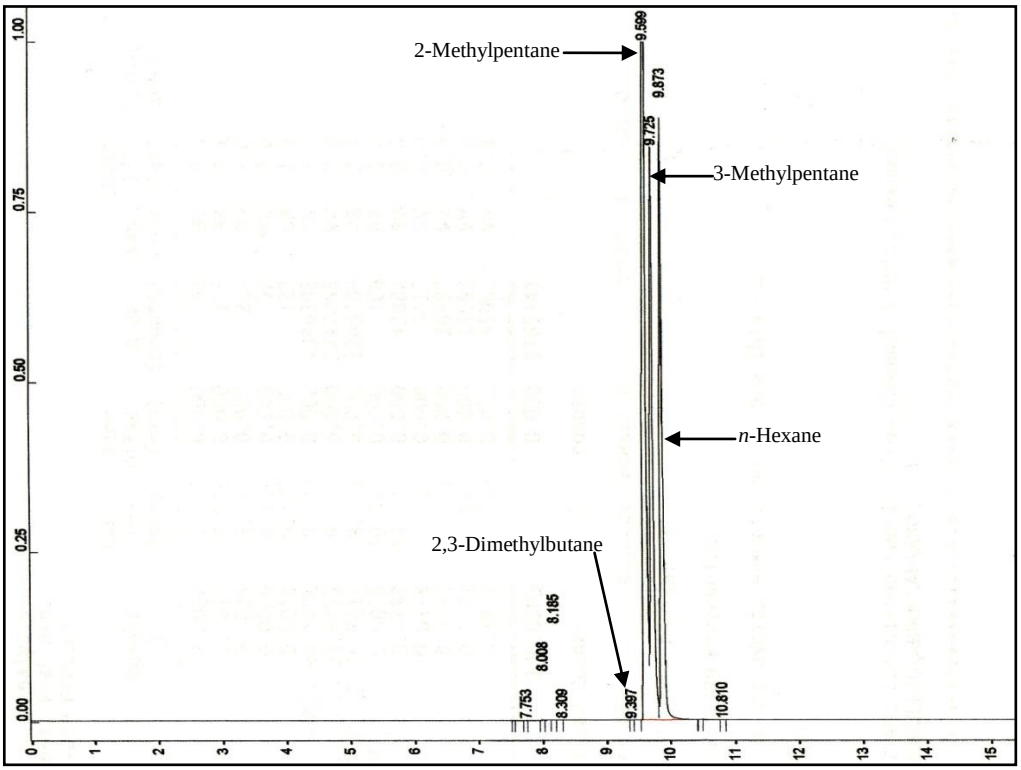

Figure 2.12 GC trace of 2-methylpentane isomers produced from hydrodeoxygenation MIBK over Ru/CsPW using column B

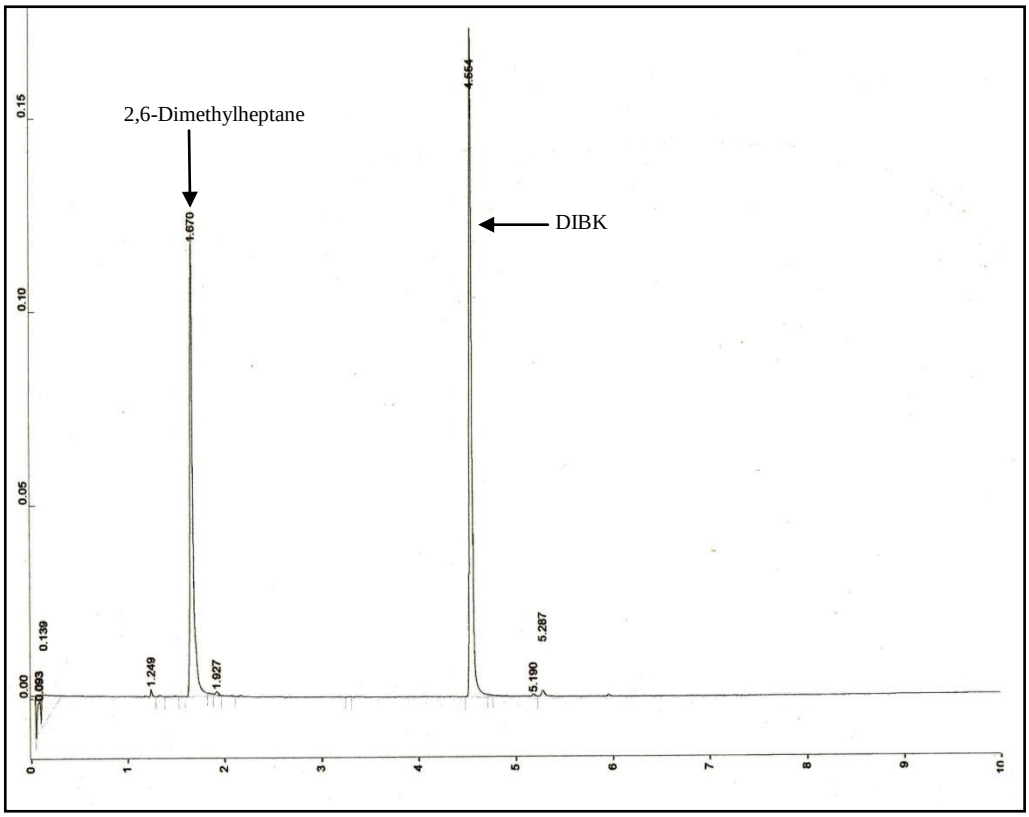

Figure 2.13 GC trace of DIBK hydrodeoxygenation over Pt/CsPW using column A

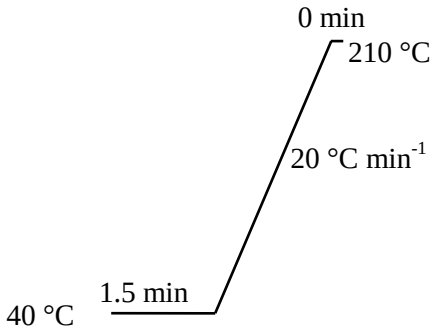

Injector temperature = 250 °C

Detector temperature = 250 °C

Figure 2.14 Conditions of column A and detector of GC analysis for hydrodeoxygenation of MIBK and DIBK.

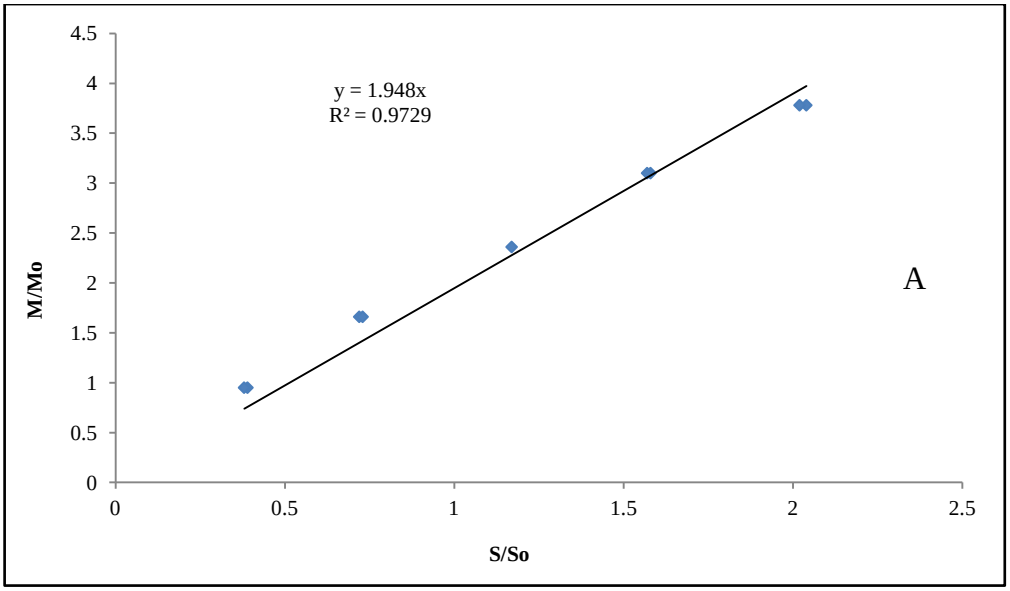
y = 1.948x
R² = 0.9729
M/Mo
S/So
A

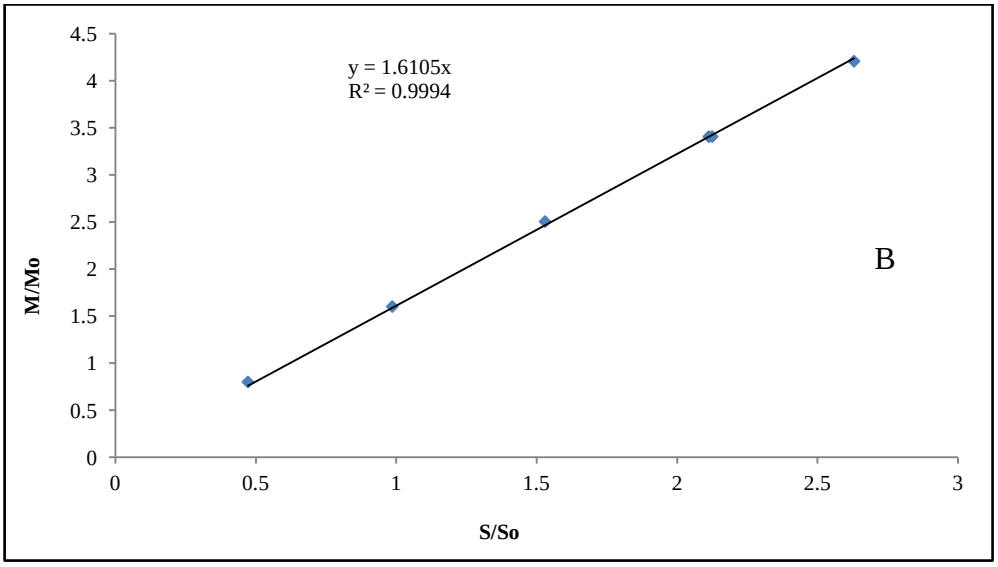
y = 1.6105x
R² = 0.9994
M/Mo
S/So
B

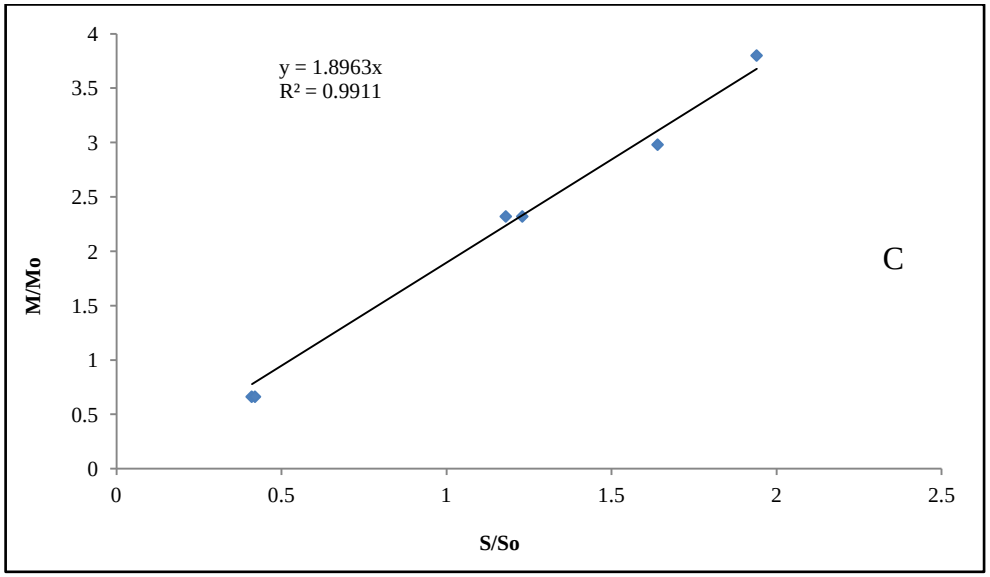
y = 1.8963x
R² = 0.9911
M/Mo
S/So
C

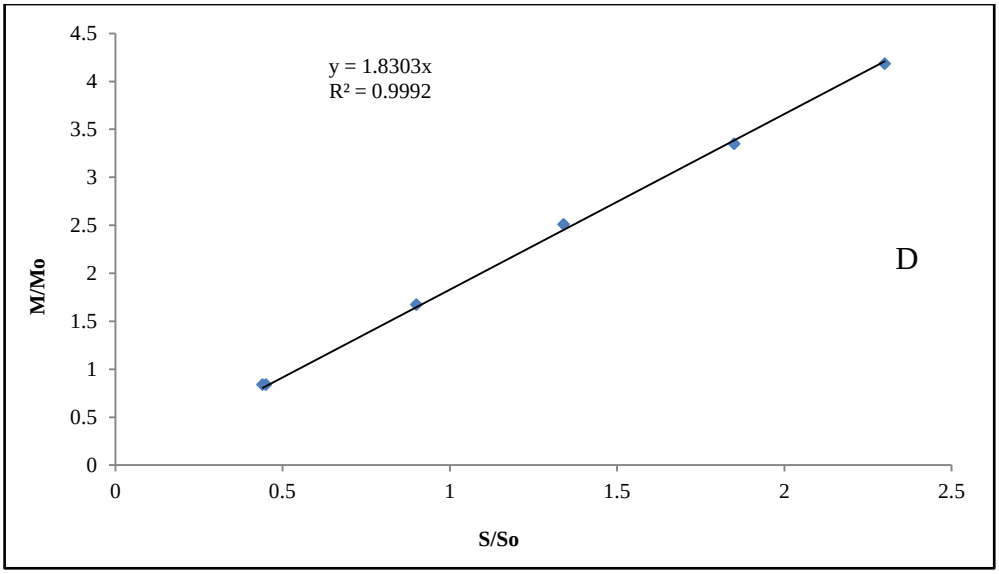

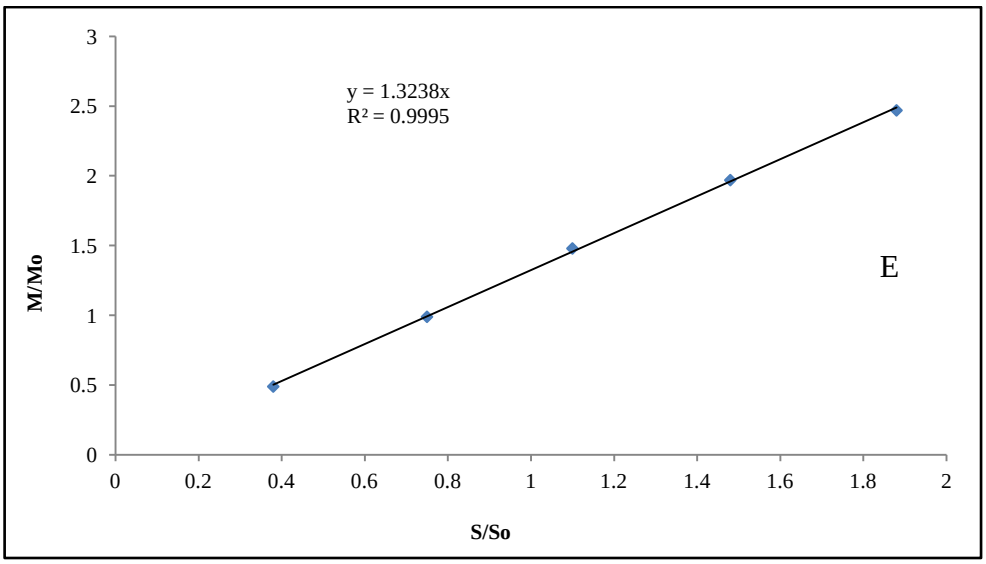

Figure 2.15 Calibration plots for some products formed in the gas phase hydrodeoxygenation of MIBK and DIBK using decane as standard: A) MIBK, B) DIBK, C) 2-methyl pentane, D) 4-methyl-2-pentanol, E) 2,6-dimethyl-4-heptanol

2.6.3 Gas chromatography-mass spectroscopy (GC-MS)

GC-MS was employed to give further evidence of the products present. In this method, a substrate is vaporised under high vacuum, then bombarded by a beam of high energy electrons. The volatile substrate undergoes fragmentation and forms an array of ions of different sizes. Equation 2.17 shows this method, where M is the substrate to be ionised, e^- is the high energy electron and $M^{+\cdot}$ is the resulting positively charged ionised molecular radical [15].

$$M + e^- \longrightarrow M^{+\cdot} + 2e^- \qquad (2.17)$$

The resultant ions are measured by accelerating them in an electric field and deflecting them in a magnetic field, where their deflection can be interpreted in terms of their mass/charge ratio (m/z).

In this study, GC-MS analysis was carried out using a TRIO-1000 GC-MS spectrometer, which is available in the Department of Chemistry at Liverpool University. Figures 2.16 and 2.17 show the GC-MS results for the main products of deoxygenation of propionic acid and hydrodeoxygenation of MIBK in the gas phase.

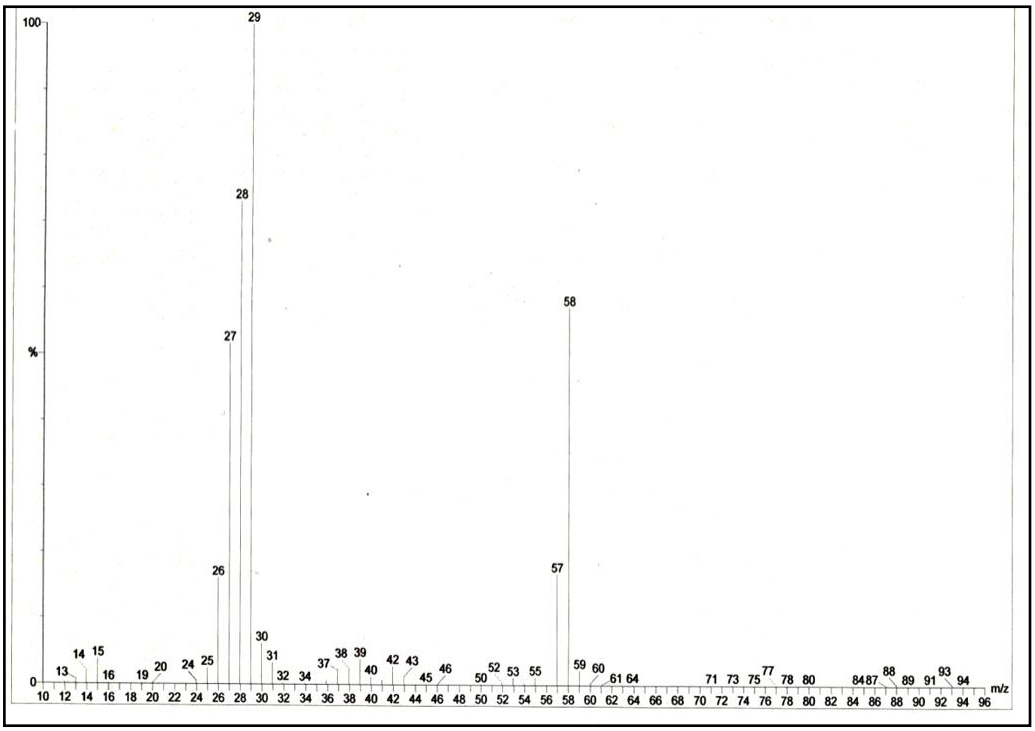

Figure 2.16 Mass spectrum of propanal. Relative molecular mass = 58.

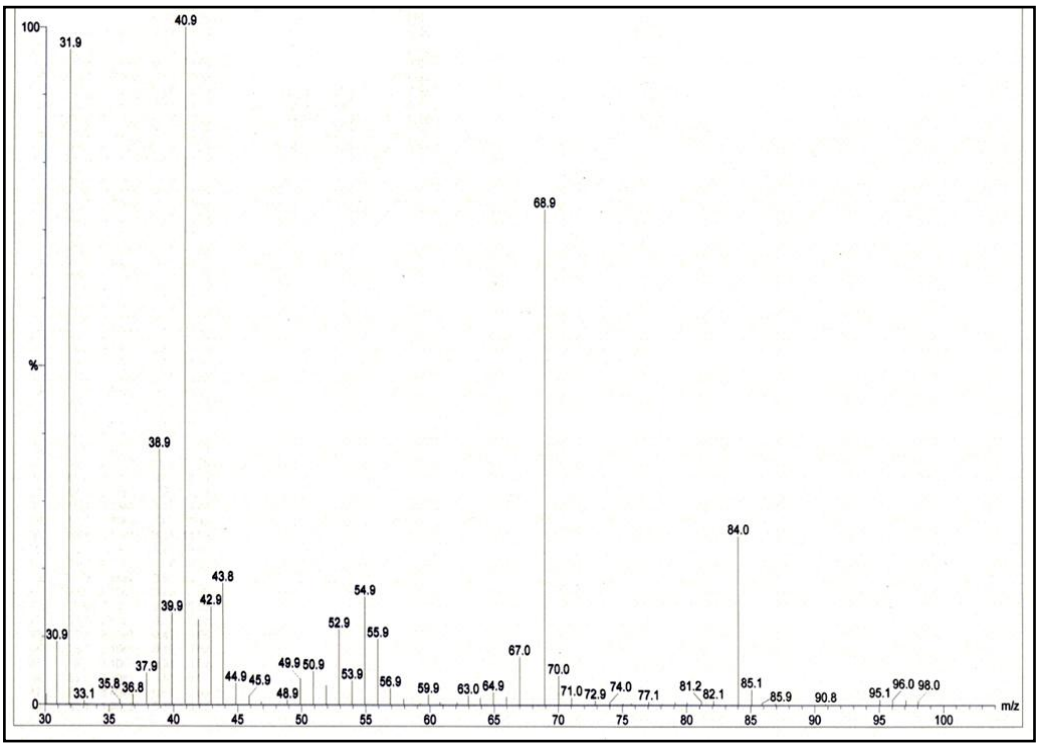

Figure 2.17 Mass spectrum of methylpentane. Relative molecular mass = 84.

References

[1] I.V. Kozhevnikov, K.R. Kloetstra, A. Sinnema, H.W. Zandbergen, H. van Bekkum, J. Mol. Catal. A 114 (1996) 287.

[2] S. Tatematsu, T. Hibi, T. Okuhara, M. Misono, Chem. Lett. (1984) 865.

[3] E.F. Kozhevnikova, E. Rafiee, I.V. Kozhevnikov, Appl. Catal. A 260 (2004) 25.

[4] T.T. Pham, L.L. Lobban, D.E. Resasco, R.G. Mallinson, J. Catal. 266 (2009) 9.

[5] A. Alhanash, E.F. Kozhevnikova, I.V. Kozhevnikov, Catal. Lett. 120 (2008) 307.

[6] A.C.M. van den Broek, J. van Grondelle, R.A. van Santen, J. Catal. 167 (1997) 417.

[7] J. de Graaf, A.J. van Dillen, K.P. de Jong, D.C. Koningsberger, J. Catal. 203 (2001) 307.

[8] G. Leofanti, M. Padovan, G. Tozzola, B. Venturelli, Catal. Today 41 (1998) 207.

[9] J.M. Thomas, W.J. Thomas, Principles and Practice of Heterogeneous Catalysis, VCH, Weinheim, 1997.

[10] J. Rouquerol, D. Avnir, C.W. Fairbridge, D.H. Everett, J.H. Haynes, N. Pernicone, J.D.F. Ramsay, K.S.W. Sing, K.K. Unger, Pure Appl. Chem. 66 (1994) 1739.

[11] G. Rothenberg, Catalysis: Concepts and Green Applications, Wiley-VCH, Weinheim, 2008.

[12] G. Leofanti, G. Tozzola, M. Padovan, G. Petrini, S. Bordiga, A. Zecchina, Catal. Today 34 (1997) 329.

[13] G. Leofanti, G. Tozzola, M. Padovan, G. Petrini, S. Bordiga, A. Zecchina, Catal. Today 34 (1997) 307.

[14] S. Brunauer, P.H. Emmett, E. Teller, J. Am. Chem. Soc. 60 (1938) 309.

[15] D. Kealey, D.J. Haines, Analytical Chemistry, 1st ed., Bio scientific, Oxford, 2002.

[16] P.W. Atkins, Physical Chemistry, Oxford University Press, 1998.

[17] A.W. Burton, Zeolite Characterization and Catalysis: A Tutorial (2009) 1.

[18] F. Pinna, Catal. Today 41 (1998) 129.

[19] J.H. Sinfelt, Rev. Mod. Phys. 51 (1979) 569.

[20] A. Dandekar, M.A. Vannice, J. Catal. 178 (1998) 621.

[21] A. Gervasini, S. Bennici, Appl. Catal. A 281 (2005) 199.

[22] J.E. Benson, M. Boudart, J. Catal. 4 (1965) 704.

[23] J.E. Benson, H.S. Hwang, M. Boudart, J. Catal. 30 (1973) 146.

[24] S.E. Wanke, Doughart.Na, J. Catal. 24 (1972) 367.

[25] K.C. Taylor, J. Catal. 38 (1975) 299.

[26] G. Prelazzi, M. Cerboni, G. Leofanti, J. Catal. 181 (1999) 73.

[27] TPD/TPR 2900 analyser, Operator's manual, VI.02, April 1993.

[28] B. Imelik, J.C. Vedrine, Catalyst Characterization, Physical Techniques for Solid Materials, Plenum Press, New York 1994.

[29] P. Patnaik, Dean's Analytical Chemistry Handbook, 2nd ed., 2004.

[30] P.G. Blake, K.J. Hole, J. Phys. Chem. 70 (1966) 1464.

[31] F. Lefebvre, F.X. Liucai, A. Auroux, J. Mater. Chem. 4 (1994) 125.

[32] V. Rakic, V. Dondur, U. Mioc, D. Jovanovic, Top. Catal. 19 (2002) 241.

[33] J.H. Ferrasse, D. Lecomte, Chem. Eng. Sci. 59 (2004) 1365.

[34] L.G. Robert, F.B. Eugene, Modern Practice of Gas Chromatography, 4th ed., Wiley-Interscience, 2004.

3. Catalyst characterisation

3.1 Introduction

This chapter details and discusses the results of catalyst characterisation. The porosity of catalysts used in this study, their surface area, the dispersion of metal on doped catalysts, crystallinity, elemental content, thermal stability and the strength and nature of acidic sites were investigated by various methods: gas adsorption, XRD, ICP, TGA, TPR, FTIR and DSC.

3.2 Elemental analysis

3.2.1 HPW-based catalysts

ICP-AEC was utilised to determine the phosphorus and tungsten composition of 30 % HPW/SiO_2 and the caesium content of HPW caesium salts ($Cs_{2.5}H_{0.5}PW_{12}O_{40}$ (CsPW) and $Cs_3PW_{12}O_{40}$). The samples were dissolved in concentrated ammonia solution. As shown in Table 3.1, the phosphorus, tungsten and caesium content (% wt) of heteropoly compound catalysts based on HPW are fairly close to the calculated theoretical values based on six water molecules in the HPW parent, as measured by TGA. Water content was taken into account during catalyst preparation and may explain the slight change in elemental content. Regarding metal-doped CsPW, Pd-, Pt-, Ru- and Cu-impregnated catalysts are based on the stoichiometric values from synthesis.

Table 3.1 ICP-AEC analysis for elemental content of HPW based catalysts

Catalyst	**Element**	**Theoretical (% wt)**	**Experimental (% wt)**
$Cs_{2.5}H_{0.5}\ PW_{12}O_{40}$	P	0.97	1.10
	W	68.7	69.50
	Cs	10.35	10.00
$Cs_3PW_{12}O_{40}$	P	0.94	1.00
	W	67.34	68.42
	Cs	12.17	12.00
30 % HPW/SiO_2	P	0.40	0.41
	W	23.00	24.3

3.2.2 Zeolites

H-ZSM-5, H-Y and NH_4-Beta were bought from Zeolyst international with specific Si/Al ratios. In this study, zeolites were used as bifunctional catalysts by doping them with Pt metal (0.5 % wt). As mentioned in the experimental chapter, NH_4-Beta was converted to the hydrogen form by calcination in air at 550 °C. Platinum content in Pt doped H-Zeolites was measured using ICP-AEC. As explained previously, Pt-doped H-zeolites were prepared by the ion exchange method, which can cause the loss of some Pt through the washing out of non-exchanged Pt (II). To study the effect of Pt loading, 0.2 % Pt/H-ZSM-5 was prepared by the same method and submitted for ICP-AEC analysis.

Pt-doped H-zeolite was prepared for analysis using ICP-AEC by dissolving the samples in a mixture of 1 eq conc. HNO_3 with 1 eq conc. HCl in the ratio of 1:3. Table 3.2 displays the Si/Al ratios of zeolites used in this study, as well as their Pt content.

Table 3.2 Si/Al ratios and Pt content of H-Zeolite doped catalysts using ICP-AEC

Catalyst	Si/Al	Pt content (%wt)	
		Theoretical	Experimentally by ICP-AEC
Pt/H-ZSM-5	12	0.5	0.30
Pt/H-ZSM-5	12	0.2	0.06
Pt/H-Beta	12	0.5	0.39
Pt/H-Y	15	0.5	0.45

3.3 Thermogravimetric analysis and carbon deposits

3.3.1 HPW-based catalysts

TGA was used to measure the number of water molecules in the catalysts and their thermal stabilities. Using the TGA measurement, the quantities of metal precursors were precisely calculated to prepare metal-doped CsPW. Table 3.3 summarises the results of submitting HPW-based catalysts to TGA at a heating ramp rate of 20 °C min^{-1} in a nitrogen flow, where KU is the Keggin unit.

Thermal analysis of 30 % HPW is shown in Figure 3.1: about 2 % weight loss was observed at 85 °C for 30 % HPW/SiO_2 catalyst, corresponding to the removal of physisorbed water that strongly depended on the number of hydration waters in the sample. A further loss of weight can be seen at 185 °C, attributed to the dehydration of the six relatively stable molecules of water which are bonded to the acidic protons in $H_3PW_{12}O_{40}$. The third peak, at 480 °C, is due to the loss of all acidic protons and the beginning of the decomposition of the Keggin structure [1-3]. The deprotonation step at 480 °C before Keggin structure collapse is a result of the formation of 1.5 water molecules from the elimination of oxygen atoms from the anion by the protons, as

confirmed by XRD [4]. It is worthy of note that the thermal stability of 30 % HPW/SiO_2 is slightly lower than its parent HPW catalyst [1]. The thermal analysis of HPW can be represented in Scheme 3.1.

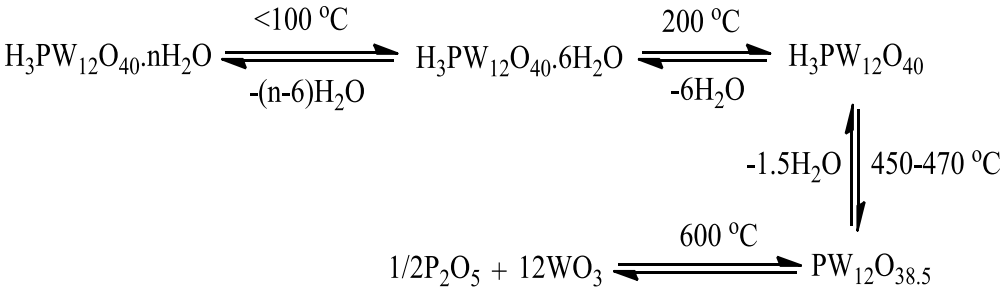

$H_3PW_{12}O_{40}.nH_2O \rightleftharpoons H_3PW_{12}O_{40}.6H_2O \rightleftharpoons H_3PW_{12}O_{40}$

$H_3PW_{12}O_{40} \rightleftharpoons 1/2P_2O_5 + 12WO_3 \rightleftharpoons PW_{12}O_{38.5}$

Scheme 3.1 Thermal decomposition of $H_3PW_{12}O_{40}$ hydrate [2]

Table 3.3 TGA results for HPW-based catalysts

Catalyst	T (°C)	Weight loss		
		%	H_2O, mol/KU	Total (20-700) °C
30 % HPW/SiO_2	85 185 480	2.10 0.60 1.50	1.00 0.25 0.60	4.20
$Cs_{2.5}H_{0.5}PW_{12}O_{40}$	85 550	2.40 0.40	4.50 1.00	2.80
$Cs_3PW_{12}O_{40}$	85	1.50	3.00	1.50
0.5 % Pd/$Cs_{2.5}H_{0.5}PW_{12}O_{40}$	85 430	2.50 1.00	4.00 1.40	3.50
0.5 % Pt/$Cs_{2.5}H_{0.5}PW_{12}O_{40}$	90 480	1.00 0.80	1.50 1.50	1.80
5 % Cu/$Cs_{2.5}H_{0.5}PW_{12}O_{40}$	90 430	0.94 0.20	1.65 0.35	1.14
5 % Ru/$Cs_{2.5}H_{0.5}PW_{12}O_{40}$	100 480	1.10 0.40	1.20 0.25	1.50

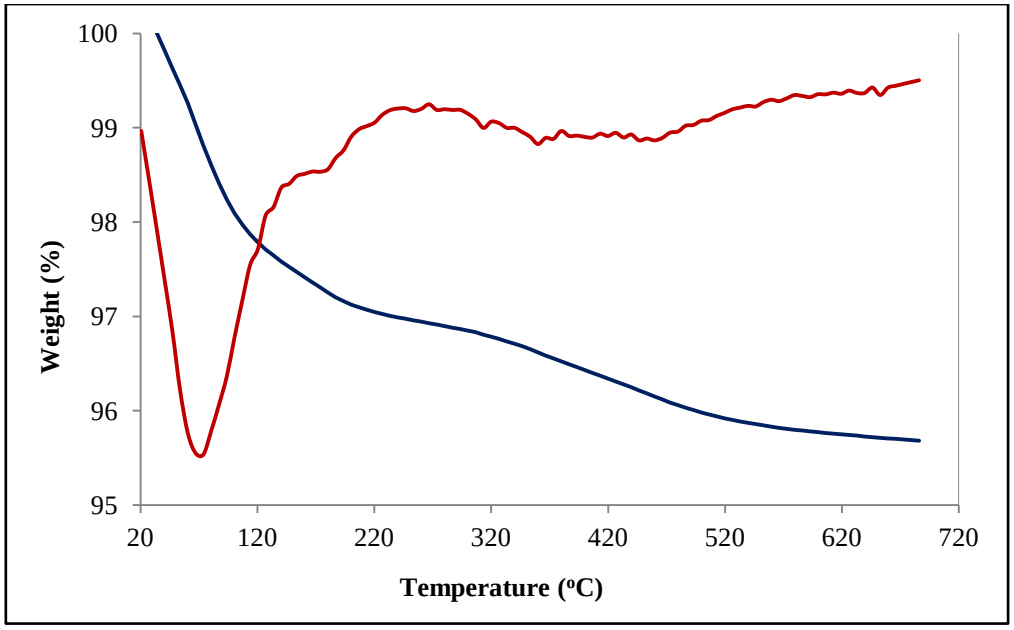

Figure 3.1 TGA of fresh 30 % HPW/SiO_2

$Cs_{2.5}H_{0.5}PW_{12}O_{40}$ (CsPW) has been demonstrated to be insoluble in water and other polar solvents and thermally stable up to 600 °C [1, 5]. Figure 3.2 displays the thermal analysis for CsPW. The 2.4 % weight loss in the range of 20-300 °C corresponds to the departure of about 4.5 molecules of water per Keggin unit, as physisorbed and crystallisation water. The further weight loss observed at 586 °C can be attributed to the deprotonation of the catalyst as described above. As seen in Figures 3.3-3.5, Pd-, Pt-, Cu- and Ru-doped CsPW had similar TGA profiles, which can be attributed to the similarity of preparation conditions.

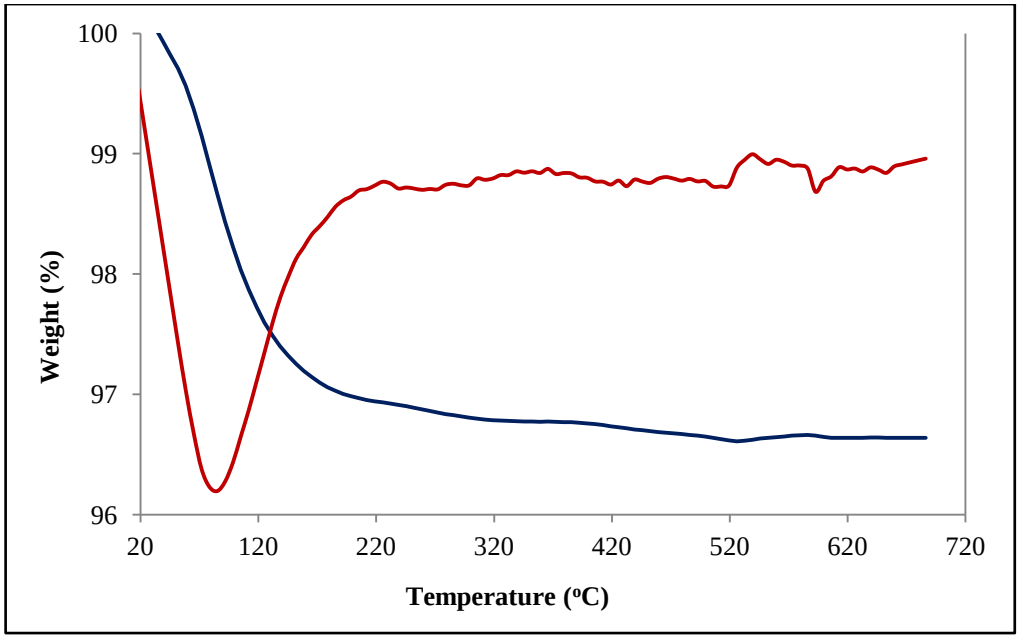

Figure 3.2 TGA of fresh CsPW

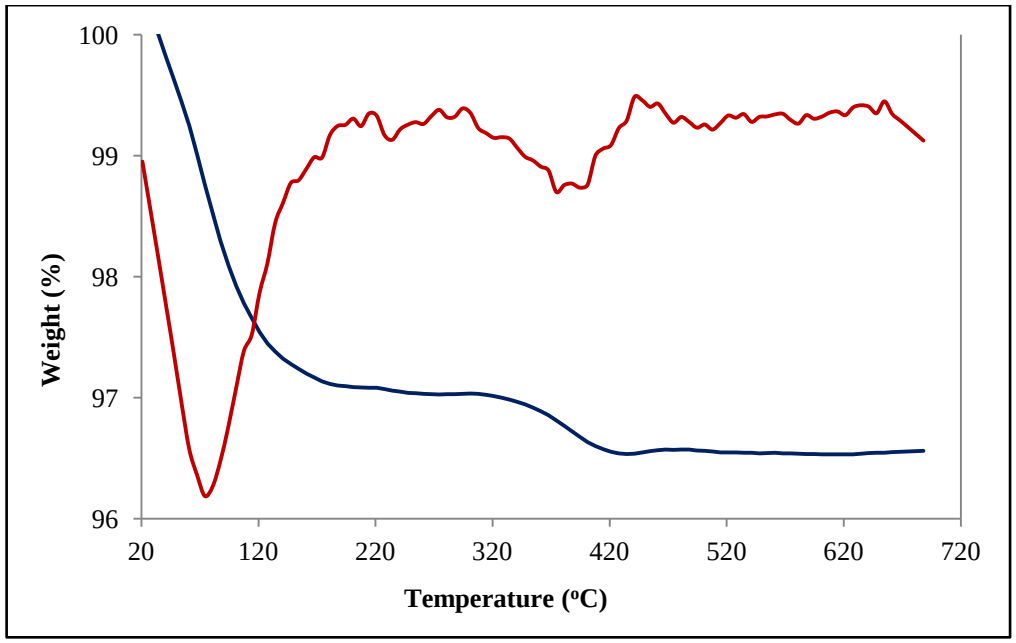

Figure 3.3 TGA of fresh 0.5 % Pd/CsPW

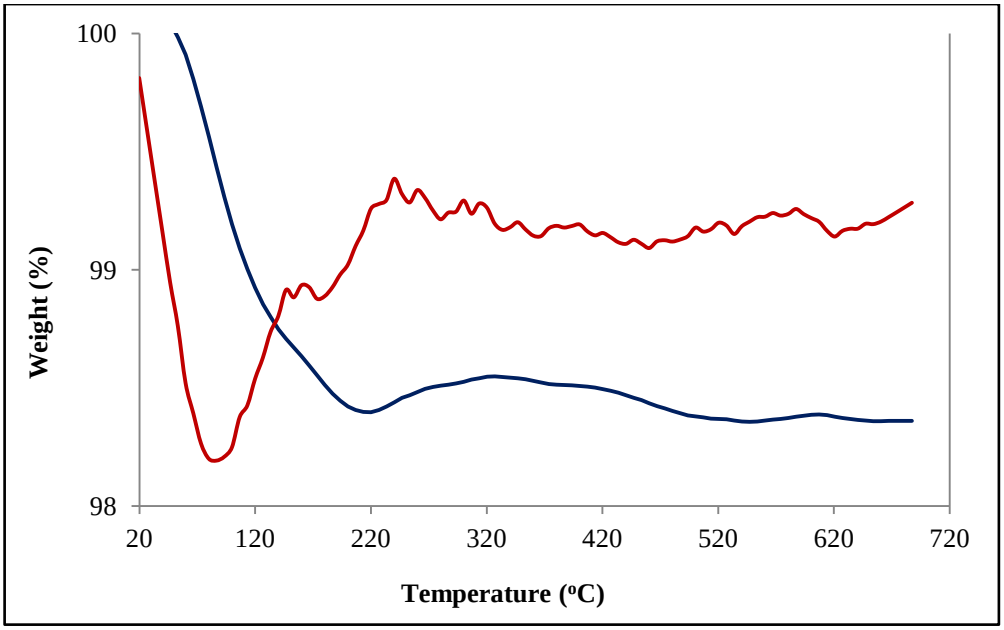

Figure 3.4 TGA of fresh 0.5 % Pt/CsPW

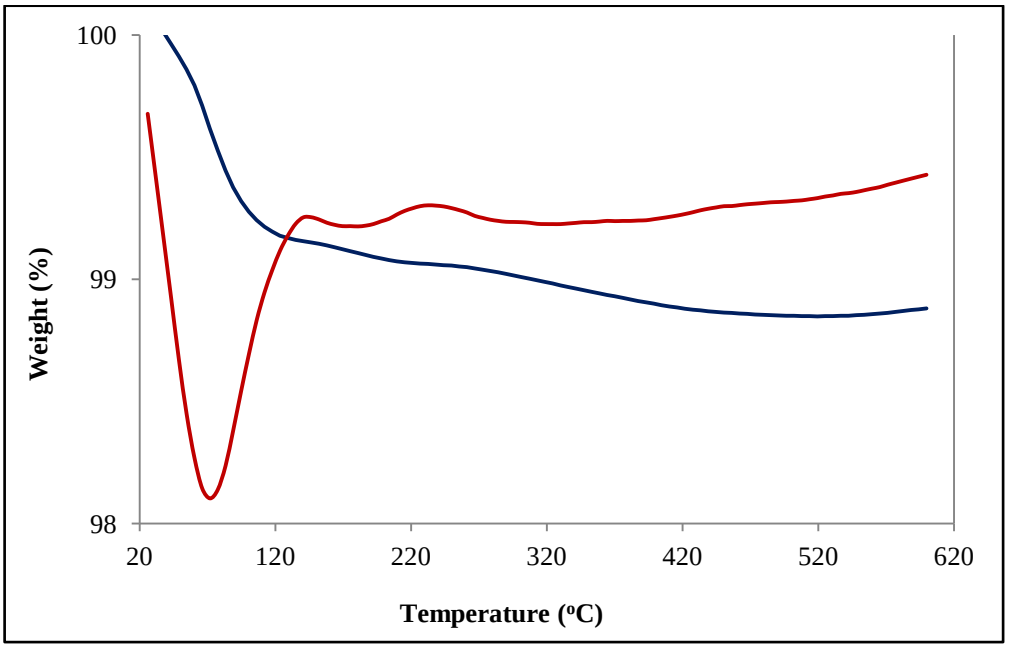

Figure 3.5 TGA of fresh 5.0 % Cu/CsPW

Unlike the other HPW-based catalysts analysed, neutral Cs salt ($Cs_3PW_{12}O_{40}$) did not have a crystallisation water removal peak at 300 °C. This can be explained by the absence of protons, following their complete substitution by Cs atoms. Only one peak can be seen, around 85 °C, due to physisorbed water molecules, as shown in its TGA profile (Figure 3.6).

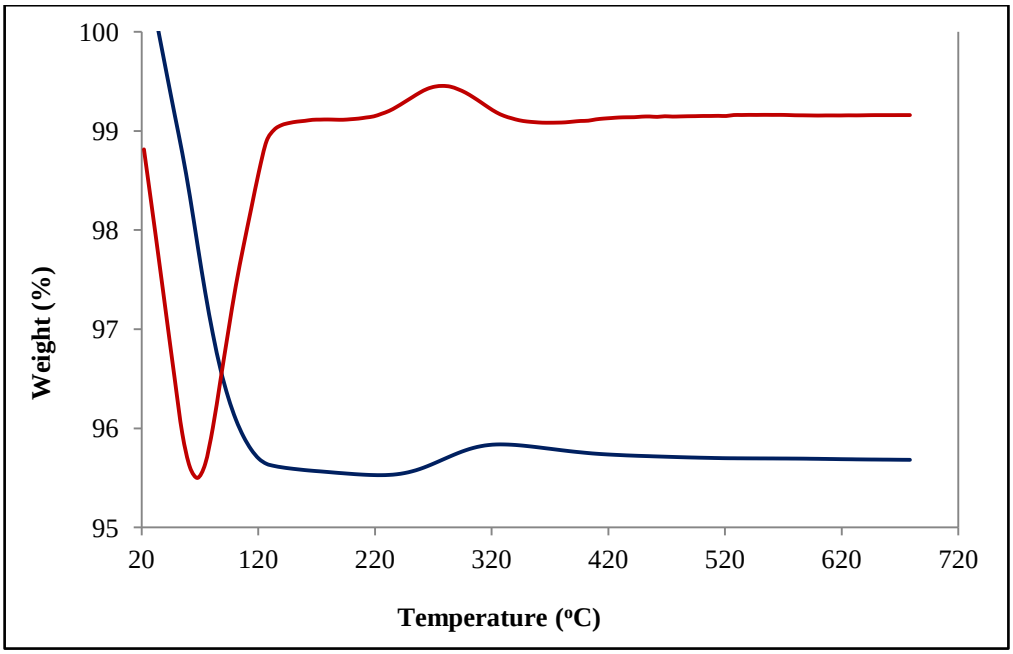

Figure 3.6 TGA of fresh $Cs_3PW_{12}O_{40}$

Substitution of N_2 gas in the TGA instrument by air (TGA/TPO) can be used to determine carbonaceous deposits on spent HPW-based catalysts after reaction to study the amount and nature of coking [6, 7]. As is shown in Figure 3.7, all catalysts used in the gas phase deoxygenation of propionic acid had an obvious peak before 150 °C attributed to the desorption of hydration water, which is produced as a by-product in this reaction. In addition, there are peaks before 350 °C that can be explained by the burning of aliphatic carbonaceous deposits (soft coke). This type of carbon deposit can

be treated by burning the HPW catalyst in air below its decomposition temperature to regenerate it [2, 6, 7]. All spent catalysts, except 5.0 % Cu/CsPW, had obvious peaks at 520 °C, which can be attributed to polyaromatic carbonaceous deposits (hard coke), which are difficult to treat in HPW-based catalysts [2, 6]. As demonstrated by combustion analysis, when CsPW catalysts were doped with metals, the amount of carbonaceous deposits decreased [6, 8].

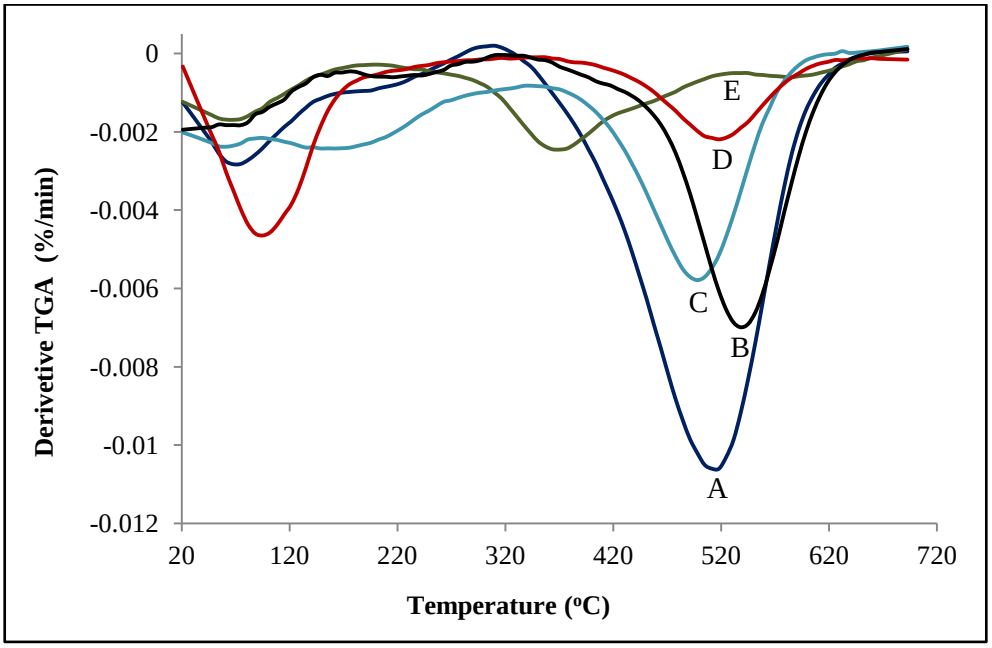

Figure 3.7 TG/TPO analysis for spent HPW based catalysts after deoxygenation of propionic acid at (400 °C, 4 h): (A) 0.5 % Pt/CsPW, (B) 0.5 % Pd/CsPW, (C) $Cs_3PW_{12}O_{40}$, (D) 30 % HPW/SiO_2, (E) 5.0 % Cu/CsPW

Table 3.4 shows the total amount of carbon deposits in the spent catalysts used for the gas phase deoxygenation of propionic acid at 400 °C/4 h using C and H combustion analysis.

Table 3.4 C and H combustion analysis for spent HPW-based catalysts used in the gas phase deoxygenation of propionic acid at (400 °C, 4 h)

Catalyst	C (%)	H (%)
CsPW	4.43	0.54
0.5 % Pd/CsPW	2.65	0.49
0.5 % Pt/CsPW	2.83	0.48
5.0 % Cu/CsPW	2.76	0.18
30 % HPW/SiO_2	2.80	0.80
$Cs_3PW_{12}O_{40}$	3.00	0.20

Metal-doped CsPW catalysts were tested as bifunctional catalysts in the gas phase hydrodeoxygenation of MIBK. 0.5% Pt and 5% Ru supported on CsPW showed high activity toward the desirable product. Different Pt loadings on CsPW were also prepared to study the effect of Pt loading in MIBK hydrodeoxygenation. 0.5 % Pt/CsPW and $Cr_2Cu_2O_5$ were chosen for DIBK hydrodeoxygenation. The resulting carbon deposits on these catalysts are listed in Table 3.5. The amount of carbonaceous deposits was in the range of 0.5-1.5 % for spent Pt/CsPW and around 2 % for spent $Cr_2Cu_2O_5$ after hydrodeoxygenation of DIBK.

Table 3.5 C and H combustion analysis for spent Pt-doped CsPW and $Cr_2Cu_2O_5$ catalysts after hydrodeoxygenation of MIBK and DIBK at 100 °C/ 6 h.

Catalyst	C (%)	H (%)
0.25 % Pt/ CsPW[a]	1.00	0.10
0.5 % Pt/ CsPW[a]	1.24	0.08
1.0 % Pt/ CsPW[a]	0.60	0.08
5.0 % Ru/ CsPW[a]	1.40	0.15
0.5 % Pt/ CsPW[b]	1.27	0.15
$Cr_2Cu_2O_5$[b,c]	1.84	0.30

a) After hydrogenation of MIBK.

b) After hydrogenation of DIBK.

c) After reaction at 300 °C

3.3.2 Pt-doped H-zeolites

Zeolites are thermally stable up to 1300 °C depending on their composition, in particular the ratio of silica to aluminium oxide. More energy is required to break the Si-O bond than to break the Al-O bond; therefore the thermal stability of zeolites with a low silica content is lower than those with a high Si content. It has been found by TGA/DTG that zeolites with an Si/Al ratio above 3.8 are always thermally stable, while zeolites with Si/Al ≤ 1.28 are unstable [9].

Three types of H-zeolite doped with Pt were used in the gas phase hydrodeoxygenation of MIBK: H-ZSM-5 (two loading amounts), H-Beta and H-Y. Their Si/Al ratios were 12, 12 and 15 respectively, making them thermally stable at the temperatures tested. Table 3.6 provides a summary of the TGA results of Pt-doped H-zeolites.

Table 3.6 TGA results for Pt-doped H-zeolites

Catalyst	Weight loss (%)		
	T (20-200 °C)	T (250-700 °C)	Total T (30-700 °C)
0.30 % Pt/H-ZSM-5	4.8	1.2	6.0
0.06 % Pt/H-ZSM-5	4.3	1.1	5.4
0.39 % Pt/H-Beta	10.1	1.9	12.0
0.45 % Pt/H-Y	8.1	1.2	10.3

As can be seen from the TG/DTG analysis profiles of Pt-doped H-zeolites in Figures 3.8-3.10, the amount of physisorbed water on the external surface of catalysts appeared to fall in the temperature range of 20-200 °C. Further changes to the TGA curves above 250 °C are attributed to the removal of adsorbed water molecules within the micropores of the zeolites [10].

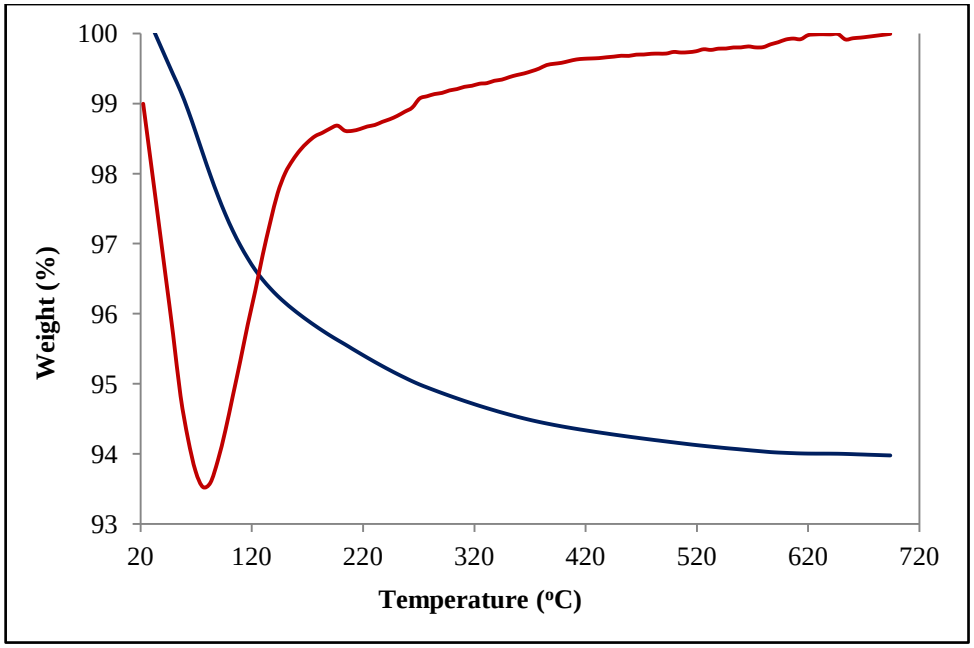

Figure 3.8 TGA profile of fresh 0.30 % Pt/H-ZSM-5

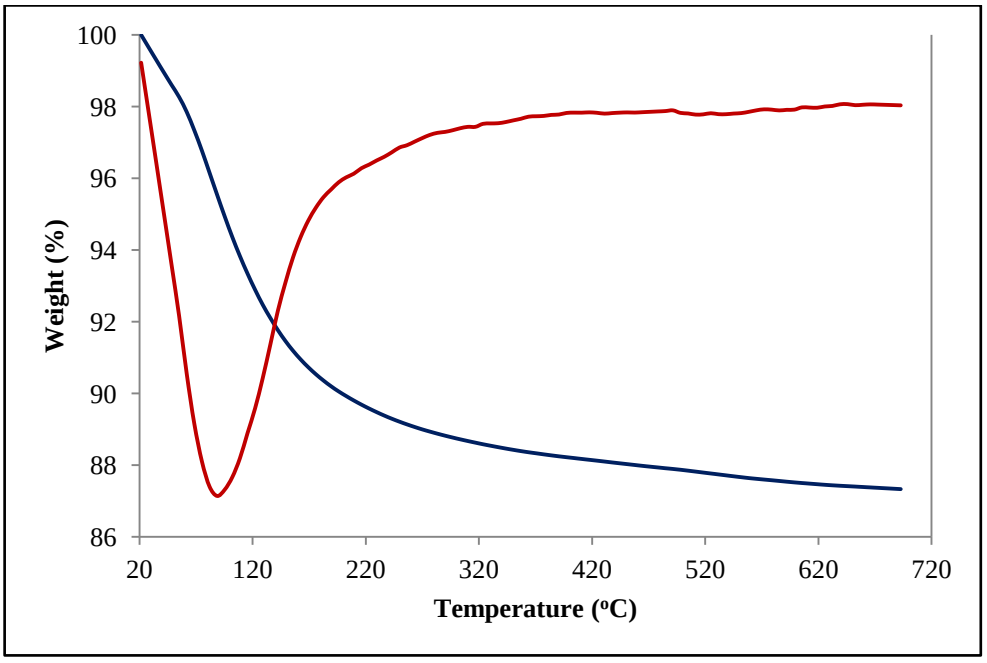

Figure 3.9 TGA profile of fresh 0.39 % Pt/H-Beta

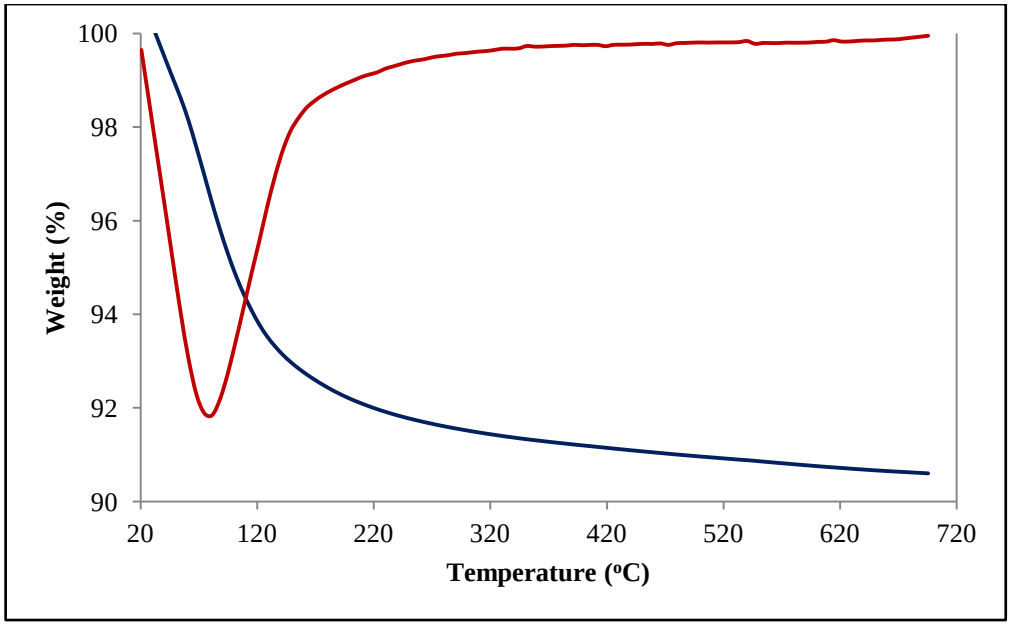

Figure 3.10 TGA profile of fresh 0.45 % Pt/H-Y

DTG/TPO analysis of spent 0.30 % Pt/HZSM-5, 0.39 % Pt/H-Beta and 0.45 % Pt/H-Y are shown in Figure 3.11 after reaction in the gas phase hydrodeoxygenation of MIBK at 200 °C/ 6 h. The spent catalysts lost hydration water below 170 °C amounting to about 3.9 % of their weight, as shown in Table 3.7. Furthermore, obvious peaks appeared for all catalysts used, in the range of 170-400 °C, which can be explained by the presence of aliphatic carbonaceous deposits. The profiles of spent Pt-doped H-Beta and H-Y have broad peaks in the range of 400-700 °C, attributed to polyaromatic carbonaceous deposits on these catalysts. In contrast, the TPO profile of Pt/H-ZSM-5 shows no weight loss in this region. The formation of hard coke can be explained by the formation of C_{6+} condensation by-products using 0.39 % Pt/H-Beta and 0.45 % Pt/H-Y catalysts. The amount of carbon formed increased with the pore size of the zeolites: H-ZSM-5 (5.5 Å) < H-Beta (7.6 x 6.4 Å) < H-Y (7.5 Å). This order was confirmed by C and H elemental analysis, as shown in Table 3.8.

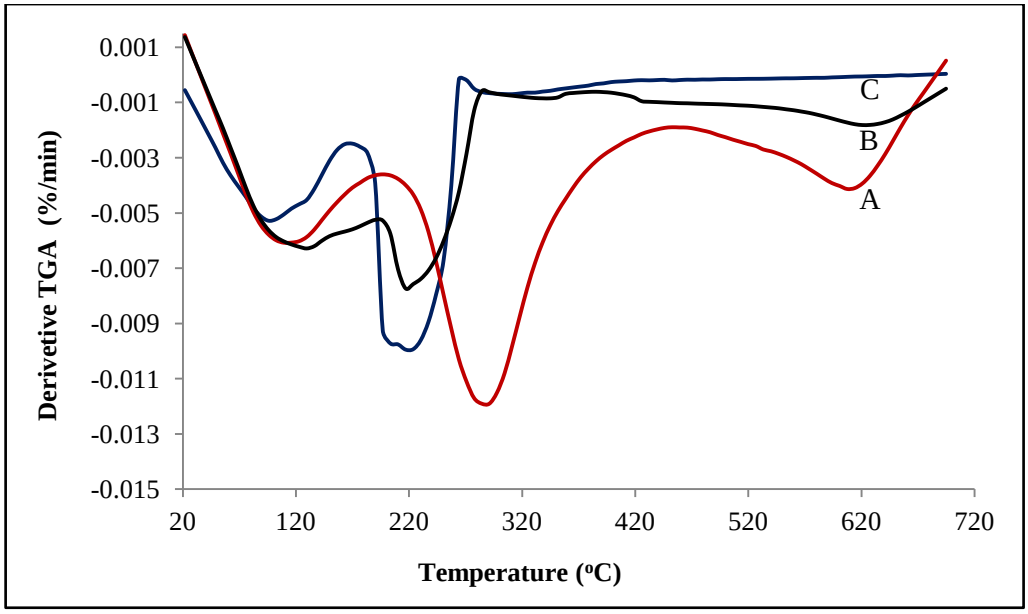

Figure 3.11 TG/TPO profile of spent Pt-doped H-zeolites used in the gas phase hydrodeoxygenation of MIBK at 200 °C/ 6 h: (A) 0.39 % Pt/H-Beta, (B) 0.45 % Pt/H-Y, (C) 0.30 % Pt/HZSM-5

Table 3.7 TG/TPO analysis of spent Pt/H-zeolites used in the gas phase hydrodeoxygenation of MIBK at 200 °C/ 6 h.

Catalyst	Weight loss (%)		
	T (30-170 °C)	T (170-400 °C)	T (400-700 °C)
0.30 % Pt/H-ZSM-5	3.9	6.6	0
0.39 % Pt/H-Beta	3.9	8.1	4.3
0.45 % Pt/H-Y	3.9	8.5	4.1

Table 3.8 C and H combustion analysis of spent Pt/H-zeolites used in the gas phase hydrodeoxygenation of MIBK at 200 °C/ 6 h.

Catalyst	C (%)	H (%)
0.30 % Pt/H-ZSM5	5.9	0.94
0.39 % Pt/H-Beta	10.5	1.79
0.45 % Pt/H-Y	11.9	1.72

3.4 Surface area and porosity studies

3.4.1 Introduction

Nitrogen physisorption at -196 °C has been widely utilised to measure catalyst surface area and porosity. Initially, determination of the adsorption isotherm is vital to recognise the type of solid catalyst, by plotting the volume of nitrogen adsorbed *versus* its relative pressure. The isotherm obtained has a unique shape that depends on the porous texture of the solid catalyst. IUPAC classifies six types of isotherm, as shown in Figure 3.12 [11]. However, only four types, I, II, IV and VI, are usually found in solid catalyst characterisation, representing microporous, macroporous, mesoporous and uniform ultramicroporous solid materials respectively [11-13].

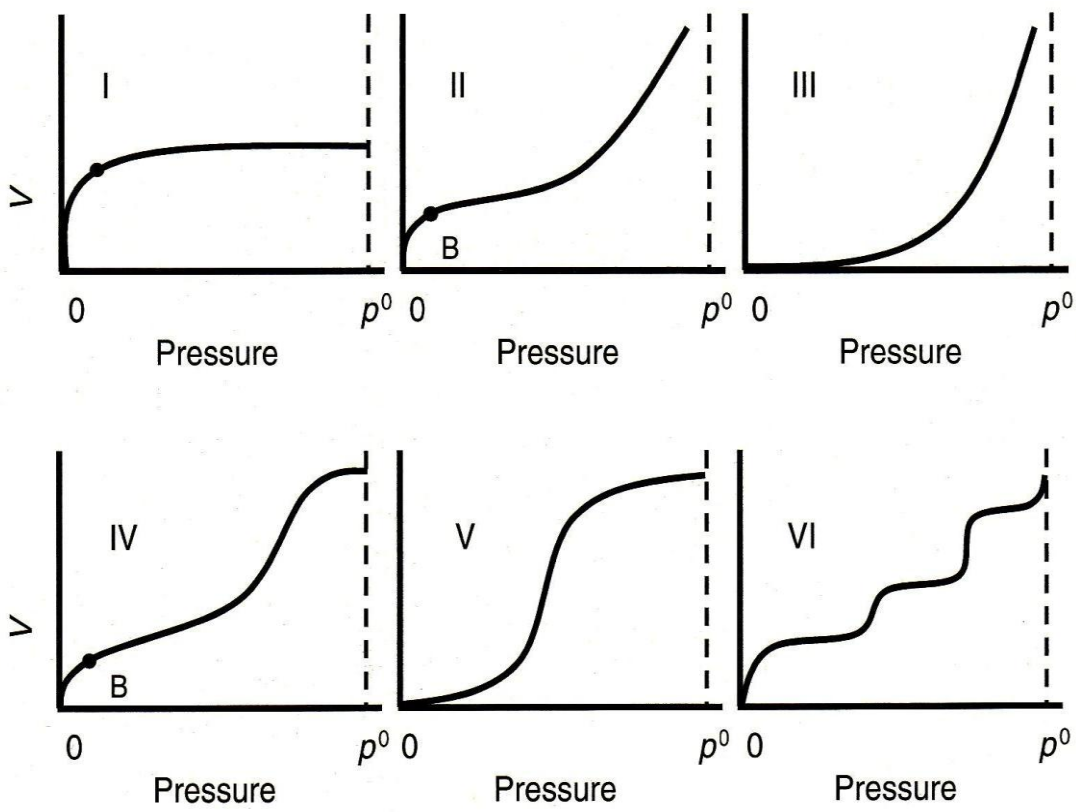

Figure 3.12 The six types of N_2 adsorption isotherm [11]

Regarding macroporous solids (type II), the creation of a monolayer of adsorbed molecules takes place at low relative pressure, whereas at high relative pressure, multilayer adsorption occurs. As pressure rises, the thickness of the adsorbate increases until condensation has been reached.

On mesoporous solids (type IV), the same process happens at low pressure, while at high relative pressure, adsorption in the mesopores leads to the formation of multilayers until condensation occurs. This strongly depends on the solid pore size, the larger mesopore size and the higher condensation pressure. The adsorption continues on the low external surface when the mesopores are completely filled. The most important catalysts are those of type IV, because the majority of substrates are within the mesopore diameter range [11]. HPA catalysts are typical examples of such materials.

On microporous solids (type I), adsorption occurs at very low relative pressure, due to strong interaction between pore walls and adsorbate without capillary condensation in the low relative pressure area (< 0.3). At high relative pressure, the pores are completely filled by interaction between adsorbed molecules. As with macro- and mesoporous solids, when the micropores are filled, adsorption continues on the external surface. Zeolites are prime examples of microporous solids.

In uniform ultramicroporous solids (type VI), the pressure at which adsorption occurs depends on the interaction between the solid surface and the adsorbate. Therefore, the adsorption of a uniform solid takes place at a well defined pressure. The successive steps of the isotherm correspond to adsorption on the first and subsequent monolayers.

Desorption of adsorbed nitrogen occurs after saturation of the adsorbate by releasing adsorbates from the pores and the surface in the opposite direction to adsorption. Nevertheless, the departure of the adsorbates from the mesopores occurs at a pressure lower than that of capillary condensation, giving a hysteresis loop. Regarding the IUPAC classification, four types of hysteresis have been documented, as displayed in Figure 3.13 [12].

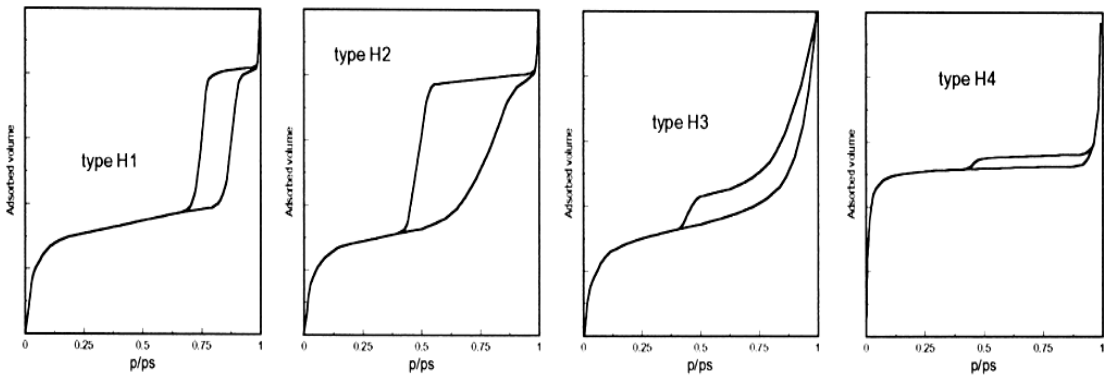

Figure 3.13 The four hysteresis types usually observed in N_2 adsorption [12]

Types H1 and H2 hysteresis are formed when the analysed solids consist of particles crossed by channels close to cylindrical in shape, or of spheroidal aggregates (consolidated) or agglomerates (unconsolidated). In catalysts showing an H1 hysteresis, pores of uniform size and shape are presented, while those displaying an H2 hysteresis have non-uniform size and shape. These two hysteresis loops are related to size differences between pore mouth and pore body (e.g. ink-bottle-shaped pores) and/or a different behaviour in adsorption and desorption close to cylindrical pores. The majority of mesoporous materials such as HPAs belong to this hysteresis category [12].

Types H3 and H4 hysteresis are associated with solid materials that consist of aggregates or agglomerates of particles producing slit-shaped pores (plates or edged particles like cubes). Pores of uniform size and/or shape result in H4 hysteresis, while

H3 hysteresis corresponds to non-uniform pore size and/or shape. Zeolites are typical examples of this hysteresis class.

In some cases, no hysteresis loop is observed and this is attributed to solids with blind cylindrical, cone-shaped and wedge-shaped pores. However, in practice, only materials with a much reduced hysteresis will be observed, because of their irregular pore shapes and sizes. As for the closure of a hysteresis isotherm, this takes place at a low relative pressure of 0.42, due to liquid adsorbate properties, regardless of the adsorbent or the pore size distribution.

The methods of measuring the surface area and porosity texture are described in detail in Section 2.4.1. The total surface area of the catalysts under study was determined using the BET method [14]. The Barrett, Joyner, and Halenda (BJH) method was used to calculate pore size distribution and total pore volume [15].

3.4.2 HPW-based catalysts

The surface area and porous texture of bulk HPW, silica-supported HPW and their Cs salts have been extensively studied and well-documented [1, 5, 16, 17]. HPW typically has a very low surface area, in the range of 1-10 $m^2 g^{-1}$, and is highly soluble in water. The BET surface area and porous texture of HPW-based catalysts used in this study are listed in Table 3.9, which also lists SiO_2-supported metals and some selected commercial catalysts for comparison. All catalysts were calcined under vacuum at 250 °C. As can be seen from the table, the HPW-based catalysts were all mesoporous solids with average pore diameter of 26-96 Å. CsPW and their doped metals have a relatively high surface area (75-111 $m^2 g^{-1}$) and low porosities. These results are in

agreement with the literature [18-21]. SiO_2-supported catalysts had larger surface areas (160-287 $m^2\ g^{-1}$) and higher porosities.

Table 3.9 Results of N_2 adsorption measurement for HPW-based catalysts used in this work, together with silica-supported metals and commercial metal-doped activated carbon and copper chromite

Catalyst[a]	S_{BET}[b] ($m^2\ g^{-1}$)	Pore diameter[c] (Å)	Pore volume[d] ($cm^3\ g^{-1}$)
30 % HPW/SiO_2	160	96	0.40
CsPW	111	26	0.07
$Cs_3PW_{12}O_{40}$	124	48	0.08
0.5 % Pd/CsPW	87	29	0.06
0.5 % Pt/CsPW	100	28	0.07
5.0 % Cu/CsPW	75	30	0.06
0.5 % Ru/CsPW	108	30	0.09
5.0 % Ru/CsPW	105	36	0.09
0.5 % Pd/SiO_2	255	106	0.68
0.5 % Pt/SiO_2	287	74	0.52
5 % Cu/SiO_2	251	118	0.74
$Cr_2Cu_2O_5$[e,f]	55	93	0.13
10 % Pt/C[f]	801	29	0.58
5 % Pd/C[f]	924	25	0.58
10 % Pd/C[f]	823	28	0.57
5 % Ru/C[f]	792	32	0.64

a) HPW = $H_3PW_{12}O_{40}$, CsPW = $Cs_{2.5}H_{0.5}PW_{12}O_{40}$

b) BET surface area

c) Average BET pore diameter

d) Single point total pore volume

e) After reduction in H_2 at 400 °C for 2 h

f) Commercial catalysts used in MIBK and DIBK hydrodeoxygenation

The BET isotherm of 30 % HPW/SiO_2 is displayed in Figure 3.14, which shows that this catalyst was of isotherm type IV with a type H3 hysteresis loop, representing a mesoporous solid non-uniform in size and/or shape. Figure 3.15 shows that the CsPW catalyst was of isotherm type IV, with a type H2 hysteresis loop, indicating the existence of a mesoporous material of non-uniform shape. Additionally, the steep increase in nitrogen adsorption in the low pressure region indicates the presence of micropores as well as mesopores in CsPW. This result is in agreement with previous studies [22-24]. As can be seen from Figure 3.16, the pore size distribution of CsPW obtained from the BJH method shows a sharp peak at about 35 Å diameter. This result is comparable to a previous study of CsPW [25].

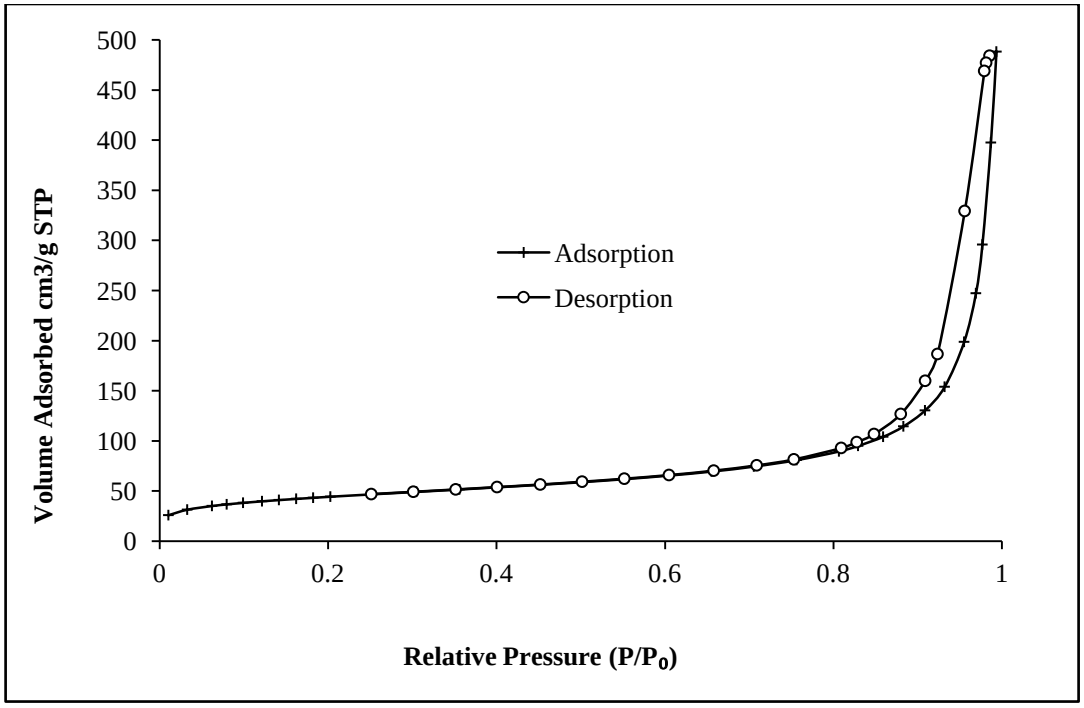

Figure 3.14 N_2 adsorption on 30 % HPW/SiO_2

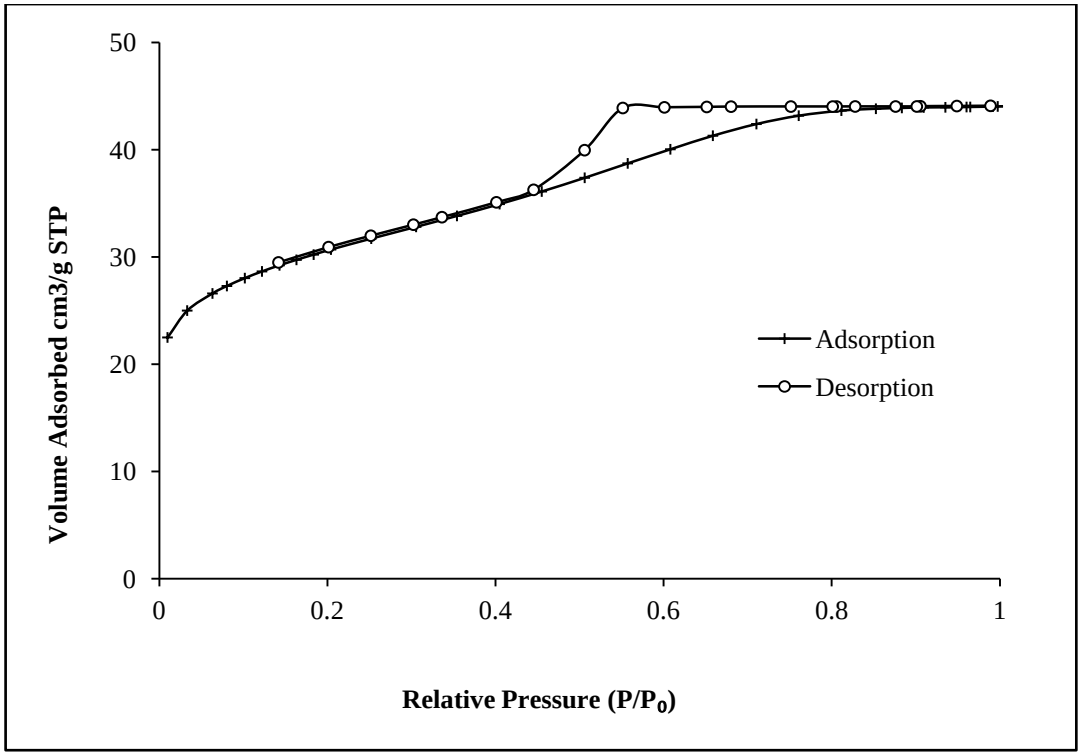

Figure 3.15 N_2 adsorption on CsPW

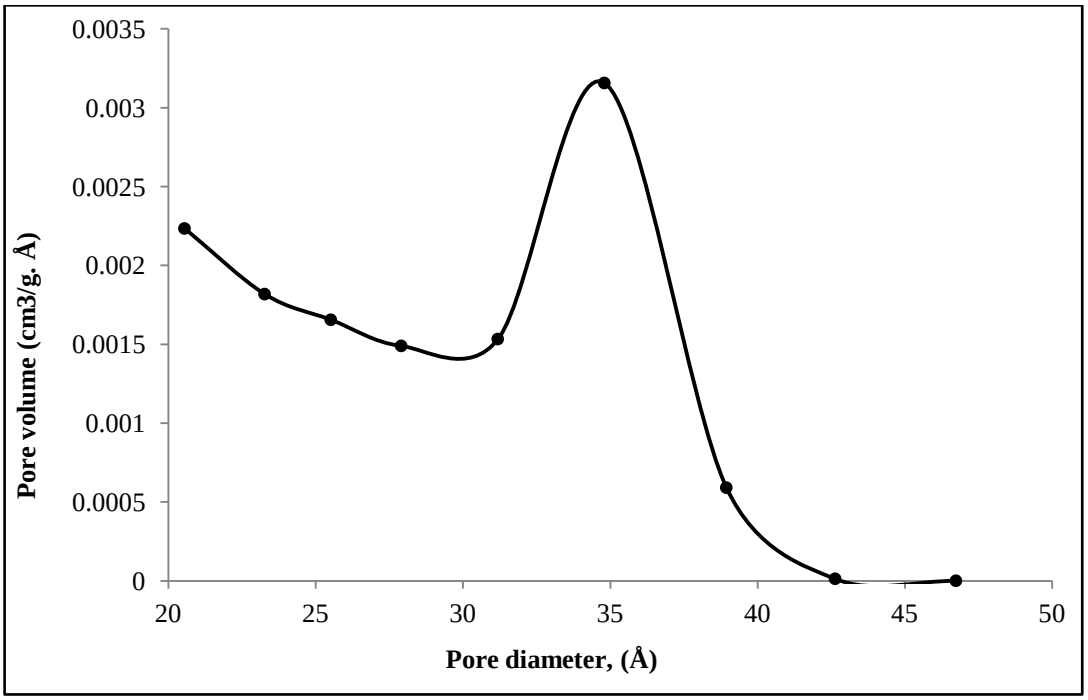

Figure 3.16 Pore size distribution of CsPW

Preparation of metal-doped CsPW differs in using water or benzene as solvent. However, no significant changes are shown in the N_2 adsorption isotherms of metal-doped CsPW catalysts, as shown in Figures 3.17-3.20. On the other hand, the BET surface area of Pd-, Pt-, Cu- and Ru-doped CsPW were lower than this in bulk CsPW, as expected. This is evidence of the presence of metal on the surface of the doped CsPW catalysts.

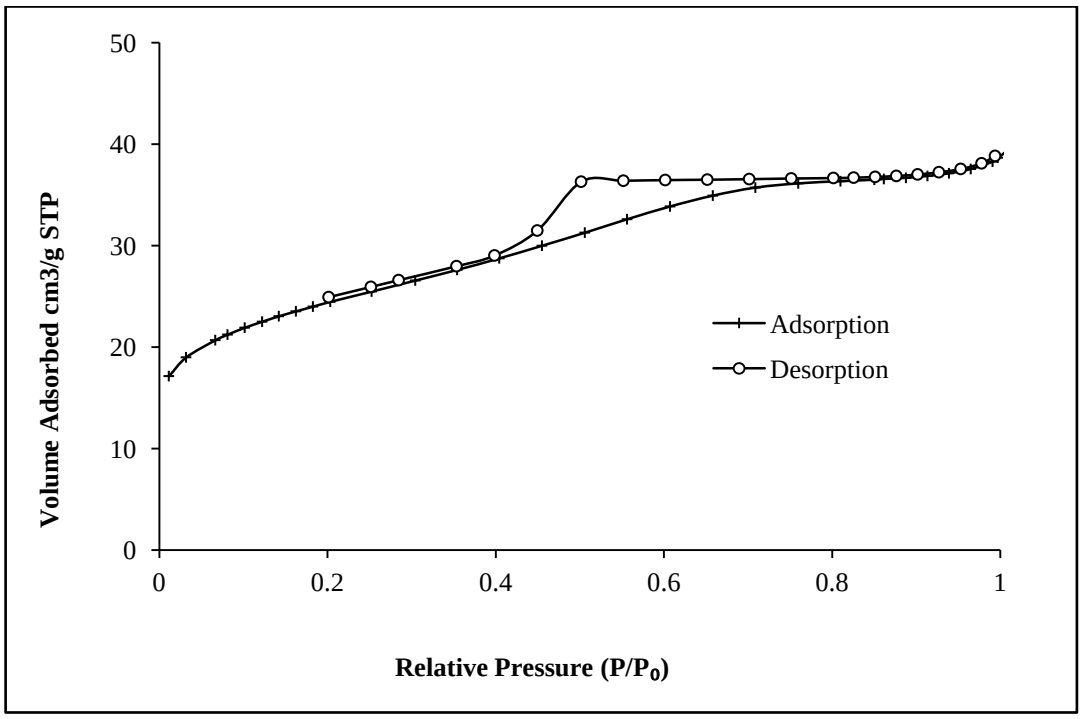

Figure 3.17 N_2 adsorption on 0.5 % Pd/CsPW

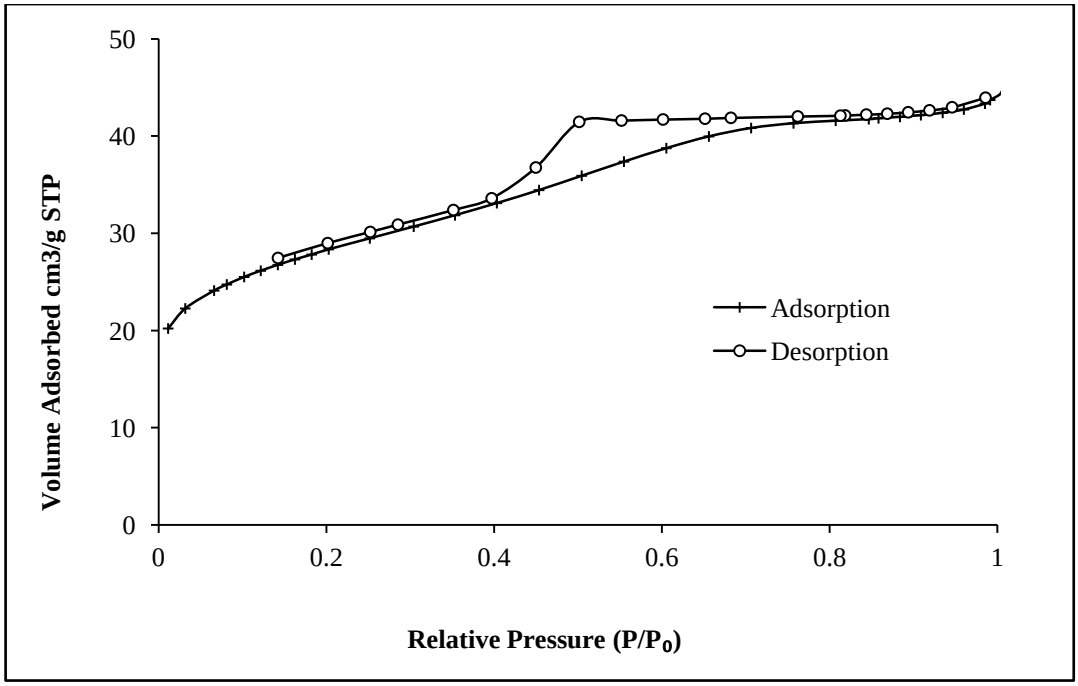

Figure 3.18 N_2 adsorption on 0.5 % Pt/CsPW

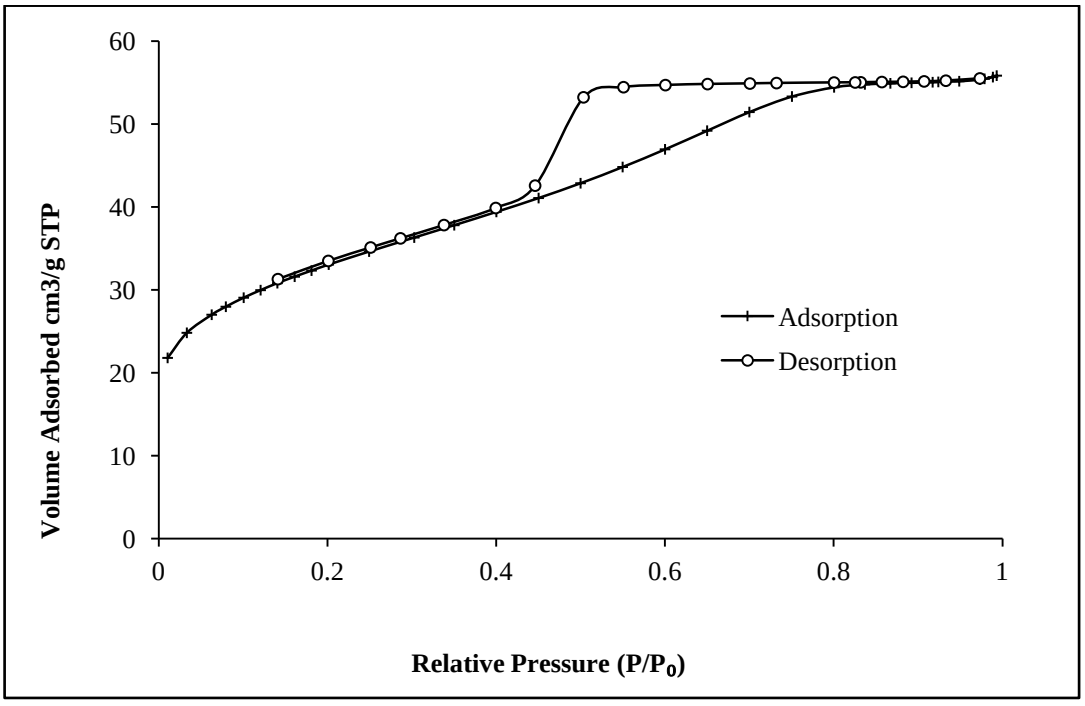

Figure 3.19 N_2 adsorption on 0.5 % Ru/CsPW

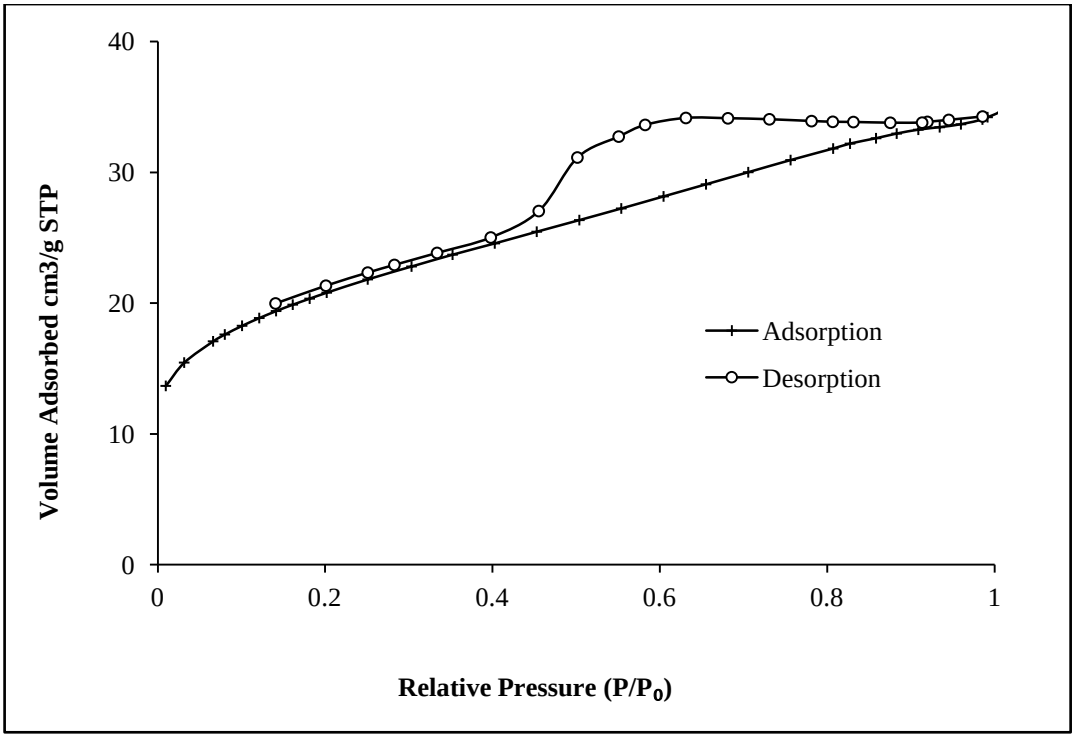

Figure 3.20 N_2 adsorption on 5.0 % Cu/CsPW

The BET surface area and porous texture of spent 30 % HPW/SiO_2, CsPW and Pd-, Pt- and Cu-doped CsPW were measured after deoxygenation with propionic acid at 400 °C. Significant reductions in surface area were observed in CsPW and the doped catalysts, as shown in Table 3.10. There was no change in the pore diameter of any spent catalyst at this temperature, except for a slight change in the case of 30 % HPW/SiO_2, accompanied by a sharp decrease in pore volume compared to fresh catalysts. This can be explained by the formation of carbonaceous deposits inside the catalyst pores after the reaction.

Table 3.10 N_2 adsorption measurements for spent 30 % HPW/SiO_2, CsPW and their metal-doped catalysts after propionic acid deoxygenation in the gas phase[a]

Catalyst[b]	S_{BET}[c] ($m^2\ g^{-1}$)	Pore diameter[d] (Å)	Pore volume[e] ($cm^3\ g^{-1}$)
30 % HPW/SiO_2	137	89	0.30
CsPW	21	28	0.02
0.5 % Pd/CsPW	27	27	0.03
0.5 % Pt/CsPW	17	25	0.02
5.0 % Cu/CsPW	35	26	0.03

a) Reaction conditions: 400° C, 1 bar, 10 ml min^{-1} H_2, 4 h, 2 % vol, propionic acid and 0.2 g catalyst

b) Catalyst dried under N_2 at 400 °C for at least 2 hours before degassing at 250 °C in BET instrument

c) BET surface area

d) Average BET pore diameter

e) Single point total pore volume

Platinum-doped CsPW was utilised in loadings of 0.25, 0.5 and 1.0 % wt in the gas phase hydrodeoxygenation of MIBK. Table 3.11 displays the characterisation data for these catalysts, including BET analysis of texture (surface area, pore diameter and pore volume). No significant change was found in surface area or porous texture of Pt-doped CsPW catalysts after MIBK hydrogenation reaction at 100 °C.

Table 3.11 N_2 adsorption results for fresh and spent Pt-doped CsPW after MIBK hydrodeoxygenation in the gas phase[a]

Catalyst[b]	S_{BET}[c] ($m^2\ g^{-1}$)	Pore diameter[d] (Å)	Pore volume[e] ($cm^3\ g^{-1}$)
0.25 % Pt/CsPW	101 (80)	26 (26)	0.06 (0.05)
0.50 % Pt/CsPW	100 (67)	28 (28)	0.07 (0.05)
1.0 % Pt/CsPW	106 (90)	25 (26)	0.07 (0.05)

a) In brackets are the values for spent catalysts after reaction conditions: 100° C, 1 bar, 20 ml/min H_2, 14 h, 3.6%Vol. MIBK, and 0.2g catalyst

b) The catalyst was dried under N_2 at 100 °C for at least 2 hours before degassing at 250 °C in BET instrument

c) BET surface area

d) Average BET pore diameter

e) Single point total pore volume

3.4.3 Doped-zeolite catalysts

ZSM-5 is an important zeolite in terms of its application. It consists of two vertically intersecting 10-ring channel structures that produce a three-dimensional framework with average pore size of 5.5 Å. Zeolite Beta has pore system with a minimum of 12 rings, producing openings with average pore size of 7.6 × 6.4 Å. Zeolite Y has pore channels wider than those of ZSM-5 and Beta, its average pore size being 7.5 Å. The 12-ring pore openings and 3-dimensional channel structure make this type of zeolite thermally stable and convenient for many catalytic applications [26-28].

The nitrogen adsorption isotherms of 0.30 % Pt/H-ZSM-5, 0.39 % Pt/H-Beta and 0.45 % Pt/H-Y are shown in Figures 3.21-3.23. Both Pt-doped H-ZSM-5 and H-Y yielded type I isotherms with H4 hysteresis loops, indicating uniform microporous solids with slit-shaped pores. Pt-doped H-Beta was found to be of the same isotherm type, but with an H3 hysteresis loop, representing a nonuniform microporous material [12, 28]. As NH_4-Beta was calcined to convert it into H form, the calcination conditions may have affected the shape and distribution of the pores. Figure 3.24 shows the pore distribution of Pt-doped H-zeolites, all of which had mesopores at about 40 Å as well as micropores. Pt/H-Beta showed a much broader spread in the region of mesopores, indicating that the calcination step, converting zeolite Beta to the H-form, had changed the pore distribution of this catalyst.

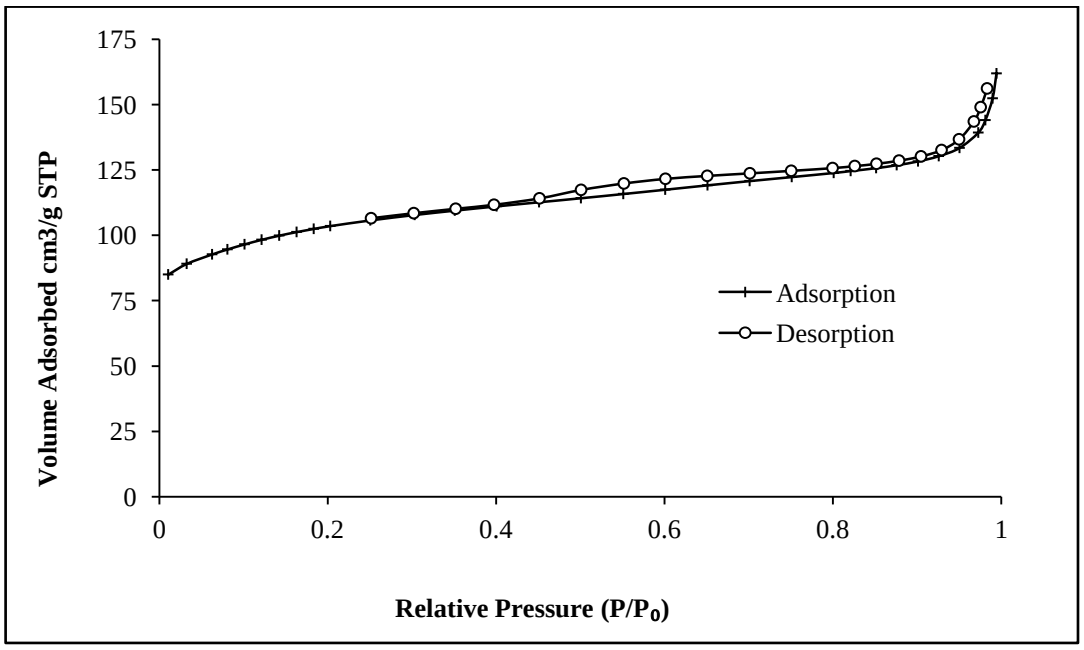

Figure 3.21 N_2 adsorption of 0.30%Pt/H-ZSM-5

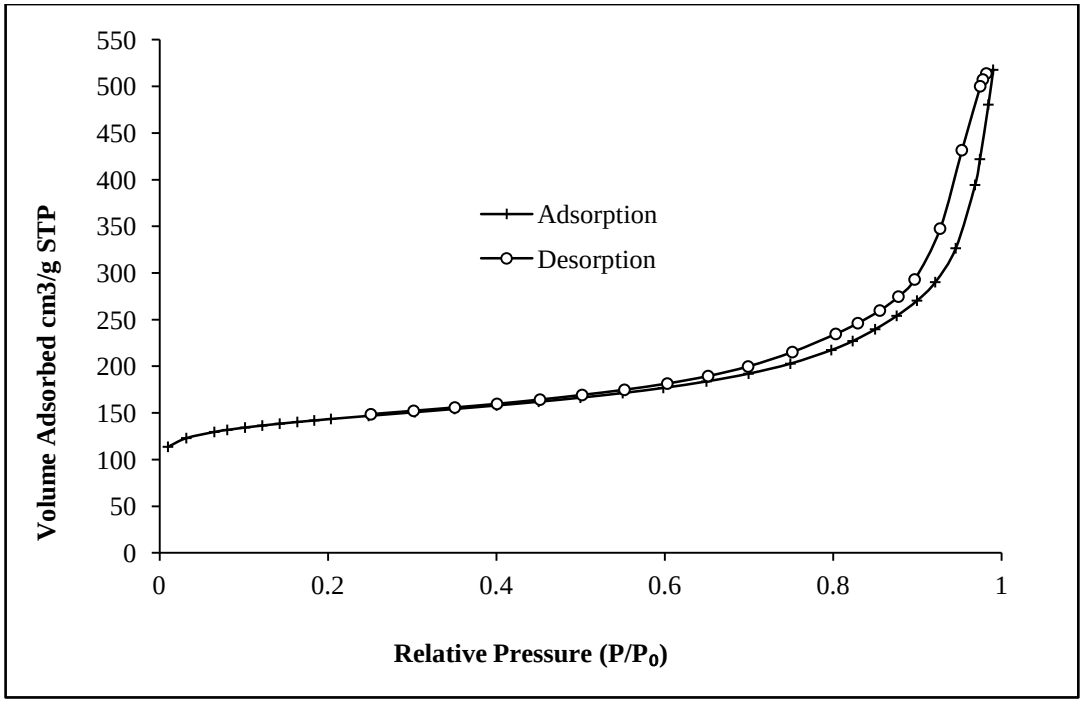

Figure 3.22 N_2 adsorption of 0.39%Pt/H-Beta

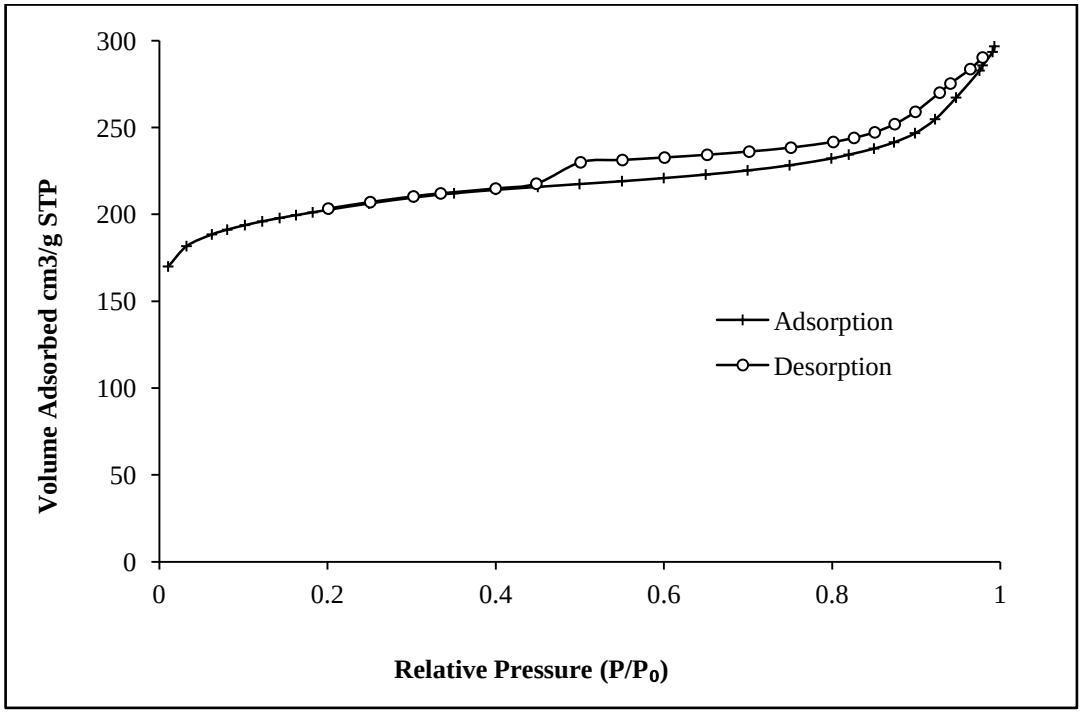

Figure 3.23 N_2 adsorption of 0.45%Pt/H-Y

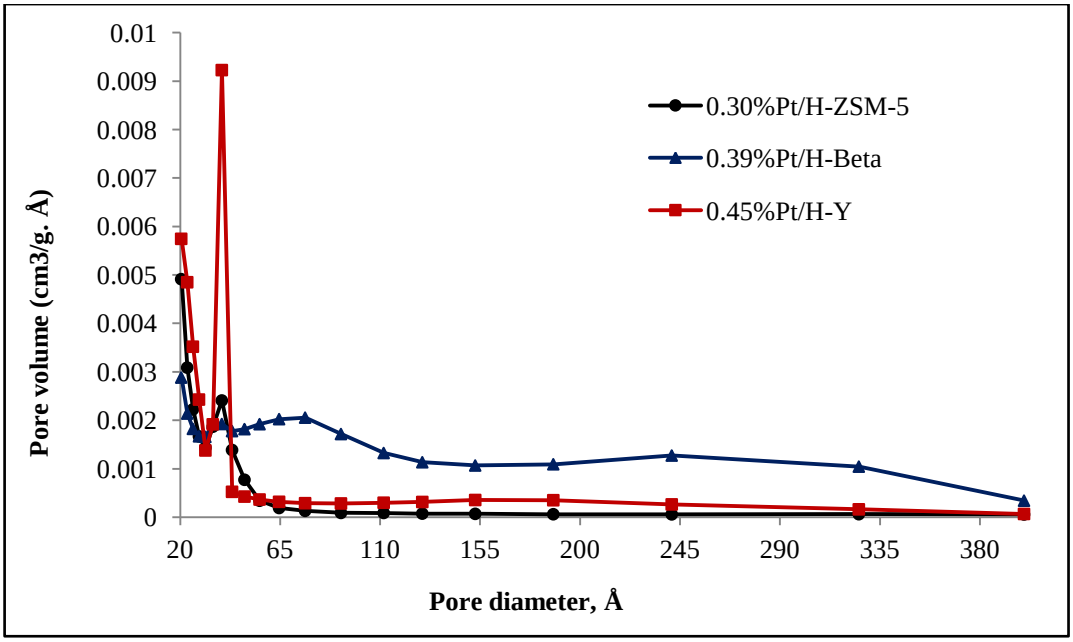

Figure 3.24 Pore size distribution of Pt doped H-zeolites

Table 3.12 is a summary of surface areas and porous texture for Pt-doped H-zeolite catalysts prepared and tested for hydrodeoxygenation of MIBK in the gas phase.

Table 3.12 Results of N_2 adsorption analysis for fresh Pt-doped H-zeolites used in the gas phase hydrodeoxygenation of MIBK

Catalyst	S_{BET} (m^2g^{-1})	Pore diameter[c] (Å)	Pore volume[d] (cm^3g^{-1})
0.30 % Pt/H-ZSM5	362 (403)[a]	25	0.23
0.06 % Pt/H-ZSM5	357 (403)[a]	24	0.22
0.39 % Pt/H-Beta	491 (608)[b]	50	0.61
0.45 % Pt/H-Y	690 (780)[a]	26	0.44

a) BET surface area for hydrogen form of bulk zeolite as received from supplier

b) BET surface area for NH_4^+ form of bulk zeolite as received from supplier, which then was calcined to 550 °C under air to obtain the hydrogen form

c) Average pore diameter by BET method

d) Single point total pore volume

3.5 Metal dispersion of bifunctional catalysts

3.5.1 Metal-doped CsPW and SiO_2

0.5 % Pd-, 0.5 % Pt- and 5.0 % Cu-doped CsPW and SiO_2 were used in the gas phase deoxygenation of propionic acid. The loading was higher for Cu catalysts to compensate for their lower catalytic activity compared to Pd and Pt. In addition, 0.5 % and 5.0 % Ru-doped CsPW were tested in the gas phase hydrodeoxygenation of MIBK. N_2O chemisorption followed by H_2-TPR was used to determine the Cu metal dispersion in 5.0 % Cu/CsPW and 5.0 % Cu/SiO_2. For the Pd-, Pt- and Ru-doped catalysts, the dispersion of these metals was calculated using the pulse H_2 chemisorption method. Hydrogen did not adsorb on CsPW and SiO_2 under such conditions, while no reduction of CsPW in the metal-doped catalysts was observed at 100 °C, as found by TPR (see section 3.7). In addition, XRD and TEM/STEM-EDX were used to estimate metal particle size for some of these catalysts. For instance, the metal particle size of 0.5%Pd/CsPW was measured by STEM-EDX (mean surface particle diameter) [29]. For 5%Cu/SiO_2, the metal particle size was also determined by TEM as well as by XRD using the Scherrer equation, with line broadening assessed as the full width at half maximum intensity (FWHM).

Table 3.13 shows the dispersion of Pd and Pt in fresh and spent catalysts after deoxygenation of propionic acid in the gas phase at 300 °C, determined by H_2 chemisorption. From these data, the average diameter of Pd and Pt particles on CsPW and SiO_2 in fresh catalysts was between 1.5 and 3.3 nm. For the fresh Pd/CsPW, the average diameter of Pd particles obtained from H_2 chemisorption (2.4 nm) was in excellent agreement with the value of 2.5 nm obtained from STEM. Figure 3.25a shows

an STEM-EDX image of this catalyst, with Pd particles in the size range of 0-14 nm. The metal dispersion predictably reduced after reaction, with Pd dispersion reducing to a greater extent than Pt. Pd and Pt nanoparticles on amorphous silica were more stable towards sintering than those on crystalline CsPW, which indicates stronger metal-support interaction with silica.

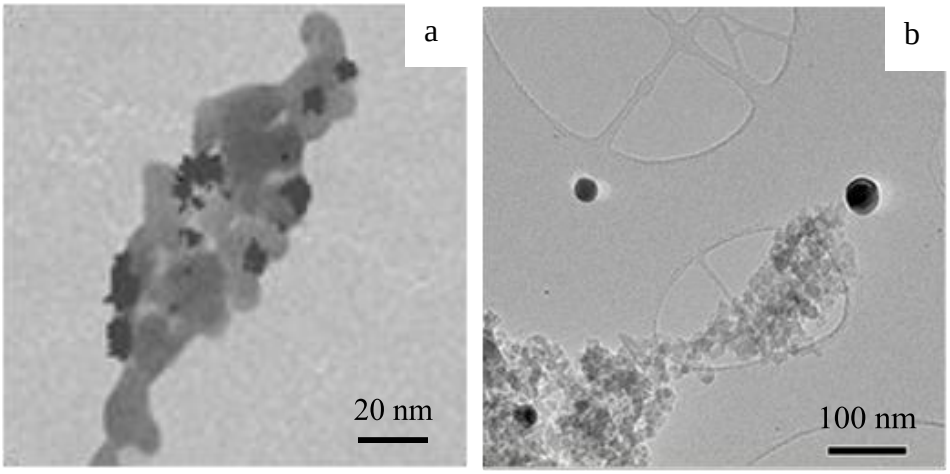

Figure 3.25 STEM-EDX image for fresh 0.5%Pd/CsPW [29] (a) and TEM image for fresh 5%Cu/SiO_2 (b) showing metal particles as dark spots.

From N_2O uptake, Cu dispersion on SiO_2, D = 0.055, was obtained. This corresponds to a Cu metal particle size of 20 nm. A close value of 35 nm was obtained from TEM (Fig. 3.25b). 5% Cu/CsPW had smaller Cu particles and had a Cu metal dispersion of 0.11, corresponding to a metal particle size of 10 nm. Fresh and spent Cu catalysts had about the same metal dispersion within the accuracy of measurement. The higher Cu dispersion in Cu/CsPW compared to Cu/SiO_2 may be due to ion exchange of Cu^{2+} with strong proton sites in CsPW upon impregnation of CsPW with $Cu(NO_3)_2$ aqueous solution, which may also explain the H_2 uptake of Cu on CsPW at a

temperature higher than for the Cu on SiO_2 catalyst, as shown in Figure 3.26. For Pd and Pt catalysts, no significant difference in metal dispersion on CsPW and SiO_2 was observed (Table 3.13). This may be explained by the different preparation of these catalysts, namely, using non-ionic metal precursors and a non-polar solvent (benzene) for the impregnation.

Table 3.13 Particle size and dispersion of metals on CsPW and SiO_2

Catalyst	D [a]	d [b] (nm)
0.5 % Pd/CsPW	0.37 (0.07)	2.4[c], 2.5[f]
0.5 % Pt/CsPW	0.48 (0.25)	1.9[c]
0.5 % Pd/SiO_2	0.62 (0.49)	1.5[c]
0.5 % Pt/SiO_2	0.27 (0.26)	3.3[c]
5% Cu/CsPW	0.11	10[d]
5% Cu/SiO_2	0.055	20,[d] 45[e], 35[f]
0.5 % Ru/CsPW	0.24	3.8[c]
5.0 % Ru/CsPW	0.11	8.2[c]

a) Metal dispersion in fresh catalysts and in brackets in spent catalysts after reaction of propionic acid at 300 °C in H_2, as determined from chemisorption of H_2 (Pd, Pt) or N_2O (Cu)

b) Metal particle diameter

c) Values obtained from the equation d (nm) = 0.9/D [30]

d) Values obtained from the equation d (nm) = 1.1/D [31]

e) From XRD

f) From TEM and STEM-EDX analysis

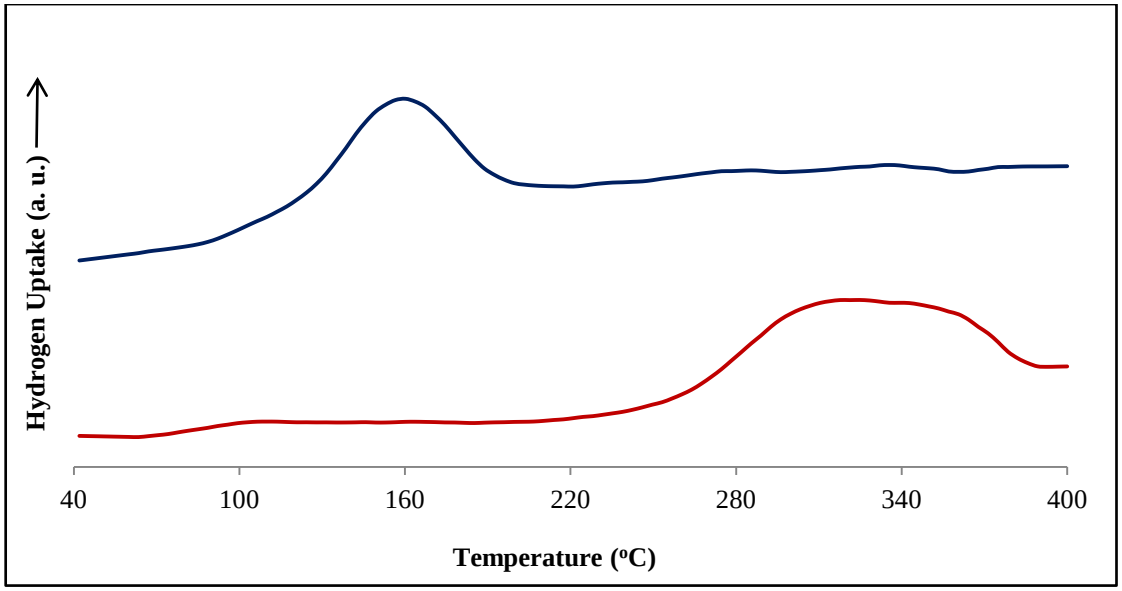

Figure 3.26 TPR profile of Cu-doped CsPW (bottom) and SiO_2 (top) after dissociative adsorption of N_2O

Ru-doped CsPW was used as a bifunctional catalyst in the hydrodeoxygenation of MIBK in the gas phase, at loadings of 0.5 and 5.0 %. The dispersion of Ru on 5.0 % Ru/CsPW was 0.11, corresponding to an average particle size of 8.2 nm. Decreasing Ru loading to 0.5 % caused an expected increase of ruthenium dispersion to 0.24 with 3.8 nm Ru particle size.

Pt-doped CsPW was also used at different loadings in the gas-phase hydrodeoxygenation of MIBK. As can be seen from Table 3.14, the dispersion of Pt particles increased as platinum loading decreased, resulting from the available catalyst surface at low loading. As this catalyst has excellent performance at 100 °C, the dispersion and particle size of spent catalysts was determined at this temperature, as shown in Table 3.14. Platinum dispersion on CsPW did not change after 14 hours TOS.

Table 3.14 Particle size and dispersion of Pt on CsPW in MIBK hydrodeoxygenation

Catalyst	D [a]	d [b] (nm)
0.25 % Pt/CsPW	0.80 (0.80)	1.1
0.5 % Pt/CsPW	0.36 (0.36)	2.5
1.0 % Pt/CsPW	0.18 (0.18)	5.0

(a) Platinum dispersion of fresh catalyst. Value of spent catalyst at 100 °C is in brackets

(b) Particle diameter, obtained from the equation d (nm) = 0.9/D [30]

3.5.2 Pt-doped H-zeolites

Pt-doped H-ZSM-5, H-Beta and H-Y were prepared by ion exchange [32, 33], which is described as an irreversible chemical reaction. Preparing Pt-doped zeolite by ion exchange has been found to produce a high platinum dispersion and small particle size compared to preparation by the impregnation method [34]. This can be explained by the depositing of platinum precursors on the external surface of the zeolite after impregnation, which then agglomerate during the calcination and/or reduction step, whereas platinum is deposited inside the channels of zeolites prepared by ion exchange [34]. The calcination step plays an important role in decomposing the $[Pt(NH_3)_4]^{2+}$ complex at a certain temperature (≈ 450 °C), thus having a great influence on platinum dispersion on the zeolite and the position of platinum particles [35]. The rate of heating in the calcination step has been found to be critical in keeping the platinum particles inside the zeolite channels during decomposition of the Pt precursor [32, 33]. Reduction by H_2 is also important to form active metal sites, Pt^0, in zeolite bifunctional catalysts.

The preparation conditions of Pt-doped H-zeolites used in the gas phase hydrodeoxygenation of MIBK and DIBK are explained in more detail in section 2.4.6.

Table 3.15 lists the dispersion and particle size of platinum deposited on H-zeolites using H_2-O_2 titration. All platinum catalysts were highly dispersed with platinum nanoparticles of 1.02-1.45 nm, which is consistent with Pt catalysts prepared in such conditions [32, 33].

Table 3.15 Results of H_2 chemisorption experiments for Pt-doped H-zeolites

Catalyst	D [a]	d [b] (nm)
0.30 % Pt/H-ZSM-5	0.88	1.02
0.06 % Pt/H-ZSM-5	0.87	1.03
0.39 % Pt/H-Beta	0.72	1.25
0.45 % Pt/H-Y	0.62	1.45

(a) Metal dispersion

(b) Particle diameter, calculated using the equation, $d = 0.9/D$ [30]

3.6 X-ray diffraction

3.6.1 HPW-based catalyst

Powder XRD was recorded for fresh and spent CsPW-doped catalysts, as well as SiO_2-doped copper, to calculate metal particle size using the Scherrer equation. The XRD pattern for CsPW has been widely studied and is similar to its parent HPW [19, 25].

Powder XRD patterns for fresh and spent catalysts after deoxygenation of propionic acid at 400 °C in H_2 are shown in Figure 3.27. XRD analysis of fresh Pd and Pt catalysts did not reveal any metal phase on CsPW and SiO_2; this is probably due to the fine dispersion and low concentration of metal in these catalysts. This is in agreement with equivalent observations for CsPW in the literature [19]. XRD patterns for spent CsPW doped catalysts after 400 °C in hydrogen gas showed no change, indicating that they retained the CsPW crystal (secondary) structure.

5 % Cu/SiO_2 exhibited the sharp XRD pattern of Cu metal (Fig. 3.27h), with the (111) and (200) reflections occurring at 43.4 and 50.5° respectively, which is in agreement with the standard values of 43.3 and 50.4° (JCPDS, copper 04-0836). From these, a mean diameter of 45 nm for Cu particles was obtained using the Scherrer equation, which is in reasonable agreement with the TEM value and the result calculated from N_2O uptake (section 3.5.1). As for the 5 % Cu/CsPW, it clearly displayed the XRD pattern of crystalline CsPW, but only traces of Cu metal phase could be seen (111 reflections at 43.4°) (Fig. 2.27a,b).

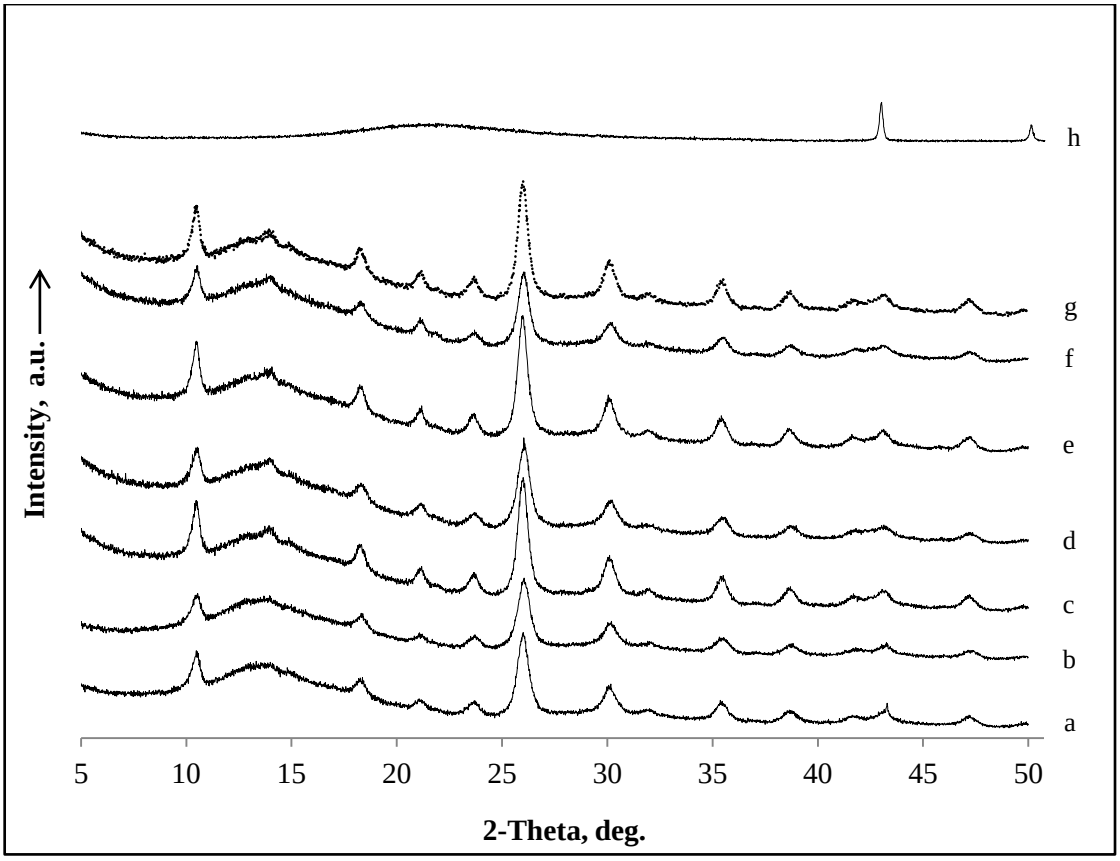

Figure 3.27 XRD patterns (Cu Kα radiation) for fresh and spent catalysts after deoxygenation of propionic acid at 400 °C in H_2: (a) spent 5 % Cu/CsPW, (b) fresh 5 % Cu/CsPW, (c) spent 0.5 % Pd/CsPW, (d) fresh 0.5 % Pd/CsPW, (e) spent 0.5 % Pt/CsPW, (f) fresh 0.5 % Pt/CsPW, (g) fresh CsPW, (h) fresh 5 % Cu/SiO_2

$Cr_2Cu_2O_5$ was used in the gas phase hydrodeoxygenation of MIBK and DIBK after reduction at 400 °C under H_2. XRD was employed for the oxide to identify the active phase of this catalyst. As shown in Figure 3.28, the oxide was amorphous before reduction, then exhibited the crystalline Cu metal phase after reduction under H_2 at 400 °C.

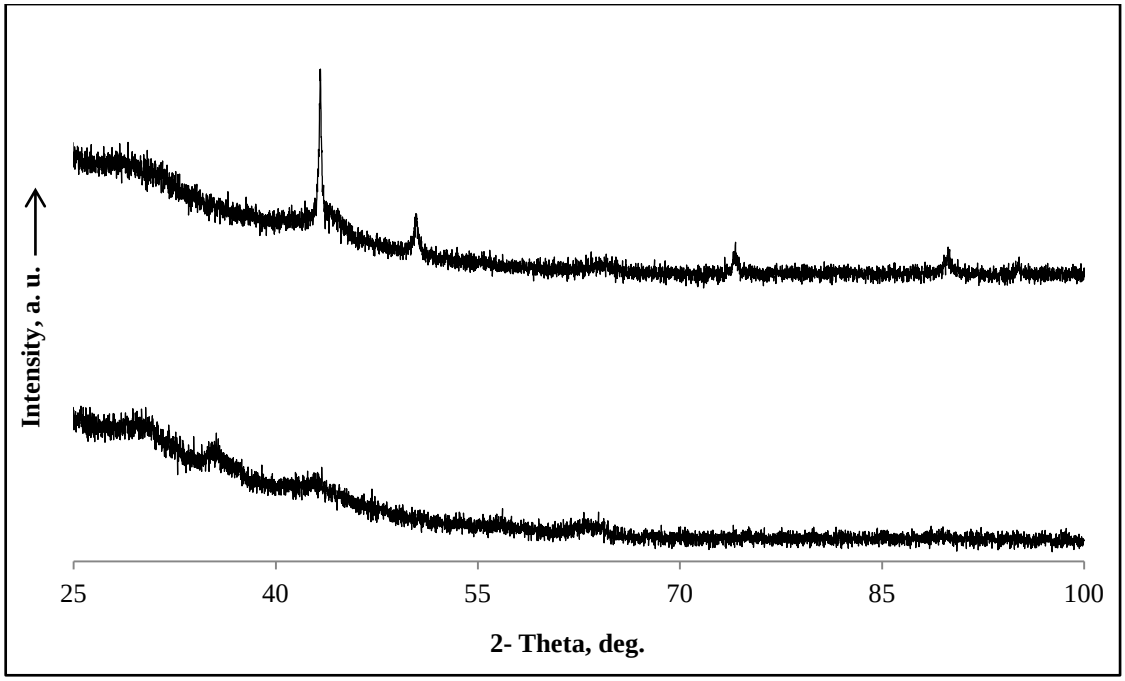

Figure 3.28 XRD patterns (Cu Kα radiation) for copper chromite catalysts: $Cr_2Cu_2O_5$ unreduced (bottom) and reduced at 400 °C in H_2 for 2 h (top)

3.6.2 Pt-doped H-zeolites

Zeolites are crystalline solid materials. Therefore, studying their crystalline structure, such as crystallinity and average crystallite size, is very important for their efficiency as catalysts [36]. As can be seen from the XRD patterns in Figures 3.29-3.31, H-ZSM-5, H-Beta and H-Y had the typical fingerprints of their zeolite type, as did the Pt-doped catalysts, findings which are in strong agreement with the literature [37, 38].

The structure of bulk zeolites after depositing Pt remained unchanged as the crystallinity of Pt/H-zeolites changed, as displayed in the figures. It should be noted that the XRD patterns of Pt-doped zeolites did not show a Pt phase, which would have shown at about 39.9° [37]. This confirms the high dispersion of Pt on H-zeolites.

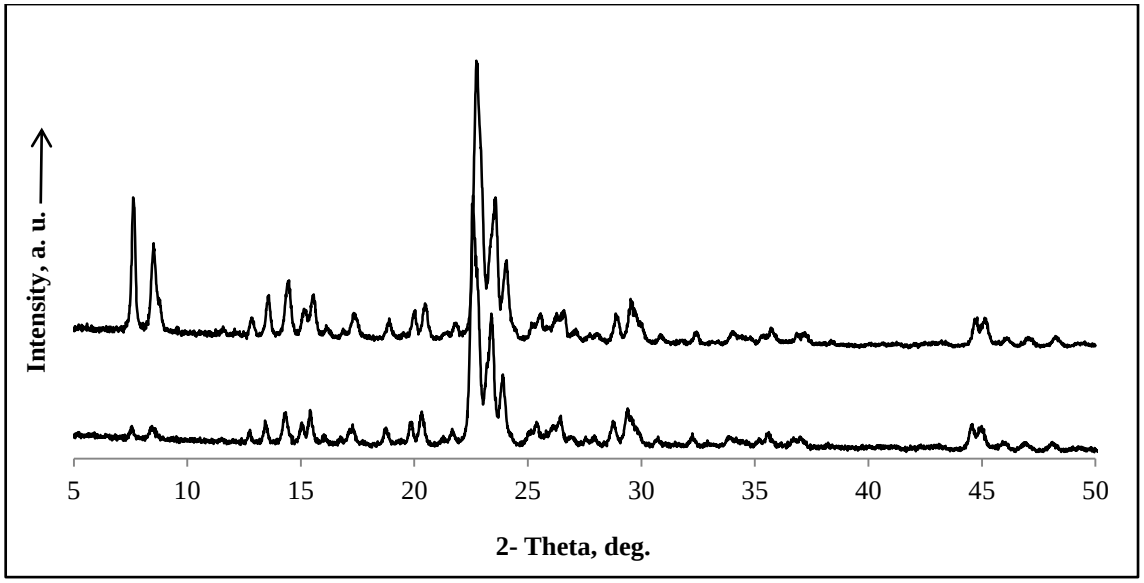

Figure 3.29 XRD patterns (Cu Kα radiation) for H-ZSM-5 (top) and Pt/H-ZSM-5 reduced at 400 °C in H_2 for 2 h (bottom)

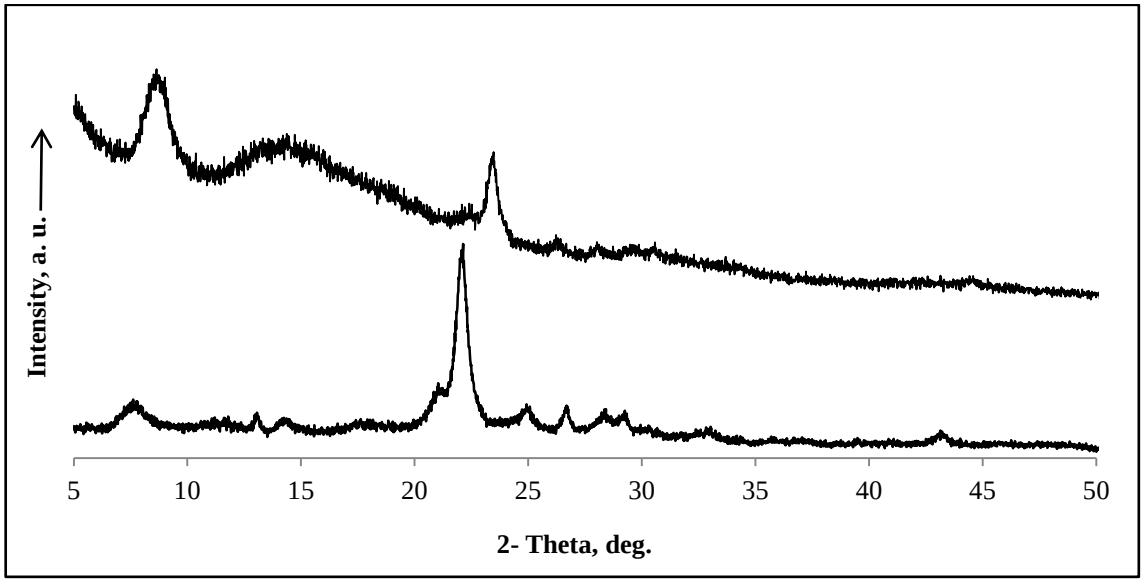

Figure 3.30 XRD patterns (Cu Kα radiation) for H-Beta (bottom) and Pt/H-Beta reduced at 400 °C in H_2 for 2 h (top)

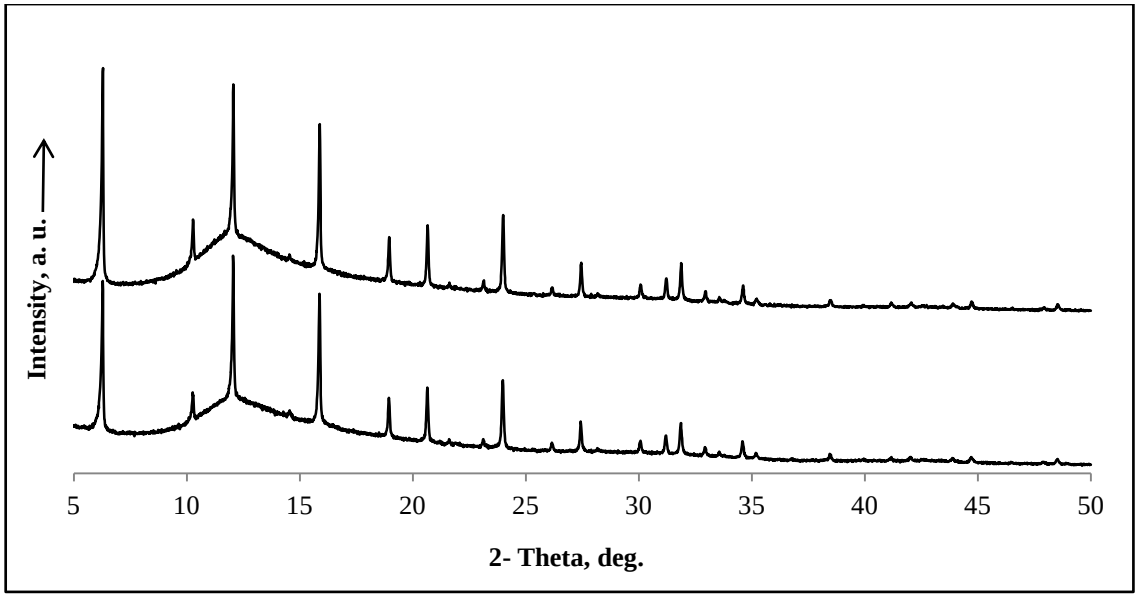

Figure 3.31 XRD patterns (Cu Kα radiation) for H-Y (top) and Pt/H-Y reduced at 400 °C in H_2 for 2 h (bottom)

3.7 Temperature programmed reduction (TPR)

Reducibility values for HPW-based catalysts were determined by TPR. Fig. 3.32 shows H_2-TPR profiles for the HPW and CsPW catalysts. The TPR profile of HPW peaked at 530 °C, with a reduction onset at ~ 400 °C. For CsPW, these temperatures were 750 and ~ 650 °C. These results are in agreement with previous reports [39, 40]. The TPR profiles for Pd/CsPW and Pt/CsPW peaked at 710 and 730 °C respectively, both with a reduction onset at ~ 600 °C. Since Pd and Pt are already reduced in these catalysts and Cs^+ will not be reduced under these conditions, it leaves W(VI) reduction as the source of the H_2-TPR signals. Therefore, all these catalysts should be resistant to reduction with H_2 upon propionic acid and MIBK conversions at the chosen reaction temperatures (100-400 °C), although partial reduction at their surface to form oxygen vacancies cannot be excluded.

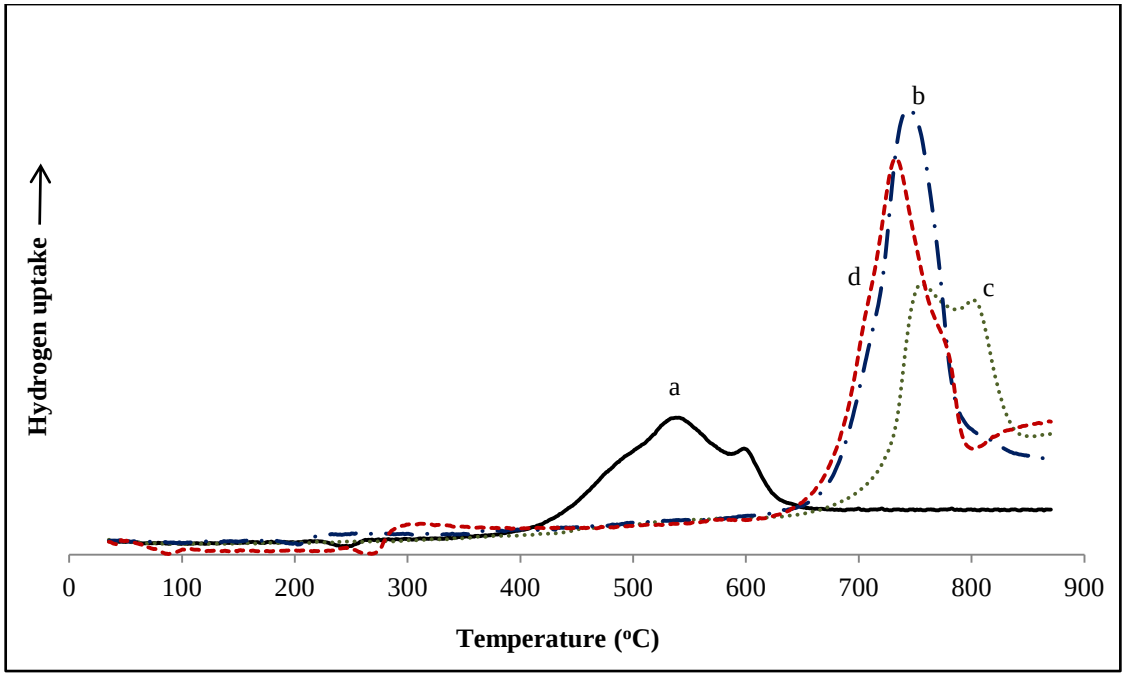

Figure 3.32 H_2-TPR for HPW (a), 0.5 % Pt/CsPW (b), CsPW (c) and 0.5 % Pd/CsPW (d). Catalysts were pretreated at 300 °C/1 h in N_2, 10 °C min^{-1} temperature ramp rate.

3.8 Fourier transform infrared spectroscopy (FTIR)

FTIR is one of the techniques most frequently used to characterise Keggin structure in HPAs, which is seen as a fingerprint in the region between 500-1200 cm^{-1} [4, 16]. The Keggin structure of bulk HPW, supported HPW and CsPW has been studied [41]. A similarity has been found between the FTIR results for HPW and its Cs salt in the following absorption bands: 1080 cm^{-1} for P-O in the central tetrahedron, 984 cm^{-1} for terminal W=O and 897 cm^{-1} for W-O-W related to the asymmetric vibration in the Keggin polyanion. In addition, Alsalme *et al.* [42] examined the Keggin structure of 15 % HPW/SiO_2, which exhibited an identical IR spectrum.

Figures 3.33 and 3.34 show the DRIFT spectra for fresh and spent HPW catalysts after deoxygenation of propionic acid in the characteristic region of the Keggin structure. All spent catalysts based on CsPW after reaction at 400 °C in H_2 exhibited the well-known spectrum of the Keggin anion $[PW_{12}O_{40}]^{3-}$ (Fig. 3.33), with strong bands of stretching vibrations at 1080 (P-O), 987 (terminal W=O group), 890 and 800 cm^{-1} (edge- and corner-sharing W-O-W groups), matching exactly the spectrum of fresh CsPW [4, 16, 43]. This shows that bulk CsPW and CsPW-supported Pd, Pt and Cu catalysts retained their primary structure (the Keggin structure of HPA) intact after reaction at 400 °C in H_2. Moreover, all these catalysts, fresh and spent, show the same XRD pattern of crystalline CsPW as explained previously (Fig. 3.27). Therefore, the CsPW catalysts retained their primary and secondary (crystal) structures after reaction, in contrast to the less stable P-Mo-V HPAs studied previously [44, 45].

In the DRIFT spectrum for fresh 30 % HPW/SiO_2 (Fig. 3.34a), silica exhibits strong bands at 1100 and 806 cm^{-1}, obscuring the HPW bands at 1080 and 800 cm^{-1}, but the vibrations at 987 (W=O) and 890 (W-O-W) appear in their normal positions with unchanged relative intensity. This shows that HPW retained the Keggin structure in the fresh catalyst. From spectra b–e in Figure 3.34, it is evident that the HPW primary structure remained stable after reaction at ≤ 350 °C in N_2, but decomposed at 400 °C.

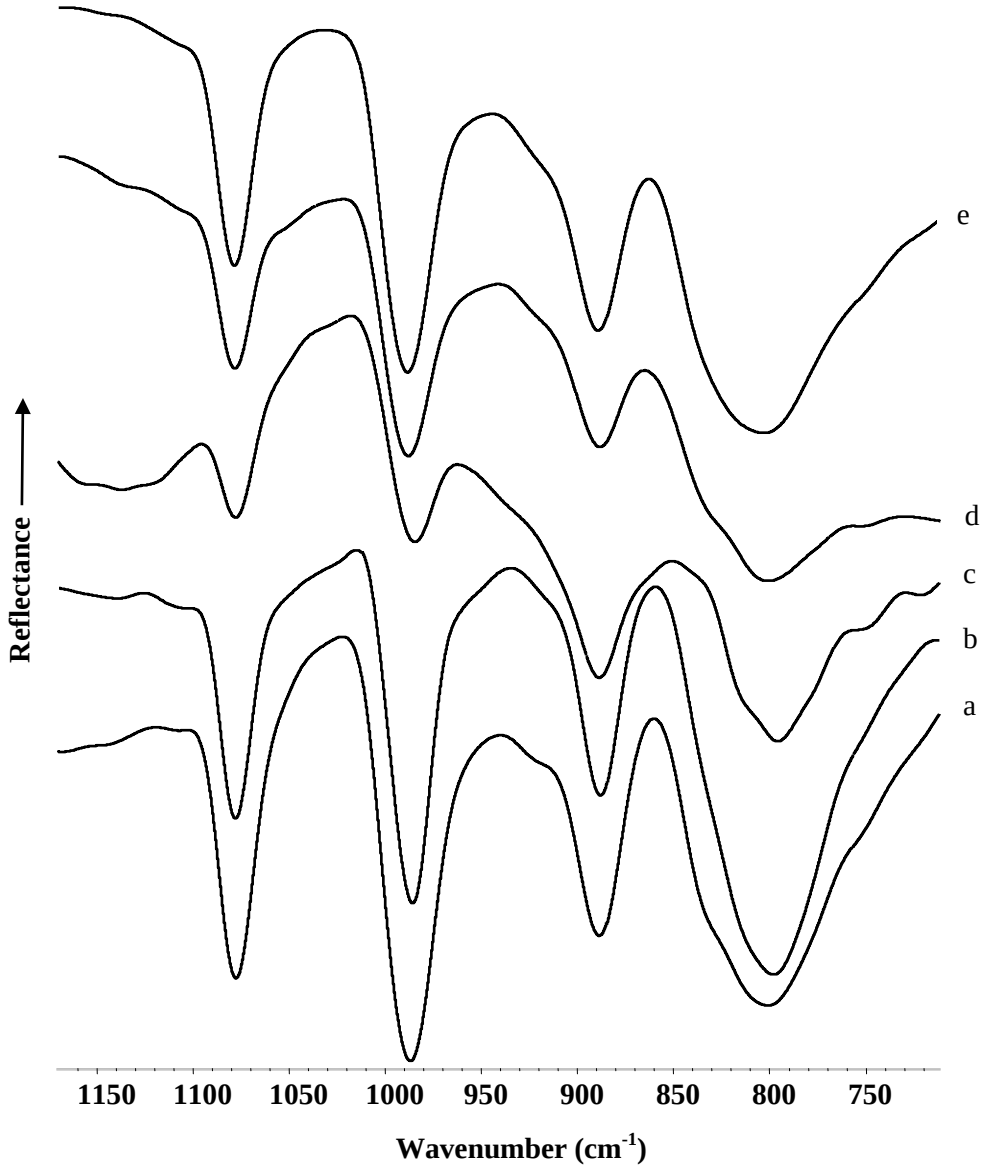

Figure 3.33 DRIFT spectra of spent catalysts after reaction at 400 °C in H_2: 0.5 % Pt/CsPW (a), $Cs_3PW_{12}O_{40}$ (b), CsPW (c), 0.5 % Pd/CsPW (d) and 5 % Cu/CsPW (e)

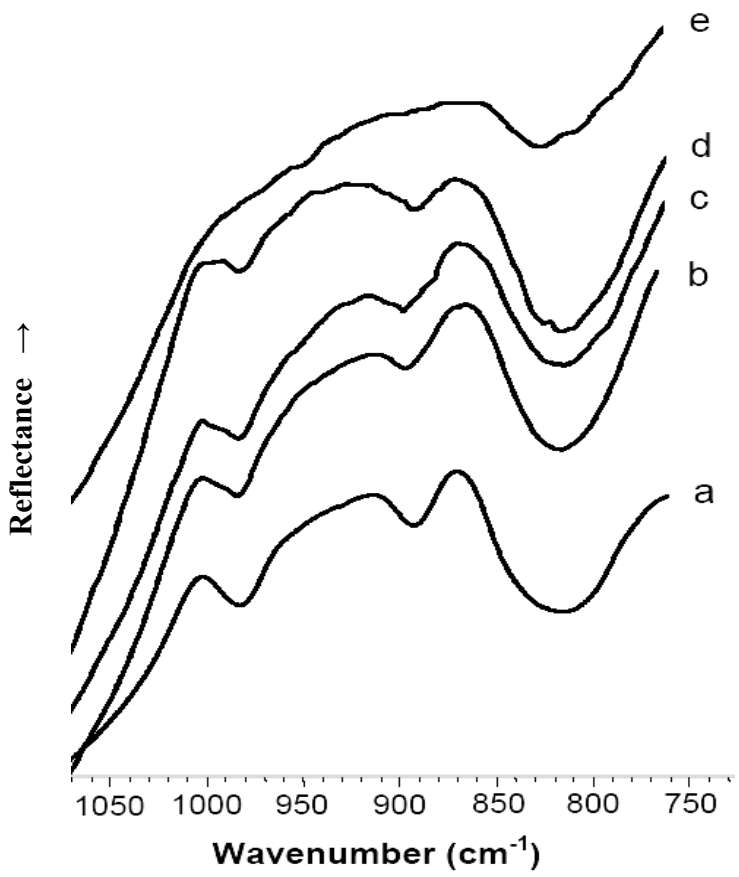

Figure 3.34 FTIR spectra of fresh (a) and spent 30 % HPW/SiO_2 catalyst after reaction in N_2 at 250 °C (b), 300 °C (c), 350 °C (d) and 400 °C (e)

3.9 Acidity measurements

Measurements of the strength and nature of acid sites of selected catalysts in this study were performed using differential scanning calorimetry of NH_3 adsorption and FTIR of pyridine adsorption. The experimental procedures for these measurements are explained in the experimental chapter.

3.9.1 Pulse ammonia adsorption analysis

The strength of acid sites in the catalysts under study was measured by determining the enthalpy (ΔH) of adsorbed ammonia in the gas-solid phase. It should be noted that discrimination between Brønsted and Lewis acid sites cannot be made by this method. Table 3.16 lists the ΔH values of the catalysts and the calcination temperature before measurements.

Table 3.16 Initial enthalpies of ammonia adsorption at 100 °C

Catalyst	Calcination temperature (°C)	-ΔH (kJ mol^{-1})
30 % HPW/SiO_2	300	160
$Cs_{2.5}H_{0.5}PW_{12}O_{40}$	300	165
$Cs_3PW_{12}O_{40}$	300	103
H-ZSM-5	300	143

Figure 3.35 plots the initial enthalpies of NH_3 adsorption, ΔH, for 30 % HPW/SiO_2, $Cs_{2.5}H_{0.5}PW_{12}O_{40}$, $Cs_3PW_{12}O_{40}$ and H-ZSM-5. The values obtained are in excellent agreement with previous studies [5, 42, 43, 46]. The substitution of protons in Cs_3PW indicates low acidity strength compared to CsPW, with initial ΔH of -103 kJ mol^{-1} [16, 47]. In this study, H-ZSM-5, H-Beta and H-Y with close Si/Al ratios (12-15) and comparable proton site densities were chosen to study the influence of zeolite structural factors. Their acid strength decreased in the order H-ZSM-5 > H-Beta > H-Y, as demonstrated in the literature [46, 48, 49]. The acid strength of the catalysts under study increased in the order: Cs_3PW << H-ZSM-5 < 30 % HPW/SiO_2 ≤ CsPW.

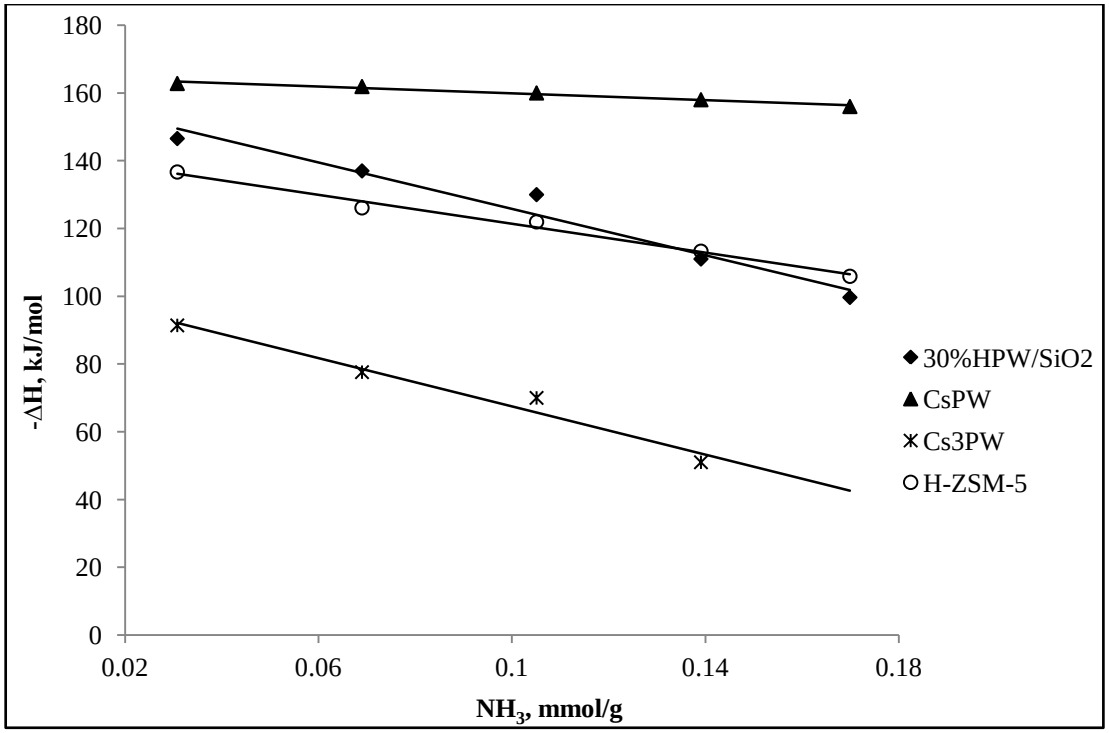

Figure 3.35 The plot of enthalpies of NH_3 adsorption against NH_3 uptake for 30 % HPW/SiO_2, $Cs_{2.5}H_{0.5}PW_{12}O_{40}$ (CsPW), $Cs_3PW_{12}O_{40}$ and H-ZSM-5

3.9.2 FTIR study of pyridine adsorption

The characterisation of the nature of surface acid sites in heterogeneous catalysis is a major step in developing a clear understanding of the reaction mechanisms. Pyridine is a probe molecule whose adsorption on the catalyst surface can be used to characterise the nature of surface acid sites [50-52]. Pyridine reacts with a Brønsted acid site to produce a pyridinium ion, which gives an IR band at 1540 cm^{-1}, while a coordinatively bonded Lewis acid site exhibits a vibration at 1450 cm^{-1} [53].

The FTIR spectra of adsorbed pyridine were examined for selected catalysts used in this study. CsPW-based catalysts and H-ZSM-5 have both Brønsted and Lewis acid sites, as clearly identified in various studies [1, 54, 55]. Figure 3.36 shows spectra of pyridine adsorbed on CsPW, 0.5 % Pt/CsPW and reduced $Cr_2Cu_2O_5$.

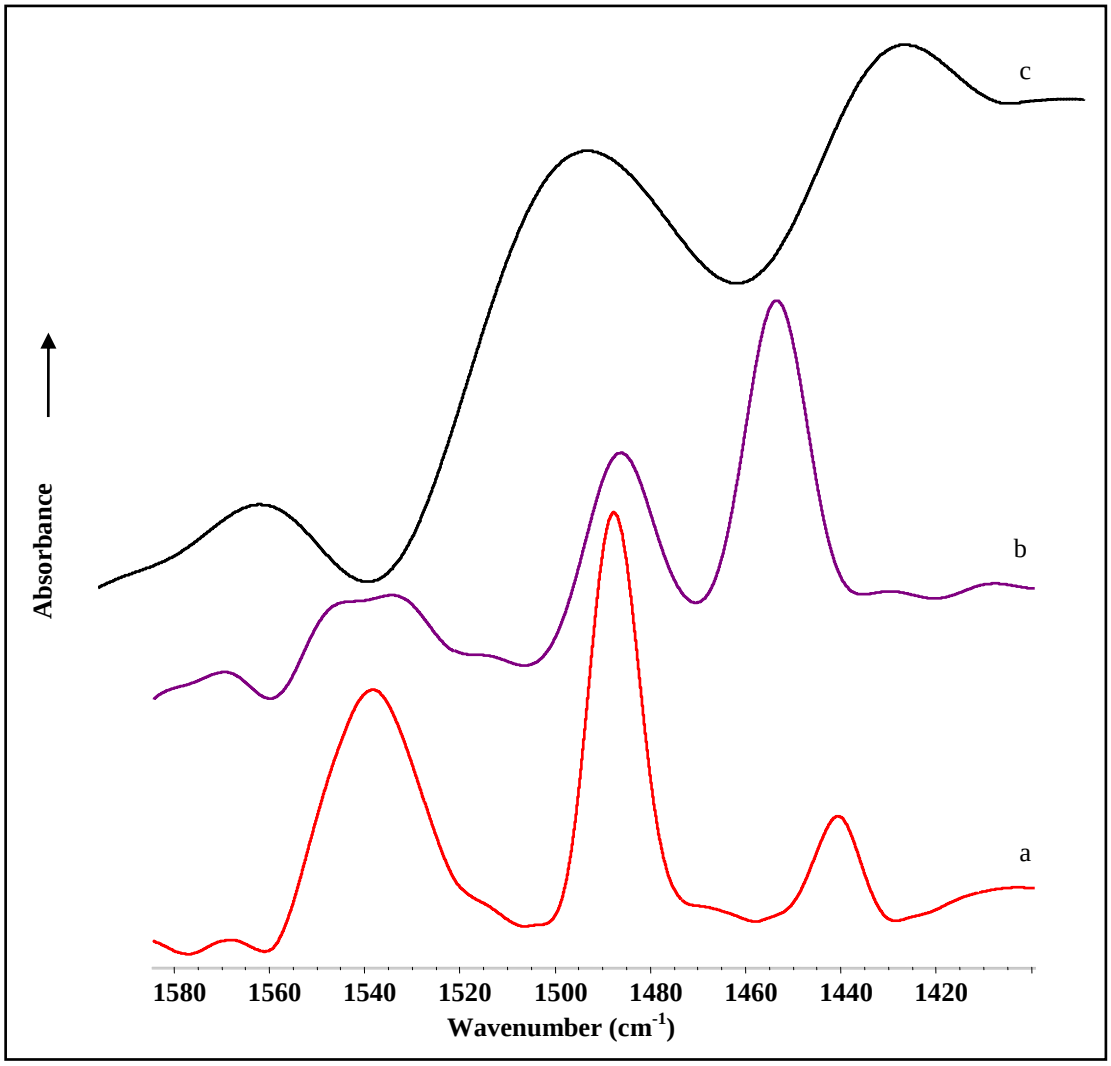

Figure 3.36 DRIFT spectra of pyridine adsorbed on (a) CsPW (b) 0.5 % Pt/CsPW and (c) reduced $Cr_2Cu_2O_5$

CsPW, 0.5 % Pt/CsPW and reduced $Cr_2Cu_2O_5$ all displayed a band at about 1450 cm^{-1}, attributed to the presence of Lewis sites. In addition, all showed IR bands at about 1540 cm^{-1}. This is in agreement with previous research [51, 56, 57]. Doping of CsPW by Pt affected the strength of the IR band for Brønsted sites, which can be explained by interaction between the acid site and a fraction of Pt metal.

Bulk H-ZSM-5 and 0.5 % Pt-doped H-ZSM-5 DRIFT spectra after pyridine adsorption are shown in Figure 3.37. In agreement with the literature [54, 58], H-ZSM-5 and its doped catalyst possess Brønsted and Lewis sites, as observed at the 1540 and 1450 cm^{-1} IR bands respectively.

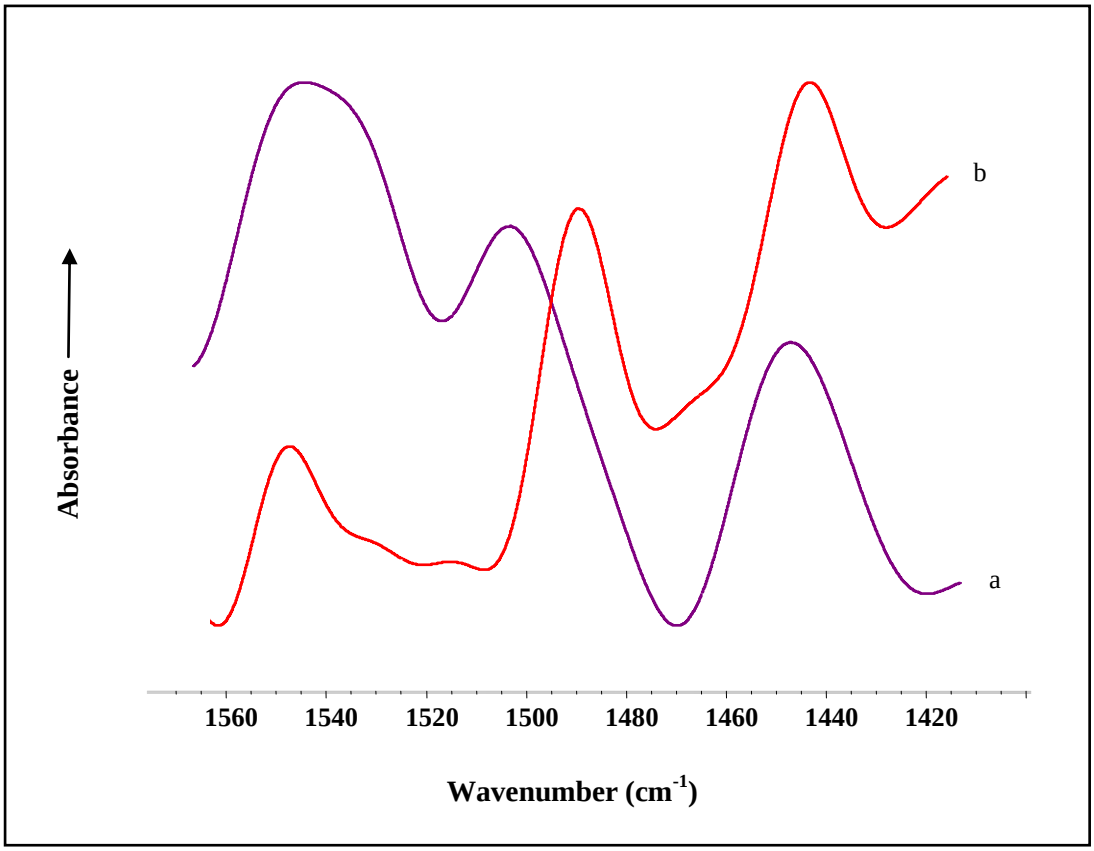

Figure 3.37 DRIFT spectra of pyridine adsorbed on (a) 0.5 % Pt/H-ZSM-5 (b) H-ZSM-5

3.10 Conclusions

The surface area and porosity of catalysts were determined using N_2 physisorption. The HPW-based catalysts under study were all mesoporous solids with average pore diameter of 26-96 Å and relatively high surface area (75-160 m^2 g^{-1}). Pt-doped H-ZSM-5, H-Beta and H-Y were found to be microporous materials having a large surface area (357-690 m^2 g^{-1}) and average pore diameter of 24-50 Å. As shown by FTIR spectra, CsPW and its doped metal catalysts retained their primary Keggin structure after use in the gas phase deoxygenation of propionic acid at 400 °C, whereas the primary structure of 30 % HPW/SiO_2 remained stable after reaction at ≤ 350 °C but decomposed at 400 °C.

XRD measurement revealed that all catalysts used in this study were crystalline and did not show any Pd or Pt metal phase on CsPW, H-ZSM-5, H-Beta and H-Y, indicating that the metals were finely dispersed. CsPW-based catalysts, fresh and spent after deoxygenation of propionic acid at 400 °C, showed the same XRD pattern as crystalline CsPW. Therefore, the CsPW catalysts also retained their secondary (crystal) structure after reaction.

Hydrogen titration experiments demonstrated the presence of Pd, Pt and Ru in high dispersion in CsPW and Pt on H-zeolites used in this study as bifunctional catalysts. Nitrous oxide adsorption was used to calculate the particle size of Cu atoms and to estimate Cu dispersion in CsPW and SiO_2. TPR experiments confirmed that all HPW-based catalysts were resistant to reduction with H_2 at reaction temperatures of 100-400 °C. ICP analysis precisely determined the composition of in-house-made

HPW-based catalysts and Pt content in H-zeolites prepared by the ion exchange method.

HPW-based catalysts and H-zeolites possess both Brønsted and Lewis sites, as indicated by FTIR spectra of adsorbed pyridine. Using ammonia adsorption calorimetry, the acid strength of catalysts under study was found to increase in the order: Cs_3PW << H-ZSM-5 < 30 % HPW/SiO_2 ≤ CsPW.

References

[1] I.V. Kozhevnikov, Catalysts For Fine Chemical Synthesis, Catalysis by Polyoxometalates, Wiley Chichester, 2002.

[2] I.V. Kozhevnikov, J. Mol. Catal. A 262 (2007) 86.

[3] I.V. Kozhevnikov, Chem. Rev. 98 (1998) 171.

[4] J.B. Moffat, Metal-Oxygen Clusters: The Surface and Catalytic Properties of Heteropoly Oxometalates, Kluwer, New York, 2001.

[5] T. Okuhara, Chem. Rev. 102 (2002) 3641.

[6] M.R.H. Siddiqui, S. Holmes, H. He, W. Smith, E.N. Coker, M.P. Atkins, I.V. Kozhevnikov, Catal. Lett. 66 (2000) 53.

[7] M. Musawir, E.F. Kozhevnikova, I.V. Kozhevnikov, J. Mol. Catal. A 262 (2007) 93.

[8] J. Barbier, Appl. Catal. 23 (1986) 225.

[9] G. Cruciani, J. Phys. Chem. Solids 67 (2006) 1973.

[10] K. Akcay, A. Sirkecioglu, M. Tatlier, O.T. Savasci, A. Erdem-Senatalar, Powder Technol. 142 (2004) 121.

[11] G. Rothenberg, Catalysis: Concepts and Green Applications, Wiley-VCH, Weinheim, 2008.

[12] G. Leofanti, M. Padovan, G. Tozzola, B. Venturelli, Catal. Today 41 (1998) 207.

[13] S.J. Gregg, K.S.W. Sing, Adsorption, Surface Area and Porosity, Academic Press, London, 1982.

[14] S. Brunauer, P.H. Emmett, E. Teller, J. Am. Chem. Soc. 60 (1938) 309.

[15] L.G. Joyner, E.P. Barrett, R. Skold, J. Am. Chem. Soc. 73 (1951) 3155.

[16] T. Okuhara, N. Mizuno, M. Misono, Adv. Catal. 41 (1996) 113.

[17] I.V. Kozhevnikov, Catal. Rev. 37 (1995) 311.

[18] P. Sun, D.H. Yu, Y. Hu, Z.C. Tang, J.J. Xia, H. Li, H. Huang, Korean J. Chem. Eng. 28 (2011) 99.

[19] J.A. Dias, E. Caliman, S.C.L. Dias, Micropor. Mesopor. Mat. 76 (2004) 221.

[20] Y. Izumi, M. Ono, M. Kitagawa, M. Yoshida, K. Urabe, Microporous Mater. 5 (1995) 255.

[21] A. Alhanash, E.F. Kozhevnikova, I.V. Kozhevnikov, Catal. Lett. 120 (2008) 307.

[22] N. Mizuno, M. Misono, Chem. Rev. 98 (1998) 199.

[23] T. Yamada, Y. Yoshinaga, T. Okuhara, B Chem. Soc. Jpn. 71 (1998) 2727.

[24] T. Nakato, Y. Toyoshi, M. Kimura, T. Okuhara, Catal. Today 52 (1999) 23.

[25] T. Okuhara, H. Watanabe, T. Nishimura, K. Inumaru, M. Misono, Chem. Mater. 12 (2000) 2230.

[26] P.B. Venuto, Microporous Mater. 2 (1994) 297.

[27] H. van Bekkum, E. M. Flanigen, P. A. Jacobs, J.C. Jansen, Introduction to Zeolite Science and Practice, 2nd ed., Elsevier, Amsterdam, 2001.

[28] P.A. Zielinski, A. Vanneste, D.B. Akolekar, S. Kaliaguine, Microporous Mater. 5 (1995) 123.

[29] R. Hetterley, Ph.D Thesis, Department of Chemistry, University of Liverpool, UK, 2008.

[30] J.E. Benson, H.S. Hwang, M. Boudart, J. Catal. 30 (1973) 146.

[31] A. Dandekar, M.A. Vannice, J. Catal. 178 (1998) 621.

[32] J. de Graaf, A.J. van Dillen, K.P. de Jong, D.C. Koningsberger, J. Catal. 203 (2001) 307.

[33] A.C.M. van den Broek, J. van Grondelle, R.A. van Santen, J. Catal. 167 (1997) 417.

[34] R.M. Jao, L.J. Leu, J.R. Chang, Appl. Catal. A 135 (1996) 301.

[35] C. Bigey, B.L. Su, J. Mol. Catal. A 209 (2004) 179.

[36] R. van Grieken, J.L. Sotelo, J.M. Menendez, J.A. Melero, Micropor. Mesopor. Mat. 39 (2000) 135.

[37] J.I. Villegas, N. Kumar, T. Heikkila, V.P. Lehto, T. Salmi, D.Y. Murzin, Chem. Eng. J. 120 (2006) 83.

[38] A.W. Burton, Zeolite Characterization and Catalysis: A Tutorial (2009) 1.

[39] S. Yoshida, H. Nilyama, E. Echigoya, J. Phys. Chem. 86 (1982) 3150.

[40] K.M. Parida, S. Rana, S. Mallick, D. Rath, J. Colloid Interf. Sci. 350 (2010) 132.

[41] S.M. Choi, Y. Wang, Z.M. Nie, J. Liu, C.H.F. Peden, Catal. Today 55 (2000) 117.

[42] A.M. Alsalme, P.V. Wiper, Y.Z. Khimyak, E.F. Kozhevnikova, I.V. Kozhevnikov, J. Catal. 276 (2010) 181.

[43] A. Alhanash, E.F. Kozhevnikova, I.V. Kozhevnikov, Appl. Catal. A 378 (2010) 11.

[44] H. Benaissa, P.N. Davey, E.F. Kozhevnikova, I.V. Kozhevnikov, Appl. Catal. A 351 (2008) 88.

[45] H. Benaissa, P.N. Davey, Y.Z. Khimyak, I.V. Kozhevnikov, J. Catal. 253 (2008) 244.

[46] M. Brandle, J. Sauer, J. Am. Chem. Soc. 120 (1998) 1556.

[47] M. Misono, Chem. Comm. (2001) 1141.

[48] S.G. Hegde, R. Kumar, R.N. Bhat, P. Ratnasamy, Zeolites 9 (1989) 231.

[49] D. Barthomeuf, Mater. Chem. Phys. 17 (1987) 49.

[50] B.M. Devassy, S.B. Halligudi, J. Catal. 236 (2005) 313.

[51] B.M. Devassy, F. Lefebvre, S.B. Halligudi, J. Catal. 231 (2005) 1.

[52] H. Sachsenroder, E. Brunner, M. Koch, H. Pfeifer, B. Staudte, Microporous Mater. 6 (1996) 341.

[53] B.H. Davis, R.A. Keogh, S. Alerasool, D.J. Zalewski, D.E. Day, P.K. Doolin, J. Catal. 183 (1999) 45.

[54] J.F. Haw, Phys. Chem. Chem. Phys. 4 (2002) 5431.

[55] C. Busco, A. Barbaglia, M. Broyer, V. Bolis, G.M. Foddanu, P. Ugliengo, Thermochim. Acta. 418 (2004) 3.

[56] A.A. Khasin, T.M. Yur'eva, L.M. Plyasova, G.N. Kustova, H. Jobic, A. Ivanov, Y.A. Chesalov, V.I. Zaikovskii, A.V. Khasin, L.P. Davydova, V.N. Parmon, Russ. J. Gen. Chem. 78 (2008) 2203.

[57] K. Okumura, K. Yamashita, M. Hirano, M. Niwa, J. Catal. 234 (2005) 300.

[58] D.T. On, S. Kaliaguine, Angew. Chem. Int. Edit. 41 (2002) 1036.

4. Deoxygenation of propionic acid on heteropoly acid and bifunctional metal-loaded heteropoly acid catalysts

4.1 Introduction

Carboxylic acids are readily available from natural sources and are attractive as renewable resources for the production of value-added chemicals and biofuel components [1, 2]. For fuel applications, carboxylic acids require reduction in their oxygen content, i.e. deoxygenation [3]. Therefore, much recent research has focused on the deoxygenation of carboxylic acids using heterogeneous catalysis [4-10].

Heteropoly compounds comprising polyoxometalates (POMs), i.e. metal-oxygen cluster anions, have found numerous applications as catalysts, offering significant economic and environmental benefits [11-13]. P-Mo-V heteropoly compounds of Keggin structure have been studied in this group as catalysts for the gas-phase hydrogenation and ketonisation of aliphatic carboxylic acids [14, 15]. However, due to their relatively low thermal stability (< 400 °C), these POMs decompose in situ to form Mo and V oxides, which are the true catalysts, rather than the POMs themselves.

In this chapter, key reaction pathways of the gas-phase deoxygenation of propionic acid catalysed by POMs and metal-loaded POMs with proven on-stream stability are presented and discussed. Propionic acid is chosen as a representative of carboxylic acids with the number of carbon atoms $n \leq 6$ derived from carbohydrate feedstocks [1, 16]. As catalysts, we choose tungstophosphoric Keggin heteropoly acid $H_3PW_{12}O_{40}$ (HPW) and its Cs acidic salt $Cs_{2.5}H_{0.5}PW_{12}O_{40}$ (CsPW), which possess sufficiently high thermal stability, with respective decomposition temperatures of 450

and > 500 °C [13]. These compounds have a very strong Brønsted acidity and are well-documented as acid catalysts [11-13]. Pd-, Pt- and Cu-loaded CsPW are studied as bifunctional metal-acid catalysts. In particular, it should be interesting to compare Pd and Pt catalysts with Cu catalysts, because they preferably catalyse C=C and C=O bond hydrogenation respectively. These catalysts are compared with the corresponding SiO_2-supported metal catalysts regarding their selectivity and turnover rate. The catalysts studied together with their characterisation data are summarised in Table 4.1, which was deeply discussed in Chapter 3.

Table 4.1 Catalyst characterisation

Catalyst[a]	S_{BET}[b] (m^2g^{-1})	D[c]	d[d] (nm)
30%HPW/SiO_2	160		
CsPW	111		
$Cs_3PW_{12}O_{40}$	124		
0.5% Pd/CsPW	87	0.37 (0.07)	2.4[e], 2.5[f]
0.5% Pt/CsPW	100	0.48 (0.25)	1.9[e]
0.5% Pd/SiO_2	255	0.62 (0.49)	1.5[e]
0.5% Pt/SiO_2	287	0.27 (0.26)	3.3[e]
5%Cu/CsPW	75	0.11	10[g]
5%Cu/SiO_2	251	0.055	20,[g] 45,[h] 35[f]

(a) HPW = $H_3PW_{12}O_{40}$, CsPW = $Cs_{2.5}H_{0.5}PW_{12}O_{40}$.

(b) BET surface area.

(c) Metal dispersion in fresh catalysts (and in brackets in spent catalysts) after reaction of propionic acid at 300 °C in H_2, as determined from chemisorption of H_2 (Pd, Pt) or N_2O (Cu).

(d) Metal particle diameter.

(e) Values obtained from the equation d (nm) = 0.9/D [17].

(f) From TEM and STEM-EDX analysis.

(g) Values obtained from the equation d (nm) = 1.1/D [18].

(h) From XRD.

The reaction was carried out in the gas phase both in flowing H_2 and in a hydrogen-free system (in N_2). The catalysts were tested at 250-400 °C under atmospheric pressure in a Pyrex fixed-bed down-flow reactor fitted with an online gas chromatograph. The gas feed contained 2.0% propionic acid in N_2 or H_2 as a carrier gas. The acid was fed by passing the carrier gas flow, controlled by a Brooks mass flow controller, through a stainless steel saturator which held liquid propionic acid at 47 °C to maintain the chosen reactant concentration. The gas feed entered the reactor at the top at a flow rate of 10 ml min^{-1} unless stated otherwise (space time W/F = 8.0 h g mol^{-1}, where W is the catalyst weight (g) and F the total molar flow rate (mol h^{-1})). The reactor was packed with 0.2 g of catalyst. Prior to reaction, the catalysts were pre-treated in H_2 for 1 h at the reaction temperature. Once the reaction had started, the downstream gas flow was analysed by the online GC to determine propionic acid conversion and product selectivity. The selectivity was defined as moles of product formed per mole of propionic acid converted and quoted in mole per cent (Section 2.5.1). The run-to-run deviation of conversion and selectivity was usually estimated from the mean of three parallel experiments and was typically within 15%. The rates of overall propionic acid conversion over different metal catalysts were measured at 250 °C under differential conditions within the conversion range < 10%. To fit these conditions, the quantity of catalyst was reduced to 0.050 g and diluted with 0.15 g silica.

4.2 Deoxygenation of propionic acid over 30%HPW/SiO_2 and CsPW catalysts

The performance of 30%HPW/SiO_2 and CsPW catalysts is shown in Figures 4.1 and 4.2 respectively as a function of reaction temperature.

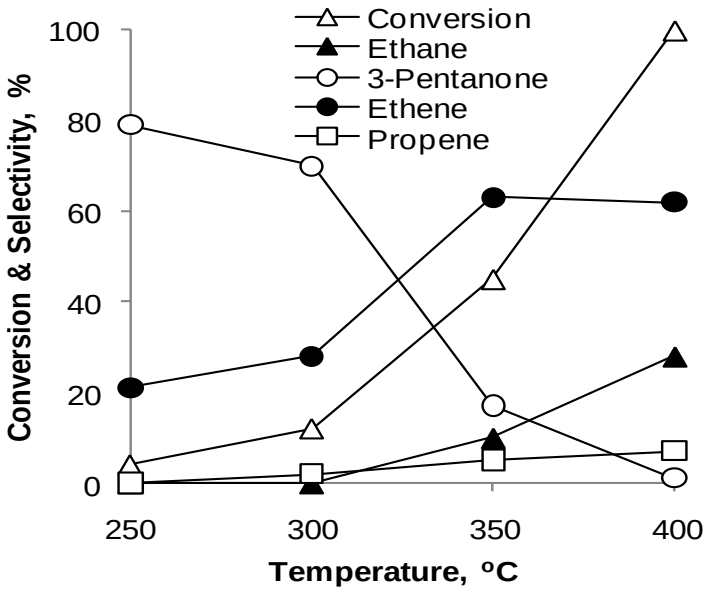

Figure 4.1 Variation of propionic acid conversion and selectivity to main reaction products with reaction temperature during the deoxygenation of propionic acid over 30%HPW/SiO_2. Reaction conditions: 0.2 g catalyst, 2.0% propionic acid in H_2 flow, 10 ml min^{-1} flow rate, 3 h time on stream. Similar performance was observed in N_2.

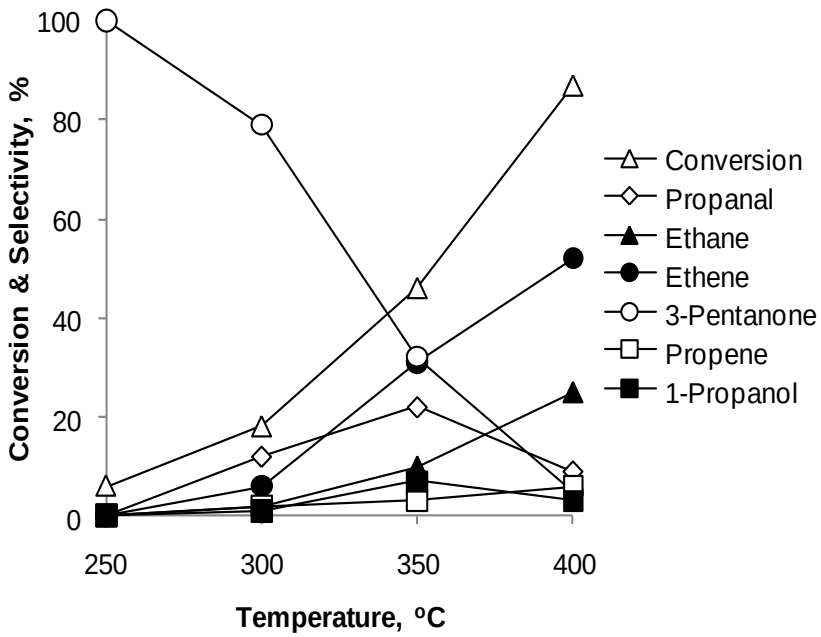

Figure 4.2 Variation of propionic acid conversion and selectivity to main reaction products with reaction temperature during the deoxygenation of propionic acid over CsPW. Reaction conditions: 0.2 g catalyst, 2.0% propionic acid in H_2 flow, 10 ml min^{-1} flow rate, 3 h time on stream. Similar performance was observed in N_2.

Both catalysts exhibited good performance stability, reaching steady state within 1 h, as shown for CsPW in Figure 4.3. A moderate decrease in propionic acid conversion that can be seen during 6 h on stream was probably due to catalyst coking; 3-5% of carbon was found in spent 30%HPW/SiO_2 and CsPW catalysts, as presented in Chapter 3. The carbon balance was 88-92% depending on the time on stream. A larger amount of carbon loss was observed in the beginning of reaction and decreased with time on stream. In addition to catalyst coking, the carbon loss can be attributed to CO and CO_2 formed as by-products in the reaction. Both catalysts (30%HPW/SiO_2 and CsPW) displayed an exponential growth of substrate conversion with temperature. Approximate values of apparent activation energy were calculated to be 55 and 40 kJ

mol^{-1} for 30%HPW/SiO_2 and CsPW respectively, in the temperature range of 250-300 °C, which implies the absence of mass transport limitations in this temperature range. Between 250 and 300 °C, these catalysts, both in H_2 and in N_2, exhibited ketonisation activity to yield 3-pentanone (Equation 4.1), with CsPW being more selective than HPW. This compares favourably with the ketonisation performance of CeO_2-ZrO_2 and CeO_2-MnO_x catalysts, which have been found active at higher temperatures of 300-450 °C [16, 19, 20].

$$2\ CH_3CH_2COOH \rightarrow (CH_3CH_2)_2CO + CO_2 + H_2O \qquad (4.1)$$

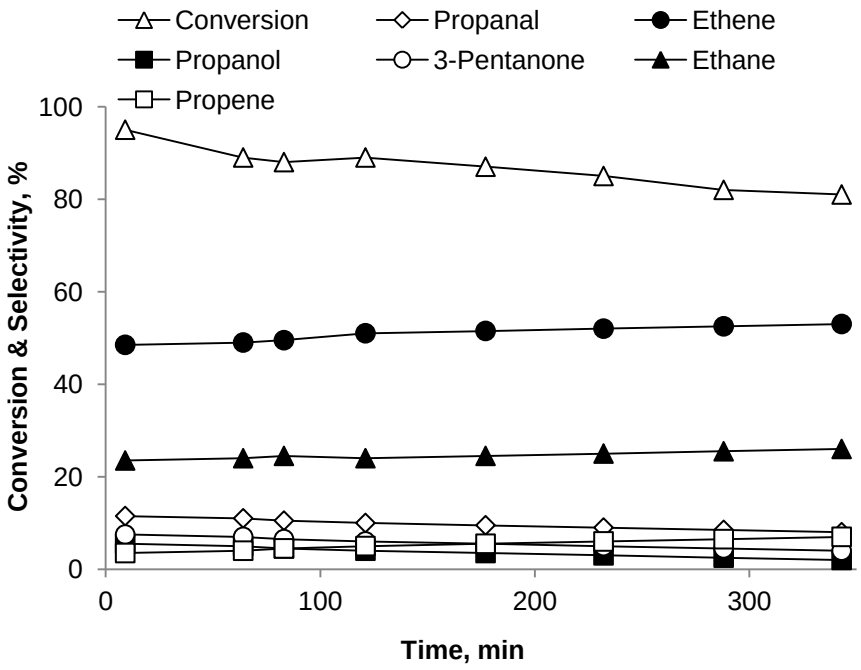

Figure 4.3 Time course for propionic acid conversion over CsPW at 400 °C in H_2

As can be seen in Figures 4.1 and 4.2, ketonisation over 30%HPW/SiO_2 and CsPW diminished at higher temperatures 350-400 °C, giving rise to the formation of ethene and ethane (Equations 4.2 and 4.3).

$$CH_3CH_2COOH \rightarrow C_2H_6 + CO_2 \quad (4.2)$$

$$CH_3CH_2COOH \rightarrow C_2H_4 + CO + H_2O \quad (4.3)$$

CO and CO_2 were detected by IR spectroscopy in the downstream gas flow after the reactor; CO was identified by its well-known rotational-vibrational spectrum [21] and CO_2 by its asymmetric stretch at 2350 cm^{-1}, as shown in Figure 4.4.

Several mechanisms have been proposed for the ketonisation of carboxylic acids. These include: (i) decomposition of metal carboxylate, (ii) via acid anhydride intermediate, (iii) via β-keto acid intermediate and (iv) via ketene intermediate route [22-24]. Previous studies of the ketonisation of carboxylic acids over Keggin-type P-Mo-V heteropoly acids and their Cs salts have revealed a direct correlation between ketonisation selectivity and Cs substitution in P-Mo-V heteropoly acids [14, 15]. On this basis, it has been suggested that ketonisation occurs via Cs carboxylate intermediates. It should be noted, however, that the P-Mo-V heteropoly compounds were catalyst precursors rather than the true catalysts, decomposing in situ to form catalytically active Mo and V oxides [14, 15]. For the more stable HPW and CsPW catalysts, no correlation was observed between ketonisation selectivity and Cs content. Moreover, the formation of CO, CO_2 and ethene from propionic acid over HPW/SiO_2 and CsPW may indicate the intermediate formation of methylketene, which is known to form these products upon its thermal decomposition [25]. Indeed, traces of methylketene were detected by IR spectroscopy along with CO and CO_2, as shown in Figure 4.4. This spectrum clearly shows the characteristic asymmetric stretch of methylketene at 2130 cm^{-1} [26], which stands out from the C=O bands of other carbonyl compounds (aldehydes, ketones and acids) and hence can be used for methylketene detection [25]. It should be noted that mass spectrometry is not suitable

for this, since it cannot distinguish methylketene from acrolein, the isomer of methylketene [22]. The observation of traces of methylketene may favour the mechanism via ketene intermediate for propionic acid ketonisation over HPW and CsPW; however, more evidence is required to prove this.

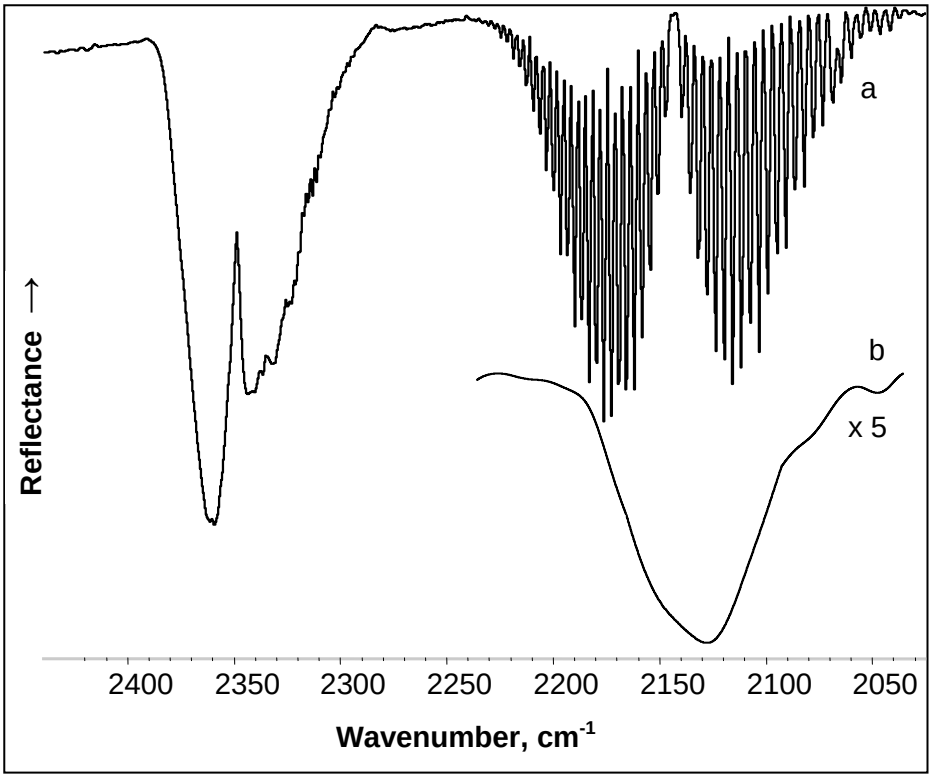

Figure 4.4 IR spectra of gaseous products of catalytic conversion of propionic acid over CsPW at 350 °C in N_2: (a) CO (rotational-vibrational band centred at 2140 cm^{-1}) and CO_2 (rotational-vibrational band of the asymmetric stretch centred at 2350 cm^{-1} with unresolved rotational fine structure), (b) methylketene (asymmetric stretch at 2130 cm^{-1}, the intensity scaled up 5-fold compared to that of CO and CO_2).

The neutral salt $Cs_3PW_{12}O_{40}$ was inactive for ketonisation of propionic acid. It exhibited zero acid conversion at 250-300 °C and at 350-400 °C produced ethene as the main product, together with ethane and a little propene, as presented in Table 4.2. This

is inconsistent with ketonisation occurring via Cs carboxylate intermediate and thus may support the intermediacy of methylketene for this reaction.

Table 4.2 Hydrogenation of propionic acid over $Cs_3PW_{12}O_{40}$[a]

Temperature (°C)	Conversion (%)	Selectivity (mol %)		
		Ethane	Ethene	Propene
350	21	20	61	19
400	80	30	63	7

(a) 0.2 g catalyst, 2.0% propionic acid in H_2 flow, 10 ml min^{-1} flow rate, 3 h time on stream.

The general picture emerging from these results is as follows. First, propionic acid is probably dehydrated on HPW or CsPW to form a short-lived methylketene intermediate (Equation 4.4) with the aid of Brønsted acid catalysis. This is followed by its interaction with propionic acid molecules to yield 3-pentanone (Equation 4.5).

$$CH_3CH_2COOH \rightarrow CH_3CH=C=O + H_2O \quad (4.4)$$

$$CH_3CH=C=O + CH_3CH_2COOH \rightarrow (CH_3CH_2)_2CO + CO_2 \quad (4.5)$$

The mechanism of ketonisation via ketene intermediate has been discussed in more detail [23]. Regarding this mechanism, the ketonisation of acetic acid over various metal oxides involves the coupling reaction between one adsorbed acetic acid molecule that strongly interacts with the surface catalyst through the α-hydrogen atom and another adjacent adsorbed acetic acid molecule, as illustrated in Scheme 4.1.

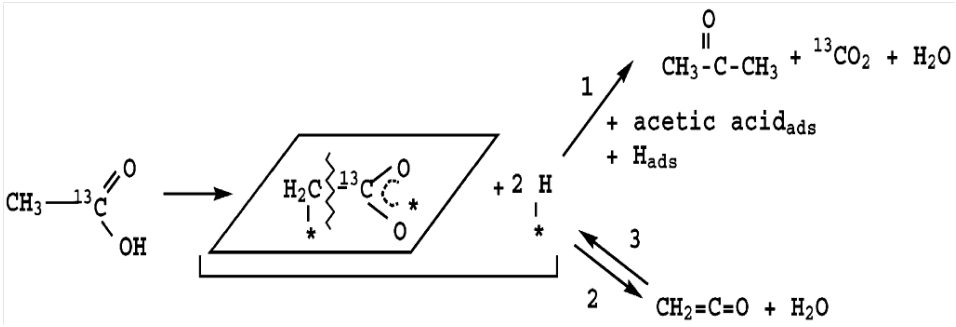

Scheme 4.1 Proposed mechanism for ketone production from acetic acid via ketene intermediacy [23]

3-Pentanone, the main product in the temperature range 250-350 °C, was found to be stable in the presence of HPW and CsPW in this temperature range. As the temperature is increased, methylketene increasingly decomposes to yield ethene and CO at the expense of 3-pentanone. Direct decarbonylation (Equation 4.3) is probably inefficient in this system; it appears to play a significant role in the presence of metal catalysts. Decarboxylation (Equation 4.2) occurs in parallel with ethene formation to yield ethane and CO_2 (Figures 4.1 and 4.2).

In flowing H_2, CsPW gave a small amount of propanal and 1-propanol, which peaked at ~350 °C, as shown in Figure 4.2. This reaction appears to be similar to that occurring on P-Mo-V [15] and is discussed later in Section 4.3. In the presence of H_2, both CsPW and HPW/SiO_2 also produced some propene, which probably formed through 1-propanol dehydration.

4.3 Deoxygenation of propionic acid over metal catalysts

This section focuses on metal-loaded CsPW catalysts, with Pd, Pt and Cu as the metal additives. As demonstrated by the TPR, FTIR and XRD results reported in Chapter 3, these catalysts are stable towards reduction in H_2, and CsPW retains its primary and secondary structures within the required temperature range. Since CsPW has strong Brønsted acidity, these materials can act as metal-acid bifunctional catalysts. For comparison, we will also look at the performance of these metals supported on silica as monofunctional metal catalysts.

The activity of catalysts was examined under H_2 and under N_2 in the temperature range of 250-400 °C for 3 h on stream. During this time, the activity was fairly stable and the catalysts reached steady state within 1 h. Figures 4.5-4.8 and Table 4.3 illustrate catalyst performance as a function of temperature.

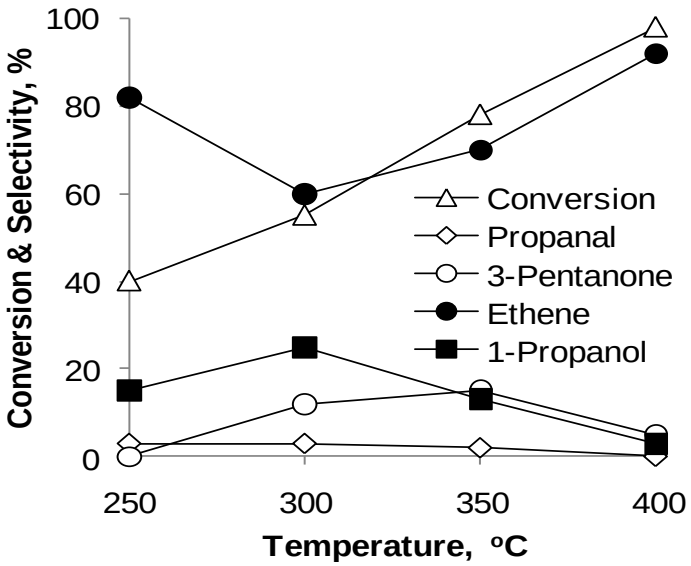

Figure 4.5 Variation of propionic acid conversion and selectivity to main reaction products with reaction temperature during the deoxygenation of propionic acid over 0.5%Pd/CsPW. Reaction conditions: 0.2 g catalyst, 2.0% propionic acid in H_2 flow, 10 ml min^{-1} flow rate, 3 h time on stream.

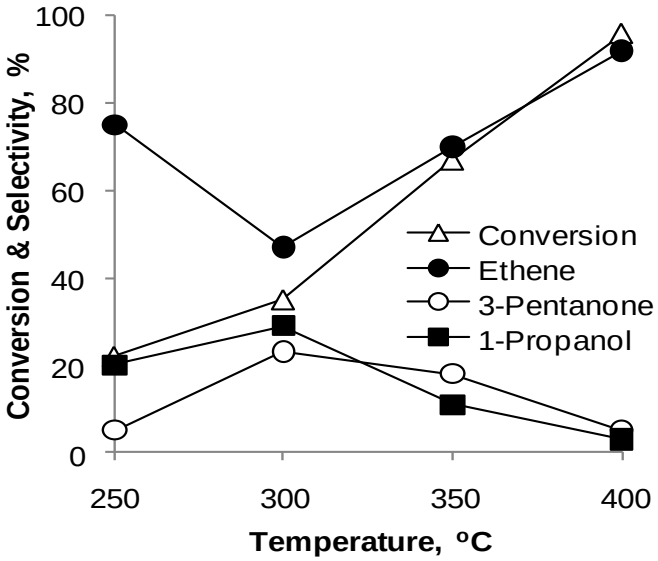

Figure 4.6 Variation of propionic acid conversion and selectivity to main reaction products with reaction temperature during the deoxygenation of propionic acid over 0.5%Pt/CsPW. Reaction conditions: 0.2 g catalyst, 2.0% propionic acid in H_2 flow, 10 ml min^{-1} flow rate, 3 h time on stream.

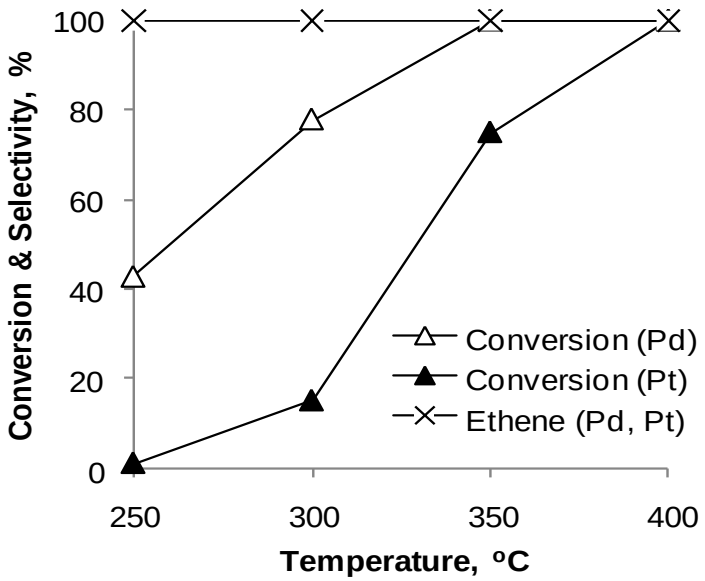

Figure 4.7 Variation of propionic acid conversion and selectivity to ethene with reaction temperature during the deoxygenation of propionic acid over 0.5%Pd/SiO_2 and 0.5%Pt/SiO_2. Reaction conditions: 0.2 g catalyst, 2.0% propionic acid in H_2 flow, 10 ml min^{-1} flow rate, 3 h time on stream.

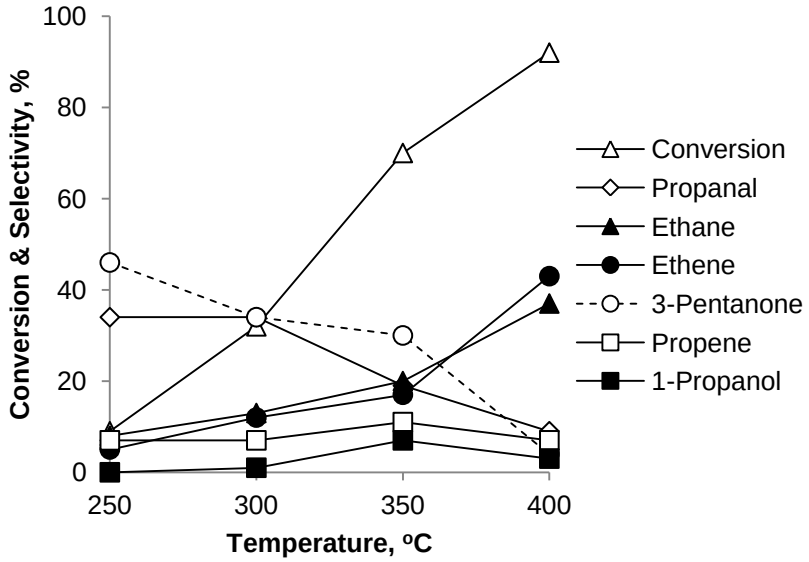

Figure 4.8 Variation of propionic acid conversion and selectivity to main reaction products with reaction temperature during the deoxygenation of propionic acid over 5%Cu/CsPW. Reaction conditions: 0.2 g catalyst, 2.0% propionic acid in H_2 flow, 10 ml min^{-1} flow rate, 3 h time on stream.

Table 4.3 Hydrogenation of propionic acid over 5%Cu/SiO_2[a]

T (°C)	Conversion (%)	Selectivity (mol %)				
		Propanal	Ethane	Ethene	Propene	1-Propanol
250	2.5	100				
300	34	36	0.2	0.5	0.3	63
350	80	60	0.5	0.4	0.4	39
350[b]	80	59	0.4	0.5	0.5	40
350[c]	65	60	0.3	0.5	0.4	39
400	87	79	1.7	0.5	0.5	19

(a) 0.2 g catalyst, 2.0% propionic acid in H_2 flow, 10 ml min^{-1} flow rate (W/F = 8.0 h g mol^{-1}), 3 h time on stream.

(b) 20 ml min^{-1} flow rate (W/F = 4.0 h g mol^{-1}).

(c) 40 ml min^{-1} flow rate (W/F = 2.0 h g mol^{-1}).

All of these catalysts except 0.5%Pd/CsPW exhibited the usual exponential growth of substrate conversion (S-shaped curve) with an apparent activation energy $E \geq$ 30 kJ mol^{-1} in the 250-300 °C range (Table 4.4). This implies the absence of mass transport limitations for these catalysts under such conditions. It should be noted that bifunctional metal/CsPW catalysts had lower E values than the corresponding metal/SiO_2 catalysts, which points to more efficient catalysis with the former compared to the latter catalysts. 0.5%Pd/CsPW had a smaller E value of ca. 20 kJ mol^{-1} and displayed almost linear growth in conversion with the temperature, as shown in Figure 4.5. This may indicate mass transport limitations. However, the activity of 0.5%Pd/CsPW is close to that of 0.5%Pt/CsPW as presented in Figure 4.6, which suggests similar reaction regimes in both cases. Another possible explanation is that 0.5%Pd/CsPW catalyst suffers from deactivation due to Pd sintering, because after the

reaction under H_2 at 300 °C, Pd dispersion dropped from 0.37 in fresh catalyst to 0.07 in spent catalyst, as can be seen in Table 4.1. For other Pd and Pt catalysts, the metal dispersion did not change significantly after reaction. However, more rigorous kinetic studies are required for the reaction regime to be assessed.

Table 4.4 Apparent activation energies for propionic acid conversion over metal catalysts[a]

Catalyst	Pd/CsPW	Pd/SiO_2	Pt/CsPW	Pt/SiO_2	Cu/CsPW	Cu/SiO_2
E (kJ mol^{-1})	20	35	30	150	75	140

(a) Calculated in the temperature range of 250-300 °C.

Overall, the picture emerging from these results is twofold. First, the metal loading onto CsPW and SiO_2 has a profound effect on catalyst performance in flowing H_2 but hardly any effect in N_2; secondly, the performance of Pd and Pt catalysts is very different from that of Cu catalysts. In flowing H_2, bifunctional metal-acid catalysts comprising Pd and Pt supported on CsPW exhibited greatly enhanced activity towards decarbonylation (Eq. 4.3) to form ethene (Figures 4.5 and 4.6) at the expense of ketonisation and decarboxylation, as compared to the metal-free CsPW (Figure 4.2). With both Pd and Pt catalysts, the selectivity to ethene increased to 92% at almost 100% conversion at 400 °C. Previously, for acetic acid deoxygenation on TiO_2 it has been found that loading TiO_2 with Pt suppresses ketonisation to acetone and enhances acid decomposition to CH_4, CO and CO_2 [27]. For acetic acid deoxygenation, however, it is not possible to discriminate between decarbonylation and decarboxylation pathways, since methane will form in either case. In our case, neither Pd/CsPW nor

Pt/CsPW showed any activity towards decarboxylation of propionic acid to form ethane (Eq. 4.2). The fact that propionic acid decarbonylation to ethene over the Pd and Pt catalysts occurred under H_2 but not under N_2, although by stoichiometry H_2 is not required for decarbonylation, suggests that the reaction proceeds via hydrogenolysis of C-O and/or C-C bond and hence can be referred to as hydrodeoxygenation.

With Pd/CsPW and Pt/CsPW, the total selectivity to propanal and its consecutive hydrogenation product 1-propanol increased in the temperature range of 250-300 °C, as compared to the metal-free CsPW (cf. Figure 4.2 and Figures 4.5 and 4.6). In contrast, Pd/SiO_2 and Pt/SiO_2 yielded no significant quantity of 1-propanol or propanal. These results suggest that propanal is formed by propionic acid hydrogenation on the CsPW polyoxometalate, possibly by the Mars-van Krevelen mechanism proposed earlier for the reaction on P-Mo-V POMs [14, 15]. The enhancement of propanal formation on CsPW loaded with Pd and Pt may be explained by hydrogen spillover from Pt and Pd to CsPW. This involves dissociative adsorption of H_2 on the platinum group metal, followed by hydrogen migration to CsPW to create active sites (oxygen vacancies), where hydrogenation of propionic acid could take place. A similar mechanism has been proposed for the hydrogenation of acetic acid on Pt/TiO_2 [27].

0.5%Pd/SiO_2 and 0.5%Pt/SiO_2 were found to exhibit almost 100% selectivity to ethene at 100% propionic acid conversion in flowing H_2 at 250-400 °C (Fig. 4.7). It has been reported that the gas-phase deoxygenation of longer-chain carboxylic acids over 7%Pd/SiO_2 in H_2 at 330 °C occurs via a decarboxylation pathway to yield C_{n-1} alkanes [9]. For example, heptanoic and octanoic acids give hexane and heptane with respective yields of 98% and 97%. On the other hand, cyclopentanecarboxylic acid

gives a mixture of 40% cyclopentane and 45% cyclopentene [9]. The formation of ethene rather than ethane from propionic acid, in contrast to the deoxygenation of higher acids, may be explained by ethene being rapidly desorbed from the catalyst before being hydrogenated to ethane as a result of competing adsorption of CO, propionic acid and water present in the reaction system. In principle, ethene could have formed by dehydrogenation of ethane precursor, but this would have unfavourable thermodynamics at our reaction temperatures. Ethane dehydrogenation is an equilibrium-controlled process; it requires a temperature of 710 °C to reach 50% conversion at 1 bar ethane pressure [28].

Reaction selectivities observed for supported Cu catalysts were very different from those for the Pd and Pt catalysts. Thus, 5%Cu/CsPW, in contrast to 0.5%Pd/CsPW and 0.5%Pt/CsPW, clearly exhibited a preference towards hydrogenation of the C=O bond, giving propanal and 3-pentanone as the main products at 250-300 °C, whereas ethene, ethane and propene dominated at 400 °C (Fig. 4.8). 5%Cu/SiO_2 showed even higher selectivity for C=O bond hydrogenation, yielding almost exclusively propanal and 1-propanol (Table 4.3). The propanal/1-propanol ratio increased with temperature between 300 and 400 °C and was independent of contact time, which indicates that reaction equilibrium was approached.

The preference of Cu for C=O bond hydrogenation and Pd and Pt for decarbonylation via C-C bond hydrogenolysis has been recognised previously in hydrogenation and hydrodeoxygenation of aldehydes and ketones ([29-31] and references therein). Our study demonstrated that this is also the case in carboxylic acid hydrodeoxygenation.

4.4 Turnover frequency

Turnover frequency (TOF) is an accurate measurement value that can be used to calculate the catalyst activity. It can be defined as the number of reacted molecules per catalytic site per unit time [32]. The turnover rate of propionic acid conversion over different metal catalysts was measured at 250 °C under differential conditions (conversion < 10%). Under such conditions, the activity of CsPW support was negligible and the entire conversion could be attributed to metal nanoparticles. TOFs were calculated per surface metal atom using metal dispersions for fresh catalysts (Table 4.1), which were obtained from H_2 chemisorption for Pd and Pt, and from N_2O chemisorption for Cu. The TOF values for the overall conversion of propionic acid thus obtained follow the order Pd > Pt > Cu for both CsPW and SiO_2 supports (Table 4.5).

Table 4.5. TOF values per surface metal atom for the conversion of propionic acid at 250 °C[a]

Catalyst	Pd/CsPW[b]	Pt/CsPW[b]	Cu/CsPW
TOF (h^{-1})	67	28	1.0
Catalyst	Pd/SiO_2[b]	Pt/SiO_2	Cu/SiO_2
TOF (h^{-1})	34	3.3	1.3

(a) 0.2 g catalyst, 2.0% propionic acid in H_2 flow, 10 ml min^{-1} flow rate, 3 h time on stream, < 10% conversion.

(b) Catalyst bed: 0.05 g catalyst + 0.15 g SiO_2.

The TOFs calculated using the metal dispersion for spent catalysts were higher in value, as expected, but the order of relative metal activity remained the same. Pd and Cu nanoparticles supported on CsPW and SiO_2 exhibited close turnover rates, whereas Pt was significantly more active on CsPW than on SiO_2. The latter may be attributed to a stronger ability of Pt to form covalent bonds due to its larger number of electrons, resulting in stronger metal-support interaction in the case of Pt compared to Pd and Cu. The better sintering resistance of Pt nanoparticles on amorphous silica compared to crystalline CsPW indicates stronger interaction of Pt with silica than with CsPW, reducing the relative activity of Pt/SiO_2 catalyst.

4.5 Conclusions

The catalysed gas-phase deoxygenation of propionic acid was investigated in a fixed-bed reactor at 250-400 °C in flowing H_2 or N_2 in the presence of Keggin-type heteropoly acid $H_3PW_{12}O_{40}$ (HPW) supported on silica and its bulk acidic salt $Cs_{2.5}H_{0.5}PW_{12}O_{40}$ (CsPW), as well as with Pd-, Pt- and Cu-loaded CsPW bifunctional metal-acid catalysts. These catalysts were compared with the corresponding SiO_2-supported metal catalysts. CsPW itself and CsPW-supported Pd, Pt and Cu catalysts retained the Keggin structure of their polyanion (primary structure), as well as the CsPW crystal structure (secondary structure), after the reaction at 400 °C in H_2, whereas HPW decomposed above 350 °C in N_2. The reaction was found to involve several pathways such as ketonisation, decarbonylation, decarboxylation and hydrogenation, leading to partial or total deoxygenation of propionic acid. HPW and CsPW, both in H_2 and in N_2, exhibited ketonisation activity between 250 and 300 °C to yield 3-pentanone, CsPW being more

selective than HPW. At 400 °C, HPW and CsPW were active for decarbonylation and decarboxylation of propionic acid to yield ethene and ethane respectively. Loading Pd or Pt onto CsPW greatly affected catalyst performance in H_2, enhancing decarbonylation of propionic acid to form ethene at the expense of ketonisation and decarboxylation. The metal loading, however, had little effect in N_2. Pd/SiO_2 and Pt/SiO_2 exhibited similar behaviour, showing almost 100% selectivity to ethene in H_2. These results are consistent with the hydrodeoxygenation of propionic acid, suggesting that hydrogenolysis of C-C bonds on Pd and Pt sites plays an essential role. In contrast to the Pd and Pt catalysts, the Cu catalysts, Cu/CsPW and Cu/SiO_2, were both active in the hydrogenation of the C=O bond to yield propanal and 1-propanol. The turnover rates of propionic acid conversion on metal catalysts were found to follow the order Pd > Pt > Cu for both CsPW-supported and silica-supported metal catalysts. The main routes of propionic acid deoxygenation with the catalysts studied are summarised below:

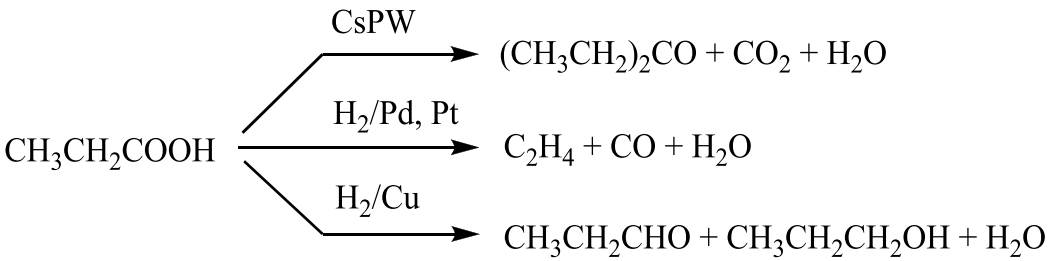

From a practical point of view, it may be desirable to produce the ketonisation products with carbon backbone upgrade ($C_n \rightarrow C_{2n-1}$) over CsPW at 250-300 °C in a hydrogen-free system, as well as the C_n hydrogenation products (aldehydes and alcohols) without carbon loss using Cu catalysts. On the other hand, Pd and Pt catalysts possessing high hydrodeoxygenation activity via the decarbonylation pathway allow the production of C_{n-1} alkenes.

References

[1] E.L. Kunkes, D.A. Simonetti, R.M. West, J.C. Serrano-Ruiz, C.A. Gartner, J.A. Dumesic, Science 322 (2008) 417.

[2] A. Corma, S. Iborra, A. Velty, Chem. Rev. 107 (2007) 2411.

[3] T.V. Choudhary, C.B. Phillips, Appl. Catal. A 397 (2011) 1.

[4] M. Snare, I. Kubickova, P. Maki-Arvela, K. Eranen, D.Y. Murzin, Ind. Eng. Chem. Res. 45 (2006) 5708.

[5] H. Bernas, K. Eranen, I. Simakova, A.R. Leino, K. Kordas, J. Myllyoja, P. Maki-Arvela, T. Salmi, D.Y. Murzin, Fuel 89 (2010) 2033.

[6] J.G. Immer, M.J. Kelly, H.H. Lamb, Appl. Catal. A 375 (2010) 134.

[7] P.T. Do, M. Chiappero, L.L. Lobban, D.E. Resasco, Catal. Lett. 130 (2009) 9.

[8] Y. Takemura, A. Nakamura, H. Taguchi, K. Ouchi, Ind. Eng. Chem. Prod. Rd. 24 (1985) 213.

[9] W.F. Maier, W. Roth, I. Thies, P.V. Schleyer, Chem. Ber-Recl. 115 (1982) 808.

[10] M. Arend, T. Nonnen, W.F. Hoelderich, J. Fischer, J. Groos, Appl. Catal. A 399 (2011) 198.

[11] T. Okuhara, N. Mizuno, M. Misono, Adv. Catal. 41 (1996) 113.

[12] J.B. Moffat, Metal-Oxygen Clusters: The Surface and Catalytic Properties of Heteropoly Oxometalates, Kluwer, New York, 2001.

[13] I.V. Kozhevnikov, Catalysts For Fine Chemical Synthesis, Catalysis by Polyoxometalates, Wiley Chichester, 2002.

[14] H. Benaissa, P.N. Davey, E.F. Kozhevnikova, I.V. Kozhevnikov, Appl. Catal. A 351 (2008) 88.

[15] H. Benaissa, P.N. Davey, Y.Z. Khimyak, I.V. Kozhevnikov, J. Catal. 253 (2008) 244.

[16] C.A. Gaertner, J.C. Serrano-Ruiz, D.J. Braden, J.A. Dumesic, J. Catal. 266 (2009) 71.

[17] J.E. Benson, H.S. Hwang, M. Boudart, J. Catal. 30 (1973) 146.

[18] A. Dandekar, M.A. Vannice, J. Catal. 178 (1998) 621.

[19] A.D. Murkute, J.E. Jackson, D.J. Miller, J. Catal. 278 (2011) 189.

[20] O. Nagashima, S. Sato, R. Takahashi, T. Sodesawa, J. Mol. Catal. A 227 (2005) 231.

[21] P.W. Atkins, Physical Chemistry, Oxford University Press, 1998.

[22] K.S. Kim, M.A. Barteau, Langmuir 4 (1988) 945.

[23] R. Pestman, A. Vanduijne, J.A.Z. Pieterse, V. Ponec, J. Mol. Catal. A 103 (1995) 175.

[24] T. Yokoyama, N. Yamagata, Appl. Catal. A. 221 (2001) 227.

[25] P.G. Blake, K.J. Hole, J. Phys. Chem. 70 (1966) 1464.

[26] F. Winther, S. Meyer, F.M. Nicolaisen, J. Mol. Struct. 611 (2002) 9.

[27] R. Pestman, R.M. Koster, J.A.Z. Pieterse, V. Ponec, J. Catal. 168 (1997) 255.

[28] G.C. Bond, Metal-Catalysed Reactions of Hydrocarbons, Springer, 2005.

[29] K.M. Parida, S. Rana, S. Mallick, D. Rath, J. Colloid Interf. Sci. 350 (2010) 132.

[30] W.A.H. B. Cornils, M. Muhler, C.-H. Wong (Eds.), Catalysis From A to Z, Wiley-VCH, Weinheim, 2007.

[31] T.T. Pham, L.L. Lobban, D.E. Resasco, R.G. Mallinson, J. Catal. 266 (2009) 9.

[32] M. Boudart, Chem. Rev. 95 (1995) 661.

5. Hydrodeoxygenation of MIBK and DIBK over bifunctional metal-loaded polyoxometalate catalyst

5.1 Introduction

Efficient utilisation of biomass resources is a major goal for academia and industry [1, 2]. Presently, about 50% of the crude oil produced worldwide is refined into transportation fuels. The use of biomass-derived fuels such as ethanol and biodiesel can significantly reduce greenhouse gas emission, diversify energy sources and improve energy security. It is expected that biomass-based *n*-butanol (biobutanol) will also play a major role in the next generation of biofuels, together with ethanol and biodiesel. Butanol produces more power than ethanol, and 85% butanol/gasoline blends can be used in unmodified petrol engines [3]. Biobutanol can be produced by the acetone-butanol fermentation of carbohydrates and cellulosic raw materials using a strain of *Clostridium acetobutylicum* which yields butanol together with acetone and ethanol in a weight ratio of 6:3:1 [4, 5]. This process, however, will produce a large surplus of acetone. Therefore, finding new outlets for acetone, preferably in the transportation fuel sector, would greatly improve the economy of biobutanol production. It is well known that acetone can be transformed into C_6, C_9 and larger organic molecules by aldol condensation. This is employed in the industrial production of methyl isobutyl ketone (MIBK) and diisobutyl ketone (DIBK) (Scheme 5.1), which are used as solvents in paints, coatings and resins [6-8]. MIBK and DIBK can be hydrogenated to alkanes, 2-methylpentane (MP) and 2,6-dimethylheptane (DMH), which can be blended with gasoline and used through the existing fuel infrastructure. However, to the best of our knowledge, there is little data available on the catalytic hydrogenation of MIBK.

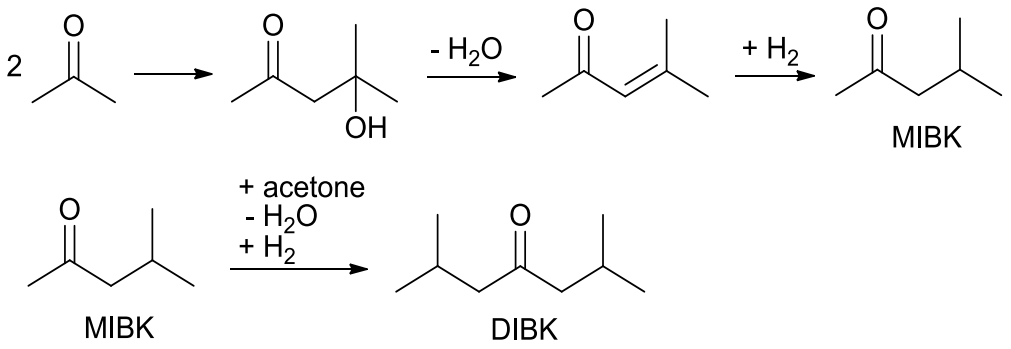

Scheme 5.1 MIBK and DIBK production from acetone. It can be performed as a one-pot process using a bifunctional metal-acid catalyst, e.g. Pd on an acidic support [6-8].

In the work reported in this chapter, the hydrodeoxygenation of MIBK was investigated in the gas phase. First, a number of conventional supported metal catalysts comprising Pd, Pt, Ru and Cu supported on silica and active carbon (monofunctional catalysts) were examined. Next, bifunctional metal-polyoxometalate catalysts comprising Pt, Pd, Ru, or Cu supported on Keggin heteropoly salt $Cs_{2.5}H_{0.5}PW_{12}O_{40}$ (CsPW) were tested. This salt is widely used as a solid acid catalyst. It is a strong Brønsted acid, almost as strong as the parent heteropoly acid $H_3PW_{12}O_{40}$, with the important advantage over the latter of having much larger surface area (111 m^2g^{-1}) and a higher thermal stability (~500 °C decomposition temperature) [9, 10], hence a longer lifetime [11, 12]. Table 5.1 lists the catalysts studied and summarises their characterisation data. The purpose of this study was to explore bifunctional metal-acid catalysed pathways to achieve MIBK-to-MP hydrogenation in one step on a single catalyst bed. Finally, the hydrogenation of DIBK in the gas phase was examined using 0.5%Pt/CsPW and reduced copper chromite for comparison as catalysts.

Table 5.1 Catalyst characterisation

Catalyst	S_{BET}[a] [m^2 g^{-1}]	D[b]
5%Cu/CsPW	75	0.11
5%Cu/SiO_2	251	0.05
0.5% Pd/CsPW	87	0.37
0.5% Pd/SiO_2	255	0.62
0.5% Pt/ CsPW	100	0.36
0.5% Pt/SiO_2	287	0.27
0.25%Pt/CsPW	101	0.80
1%Pt/CsPW	106	0.18
0.5%Ru/CsPW	118	0.24
5%Ru/CsPW	105	0.11
10%Pt/C	801	
5%Ru/C	792	
5%Pd/C	924	
10%Pd/C	823	
$2CuO{\cdot}Cr_2O_3$[c]	55	

a) BET surface area

b) Metal dispersion in fresh catalysts

c) After reduction at 400 °C in H_2 for 2 h

The hydrogenation of MIBK and DIBK was carried out in the gas phase in flowing H_2. The reaction testing procedure is described in more detail in Section 2.5.2 and summarised here for clarity. The catalysts were tested at 100-400 °C under atmospheric pressure in a Pyrex fixed-bed down-flow reactor fitted with an on-line gas chromatograph (Varian Star 3400 CX instrument with a 30 m x 0.25 mm HP INNOWAX capillary column and a flame ionisation detector). For more accurate analysis of C_1-C_5 hydrocarbon products, a 60 m x 0.32 mm GSGasPro capillary column was used, allowing for full separation of these hydrocarbons. The temperature in the

reactor was controlled by a Eurotherm controller using a thermocouple placed at the top of the catalyst bed. The gas feed contained a variable amount of MIBK or DIBK in H_2 as carrier gas. The reactants were fed by passing the carrier gas flow controlled by a Brooks mass flow controller through a stainless steel saturator which held liquid MIBK or DIBK at an appropriate temperature to maintain the chosen reactant concentration. The gas feed entered the reactor at the top at a flow rate of 20-100 ml min^{-1}. The reactor was packed with 0.2 g catalyst powder of 45-180 μm particle size. In some cases, to reduce reaction rate, a smaller amount of catalyst was used as a homogeneous mixture with silica of a total weight of 0.2 g. Prior to reaction, the catalysts were pre-treated in H_2 for 1 h at the reaction temperature. Once the reaction started, the downstream gas flow was analysed by the on-line GC to obtain reactant conversion and product selectivity. The selectivity was defined as moles of product formed per mole of reactant converted and is quoted in mole per cent.

5.2 Gas phase hydrogenation of MIBK

5.2.1 MIBK hydrogenation over conventional supported metal catalysts

A number of conventional supported metal catalysts comprising Pd, Pt, Ru and Cu supported on silica and active carbon for MIBK hydrogenation in the temperature range 100-400 °C were tested. Some representative results are shown in Tables 5.2 and 5.3.

Table 5.2 Hydrogenation of MIBK at 100 °C over conventional supported metal catalysts[a]

Catalyst	Conversion (%)	Selectivity (%)		
		MP	MP-ol	Other[c]
0.5%Pt/SiO_2	64	14	86	0
10%Pt/C	95	6	93	1
0.5%Pd/SiO_2	3	0	100	0
10%Pd/C	7	2	58	40
5%Ru/C	96	2	95	3
5%Cu/SiO_2	<1	0	100	0
$2CuO{\cdot}Cr_2O_3$[b]	92	0	100	0

a) 3.6% MIBK in H_2 flow, 20 ml min^{-1} flow rate, 0.20 g catalyst pretreated in H_2 at reaction temperature for 1 h, 4 h time on stream.

b) Pre-reduced in H_2 at 400 °C for 2 h; exhibited XRD pattern of Cu metal.

c) C_1-C_5 cracking products, mainly propene and butene, together with small amounts of C_{6+} condensation products

At 100-200 °C, these catalysts were active in the hydrogenation of MIBK to 4-methyl-2-pentanol (MP-ol). The best results were obtained for 10%Pt/C, 5%Ru/C and copper chromite, with 93-100% MP-ol selectivity and 92-96% MIBK conversion at 100 °C. Selectivity to MP-ol decreased with increasing temperature due to the formation of MP and hydrogenolysis of C-C bonds, giving C_1-C_5 hydrocarbons. The highest MP selectivities of 87-94% were observed for 10%Pt/C and 10%Pd/C catalysts at 52-84%

conversion, but only at a temperature as high as 300 °C (Table 5.3), which indicates the difficulty of direct hydrogenation of MP-ol to MP.

Table 5.3 Hydrogenation of MIBK at 200 °C on conventional supported metal catalysts[a]

Catalyst	Conversion (%)	Selectivity (%)		
		2MP	MP-ol	Other
0.5%Pt/SiO_2	46	47	53	0
10%Pt/C	47	40	56	4
10%Pt/C[b]	52	87	9	4
0.5%Pd/SiO_2	46	0	47	53
10%Pd/C	37	28	66	6
10%Pd/C[b]	84	94	5	1
5%Ru/C	65	54	26	20
5%Cu/SiO_2	34	0	100	0
2CuO·Cr_2O_3[c]	41	0	82	18

a) 3.6% MIBK in H_2 flow, 20 ml min^{-1} flow rate, 0.20 g catalyst pretreated in H_2 at reaction temperature for 1 h, 4 h time on stream.

b) At 300 °C.

c) Pre-reduced in H_2 at 400 °C for 2 h; exhibited XRD pattern of Cu metal.

d) C_1-C_5 cracking products, mainly propene and butene, together with small amounts of C_{6+} condensation products.

5.2.2 MIBK hydrogenation over bifunctional metal-polyoxometalate catalysts

Bifunctional metal-polyoxometalate catalysts comprising Pt, Pd, Ru, or Cu supported on Keggin heteropoly salt $Cs_{2.5}H_{0.5}PW_{12}O_{40}$ (CsPW) were tested. Representative results are shown in Table 5.4.

Table 5.4 Hydrogenation of MIBK at 100 °C over bifunctional metal-acid catalysts[a]

Catalyst	Conversion (%)	Selectivity (%)		
		MP	MP-ol	Other
0.5%Pt/CsPW	99	100	0	0
0.5%Pt/CsPW[b]	95	88	0	12
0.5%Pt/HZSM-5[c]	94	65	34	1
0.5%Pt/HZSM-5[b,c]	100	83	0	17
0.5%Pd/CsPW	7	34	0	66
0.5%Ru/CsPW	5	100	0	0
5%Ru/CsPW	99	100	0	0
5%Cu/CsPW	<1	100	0	0

a) 0.20 g catalyst pretreated in H_2 at reaction temperature for 1 h, 3.6% MIBK in H_2 flow, 20 ml min^{-1} flow rate, 4 h time on stream.

b) At 200 °C.

c) Atomic ratio Si/Al = 12.

d) MP isomers.

e) C_{6+} condensation products.

It can be seen that 0.5%Pt/CsPW clearly stands out amongst the bifunctional catalysts studied, yielding 99% MP at 100 °C, with 100% MP selectivity at ≥ 99% MIBK conversion (top entry in Table 5.4). Importantly, no MP isomerisation was observed at this temperature, thus allowing synthetically viable complete transformation of ketone to alkane without carbon backbone alteration. At 200 °C, about 12% of MP isomerised to form *n*-hexane, 3-methylpentane and 2,3-dimethylbutane, in agreement with the literature [13]. 0.5%Ru/CsPW matched the Pt catalyst in MP selectivity, but had much lower activity per unit metal weight. About 5% Ru loading was required to match the activity of the 0.5% Pt catalyst, but performance stability was lower than for Pt catalyst when the process ran for a long time, as will be shown later. 0.5%Pd/CsPW was inferior to the Pt catalyst regarding both catalytic activity and MP selectivity, giving a large amount of heavy condensation products. Previously, Pd/CsPW has been found to be an active bifunctional catalyst for the one-pot hydrocondensation of acetone to MIBK and further to DIBK [7]. Finally, 5%Cu/CsPW showed practically no catalytic activity at 100 °C.

5.2.2.1 Catalyst performance stability

Pt/CsPW catalyst showed excellent performance stability at 100 °C. It reached steady state in about 1 h and operated without deactivation for at least 14 h, as presented in Figure 5.1. It should be noted that to set the conversion in this run at about 80%, the amount of catalyst had to be reduced fourfold and the flow rate increased fivefold as compared to those in Table 5.4. About 1% of coke was found in the catalyst after reaction. Pt dispersion, i.e. the fraction of exposed Pt atoms, which was 0.36 in the fresh 0.5%Pt/CsPW catalyst, found from H_2 chemisorption, did not change after reaction, demonstrating high stability of Pt nanoparticles under reaction conditions. On

the other hand, 5%Ru/CsPW exhibited deactivation through its performance when running for a long time, as shown in Figure 5.2, with about 1.5% of coke deposited in the catalyst after reaction.

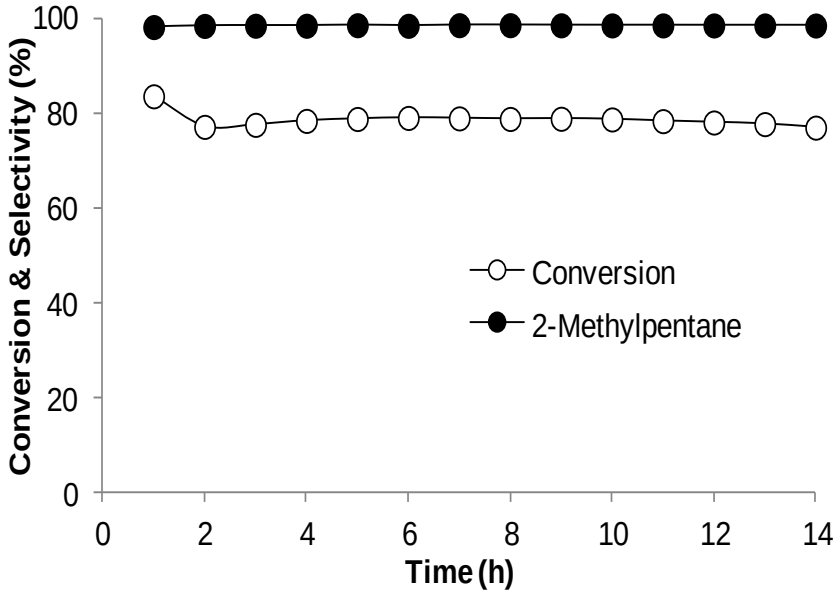

Figure 5.1 Time course of MIBK hydrogenation over 0.5%Pt/CsPW (0.05 g) at 100 °C (3.6% MIBK in H_2 flow, 100 ml min^{-1} flow rate, catalyst diluted with 0.15 g SiO_2).

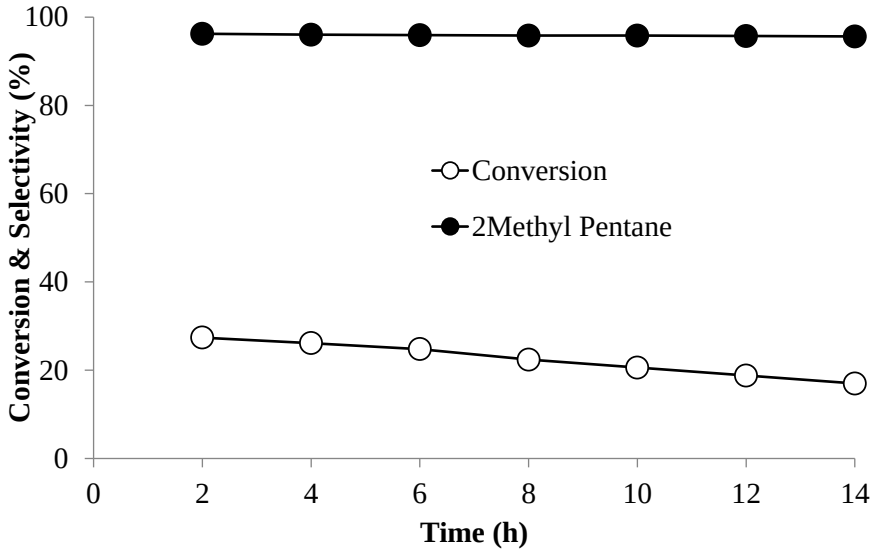

Figure 5.2 Time course of MIBK hydrogenation over 5%Ru/CsPW (0.05 g) at 100 °C (3.6% MIBK in H_2 flow, 100 ml min^{-1} flow rate, catalyst diluted with 0.15 g SiO_2).

5.2.2.2 Reaction mechanism over Pt/CsPW

Our idea was to explore a bifunctional metal-acid catalysed pathway to achieve MIBK-to-MP hydrogenation in one step on a single catalyst bed. This pathway would involve MIBK hydrogenation to MP-ol on metal sites, followed by MP-ol dehydration on acid sites to form olefin and finally olefin hydrogenation to MP on metal sites, as proposed in Scheme 5.2. Since dehydration of secondary alcohols on heteropoly acid catalysts is rapid [14, 15] and so is the hydrogenation of C=C bonds on platinum metals, the bifunctional pathway was expected to be more efficient than the hydrogenation-only pathway. Our study proved that this was indeed the case.

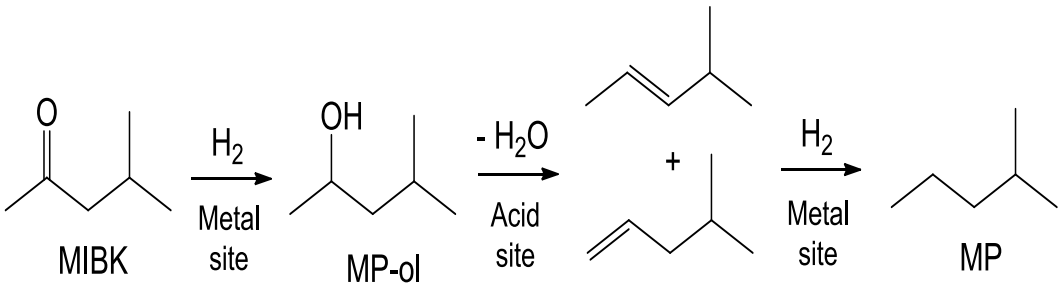

Scheme 5.2 Proposed mechanism for hydrodeoxygenation of MIBK *via* bifunctional metal-acid catalysis.

To prove the bifunctional mechanism presented in Scheme 5.2, the dehydration of MP-ol on 0.5%Pt/CsPW catalyst was tested at 100 °C under the conditions applied to MIBK hydrogenation (Table 5.4), except with N_2 (20 ml min^{-1}) instead of H_2. As expected, the reaction was very fast, yielding two olefins, 4-methylpentene-1 and 4-methylpentene-2, in about 1:1 ratio at 100% conversion, as represented in Equation 5.1. The same reaction under H_2 gave MP in a 100% yield (Equation 5.2). These results support the bifunctional mechanism for MIBK hydrogenation over 0.5%Pt/CsPW catalyst.

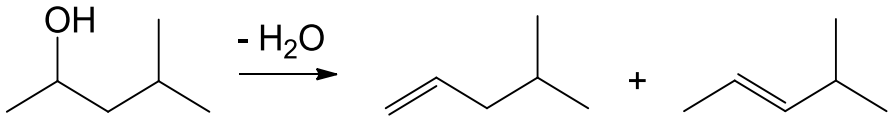

(5.1)

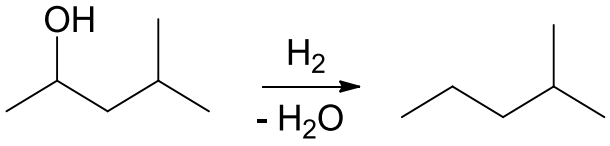

(5.2)

5.2.2.3 Preliminary kinetic study

The kinetic study of MIBK hydrogenation was performed using Pt/CsPW catalyst. To achieve this, MIBK conversion was kept below 10% by varying either or both of total flow rate of MIBK and catalyst weight. MIBK concentrations were varied between 3.6 and 6.4 vol%, the rest being hydrogen gas. The reaction rate was practically unchanged with MIBK concentration in the gas feed, as can be seen in Figure 5.3, which means that the order in MIBK was close to zero. Therefore, MIBK conversion was equivalent to the rate of MIBK consumption in our system. On the other hand, the order in the catalyst was close to one, as shown in Figure 5.4. The apparent activation energy was found to be 50 kJ mol^{-1} in the temperature range 60-100 °C, as shown in Figure 5.5, which indicates that the reaction occurred under kinetic control. From these results, the turnover frequency was estimated to be 160 h^{-1} per exposed Pt atom at 100 °C.

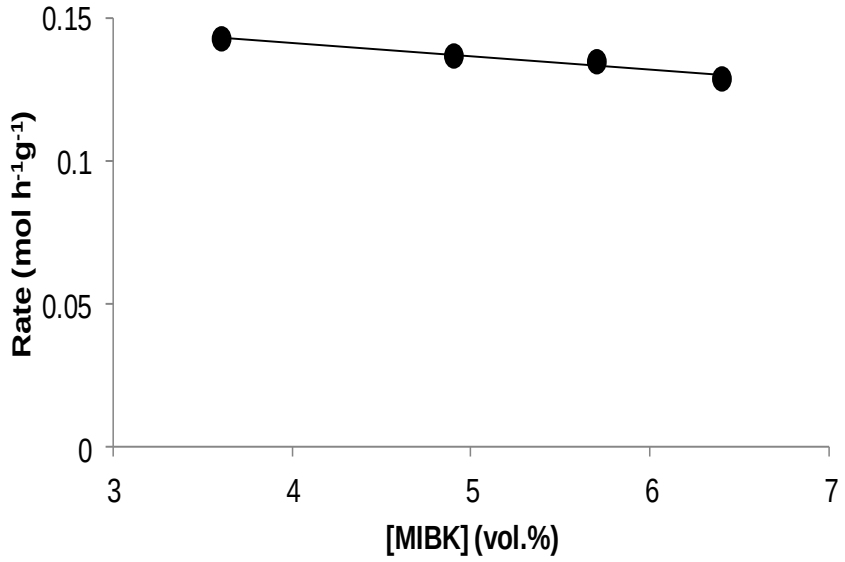

Figure 5.3 Effect of MIBK concentration on the rate of MIBK hydrogenation over 0.5%Pt/CsPW (0.025 g) at 100 °C (100 ml min^{-1} H_2 flow rate, catalyst diluted with 0.175 g SiO_2).

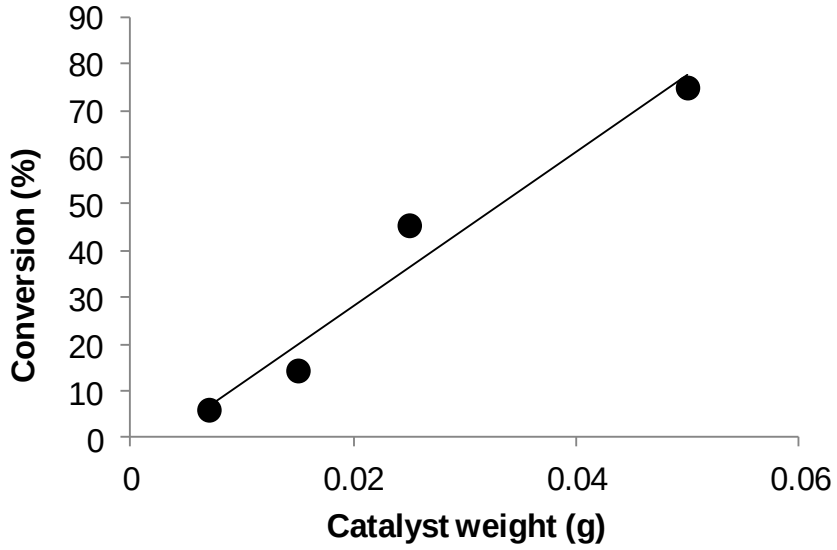

Figure 5.4 Effect of catalyst weight on conversion for MIBK hydrogenation over 0.5%Pt/CsPW at 100 °C (3.6% MIBK in H_2 flow, 100 ml min^{-1} flow rate, 0.5%Pt/CsPW + SiO_2 = 0.20 g).

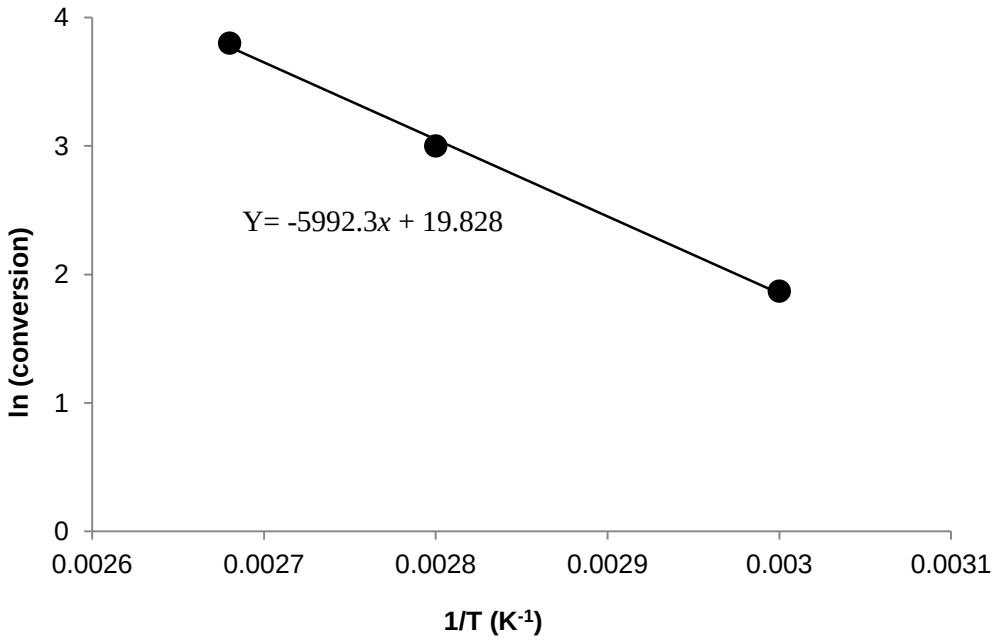

Figure 5.5 Arrhenius plot for MIBK hydrogenation over 0.5%Pt/CsPW (3.6% MIBK in H_2 flow, 100 ml min^{-1} flow rate, 0.5%Pt/CsPW + SiO_2 = 0.20 g).

To determine the rate-limiting step in the proposed mechanism of MIBK hydrogenation over Pt/CsPW catalyst that is presented in Scheme 6.2, the effect of Pt loading in Pt/CsPW catalyst on MIBK hydrogenation was investigated. As can be seen from Table 5.5, MIBK conversion increased from 30 to 100% with increasing Pt loading from 0.25 to 1%. In contrast, MP selectivity remained practically unchanged with Pt loading, being in the range of 93-100%. This clearly shows that the reaction is limited by the first step: hydrogenation of MIBK to MP-ol on Pt sites (Scheme 5.2). Subsequent dehydration and hydrogenation steps are fast under the chosen conditions. The fast dehydration of MP-ol over Pt/CsPW can be explained by the strong acidity of CsPW. Its acid strength corresponds to 165 kJ mol^{-1} in terms of the differential heat of NH_3 adsorption, as explained in Section 3.9.1. In this respect it was interesting to test a

Pt catalyst with weaker acid sites. Therefore 0.3%Pt/HZSM-5 with zeolite HZSM-5 was tested as an acidic support, possessing acid sites with a heat of NH_3 adsorption of 143 kJ mol^{-1}. At 100 °C this catalyst gave MIBK conversion close to that of 0.5%Pt/CsPW, but its MP selectivity (65%) was lower than for Pt/CsPW, due to incomplete dehydration of MP-ol on the weaker acid HZSM-5 (Table 5.4). This shows that the strong acidity of CsPW is essential for the high efficiency of the Pt/CsPW catalyst in the hydrodeoxygenation of MIBK. At 200 °C, Pt/HZSM-5 matched the performance of Pt/CsPW, but at this temperature considerable isomerisation of MP took place (Table 5.4). Hydrogenation of MIBK over Pt doped-zeolite catalysts will be discussed in more detail in Chapter 6.

Table 5.5 Effect of Pt loading in Pt/CsPW on MIBK hydrogenation[a]

Pt loading (wt%)	Conversion (%)	MP selectivity (%)
0.25	30	93
0.50	78	98
1.0	100	100

a) Catalyst mixture 0.05 g Pt/CsPW + 0.15 g SiO_2, 100 °C, 3.6% MIBK in H_2 flow, 100 ml min^{-1} flow rate, 4 h time on stream.

5.3 Gas phase hydrogenation of DIBK

The hydrogenation of DIBK over 0.5%Pt/CsPW catalyst was tested. For comparison, copper chromite was also tested and the results are shown in Table 5.6. The Pt catalyst again showed excellent performance under conditions similar to those applied to MIBK hydrogenation. At 100 °C, it gave 97% selectivity to DMH at 100% DIBK conversion, with 3% of C_9 alkane isomers also formed. No 2,6-dimethyl-4-heptanol (DMH-ol) was found amongst the reaction products.

Copper chromite, possessing weak acidity, performed differently, as in the case of MIBK reaction. At 100-200 °C, it gave DMH-ol as the main product (90-92% selectivity at 74-80% DIBK conversion). At 300 °C, it effected complete hydrogenation to give DMH with 92% selectivity at 96% DIBK conversion, with 8% selectivity to other C_9 alkane isomers.

Both catalysts, Pt/CsPW at 100 °C (Figure 5.6) and copper chromite at 300 °C, exhibited very good durability, operating without deactivation for at least 14 h. As determined with Pt/CsPW catalyst, the reactivity of DIBK was 8 times lower than that of MIBK at 100 °C. This can be explained by greater steric hindrance in the case of DIBK hydrogenation.

Table 5.6 Hydrogenation of DIBK[a]

Catalyst	Temperature (°C)	Conversion (%)	Selectivity (%)		
			DMH	DMH-ol	Other[b]
0.5%Pt/CsPW	100	100	97	0	3
$2CuO{\cdot}Cr_2O_3$[c]	300	96	92	0	8

a) 0.20 g catalyst, 1.7% DIBK in H_2 flow, 20 ml min^{-1} flow rate, 4 h time on stream.

b) Other products: C_9 alkane isomers.

c) Pre-reduced in H_2 at 400 °C for 2 h; exhibited XRD pattern of Cu metal.

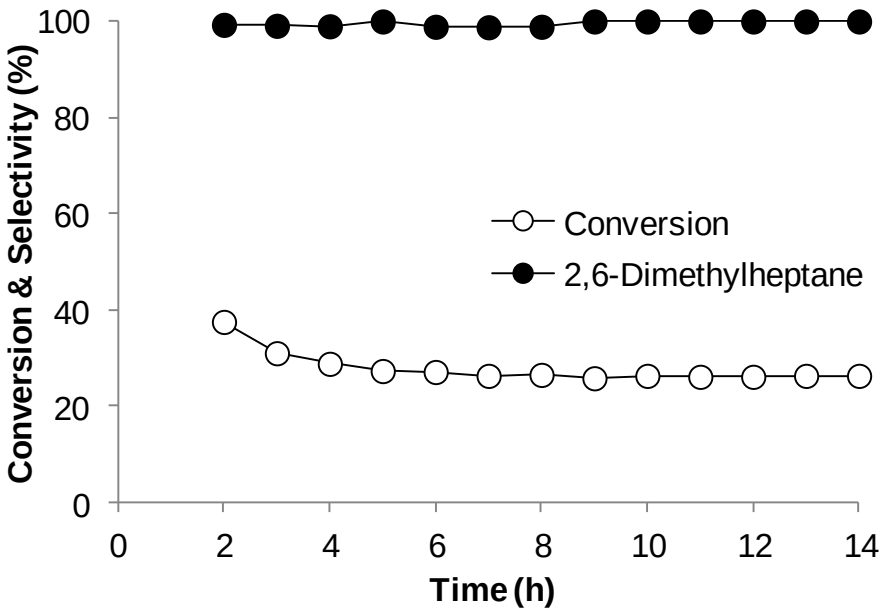

Figure 5.6 Time course for DIBK hydrogenation over 0.5%Pt/CsPW (0.05 g) at 100°C (1.7% DIBK in H_2 flow, 80 ml min^{-1} flow rate, catalyst diluted with 0.15 g SiO_2).

5.4 Conclusions

The gas phase hydrogenation of MIBK and DIBK was investigated in a fixed-bed reactor at 100-400 °C at atmospheric pressure. Bifunctional metal-doped Keggin heteropoly salt $Cs_{2.5}H_{0.5}PW_{12}O_{40}$ (CsPW) catalysts were examined. We developed a very efficient Pt/CsPW catalyst for the selective one-step hydrodeoxygenation of biomass-derived aliphatic ketones MIBK and DIBK under mild conditions (100 °C, 1 bar) without isomerisation of carbon backbone via a metal-acid bifunctional mechanism to give 2-methylpentane (MP) and 2,6-dimethylheptane (DMH) respectively, which could be blended with gasoline and used through the existing fuel infrastructure. The catalyst did not show any deactivation upon its performance for at least 14 hours on stream. Reduced copper chromite is also an efficient catalyst for DIBK hydrogenation at 300 °C.

The effects of reaction temperature, MIBK concentration, catalyst amount and Pt loading have been investigated. The catalysed reaction occurred under kinetic control. In addition, a bifunctional metal-acid catalysed mechanism to achieve MIBK-to-MP hydrogenation was proposed. This involves MIBK hydrogenation to MP-ol on metal sites followed by MP-ol dehydration on acid sites to form olefin and finally olefin hydrogenation to MP on metal sites.

References

[1] E.L. Kunkes, D.A. Simonetti, R.M. West, J.C. Serrano-Ruiz, C.A. Gartner, J.A. Dumesic, Science 322 (2008) 417.

[2] A. Corma, S. Iborra, A. Velty, Chem. Rev. 107 (2007) 2411.

[3] P. Durre, Ann. N. Y. Acad. Sci. 1125 (2008) 353.

[4] V.V. Zverlov, O. Berezina, G.A. Velikodvorskaya, W.H. Schwarz, Appl. Microbiol. Biot. 71 (2006) 587.

[5] D.T. Jones, D.R. Woods, Microbiol. Rev. 50 (1986) 484.

[6] R.D. Hetterley, R. Mackey, J.T.A. Jones, Y.Z. Khimyak, A.M. Fogg, I.V. Kozhevnikov, J. Catal. 258 (2008) 250.

[7] R.D. Hetterley, E.F. Kozhevnikova, I.V. Kozhevnikov, Chem. Comm. (2006) 782.

[8] F. Al-Wadaani, E.F. Kozhevnikova, I.V. Kozhevnikov, J. Catal. 257 (2008) 199.

[9] T. Okuhara, N. Mizuno, M. Misono, Adv. Catal. 41 (1996) 113.

[10] I.V. Kozhevnikov, Catalysts For Fine Chemical Synthesis, Catalysis by Polyoxometalates, Wiley Chichester, 2002.

[11] I.V. Kozhevnikov, J. Mol. Catal. A 305 (2009) 104.

[12] I.V. Kozhevnikov, J. Mol. Catal. A 262 (2007) 86.

[13] J. Macht, R.T. Carr, E. Iglesia, J. Catal. 264 (2009) 54.

[14] A.M. Alsalme, P.V. Wiper, Y.Z. Khimyak, E.F. Kozhevnikova, I.V. Kozhevnikov, J. Catal. 276 (2010) 181.

[15] J. Macht, M. Neurock, M. Iglesia, E., J. Am. Chem. Soc. 130 (2008) 10369.

6. Hydrodeoxygenation of MIBK over bifunctional Pt-zeolite catalyst

6.1 Introduction

Zeolites are crystalline microporous materials widely used as solid acid catalysts. Their well-defined pore dimensions allow them to be utilised for specific reactions. In addition, the acidity of zeolites is one of the most important properties in their applications [1]. For comparison with HPA catalysts, it is useful to test MIBK hydrogenation over a bifunctional metal catalyst based on zeolite. As demonstrated in Chapter 5, platinum is an active metal which, when loaded on CsPW, gave excellent performance in MIBK hydrogenation to yield 2MP.

The work reported in this chapter investigated the gas phase hydrogenation of MIBK over Pt-doped H-ZSM-5, H-Beta and H-Y. The catalysts were prepared using the ion exchange method explained in Section 2.3.6. The catalysts studied, together with their characterisation data, which were discussed in Chapter 3, are summarised in Table 6.1.

Table 6.1 Catalyst characterisation

Catalyst[a]	Si/Al[b]	S_{BET}[c] (m^2g^{-1})	D[d]	d[e] (nm)
0.30%Pt/H-ZSM-5	12	362	0.88	1.02
0.06%Pt/H-ZSM-5	12	357	0.87	1.03
0.39%Pt/H-Beta	12	491	0.72	1.25
0.45%Pt/H-Y	15	690	0.62	1.45

a) Pt loading (wt%) from ICP analysis

b) Si/Al atomic ratio in zeolites

c) BET surface area

d) Metal dispersion in fresh catalysts form H_2 chemisorption

e) Values obtained from the equation d (nm) = 0.9/D [2]

The hydrogenation of MIBK was carried out in the gas phase in flowing H_2. The catalysts were tested at 100 and 200 °C under atmospheric pressure in a Pyrex fixed-bed down-flow reactor (9 mm internal diameter) fitted with an on-line gas chromatograph (Varian Star 3400 CX instrument with a 30 m x 0.25 mm HP INNOWAX capillary column and a flame ionisation detector). For more accurate analysis of C_1-C_5 hydrocarbon products, a 60 m x 0.32 mm GSGasPro capillary column was used, allowing for full separation of these hydrocarbons. The temperature in the reactor was controlled by a Eurotherm controller using a thermocouple placed at the top of the catalyst bed. MIBK was fed by passing H_2 flow controlled by a Brooks mass flow controller through a stainless steel saturator, which held liquid MIBK at appropriate temperature to maintain the chosen reactant concentration. Typically, unless stated otherwise, the saturator temperature was 35 ± 0.3 °C, which gave the

MIBK partial pressure of 3.64 kPa (3.6 vol%) [3]. The gas feed entered the reactor at the top at a flow rate of 20 ml min^{-1}. The downstream gas lines and valves were heated to 180 °C to prevent substrate and product condensation. Unless otherwise indicated, the catalyst bed contained 0.2 g of powdered catalyst (45-180 μm particle size). In some cases, a smaller amount of catalyst diluted with silica to 0.2 g was used to reduce conversion. Prior to reaction, the catalysts were pre-treated in H_2 flow for 1 h at the reaction temperature. Once reaction started, the downstream gas flow was analysed by the on-line GC to obtain reactant conversion and product selectivity. The selectivity was defined as moles of product formed per mole of MIBK converted and is quoted in mole per cent.

6.2 MIBK hydrogenation over Pt-doped zeolites

6.2.1 Catalyst performance

This work explored a bifunctional metal-acid catalysed pathway to achieve MIBK-to-2MP hydrogenation in one step on a single catalyst bed, using platinum metal supported on zeolites as the bifunctional catalysts. This pathway would involve MIBK hydrogenation to MP-ol on metal sites followed by MP-ol dehydration on acid sites to form olefin and finally olefin hydrogenation to 2MP on metal sites, as shown in Scheme 6.1. Since the dehydration of secondary alcohols on acid catalysts is fast [4, 5] and so is the hydrogenation of C=C bonds on platinum metals, the bifunctional pathway was expected to be more efficient than the hydrogenation-only pathway.

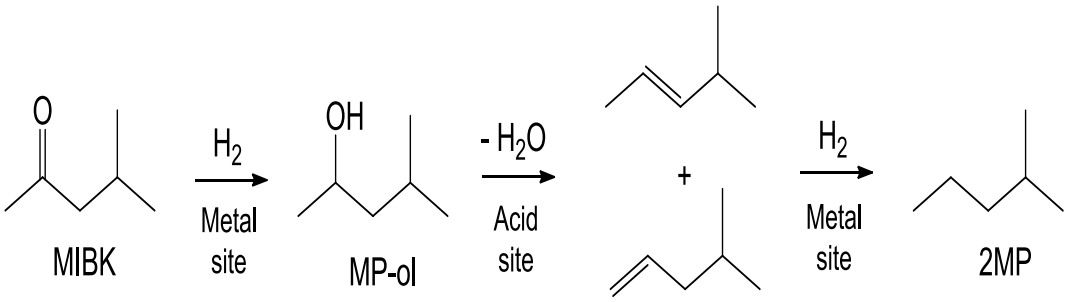

Scheme 6.1 Hydrogenation of MIBK via bifunctional metal-acid catalysis.

The zeolites used, H-ZSM-5, H-Beta and H-Y, had close Si/Al ratios (12-15) and hence comparable proton site densities. Their acid strength decreased in the order H-ZSM-5 > H-Beta > H-Y [6, 7]. The Pt/zeolite catalysts had high crystallinity and exhibited standard XRD patterns of the corresponding zeolites, as presented in Section 3.6.2. Despite Pt doping being carried out similarly for all zeolites (0.5 wt% using the ion exchange method), the final Pt loading varied between 0.30 and 0.45 wt%, as shown in Table 6.1, increasing with the pore diameter of the zeolite. This indicates that Pt loading was controlled by the zeolite pore size.

Representative results are shown in Table 6.2, with zeolite catalysts placed in order of increasing pore size.

Table 6.2 Hydrogenation of MIBK over bifunctional Pt/zeolite catalysts[a]

Catalyst	Temperature (°C)	Conversion (%)	Selectivity (%)			
			2MP	3MP	MP-ol	Other
H-ZSM-5	100	0	0	0	0	0
H-ZSM-5	200	20	9	0	7	84[b]
0.30%Pt/H-ZSM-5	100	94	65	0	34	1
0.30%Pt/H-ZSM-5	200	100	83	17	0	0
0.39%Pt/H-Beta	100	92	58	0	38	4
0.39%Pt/H-Beta	200	44	70	4	0	26[c]
0.45%Pt/H-Y	100	98	36	0	49	15
0.45%Pt/H-Y	200	81	55	2	0	43[c]

a) 0.20 g catalyst pre-treated in H_2 at reaction temperature for 1 h, 3.6% MIBK in H_2 flow, 20 ml min^{-1} flow rate, 4 h time on stream

b) C_1-C_5 cracking products, mainly propene and butene, together with small amounts of C_{6+} condensation products

c) C_{6+} condensation products.

In a blank run, H-ZSM-5 itself was not active at all at 100 °C. At 200 °C, it converted 20% of MIBK to give mainly C_1-C_5 cracking products, mostly propene and butenes, together with small amounts of 2MP and MP-ol.

Doping of zeolites with Pt greatly increased catalyst activity even at 100 °C, giving 92-98% MIBK conversion to a mixture of 2MP and MP-ol in a molar ratio of 1:(0.5-1.4). Therefore, at this temperature the dehydration of MP-ol was not complete and the MP-ol/2MP ratio decreased with increasing zeolite acid strength: 1.36 (H-Y) >

0.66 (H-Beta) > 0.52 (H-ZSM-5), which can be explained by the acceleration of alcohol dehydration with increasing catalyst acid strength. It should be noted that no 2MP isomerisation was observed at 100 °C.

Increasing the temperature to 200 °C led to the complete dehydration of MP-ol, giving 2MP as the main product with 55-83 selectivity. At 200 °C, 2MP isomerised to form 3-methylpentane (3MP) and traces of *n*-hexane, in agreement with the literature [8]. As expected, the isomerisation correlates with zeolite acid strength, as indicated by the 3MP/2MP product ratio: 0.20 (Pt/H-ZSM-5) > 0.057 (Pt/H-Beta) > 0.036 (Pt/H-Y) (Table 6.2). The mechanism of alkane isomerisation over bifunctional catalysts has been discussed elsewhere ([8] and references therein). It involves alkane dehydrogenation on Pt to form an alkene followed by alkene skeletal isomerisation on acid sites and finally alkene hydrogenation on Pt to yield the corresponding alkane isomer. In our case, 4-methylpentene-1 and 4-methylpentene-2 formed in MP-ol dehydration (Scheme 6.1) may isomerise on zeolite acid sites to give 3MP eventually. The total selectivity to methylpentanes increased in the order: Pt/H-Y (57%) < Pt/H-Beta (74%) < Pt/H-ZSM-5 (>99%). Therefore, amongst the Pt/zeolite catalysts studied, Pt/H-ZSM-5 clearly stands out, giving >99% selectivity to methylpentanes and 100% MIBK conversion at 200 °C (Table 6.2). Other catalysts, Pt/H-Beta and Pt/H-Y, gave significant amounts of unidentified C_{6+} condensation by-products, which can be attributed to aldol condensation of MIBK. The quantity of bulky C_{6+} by-products formed increased with the pore size of zeolites: H-ZSM-5 (5.5 Å) < H-Beta (7.6 x 6.4 Å) < H-Y (7.5 Å), which is an indication of "shape-selective" catalysis. The quantity of coke (C wt%) found in spent catalysts after reaction (200 °C, 6 h) also increased in this order: 5.9 (H-ZSM-5) < 10.5 (H-Beta) < 11.9 (H-Y), as explained in

Section 3.3.2. This is probably the reason for the drop in MIBK conversion at 200 °C for the larger pore zeolites H-Beta and H-Y.

6.2.2 Catalyst performance stability

The Pt/H-ZSM-5 catalyst showed excellent performance stability. It reached steady state in about 2 h and operated without deactivation for at least 16 h, as shown in Figure 6.1. It should be noted that in this run to set the conversion of MIBK at about 70%, the amount of catalyst had to be reduced 4-fold compared to that in Table 6.2.

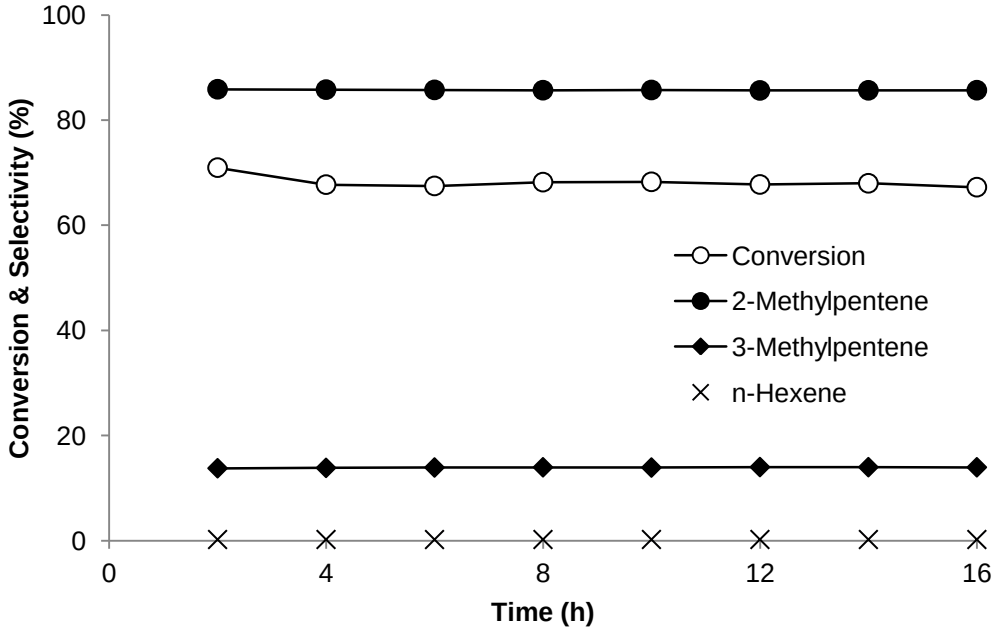

Figure 6.1 Time course for MIBK hydrogenation over 0.3%Pt/H-ZSM-5 (0.05 g) diluted with 0.15 g SiO_2 at 200 °C, 3.6% MIBK, 20 ml min^{-1} H_2 flow rate

6.2.3 Preliminary kinetic study

A kinetic study was carried out on MIBK hydrogenation using Pt/H-ZSM-5 catalyst. To achieve this, MIBK conversion was kept between 6 to 10%. MIBK concentrations were varied between 3.6 and 6.4 vol%, the rest being hydrogen gas.

The rate of reaction was practically unchanged with MIBK concentration in the gas feed, as presented in Table 6.3, indicating that the order in MIBK was close to zero. Therefore, in this system, MIBK conversion was directly proportional to the reaction rate.

Table 6.3 Effect of MIBK concentration on reaction rate[a]

[MIBK] (vol%)	Rate (mol $h^{-1}g^{-1}$)
3.6	0.0038
4.9	0.0037
6.4	0.0036

a) 0.06%Pt/H-ZSM-5 (0.05 g) diluted with 0.15 g SiO_2, 200 °C, 20 ml min^{-1} H_2 flow rate, 5 h time on stream.

The reaction had a rather low activation energy of 18 kJ mol^{-1}, as determined for 0.06%Pt/H-ZSM-5 catalyst in the temperature range of 185-230 °C (Figure 6.2). This implies that the reaction may be controlled by internal diffusion in zeolite micropores.

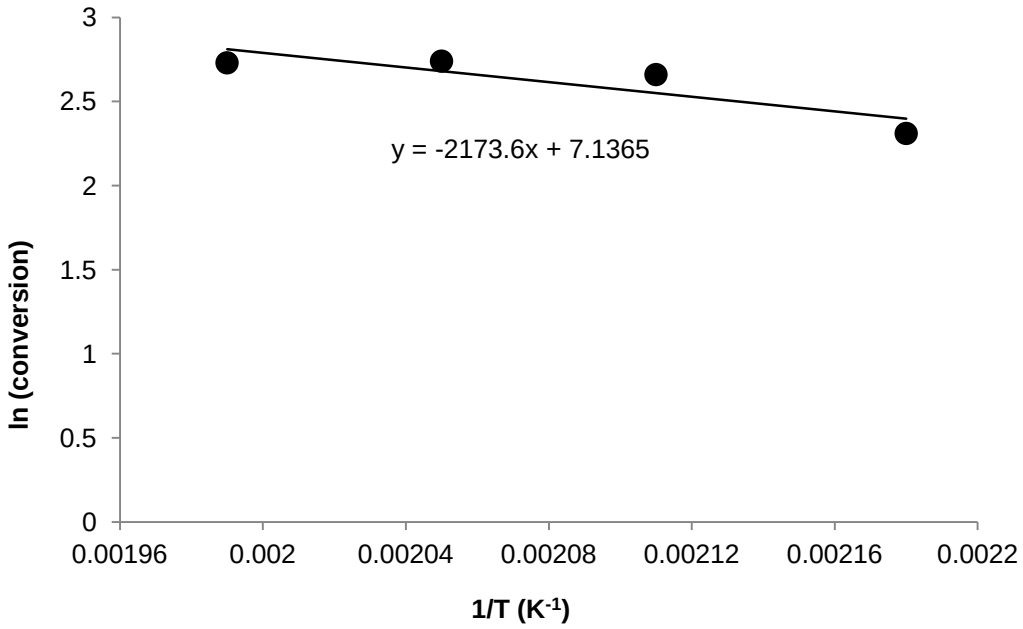

Figure 6.2 Arrhenius plot for MIBK hydrogenation over 0.06%Pt/H-ZSM-5 (0.05 g) diluted with 0.15 g SiO_2, 3.6% MIBK, 20 ml min^{-1} H_2 flow rate, 3 h time on stream

MIBK conversion was found to increase from 11 to 67% with increasing Pt loading from 0.06 to 0.30% (Table 6.4), that is, scaled almost proportionally with the Pt loading. Given that Pt dispersion was about the same for these loadings (Table 6.1), this means that the reaction order in Pt was close to one. From these results, the apparent turnover frequency was estimated to be 1200 h^{-1} per exposed Pt atom at 200 °C. This value, however, may be restricted by diffusion limitations. Importantly, the selectivity to 2MP and 3MP was practically unchanged with Pt loading (Table 6.4) and MIBK conversion (cf. entry 4 in Table 6.2 with entry 2 in Table 6.4), which suggests that the hydrogenation of MIBK to MP-ol on Pt sites is the slowest step in Scheme 6.1; subsequent dehydration and hydrogenation steps appear to be fast under the chosen conditions at 200 °C.

Table 6.4 Effect of Pt loading[a]

Catalyst	Pt dispersion	Conversion (%)	Selectivity (%)			
			2MP	3MP	n-Hexane	Other
0.06%Pt/H-ZSM-5	0.87	11	75	15	2	8
0.3%Pt/H-ZSM-5	0.88	67	86	14	<1	<1

a) 0.05 g catalyst diluted with 0.15 g SiO_2, 200 °C, 3.6% MIBK, 20 ml min^{-1} H_2 flow rate, 6 h time on stream.

6.2.4 Reaction mechanism over Pt/H-ZSM-5

The dehydration of MP-ol over 0.3%Pt/H-ZSM-5 was tested to prove the bifunctional mechanism of MIBK hydrogenation as proposed in Scheme 6.1. This was carried out under the conditions applied to MIBK hydrogenation (Table 6.2), except with N_2 (20 ml min^{-1}) instead of H_2. The reaction was very fast, yielding two olefins, 4-methylpentene-1 and 4-methylpentene-2, at 100% MIBK conversion, as presented in Equation 6.1. The same reaction under H_2 gave 2- and 3-methylpentanes at a 100% yield (Equation 6.2). These results support the bifunctional mechanism for MIBK hydrogenation over Pt/H-ZSM-5 catalyst as proposed for this reaction using Pt/CsPW in Chapter 5.

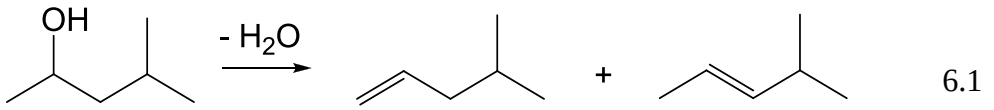

6.1

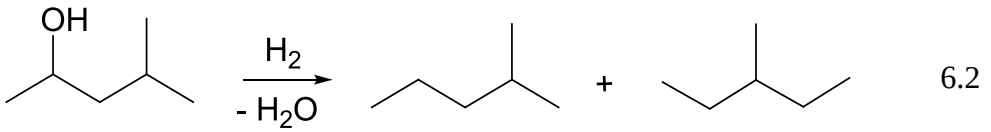

6.2

6.3 Conclusions

The gas phase hydrogenation of MIBK was investigated in a fixed-bed reactor at 100 and 200 °C and atmospheric pressure using three kinds of zeolites (H-ZSM-5, H-Beta, and H-Y) with close Si/Al ratio as acidic support for Pt metal. MIBK may be viewed as a key intermediate in the conversion of biomass-derived acetone to transportation fuel. Produced by one-step (one-pot) hydrocondensation of acetone [9-11], MIBK can be further efficiently hydrogenated via a metal-acid bifunctional pathway on a single bed containing Pt/H-ZSM-5 catalyst to give methylpentanes with > 99% yield at 200 °C. At this temperature, 2MP isomerised to form 3-methylpentane (3MP) and traces of *n*-hexane. The isomerisation increased with increasing zeolite acid strength in the order H-ZSM-5 > H-Beta > H-Y.

The effects of reaction temperature, MIBK concentration, catalyst weight and Pt loading have been studied. The reaction may be controlled by internal diffusion in zeolite micropores. The mechanism of MIBK hydrogenation to yield MP was investigated using Pt/H-ZSM-5. It consists of MIBK hydrogenation to MP-ol on metal sites followed by MP-ol dehydration on H-ZSM-5 acidic sites to form olefin and finally olefin hydrogenation to MP on metal sites.

References

[1] B.C. Gates, Catalytic Chemistry, Wiley, 1992.

[2] J.E. Benson, H.S. Hwang, M. Boudart, J. Catal. 30 (1973) 146.

[3] CRC, Handbook of Chemistry and Physics, 88th ed.

[4] J. Macht, M. Neurock, M. Iglesia, E., J. Am. Chem. Soc. 130 (2008) 10369.

[5] A.M. Alsalme, P.V. Wiper, Y.Z. Khimyak, E.F. Kozhevnikova, I.V. Kozhevnikov, J. Catal. 276 (2010) 181.

[6] M. Brandle, J. Sauer, J. Am. Chem. Soc. 120 (1998) 1556.

[7] S.G. Hegde, R. Kumar, R.N. Bhat, P. Ratnasamy, Zeolites 9 (1989) 231.

[8] J. Macht, R.T. Carr, E. Iglesia, J. Catal. 264 (2009) 54.

[9] R.D. Hetterley, R. Mackey, J.T.A. Jones, Y.Z. Khimyak, A.M. Fogg, I.V. Kozhevnikov, J. Catal. 258 (2008) 250.

[10] R.D. Hetterley, E.F. Kozhevnikova, I.V. Kozhevnikov, Chem. Comm. (2006) 782.

[11] F. Al-Wadaani, E.F. Kozhevnikova, I.V. Kozhevnikov, J. Catal. 257 (2008) 199.

7. Conclusions

Efficient and economical utilisation of biomass resources is a major goal for academia and industry in the 21st century. In the fast growing energy sector, approximately 50% of the crude petroleum produced worldwide is presently refined into transportation fuels. The rapidly rising use of a non-renewable feedstock has a significant impact on greenhouse gas emission. Biomass is the only renewable energy source that can be converted into liquid transportation fuels. Therefore, increasing use of biomass-derived fuel (biofuel) in the transportation sector can significantly reduce greenhouse gas emissions, as well as diversify energy sources, improving energy security and stimulating the rural economy.

Carboxylic acids are readily available from natural sources and are attractive as renewable raw materials for the production of value-added chemicals and biofuel components. For fuel applications, carboxylic acids require reduction in their oxygen content. Therefore, much recent research has focussed on the deoxygenation of carboxylic acids using heterogeneous catalysis. In this work, propionic acid was chosen as representative of carboxylic acids with the number of carbon atoms $n \leq 6$ derived from carbohydrate feedstocks.

Today's best known biofuels, biodiesel and ethanol, are derived from food crops (oils, grains or sugars), resulting in unsustainable pressure on the global food and arable land supply. Second-generation biofuels will be produced largely from a combination of non-food sources such as cellulosic biomass, inedible oils and algal oils. Biomass-based butanol (also called biobutanol) is expected to play a major role in the next generation of biofuels. Biobutanol production is largely based on the traditional

acetone-butanol fermentation of carbohydrates by a *Clostridium* strain which yields butanol together with acetone and ethanol in a ratio of 6:3:1. Therefore, if the biobutanol project goes ahead as planned, it will produce a massive surplus of acetone. For that reason, finding new outlets for acetone, preferably in the transportation fuel sector, would greatly improve the economy of biobutanol production. It is well known that acetone can be transformed into C_6, C_9 and larger organic molecules by aldol condensation. This is used for the industrial production of methyl isobutyl ketone (MIBK) and diisobutyl ketone (DIBK), which are used as solvents in paints, coatings and resins. MIBK and DIBK can be viewed as key intermediates for the conversion of biomass-derived acetone to transportation fuel.

The main aim of this work was to investigate heterogeneous catalysis using heteropoly acids (HPAs) for the deoxygenation and hydrogenation of renewable feedstocks for value-added chemicals and fuels. HPA compounds comprising polyoxometalates (POMs) have found numerous applications as catalysts, offering significant economic and environmental benefits. The main focus was on HPW and its Cs acidic salt (CsPW), which possess sufficiently high thermal stability, with decomposition temperatures of 450 and > 500 °C respectively. These compounds have a very strong Brønsted acidity and are well-documented as acid catalysts. They were used with metal-loaded CsPW as bifunctional metal-acid catalysts for the deoxygenation and hydrogenation of propionic acid, MIBK and DIBK. In addition, Pt-doped zeolites (H-ZSM-5, H-Beta and H-Y) were also investigated in MIBK deoxygenation for comparison with the metal-loaded POM catalysts.

The catalysts used in this work were prepared according to the procedures documented in the literature and characterised using various physical and chemical

techniques. The surface area and porosity of catalysts were determined using N_2 physisorption. The HPW-based catalysts under study were all mesoporous solids with an average pore diameter of 26-96 Å and relatively high surface area (75-160 $m^2\ g^{-1}$). Pt-doped H-ZSM-5, H-Beta and H-Y were found to be microporous materials having a large surface area (357-690 $m^2\ g^{-1}$) and average pore diameter of 24-50 Å. As demonstrated by FTIR spectra, CsPW and its doped metal catalysts retained their primary Keggin structure after use in the gas phase deoxygenation of propionic acid at 400 °C, whereas the primary structure of 30 % HPW/SiO_2 remained stable after reaction at ≤ 350 °C but decomposed at 400 °C. XRD measurement revealed that all catalysts used in this study were crystalline and showed no Pd or Pt metal phase on CsPW, H-ZSM-5, H-Beta and H-Y, indicating that the metals were finely dispersed. CsPW-based catalysts, fresh and spent after deoxygenation of propionic acid at 400 °C, showed the same XRD pattern as crystalline CsPW. Therefore, the CsPW catalysts also retained their secondary (crystal) structure after reaction. Hydrogen titration experiments demonstrated the presence of Pd, Pt and Ru in high dispersion in the CsPW and Pt on H-zeolites used in this study as bifunctional catalysts. Nitrous oxide adsorption was used to determine the particle size of Cu particles and to estimate Cu dispersion on CsPW and SiO_2. TPR experiments confirmed that all HPW-based catalysts were resistant to reduction with H_2 at reaction temperatures of 100-400 °C. ICP analysis precisely determined the composition of in-house-made HPW-based catalysts and the Pt content of H-zeolites prepared by the ion exchange method. HPW-based catalysts and H-zeolites possess both Brønsted and Lewis sites, as indicated by FTIR spectra of adsorbed pyridine. Using ammonia adsorption calorimetry, the acid strength of catalysts under study was found to increase in the order: Cs_3PW << H-ZSM-5 < 30 % HPW/SiO_2 ≤ CsPW.

The gas-phase deoxygenation of propionic acid was investigated at 250-400 °C in flowing H_2 or N_2 using the Keggin-type HPA $H_3PW_{12}O_{40}$ supported on silica and its bulk acidic salt $Cs_{2.5}H_{0.5}PW_{12}O_{40}$, as well as with Pd-, Pt- and Cu-loaded CsPW bifunctional metal-acid catalysts. For comparison, these catalysts were tested with the corresponding SiO_2-supported metal catalysts. Previously, P-Mo-V heteropoly compounds of Keggin structure have been studied in this group as catalysts for the gas-phase hydrogenation and ketonisation of aliphatic carboxylic acids. However, due to their relatively low thermal stability (< 400 °C), these POMs decompose in situ to form Mo and V oxides, which are the true catalysts rather than the POMs themselves. In contrast, in the present work, CsPW itself and CsPW-supported Pd, Pt and Cu catalysts were found to be thermally stable. They retained the Keggin structure of their polyanion (primary structure), as well as the CsPW crystal structure (secondary structure), after reaction at 400 °C in H_2, whereas HPW decomposed above 350 °C in N_2. The reaction was found to involve several pathways including ketonisation, decarbonylation, decarboxylation and hydrogenation, leading to partial or total deoxygenation of propionic acid. HPW and CsPW, both in H_2 and in N_2, exhibited ketonisation activity between 250 and 300 °C to yield 3-pentanone, CsPW being more selective than HPW. At 400 °C, HPW and CsPW were active for the decarbonylation and decarboxylation of propionic acid to yield ethene and ethane respectively. Loading Pd or Pt onto CsPW greatly affected catalyst performance in H_2, enhancing the decarbonylation of propionic acid to form ethene at the expense of ketonisation and decarboxylation. Metal loading had little effect in N_2, however. Pd/SiO_2 and Pt/SiO_2 exhibited similar behaviour, showing almost 100% selectivity to ethene in H_2. These results are consistent with the hydrodeoxygenation of propionic acid, suggesting that hydrogenolysis of C-C bonds on Pd and Pt sites plays an essential role. In contrast to the Pd and Pt catalysts, the Cu

catalysts, Cu/CsPW and Cu/SiO_2, were both active in the hydrogenation of the C=O bond to yield propanal and 1-propanol. The turnover rates of propionic acid conversion on metal catalysts were found to follow the order Pd > Pt > Cu for both CsPW-supported and silica-supported metal catalysts. The main routes of propionic acid deoxygenation with the catalysts studied are summarised below:

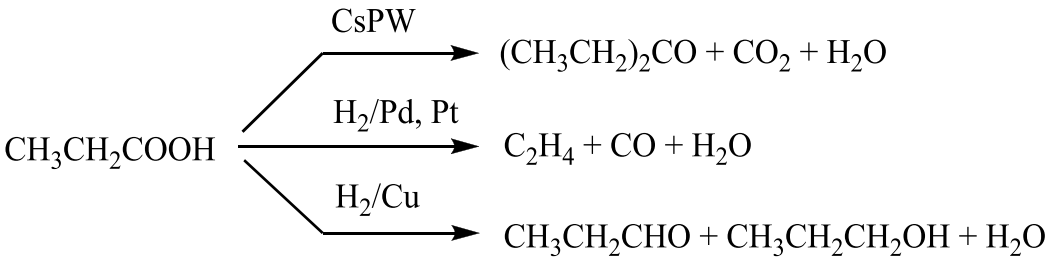

From a practical point of view, it may be desirable to produce the ketonisation products with carbon backbone upgrade ($C_n \rightarrow C_{2n-1}$) over CsPW at 250-300 °C in a hydrogen-free system, as well as the C_n hydrogenation products (aldehydes and alcohols) without carbon loss using Cu catalysts. On the other hand, Pd and Pt catalysts possessing high hydrodeoxygenation activity via the decarbonylation pathway allow the production of C_{n-1} alkenes.

The gas phase hydrogenation of MIBK and DIBK was tested at 100-400 °C under atmospheric pressure. Bifunctional Pd-, Pt-, Ru- and Cu-loaded Keggin heteropoly salt $Cs_{2.5}H_{0.5}PW_{12}O_{40}$ (CsPW) catalysts were used. Pt/CsPW was found to be a very efficient catalyst for the selective one-step hydrodeoxygenation of MIBK and DIBK under mild conditions (100 °C, 1 bar) without isomerisation of carbon backbone via a metal-acid bifunctional mechanism to give a 97-99% yield of 2-methylpentane (MP) and 2,6-dimethylheptane (DMH) respectively , which could be blended with gasoline and used through the existing fuel infrastructure. The catalyst showed no

deactivation of its performance for at least 14 hours on stream. In addition, reduced copper chromite was found to be an efficient catalyst for DIBK hydrogenation at 300 °C. The catalysed reaction of MIBK hydrodeoxygenation using Pt/CsPW occurred under kinetic control. The bifunctional metal-acid catalysed mechanism to achieve MIBK-to-MP hydrogenation involves MIBK hydrogenation to MP-ol on metal sites, followed by MP-ol dehydration on acid sites to form olefin and finally olefin hydrogenation to MP on metal sites.

Pt/zeolites were examined for MIBK hydrogenation in the gas phase. Three kinds of zeolites (H-ZSM-5, H-Beta and H-Y) were chosen at close Si/Al ratios (12-15). Among the Pt-loaded H-zeolites used in this reaction, Pt/H-ZSM-5 was the most efficient bifunctional catalyst that was highly selective for the desired product. At 100 °C, Pt/H-ZSM-5 gave MIBK conversion close to that of Pt/CsPW, but its MP selectivity (65%) was lower than that of Pt/CsPW, due to incomplete dehydration of MP-ol on the H-ZSM-5 catalyst. This shows that the strong acidity of CsPW is essential for the high efficiency of the Pt/CsPW, as demonstrated by the differential scanning calorimetry of NH_3 adsorption. At 200 °C, Pt/ZSM-5 matched the catalytic performance of Pt/CsPW, but at this temperature considerable isomerisation of MP took place to give methylpentanes with > 99% yield. 2MP isomerised to form 3MP and traces of *n*-hexane. The isomerisation increased with increasing of zeolite acid strength, following the order H-ZSM-5 > H-Beta > H-Y. The reaction may be controlled by internal diffusion in H-ZSM-5 micropores.

Further work would be of interest on MIBK and DIBK hydrogenation using a wide range of acidic solid catalysts.